Cell-Penetrating Peptides (CPPs) Based on an Oligoproline Scaffold – Design, Synthesis and Biological Evaluation

&

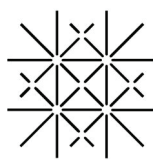# Conformational Analysis of Functionalized Proline Derivatives

Inauguraldissertation

zur
Erlangung der Würde eines Doktors der Philosophie

vorgelegt der
Philosophisch-Naturwissenschaftlichen Fakultät
der Universität Basel

UNI BASEL

von
Yvonne Alice Nagel
aus Freiburg im Breisgau (Deutschland)
Basel 2014

Genehmigt von der Philosophisch-Naturwissenschaftlichen Fakultät der Universität Basel auf Antrag von

Prof. Dr. Helma Wennemers

Prof. Dr. Florian Seebeck

Basel, den 11. Dezember 2012

Prof. Dr. Jörg Schibler

Dekan

Abstract

The effective delivery of drugs and other biomolecules into cells is challenging, since poor translocation across the plasma membrane is a major limitation. Cell-penetrating peptides (CPPs) are a promising tool to address this issue. Despite the progress that has been made in recent years, there is still a need for the development of new CPPs with superior physicochemical properties, enhanced uptake efficiency, intracellular targeting of specific organelles and proteolytic stability. Herein we present a novel type of oligoproline-based CPPs that shows a number of advantages over existing systems. The approach exploits the conformationally well-defined and functionalizable polyproline type II (PPII) helix of Azp-containing oligoprolines as a scaffold. Peptides bearing either (4*R*)- or (4*S*)-configured amino or guanidino proline residues with different geometrical designs along the helical axis as well as different chain lengths were prepared and their cellular uptake was evaluated. All of these oligoproline-based CPPs penetrate into different human cancer cells under physiological conditions. Members of these novel CPPs have higher levels of internalization than the established reference peptides Tat(48-60), octaarginine, and penetratin. Confocal microscopy studies demonstrated that the oligoproline-based CPPs localize in the nucleus of HeLa cells. The proteolytic stability of the CPPs proved to be high and it was shown that all L- and D-oligoproline-based CPPs are stable towards trypsin and in human blood serum for at least 48 h. In addition, the peptides have only a low cytotoxicity towards HeLa cells and no haemolytic activity against human erythrocytes. A preliminary siRNA delivery experiment showed a promising delivery potential into HeLa cells, compared to the reference peptides Tat(48-60) and octaarginine. These results demonstrate the potential of the novel oligoproline-based CPPs for future biomedical applications.

A second goal of this work was to investigate structure directing properties of electron-withdrawing groups (EWGs) derived from an azide at the C(4) position of proline. In the course of the studies C(4)-*endo* puckered amino proline derivatives favoring a *trans* conformation around the tertiary prolyl amide bond were developed. Such conformers with an *endo* ring pucker favoring a *trans* amide bond had not been established before. In these derivatives a hydrogen bond between the substituent at C(4) and the carbonyl group of the amide backbone stabilizes the *endo* ring pucker and favors the *trans* amide conformer. Furthermore we demonstrated that these derivatives are valuable tools to tune the *cis/trans* amide bond ratio within peptides.

The following dissertation was carried out under the supervision of Prof. Dr. Helma Wennemers at the University of Basel from June 2008 until November 2011 and at ETH Zürich from December 2011 until December 2012.

During the course of this work, the following Master theses and internships affiliated to the project of this thesis were supervised:

Master thesis:

Philipp Raschle   June 2011 – November 2011
Title: "Synthese und Zellgängigkeit von stereoisomeren kationischen Oligoprolinen"

Alba Mascarin   September 2010 – February 2011
Title: "Cell-penetrating Properties of Functionalized Oligoprolines and Synthesis of a Releasable Linker System for Cell-penetrating Peptides"

Internships:

Cedric Hugelshofer   September 2011
Simon Bertschi   June 2011
Lucia Buglione   May 2011

Parts of this work were published:

Y. A. Nagel, M. Kuemin, H. Wennemers, „Functionalizable Oligoprolines as Molecular Scaffolds", *Chimia* **2011**, *65,* 264-267.

M. Kuemin, Y. A. Nagel, S. Schweizer, F. W. Monnard, C. Ochsenfeld, H. Wennemers, „Tuning the *cis/trans* Conformer Ratio of Xaa–Pro Amide Bonds by Intramolecular Hydrogen Bonds: The Effect on PPII Helix Stability", *Angew. Chem. Int. Ed.* **2010**, *49*, 6324-6327.

Parts of this work were presented at the following conferences:

Oral presentations

Iberian Peptide Meeting **2012**, Alicante, Spain, *„Cell-Penetrating Peptides Based on Polyproline Scaffolds"*

Summer School **2011** - Challenges in Organic Synthesis, Villars, Switzerland, *„Cell-Penetrating Peptides Based on Polyproline Scaffolds"*

30. Regio Symposium, **2010**, Mittelwihr, France, "*Effects of Intramolecular Hydrogen Bonds on Polyproline II Helix Stability"*

Posters

Fall meeting of the Swiss Chemical Society, **2012**, ETH Zürich, Switzerland

Fall meeting of the Swiss Chemical Society, **2011**, University of Lausanne, Switzerland

46th Bürgenstock Conference, (EUCHEM Conference on Stereochemistry), **2011**, Brunnen, Switzerland

COST Meeting on Foldamers: Building Blocks, Structure and Function, (European Cooperation in Science and Technology), **2009**, Szeged, Hungary

Fall meeting of the Swiss Chemical Society, **2009**, Lausanne, Switzerland

3rd Conference on Intracellular Delivery of Therapeutic Molecules: From Bench to Bedside, **2009**, Montpellier, France

9th German Peptide Symposium, **2009**, Göttingen, Germany

Awards:

Poster award at the „Peptide Vectors and Delivery of Therapeutics" conference **2011**, Tallinn, Estonia; Title: *„Cell-Penetrating Peptides Based on Polyproline Scaffolds"*

Poster award from the Swiss Chemical Society, fall meeting **2010**, ETH Zürich, Switzerland; Title: *„Cell-Penetrating Peptides Based on Cationic Amphiphilic Polyproline Structures"*

Für meine Familie
und Carsten

Acknowledgments

Table of Contents

1. INTRODUCTION

1.1 Proline – a special amino acid

1.1.1   The *cis/trans* isomerization around the prolyl amide bond

The amino acid proline and its derivatives are unique amongst the proteinogenic amino acids due to their cyclic structure and secondary amine.[1] In Xaa-Pro amide bonds (Xaa = any amino acid, Pro = proline) the ability of the nitrogen to delocalize its free electron pair over the whole amide structure induces a partial double bond character of the C-N bond. According to the restriction of the torsion angles a planar structure results, in which two distinct conformations can be adopted, namely the *cis* and *trans* conformation. The activation energy for the *cis/trans* isomerization of amide bonds is around 20 kcal/mol.[2] It is well established that secondary peptidic amide bonds have a strong preference for the *trans* conformation (dihedral angle of $\omega = 180°$), due to the steric hindrance between the N-terminal amino acid ($C^{\alpha-1}$) and the flanking amino acid in the *cis* conformation ($\omega = 0°$), in contrast to the less unfavorable interaction between $C^{\alpha-1}$ and the amide hydrogen in the *trans* conformation (Fig. 1, right).[3] In the case of a tertiary prolyl amide bond (Xaa-Pro) the energetic gap between the *cis* and *trans* conformation is diminished, since in both isomeric forms the $C^{\alpha-1}$ atom is in *cis* conformation towards either C^{α} or C^{δ} (Fig. 1, left). Due to this steric effect the *trans* preference in Xaa-Pro bonds is less pronounced, although the overall equilibrium is still on the side of the *trans* conformer.[4]
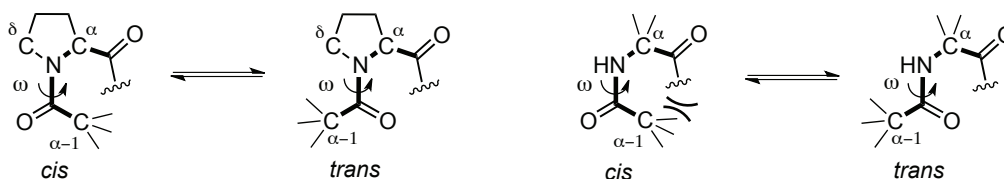
Figure 1: *Cis/trans* isomers of the tertiary prolyl amide bond (Xaa-Pro) (left) and a secondary amide (right).

In short peptides both conformations exist in a dynamic equilibrium, whereas the focus is clearly on the side of the *trans* conformation.[4-5] The conformation of prolyl amide bonds in the native, functional state of folded proteins is in most cases defined. Due to its relatively high activation energy, the *cis/trans* isomerization is a rather slow process, which turns out to be in many cases the rate-limiting step of protein folding.[2b, 3, 6]

1

Enzymes, able to catalyze this isomerization, act as protein folding chaperones and were first discovered by Fischer *et al.* in 1984. They are known as peptidyl prolyl isomerases (PPIases).[7] *Cis* conformations in Xaa-Pro bonds are often located at the first residue of certain types of tight turns within the protein backbone. Proteins that contain structural *cis*-prolines in the native state include for example ribonuclease A,[8] ribonuclease T1,[9] tryptophan synthase,[10] and some interleukins.[11]

1.1.2   Factors that influence the *cis*/*trans* isomerization

Cis/*trans* isomerizations of prolyl amide bonds play a key role in a variety of essential processes. They are not only relevant as the rate determining steps of protein folding,[2b, 3, 6] but also significantly influence the susceptibility of proximate peptide bonds to protease activity.[12] Furthermore, they are involved in protein regulation. In this case proline isomerizations act as molecular switches, which regulate the conformation of catalytic or binding sites of cellular proteins.[6e] [6f] Due to the particular importance of the isomerization processes it is of high interest to understand the factors that determine the *cis*/*trans* conformer ratio, as well as the development of tools that allow for a tuning of the equilibrium.

1.1.2.1 The n→π* interaction

To study the factors that determine the *cis*/*trans* conformer ratio of prolyl amide bonds, a series of synthetic proline derivatives were closely examined. Raines and co-workers for example examined the model compound N-formyl-proline methyl ester (Fm-Pro-OMe, **1**). A preference for the *cis* conformer would be expected based on steric considerations, to avoid a repulsion between the formyl oxygen and the methyl ester, as the Van-der-Waals radius of oxygen is larger, compared to hydrogen and the carbonyl bond is longer compared to the C-H bond. However, a *cis/trans* ratio of 1:1.8 was observed for **1** in D_2O via NMR experiments, showing that the *trans* conformer is populated to a higher amount than the *cis* conformer.[13] This observation is explained with a hyperconjugative interaction of non-bonding electrons of the amide oxygen with the electropositive carbonyl carbon atom of the methyl ester. This n→π* interaction is only possible in the *trans* conformation and therefore leads to a stabilization of the *trans* relative to the *cis* conformer (Fig. 2).
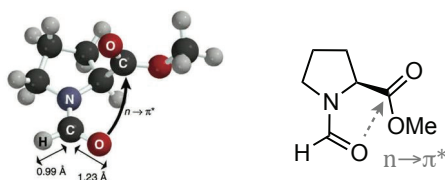
Figure 2: Structure of *N*-formyl-L-proline methylester (Fm-Pro-OMe, **1**) showing the n→π* interaction, favoring the *trans* amide conformation;[13] the C'$_{i-1}$-H and C'$_{i-1}$=O$_{i-1}$ bond lengths are from the structure of crystalline dimethyl formamide.[14]
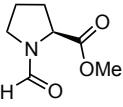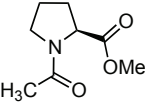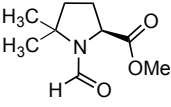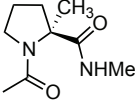
This n→π* interaction contributes significantly to the molecular conformation of proline derivatives. The contribution was estimated to be in a range of 3 kJ/mol at 25 °C for proline derivative **1**.[15] n→π* interactions are abundant in common secondary structures, such as α- or polyproline II (PPII) helices, but also in twisted β-sheets.[16] General factors influencing the strength of the n→π* interaction are the distance between the oxygen of the amide and the carbonyl carbon atom of the C-terminus, as well as the angle between them. In an ideal case, this angle corresponds to the Bürgi-Dunitz trajectory, the angle of a nucleophilic attack on a carbonyl group as an electrophile.[17] Another crucial point for the interaction is the electropositive character of the carbonyl carbon, which can be enhanced by introduction of electron-withdrawing substituents to the ester.[18]

1.1.2.2 The influence of steric factors

The influence of steric factors on the *cis/trans* conformer ratio was explored with proline derivatives, bearing sterically demanding groups in various positions. The preference of the *trans* over the *cis* conformer (**1**, $K_{trans/cis}$ = 1.8 in D_2O), proved to be even more pronounced in Ac-Pro-OMe (**2**) compared with Fm-Pro-OMe (**1**). Within Ac-Pro-OMe, (**2**) the steric repulsion of the additional methyl group with the methyl ester in the *cis* form leads to a higher population of the *trans* conformer ($K_{trans/cis}$ = 4.9 in D_2O).[1]

---

[1] $K_{trans/cis}$ of Ac-Pro-OMe (**2**) was determined *via* ^{1}H NMR analysis in D_2O. $K_{trans/cis}$ = 4.9 is obtained by Moroder *et al.* [19], while Raines and co-workers describe a value of 4.6 [13] or 5.3 [15b].

Table 1: *Trans/cis* equilibria of proline derived monomer models.
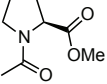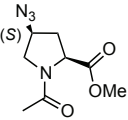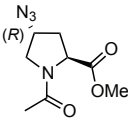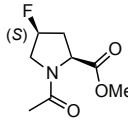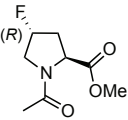
	1	2	3	4
$K_{trans/cis}$ in D_2O	1.8	4.9	25	> 98% *trans*
Ref.	[13]	[13, 15b, 19]	[6c, 13, 20]	[21]

The introduction of two methyl substituents at C^δ to the formylated proline methyl ester (**1**) leading to *N*-formyl-5,5-dimethylproline methyl ester (Fm-dmP-OMe, **3**), causes a significantly higher population of the *trans* conformer, compared to derivative **1**.[6c, 13, 20] Another interesting experiment made by Delaney *et al*. with acetylated 2-methylproline amide (Ac-2-MePro-NHMe, **4**), showed over 98% *trans* conformation in aqueous solution.[21] The substituent at C^α causes a steric repulsion with the methyl group of the acetyl group in the *cis* conformation.

1.1.2.3 The stereoelectronic gauche effect

The azido gauche effect was explored by the Wennemers group in 2006 and was found to determine the conformation of acetylated methyl esters of (4*R*)- and (4*S*)-azidoproline (Azp) (Ac-(4*R*)Azp-OMe **5R** and Ac-(4*S*)Azp-OMe **5S**, Table 2).[22] These studies were initiated by the interesting observation that the configuration of the substituent at C(4) of the pyrrolidine ring plays a significant role for the cyclization tendency of Azp derivatives.[22] It was observed that (4*S*)-configured Azp dimers and trimers generally show a higher cyclization tendency compared to the (4*R*)-diastereoisomers. Since the formation of cyclic di-and tripeptides requires all *cis* amide bonds in the linear precursor peptide, it was expected to identify a higher population of the *cis* conformer in (4*S*)- compared to (4*R*)-configured Azp derivatives. And in fact, the ^{1}H NMR spectra of the monomer model Ac-(4*S*)Azp-OMe (**5S**) and Ac-(4*R*)Azp-OMe (**5R**) revealed a *cis:trans* ratio of 1:2.6 for **5S** and 1:6.1 for **5R** in D_2O. A similar ratio was measured for the according fluorine derivatives **6S** and **6R** by Raines *et al.* The ratio for Ac-Pro-OMe (**2**) is located in between those two values with 1:4.9 (Table 2).

Table 2: *Trans/cis* equilibrium constants of Ac-Pro-OMe (**2**), Ac-(4*S*)Azp-OMe (**5S**), Ac-(4*R*)Azp-OMe (**5R**), Ac-(4*S*)Flp-OMe (**6S**) and Ac-(4*R*)Flp-OMe (**6R**).

	2	**5S**	**5R**	**6S**	**6R**
K$_{trans/cis}$ in D$_2$O	4.9	2.6	6.1	2.5	6.7
Ref.	[13, 15b, 19]	[22]	[22]	[15b]	[15b]

To explore the relation between the absolute configuration at Cγ of Azp and the observed *cis/trans* conformer ratios, the conformational properties of the monomer models **5S** and **5R** were investigated in more detail. The pyrroldine ring of Azp can adopt two main conformations, a Cγ-exo and a Cγ -endo conformation. The Cγ-exo conformation is a ring pucker, where the Cγ atom is located on the opposite site of the residue at Cα, with respect to the plane spanned by the atoms in the ring, N, Cα, Cβ and Cδ. Correspondingly, in the Cγ-endo conformation the Cγ atom is on the same side of that plane as the substituent at Cα. Analyses of the vicinal ¹H ¹H coupling constants and correlation with the Karplus equation[23] 2 revealed that both *cis* and *trans* conformers of Ac-(4*R*)Azp-OMe (**5R**) prefer a Cγ-exo conformation, whereas both conformers of Ac-(4*S*)Azp-OMe (**5S**) preferentially adopt a Cγ-endo conformation (Fig. 3).

Cγ-endo conformation   Cγ-exo conformation
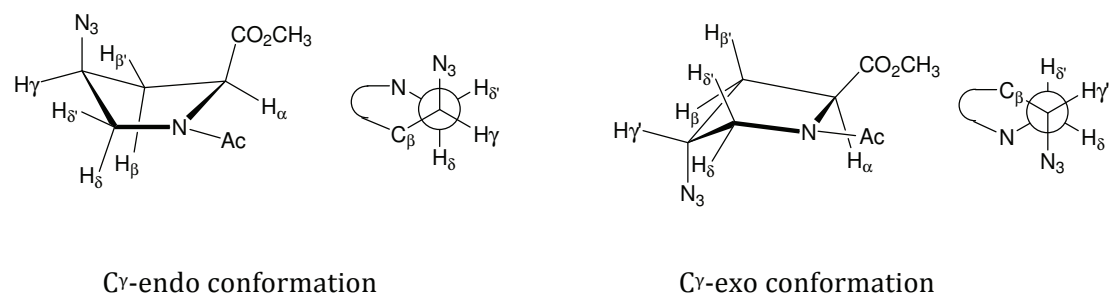
Figure 3: Cγ-exo and Cγ-endo conformations of Ac-(4*S*)Azp-OMe (**5S**) (left) and Ac-(4*R*)Azp-OMe (**5R**) (right) with Newman projections of the dihedral angles around the bond between Cγ and Cδ.[22]

---

2 With $^3J_{H,H}$ = A cos² φ + B cos φ +C, with A = 9.5, B = -1 and C = 1.4 for cyclotriproline; φ describes the dihedral angle between the vicinal protons; A, B and C are parameters used to fit the curve to specific types of molecules.

Within the preferred conformation the azido substituent in both acetylated methyl esters **5S** and **5R** is in the pseudoaxial position and as a result *gauche* to the N-acetyl group. This *gauche* conformation, rather than *anti,* might be counterintuitive at the first view. Due to a destabilization, caused by 1,3-diaxial repulsions between the azide and the methyl ester, a preference for the *anti* orientation could be expected. But the obtained data show a clear *gauche* conformation and suggest that another effect mainly influences the overall conformation of the proline derivatives **5S** and **5R**. This *gauche* conformation, also known for fluorine derivatives,[24] is preferred over an *anti* orientation due to a maximum overlap for a hyperconjugative electron donation from the σ orbital of a vicinal C-H bond to the antibonding σ* orbital of a polarized C-N bond. In this orientation the best σ-donor bond (C-H) is placed *anti* to the best σ-acceptor (C-N of the azide and amide, respectively) thus overcompensating unfavorable electronic repulsions (Fig. 4, right).
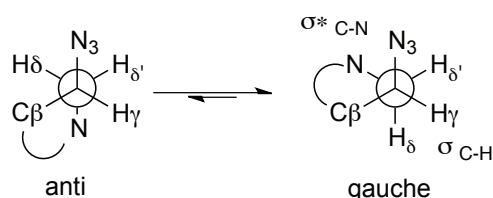
Figure 4: The azido gauche effect e.g. for Ac-(4S)Azp-OMe (**5S**): A hyperconjugative electron donation from the σ orbital of a vicinal C-H bond to the antibonding σ* orbital of a C-N bond, leading to a favored gauche conformation of the azide and amide nitrogen in the molecule.

Ab initio calculations with simple ethane derivatives demonstrated that the *gauche* effect exerted by the azido group is energetically comparable to the well-known fluorine gauche effect.[22] This is also reflected by the similar conformational properties of Azp (**5R** and **5S**) and Flp derivatives (**6R** and **6S**) shown in Table 2. Thus, both azido as well as fluorine moieties can be used as conformation directing elements in peptides, proteins, but also in other organic molecules.[25]

In the crystal structure and the predicted lowest energy structure of azidoproline **5R** the oxygen of the acetyl group is at an angle of 98° to the carbonyl group, reflecting a Bürgi-Dunitz trajectory for the approach of a nucleophile onto a carbonyl group, and the distance between the oxygen of the acetyl group and the electropositive carbonyl carbon of the methyl ester is 2.85 Å. This shows that the *trans* conformation is stabilized by a n→π* interaction between the oxygen of the acetyl group and the carbonyl group of the methyl ester, which cannot take place in the Cγ endo conformation of **5S**. As a result the

trans conformation is populated to a higher extent in (4*R*)-configured, compared to (4*S*)-configured Azp derivatives. These results also explain the observed lower cyclization tendency of (4*R*)-configured Azp derivatives compared to the (4*S*)-diastereoisomers and underlines the potency of azidoproline to tune the *trans/cis* conformer ratio of prolyl amide bonds within peptides.
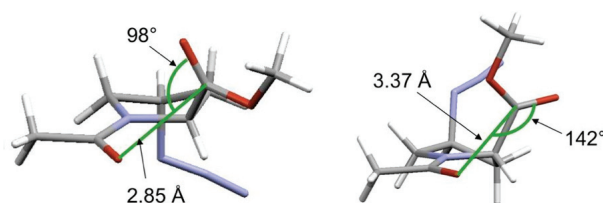
Figure 5: Crystal structures, in agreement with according *ab initio* calculations, show a n→π* interaction in the *trans* conformer of **5R** (left), whereas the *trans* conformer of the according diastereoisomer **5S** is not stabilized by this interaction.[22]

1.1.3   Applications of proline derivatives to tune the conformational properties of peptides and proteins

Synthetic proline derivatives as well as proline mimetics are successfully used to tune the *cis/trans* equilibrium of Xaa-Pro bonds within peptides and proteins.[6c, 26] For example Moroder and co-workers tuned the folding and stability of the green fluorescent protein (GFP) with (4*S*)-Flp,[27] whereas Scheraga *et al.* succeeded in retaining the *cis* conformation in tripeptide fragments of Ribonuclease A (RNAse A) by introducing 5,5-dimethylproline and therefore stabilized the biologically active form of the endonuclease.[28] By replacement of (4*R*)-hydroxy proline (Hyp) ($K_{trans/cis}$ of 6.1 in D_2O)[15b] in the Yaa position of the motif Xaa-Yaa-Gly with either (4*R*)-Flp (**6R**, $K_{trans/cis}$ of 6.7 in D_2O, see Table 2) or (4*R*)-methoxy proline (Mop) ($K_{trans/cis}$ of 6.7 in D_2O)[29] Raines and co-worker were able to enhance the triple helix stability of collagen. Studies realized in the Wennemers research group revealed that (4*R*)-Azp stabilizes the collagen triple helix to a similar extend as (4*R*)-Hyp. Additionally, it was shown that even more sterically demanding substituents like monosaccharides can be installed at defined positions along collagen model peptides (CMPs) without disrupting triple helix stability.[30] Further experiments were conducted to explore the importance of ring puckering versus interstrand hydrogen bonds for the conformational stability of collagen.[31] The ability to successfully influence the *cis/trans* equilibrium is also exploited in so-called pseudo-prolines (ψ-Pro), which were introduced as building blocks for solid phase peptide synthesis (SPPS) by Mutter *et al.* in order to minimize peptide aggregation.[32]

1.2   Polyproline

1.2.1   Structure and biological background

The unique properties of proline, its cyclic nature combined with the secondary amine, lead to constrained dihedral angles and a tertiary amide within the peptidic backbone. This causes a conformational rigidity, able to break up common secondary structures such as α-helices and β-sheets within peptides and proteins. Oligomers of proline adopt already at short chain lengths of six residues the conformationally well-defined, polyproline II (PPII) helix in aqueous solution. In this highly-symmetric structure all amide bonds are in *trans* conformation (ω = 180 °) and every third residue is stacked on top of each other with a helical pitch of ~ 9.5 Å. Thus, oligoprolines have a 3-fold symmetry axis when looking along the helical axis and appear as a prism from the side view (Fig. 6). By changing the environment to more hydrophobic solvents, e.g. *n*-PrOH, a switch to the more compact polyproline I (PPI) helix occurs. This helix is right-handed and all amide bonds are in *cis* conformation (ω = 0 °).[6d, 33] The loss of the hydrogen bond donating capability leads to the fact that in Xaa-Pro bonds no amide protons exist to stabilize the structure like an α-helix or a β-sheet.[6b]

Table 3: Main characteristics of the PPI and PPII conformation. [6d, 34]

PPI conformation	PPII conformation
Right-handed, more compact helix	Left-handed, more extended helix
All *cis* peptide bonds	All *trans* peptide bonds
ϕ = -75 °, ψ = +160 ° and ω = 0 °	ϕ = -75 °, ψ = +145 ° and ω = 180 °
~ 5.6 Å /turn	~ 9.5 Å / turn
3.3 residues per turn	3.0 residues per turn
More stable in organic solvents	More stable in aqueous solution
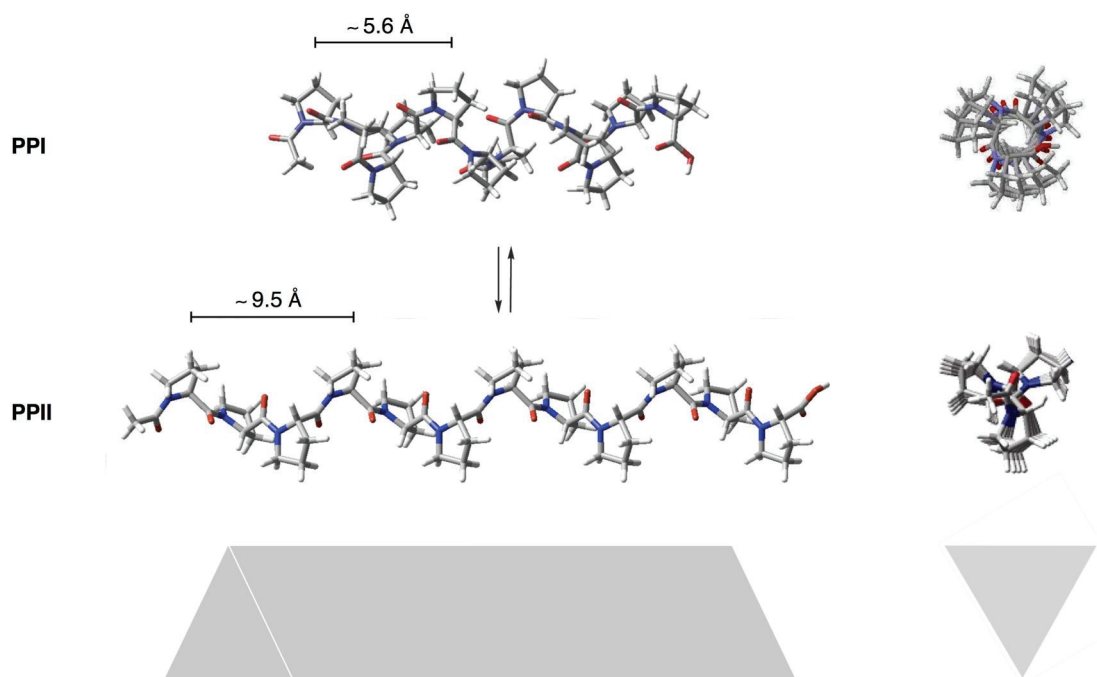
Figure 6: The right-handed PPI helix (top) with all *cis* amide bonds and the left-handed polyproline II (PPII) helix (bottom) with all amide bonds in *trans* conformation; created by using MacroModel software[35] and parameters given in Table 3.

Circular dichroism spectroscopy allows to distinguish between the PPI and PPII structures. The PPI conformation is characterized by a slight spectral minimum at ~ 232 nm and a pronounced maximum at ~ 215 nm and another slight minimum at ~ 199 nm. Spectra of the PPII conformation have a minimum at ~ 206 nm and a slight maximum at ~ 226 nm (Fig. 7).[33a, 36]
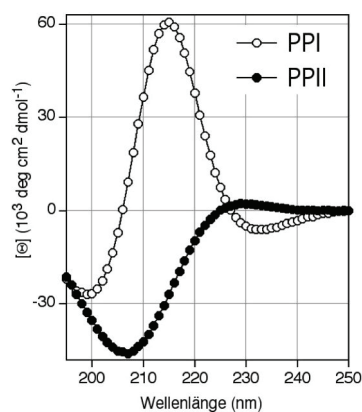
Figure 7: Characteristic circular dichroism spectra for PPI and PPII conformations of Ac-Pro$_{18}$-OH in phosphate buffer (10 mM, pH 7.2) and in 98% v/v *n*-PrOH in phosphate buffer. Spectra were recorded at a peptide concentration of 35 µM at 25 °C.[33a]

Proline-rich sequences are widespread in nature and involved in many essential processes for cell activity. In signaling pathways, for example, proline-rich motifs (PRMs) are recognized by highly abundant domains to modulate regulatory protein-protein interactions. Currently there are six distinct families of PRM-binding domains known, the SH3 domains,[37] the WW domains,[38] the EVH1 domains,[39] the GYF domains,[40] the UEV domains,[41] and the single-domain of profiling proteins.[42] Those regions are able to recognize proline-containing sequences in a range of three to six residues. Due to the special character of proline a high specificity is typically reached and K_d values are in the range of 1 to 500 µM.[43] Furthermore, self assembling PPII helical sequences that form fibrous networks are important for structural proteins like collagen[44] and elastin,[45] which are main components of the connective tissue in mammalians, but also of the cell walls of plants.[46] Proline-rich sequences are also involved in processes like cell-cell recognition[46] and cell motility.[47]

1.2.2 Functionalization and applications of oligoprolines as molecular scaffolds

In recent years the conformationally well-defined helical polyproline structure has drawn high attention as a synthetic molecular scaffold, since the facile functionalization at the γ-position of proline *via* derivatization of hydroxyl proline residues and the ability to provide a defined three-dimensional arrangement of desired moieties opens the door to a variety of applications.[35a]
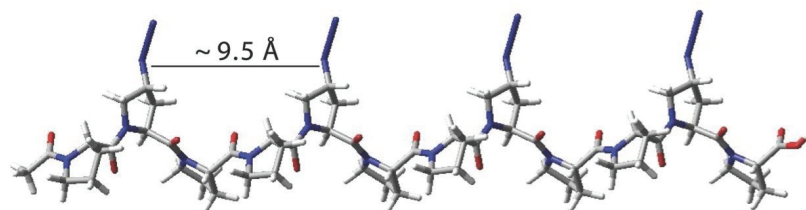
Figure 8: Model of a PPII helix of an oligoproline with Azp residues at every third position.

Common strategies for functionalization employ Azp residues (Fig. 8) allowing for subsequent reaction with alkynes using Huisgen´s 1,3-dipolar cycloaddition ("click reaction")[48] [30a] [49] [26a] [35b] or reduction of the azides to amines (Fig. 9, Scheme 1).[26b] The obtained amines then provide further sites for functionalizations.
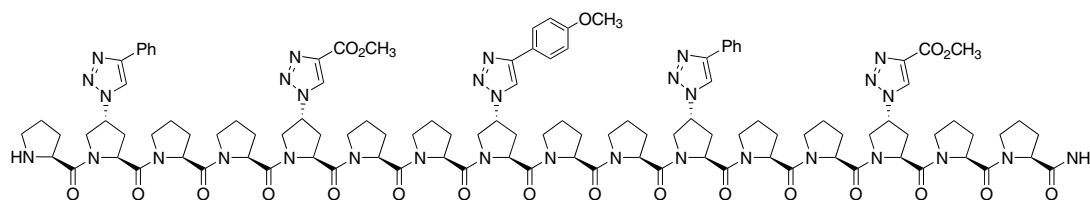
Figure 9: Manifold functionalized oligoproline synthesized by sequential peptide coupling and "click reaction" steps on solid phase.[26a] [35b]
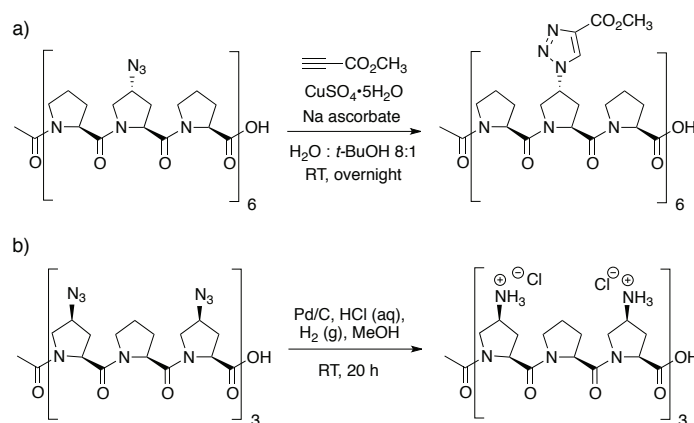
Scheme 1: Functionalization of Azp-containing oligoprolines by a) "click reaction" and b) reduction to amines.

It has also been demonstrated by Overkleeft *et al.* that the attachment of two agonists of a G-protein coupled receptor (GPCR) on an oligoproline scaffold increases the potency for tumor targeting compared to their monomeric counterpart.[50] Other examples for applications of functionalized oligoprolines are their successful use as molecular rulers for calibrating distance measurements in FRET (fluorescence resonance energy transfer) systems,[51] which have been exploited to investigate protein-protein interactions as well as conformational changes within proteins.[52] They have also shown to be of great interest to form thermally responsive materials since proline-rich peptides, due to their inverse transition temperature, aggregate at a temperature threshold around 60°C in aqueous solutions.[53] They were used as spacer units in the context of electron transfer studies, performed by Giese and co-workers as well as Meyer and co-workers.[54] Additionally proline-rich α,β-foldamers with helical conformations were described by Gellman *et al.* to exert antimicrobial properties, including efficiency against pathogens resistant to conventional antibiotics. As an additional beneficial aspect they displayed minimal activity against mammalian cells.[55] Another innovative application of polyproline structures in a biological background is taking advantage of the so-called protein grafting strategy, which is applied on the well-defined fold of the avian pancreatic polypeptide (aPP) to accomplish DNA recognition.

The interaction between the PPII helical part of aPP with its α-helix, exposed to interact with the target, is essential to stabilize the structure of this miniature protein. This special motif was manipulated by Schepartz *et al.* in a way that individual residues of the α-helix are substituted with modified residues in order to allow for an enhanced binding to target DNA with high affinity and selectivity.[56] Furthermore, the principle was extended to design potent ligands for the inhibition of protein-protein interactions. Examples are ligands for human Bcl-2 and Bcl-X$_L$, the central antagonists of programmed cell death (apoptosis), or the oncoprotein hDM2.[57] Alternatively the PPII helix of aPP has also been used to bind SH3 and EVH1 domains, respectively.[58] [59]

Our research group is using the unique features of funtionalized oligoprolines for various applications. For example, oligoproline is applied as a versatile scaffold for multivalent, peptidic tumor targeting ligands to combine the advantages of an agonist and an antagonist for an optimized binding to the gastrin-releasing peptide receptor (GRP-R).[60] Furthermore oligomers of proline with different chain lengths, which were functionalized with aldehyde groups at defined positions were recently used to control the size of silver nanoparticles (AgNPs) that are formed in the Tollens reaction. Intriguingly, the size of the AgNPs correlates linearly with the length of the scaffold.[61] We are also currently investigating the use of appropriately functionalized oligoprolines as scaffolds for the calibration of spin label systems, as well as contrast agents. Another exciting area of research, where oligoprolines can be applied as scaffolds, is the development of semiconductive materials. Furthermore, the Wennemers group is extending the research project focusing on collagen model peptides (CMP) towards the incorporation of interstrand cross-links in the collagen triple helix, accompanied by further stabilization studies to pave the way for the development of functional collagen-based materials as artificial tissues for medical applications.[62]

Last but not least, proline-rich peptides and their derivatives were also reported to be effective cell-penetrating peptides for drug delivery, which will be discussed in detail in the following chapter and is the focus of this work.

1.3   Cell-Penetrating Peptides (CPPs)

1.3.1   Introduction to intracellular drug delivery

A major challenge in the treatment of various diseases is the resistance of eukaryotic cells for active therapeutic and diagnostic agents. The plasma membrane of cells is a major barrier and protects them from uncontrolled uptake of molecules. To overcome this membrane barrier various methods have been developed in recent years. Requirements for delivery systems are in the first place an efficient uptake into the host cells, but also non-cytotoxicity and selectivity towards specific cell types. It is furthermore of interest to achieve an intracellular delivery to certain organelles, mainly the nucleus or mitochondria. In particular for *in vivo* delivery it is of great importance to overcome stability issues with respect to enzymatic degradation. Delivery strategies can be generally categorized into three groups: physical methods, viral-mediated, and nonviral-mediated transfer.

1.3.1.1 Physical methods

Physical techniques that increase cell permeability, such as electroporation or microinjection, use electric shock, mechanical pressure, hydrodynamic forces, ultrasound, magnetic fields, or laser power. Inefficient delivery and side effects like cytotoxicity and tissue damage due to the harsh experimental conditions limit their use to *in vitro* and prevent their utilization as efficient delivery systems for the treatment of several diseases *in vivo*.[63]

1.3.1.2 Viral-mediated vectors

Viral-mediated transduction is a commonly used technique in gene therapy for a variety of diseases, such as cancer, cardiovascular diseases, neurodegenerative disorders, and also infectious diseases.[64] The viral vectors are derived from naturally evolved viruses, which are able to transfer their genetic material into host cells. To achieve the expression of a desired exogenous gene in a target cell, the virus is genetically modified to lack the disease-causing sequences before the gene of interest is inserted. Viruses for transduction are in most cases replication-deficient and belong to one of the following five families of viruses: retroviruses, adenoviruses, adeno-associated viruses (AAV), herpes simplex viruses (HSV), or lentiviruses. The choice of the virus type depends strongly on the application and the host cell type.[63-64] Viral vectors are restricted to

transport DNA and cannot be used for peptides, proteins or small molecules. Despite the advantage of high delivery efficiency to a variety of cells, major drawbacks are associated with their safety and their limited ability to transfer different materials. Health problems can arise in particular in the context of immunogenicity. Adenovirus vectors are the most immunogenic of all viral vectors, since they induce multiple types of immune responses in living organisms.[64] Apart from immunogenicity issues, there is also the risk of insertion of viral DNA into the host DNA. The potential danger of viruses as vectors was demonstrated in 2002, when two children who received gene therapy against severe combined immunodeficiency disease (SCID) developed cancer. It has been shown that the retroviral vector that was chosen for therapy, had integrated itself into the DNA of the patients in or near a gene called LMO2, which can cause childhood leukaemia.[65] Since also several other studies revealed that retroviruses can potentially cause severe health problems, the use of viral vectors in gene therapy had to be reconsidered, which marked an enormous setback for the field. [66] [67] Thus, intensive research has been focused on the development of nonviral alternatives that do not integrate into the host DNA.

1.3.1.3 Nonviral-mediated vectors

The currently most effective nonviral vectors are liposomes. They were discovered in 1965 as a model for cellular membranes and were soon afterwards successfully applied to deliver different molecules into cells.[63, 68] Liposomes consist of lipid bilayers with a cationic surface at physiological pH. They adopt size-dependent vesicular structures, which are able to surround an aqueous compartment (and thus soluble cargo molecules) and separate it from its environment by a membrane. The cationic lipids themselves are amphiphilic molecules that are composed of a hydrophobic moiety (e. g. cholesterol, aliphatic chains) which is covalently linked to a cationic headgroup. These molecules self-assemble by electrostatic interactions with the negatively charged backbone of their cargo DNA and form stable DNA-liposome complexes (called lipoplexes). These lipoplexes are able to enter the cells by endocytosis and protect the DNA inside from nuclease-mediated degradation.[69] [70] They can be covalently equipped with receptor-specific ligands for targeted delivery. Advantages of liposomes as delivery systems are their ability to deliver different types of cargo, as well as their potency to protect their cargo, their ability to also transport large size DNA, their non-immunogenicity, since liposomes are in most cases well tolerated by the organism, their easy preparation, and low production cost. Unresolved issues and major drawbacks for

the use of liposomes in gene delivery are their poor cell specificity, as well as the poor endosomal release of the DNA into the cytosol, and their low efficacy *in vivo.* In a systemic context the instability of the injected lipoplex in biological fluids, containing serum proteins and physiological salt concentrations, displays a major limiting factor.[70] A range of differently formulated charged lipids are commercially available, like for example Lipofectamine[71] and a variety of different liposome-based vectors are currently under development and in clinical trials for cancer gene therapy.[72] Another non-viral approach for efficient intracellular cargo delivery is transfection *via* cationic polymers. The most widely studied cationic polymers are branched poly(L-lysine) (PLL)[73] and poly(ethylenimine) (PEI).[74] Since they are chemically assembled, modifications and ligand attachment can be easily accomplished. The advantage of PEI is its flexible buffer capacity, enabling them to act as a proton sponge within the endosomes (pH 5.5.-6.5). This effect leads to an osmotic swelling and eventual burst of the endosomes, mediating the escape of the cargo molecules into the cytosol. Since the efficacy of these systems and their toxicity depends on many factors, more studies are needed to develop optimized PEI systems.[74b, 75] A very useful property of PLL for *in vivo* applications is its biodegradability. However, it is bound to proteins within the blood plasma and rapidly eliminated through circulation. [73] Another disadvantage is the requirement of additives, e. g. chloroquine, to reduce degradation within the lysosomes and to provide a successful delivery. [76] PLL can be easily modified with histidine residues to reach a comparable proton sponge effect as PEI. Furthermore, a popular modification is PEGylation, which enhances the circulation half-life as well as the uptake efficacy. The attachment of targeting ligands to address cell selectivity can be as well implemented.[69]

New nano-materials with unique characteristics, such as quantum dots (QDs),[77] gold nanoparticles (Au NPs),[78] Iron oxide (IONPs),[79] Silica,[80] porous silicon,[81] or carbon nanotubes (CNT)[82] have attracted attention as innovative carriers for siRNA.[83] However, in many cases those carriers are highly efficient *in vitro*, but less potent *in vivo*, demonstrating the limitations of nanoparticle-based delivery. Nevertheless this technique holds a lot of promises. As the range of different nanoparticle types and applications increases rapidly, issues concerning their safety need to be thoroughly investigated to evaluate their usefulness for delivery. Nanoparticles may provoke immune responses and safety questions concerning biodistribution, accumulation, retention, and clearance. Also their toxicity profile is not sufficiently investigated yet. It is therefore of great importance for future applications to carry out further *in vivo*

studies of nanoparticles as delivery vehicles to better understand the toxicity effects associated with their exposure.[84]

Naturally derived or synthetic peptides as nonviral vectors provide another promising entity for the development of improved drug delivery systems and will be discussed in the following chapter.

1.3.2 The concept and definition of Cell-Penetrating Peptides (CPPs)

Until now, much progress has been made in the development of viral and nonviral mediated delivery systems, but only few of them have been successfully applied *in vivo* and in clinical trials due to the limitations in terms of safety, stability, efficacy, and others. Thus, there is still a demand for innovative molecular carriers. Cell-penetrating peptides (CPPs) belong to the most promising strategies for the delivery of biologically active molecules into cells. General requirements for such CPPs are a) a sufficient delivery efficiency; b) a rapid and sufficient endosomal escape in case of a endocytotic pathway of entry; c) selectivity towards certain cell types; d) the ability to reach their intracellular target; e) lack of toxicity and f) reasonable production costs.[85]

CPPs are in general peptides that are able to translocate through cell membranes and can be therefore exploited as efficient molecular transporters to deliver different biologically active, but membrane-impermeable compounds into cells, both *in vitro* and *in vivo*. They all bear cationic, and in many cases, hydrophobic residues that lead to a certain amphiphilicity of the secondary structure. CPPs have also been described as protein transduction domains (PTDs), Trojan peptides, model amphiphatic peptides (MAPs), or membrane translocating sequences (MTSs).[86] Their exact definition is difficult, due to uncertainties about their uptake mechanism. However, there is a general agreement on the definition by Ü. Langel, found in the Handbook of Cell-Penetrating Peptides:[87]

„A cell-penetrating peptide is a relatively short peptide, 5-40 amino acids, with the ability to gain access to the cell interior by means of different mechanisms, including endocytosis, and the capacity to promote the intracellular delivery of covalently or noncovalently conjugated bioactive cargoes.“

Research on cell-penetrating peptides increased continuously during the last 20 years and numerous types of CPPs have been developed. CPPs were successfully used to

deliver a variety of different biomolecules, including plasmid DNA, oligonucleotides, short interfering RNA (siRNA), peptide nucleic acids (PNA), proteins and peptides, and also small molecules into cells.[88] In the following chapters the achievements in the field, since the discovery of the first CPP 20 years ago will be highlighted, but also limitations and hurdles will be discussed. A brief overview of the history and different types of CPPs and their uptake mechanisms will be given. Examples of applications, where peptide chemistry was exploited to create novel and powerful tools for drug delivery will be illustrated.

1.3.3 Classes of CPPs

The family of CPPs is differentiated into different classes and subgroups based on their origin. Generally the three main groups are protein-derived CPPs, chimeric, and designed CPPs,[88] which will be introduced in the following sections (Table 4). CPPs can also be distinguished from a structural point of view as either being polycationic or amphiphatic, and with respect to their secondary structure.

Table 4: Overview of representative CPPs containing natural amino acids (R = Arg and K = Lys are marked in bold), [Ref.: Tat peptide,[89] penetratin,[90] pVEC,[91] VP-22[92], SynB1,[93] Pep-1,[94] transportan,[95] CADY,[96] MAP,[97] oligoarginines,[98] Bac7,[99] (PRR)$_n$ motif,[100] SAP[101]].

Cell penetrating peptide type	Sequence	Origin
Peptides derived from proteins		
Tat (48-60)	**GRKKRR**Q**RRR**PPQ	HIV Tat protein
Penetratin / pAntp	**R**QI**K**IWFQN**RR**M**K**W**KK**	Antp homeodomain
pVEC	LLIIL**RRR**I**RK**QAHAHS**K**	Murine VE-cadherin
VP-22	DAATAT**R**G**R**SAAS**R**PTER**R**A**R**SAS**R**P**RR**PVD	HSV-1 structural protein
SynB1	**R**GG**R**LSYS**RRR**FSTSTG**R**	Protegrin-1
Chimeric Peptides		
Pep-1	**K**ETWWETWWTEWSQP**KKKRK**V	Trp-rich motif-SV40 NLS
Transportan	GWTLNSAGYLL**K**INL**K**ALAALA**KK**IL	Galanin and mastoparan
Designed/synthethic peptides		
CADY	GLW**R**ALW**R**LL**R**SLW**R**LLW**R**A	Trp-and Arg rich motif
MAP	**K**ALA**K**ALA**K**ALA	
Oligoarginines	(**R**)$_n$	
Pro-rich peptides		
Bac7(1-24)	**RR**I**R**P**R**PP**R**L**R**P**R**P**R**PLPFP**R**PG	Bactenecin-7
(PRR)$_n$ motif	(**PRR**)$_n$, n = 3-6	Pro-rich and Arg-rich miniature proteins
SAP	V**R**LPPPV**R**LPPPV**R**LPPP	γ-zein

17

A third possibility to categorize CPPs refers to their delivery characteristics and differentiates peptides that require a covalent linkage to their cargo molecule and those who are able to form stable, non-covalent complexes for delivery.[85]

1.3.3.1 Protein-derived CPPs

The largest and perhaps most intensively studied group of CPPs are the protein-derived peptides, which were identified by the interesting observation that some proteins, mainly transcription factors, could move from one cell to another.[85] The discovery that a specific part of these proteins is responsible for it, forms the basis for the term PTD (protein transduction domain).[85, 102] A lot of attention was drawn in this regard to the Tat peptide, which was first discovered in 1988 independently by two research groups - the groups of Green & Löwenstein and Frankel & Pabo.[103] [104] The peptide is derived from the Tat (trans-acting activator of transcription) protein, which is able to enter cells and translocate into the nucleus. Tat is involved in the replication of HIV-1 (human immunodeficiency virus type 1), where its primary function is to enable the transcription of the viral DNA into mRNA.[105] For the Tat protein it has been demonstrated later by the research group of Lebleu that only a short peptide sequence (48-60) is sufficient for the translocation into the cell (Table 4).[106] The well-established Tat(48-60) peptide is used in the present work as a reference peptide (Fig. 10).
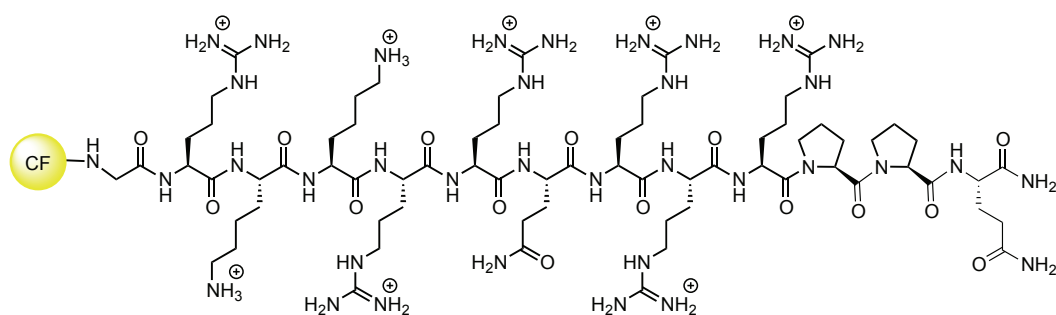
Figure 10: Structure of 5(6)-carboxyfluorescein-labeled Tat(48-60), (counterions are $CF_3CO_2^-$).

Another important example of a protein derived CPP is pAntp (or termed penetratin). It was discovered in 1991, when Prochiantz and co-workers reported the cellular uptake of the homeodomain of the Antennapedia protein of *Drosophila* into neuronal cells.[90d] Also in this case it was found that already a short peptide sequence (43-58) (for the exact sequence see Table 4), derived from the third helix of the homeodomain, is sufficient for translocation.[90c] Furthermore, a sequence from the herpes simplex virus

type 1 (HSV-1) protein VP-22 was identified as a PTD.[92] A disadvantage of members of this family is their susceptibility towards proteolytic degradation.

1.3.3.2 Chimeric peptides

Chimeric CPPs differ from protein-derived and designed ones, since the parental sequences of chimeric peptides are naturally occurring, but modifications of the sequences have been introduced. Peptides derived from signaling sequences of proteins are known to be effective in cell penetration. These sequences are recognized by specific receptors and assist in directing protein precursors to their target organelle within the cell after translation. Peptides of this type have been shown to enter different cell lines and accumulate in the nucleus, when they are connected to so-called nuclear localization sequences (NLS). Representatives of this category are peptides derived from Kaposi´s sarcoma fibroblast growth factor 1 (K-FGF),[107] the fusion sequence of HIV-1 gp41[108] or the variable light chain of immunoglobin Ig(v),[109] coupled to the NLS from the nuclear transcription factor kB (NF-kB)[110] or Simian virus 40 (SV40) T-antigen.[88, 111] Other examples are Pep-1, derived from HIV-1 gp41 and the SV40 T-antigen[94] and transportan (Table 4) that is derived from galparan,[112] a fusion between the neuropeptide galanin-1-13 and the wasp venom peptide mastoparan. It was introduced by the group of Langel,[95] and ever since various analogs were developed whereas transportan-10 (TP10) is the most effective one of them. Oehlke *et al.* discovered already in 1998 the so-called model amphiphatic peptide (MAP). It can be classified as a member of the chimeric CPPs,[85, 113] but also of the designed CPPs,[88] since its discovery was made by stepwise alterations of structure forming propensities and charge with an underlying design, but no concrete protein of origin is available. MAP showed a successful membrane translocation for different cells *in vitro*.[97b] Another example of a type of CPPs, which can be categorized as chimeric peptides, but are not derived from one specific protein, are the already mentioned oligoarginines (Table 4).[85, 98a, 113-114] They can be also classified as designed peptides, since their development was based on the general finding that the high content of basic amino acids of the early discovered CPPs, Tat and penetratin, suggested to be crucial for their internalization, since substitution (replacement by alanine) resulted in a decreased uptake efficiency.[98b, 106] These findings resulted in the development of homopolymers of arginine, containing more than six residues. They were studied and successfully applied for imaging and drug delivery by the groups of Tsien, Wender, and Futaki.[98, 114-115] It was further reported that polymers of arginine translocate across cell membranes significantly more effectively than peptides consisting of lysine, ornithine or histidine.[114]

1.3.3.3 Designed peptides & foldamers

The class of designed cell-penetrating peptides and foldamers holds a broad variety of different members. They are generally ammonium- and/or guanidinium-rich transporters composed of chemically modified amino acids or other building blocks. Compounds with modified non-peptidic backbones are as well members of this class. Several examples will be presented in this section to give an idea of the various possibilities for synthetically modified peptides and foldamers with cell-penetrating properties.

A quite recently developed peptide to improve siRNA delivery is the so-called CADY peptide, a secondary amphiphatic peptide of 20 residues, combining aromatic tryptophan and cationic arginine residues. It was designed by Divita and co-workers in 2008.[116] Also cyclic variants of the Tat peptide have been developed by Parang and co-worker in 2011 to overcome stability problems of the original Tat peptide.[116] Another possibility to generate protease stable CPPs is the use of D-amino acids, shown for example by the groups of Wender, Mitchell, and Brock for polyarginines and for the Tat peptide.[98b, 114, 117] The β-peptide analogs of polylysine and –arginine (Fig. 11), introduced and intensively studied by Seebach *et al.*, are also stable against degradation.[118] Raines and Gellman investigated the corresponding β-analog of the Tat peptide.[119] Reverse amino acid sequences, as well as retro-inverse analogs of penetratin[90b, 120] and the Tat peptide[98b] have also been tested for their cell-penetrating properties and showed comparable uptake for each system. Other design motifs, which showed cell-penetrating properties are dendrimeric and branched structures.[121]
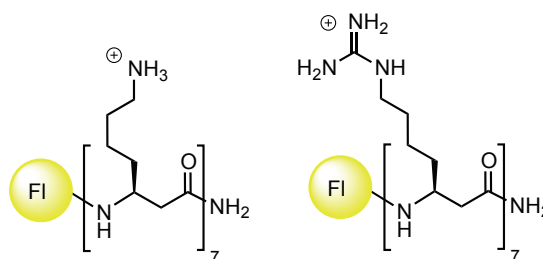
Figure 11: Structures of fluorescein-labeled β^3-oligolysine and -arginine; Fl = fluorescein, counterions not specified. [118] [122]

Also non-peptidic guanidinium-rich foldamers and peptoids have been developed, like for example carbohydrate-based compounds, where the amino groups of natural

aminoglycosides were replaced by guanidinium groups. They were developed by Luedtke *et al.* and originally designed as novel RNA ligands.[123] Other interesting examples are octaguanidinium transporters, based on an inositol dimer scaffold developed by Chung and co-workers[124] and tetraguanidinium compounds, where bicyclic guanidinium subunits were linked *via* thioether spacers by the research group of Giralt (Fig. 12).[125]
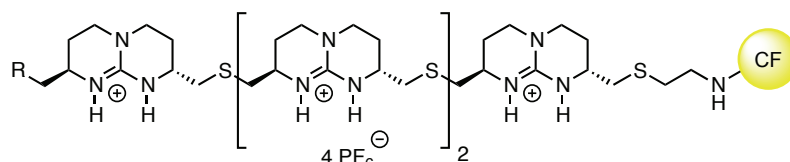
Figure 12: Structure of 5(6)-carboxyfluorescein-labeled tetraguanidinium vectors (with R = OH or SiPH$_2$^{t}Bu).[125] [122]

The group of Ly reported guanidine peptide nucleic acids (GPNAs), based on the insertion of arginines into the peptide nucleic acid (PNA) backbone (Fig. 13, left)[126] and deoxyuridine analogs containing guanidinium groups at the C5 position have been introduced by Ohmichi *et al.*[127] Also other guanidinylated DNA analogs have been reported,[128] as well as several phosphate-modified deoxynucleic guanidines (Fig. 13, right). [129] Oligocarbamate based molecular transporters were developed by Wender *et al.* with improved properties compared to D-Arg$_9$ and Tat (49-57).[130]
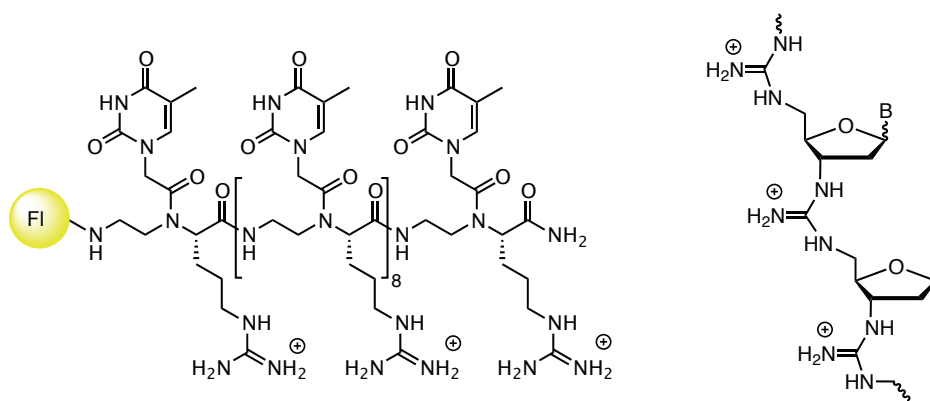
Figure 13: Structures of 5(6)-carboxyfluorescein-labeled guanidine peptide nucleic acids (left)[126] and phosphate-modified deoxynucleic guanidines (right), counterions not specified.[122, 129]

1.3.3.3.1   Pro-rich CPPs

In the context of this work cell-penetrating peptides based on oligoprolines are of particular interest. The ability of Pro-rich peptides to adopt the well-defined PPII conformation in aqueous environment (chapter 1.2.1) and its functionalizability rendered this kind of peptides very attractive for modifications and allows for a precise arrangement of cationic and hydrophobic moieties along the helix. Various different members have been reported heretofore that differ in their sequence, structure, and biological properties (Scheme 2). Sadler *et al.* reported in 2002 that certain natural proline-rich sequences, such as the antimicrobial peptide bactenecin-7 (Bac7), show cellular uptake. Bac7 bears a number of cationic amino acids, but has also a high proline content and was able to deliver a non-covalently linked protein into cells. [99]

a) proline-derived γ-peptides

imidazolidine-2-carboxylic acid

cis-γ-amino-L-proline

hydroxy proline

b) amphiphatic oligoproline helices containing modified side chains

L-proline

c) **(PPR)n, (PRR)n** miniature proteins

d) **(PX)n,** proline-rich peptides derived from the antimicrobial peptide bactenicin 7

e) **(VXLPPP)n = SAP** amphiphatic proline-rich peptides

f) proline-based dendrimers

Scheme 2: Families of proline-rich CPPs (adapted from [131]), [Ref.: a) proline-derived-γ-peptides;[132] b) amphiphatic oligoproline helices containing modified side chains;[133] c) (PPR)n and (PRR)n motifs;[100] d) bactenecin 7 derived peptides (PX)n;[99] e) amphiphatic proline-rich peptides, SAP;[101a, 101b, 131] f) proline-based dendrimers[134]].

According to this observation, also miniature proteins, consisting of repeating units of proline and arginine such as (PPR)n or (PRR)n were studied by the group of Schepartz and were shown to penetrate into mammalian cells.[100, 135] The Giralt group discovered the so-called sweet arrow peptide (SAP), derived from the N-terminal domain of γ-zein,

a maize storage protein.[101a, 101b, 131, 136] Furthermore, the exchange of a methylene group in the proline pyrrolidine ring for a dimethylsilyl group leading to a silaproline increased the hydrophobicity and also the cellular uptake of these peptides.[137] Surprisingly, also an anionic CPP was presented quite recently by Giralt and co-workers, called SAP(E).[101c] Several variations of Pro-rich CPPs and peptidomimetics with different connectivity of the backbone, consisting of proline and/or proline derivatives, have been reported. Amongst them are, for example, *cis-γ*-amino proline derived peptides (Scheme 2 and Fig. 14)[132a, 132c] and polyproline dendrimers (Scheme 2)[132b] developed by Giralt and co-workers.
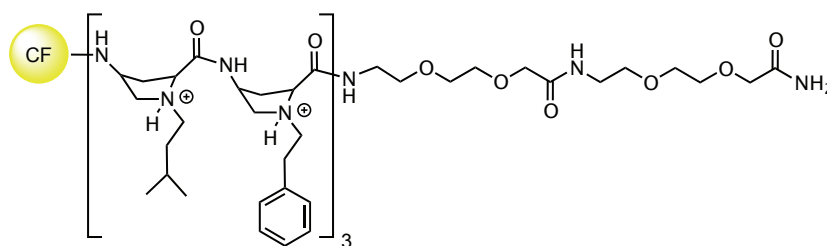
Figure 14: Structure of a 5(6)-carboxyfluorescein-labeled *cis-γ*-amino proline derived peptide, counterion not specified.[132a, 132c]

A collagen derived CPP was introduced by Ganesh *et al.*[138] Cell-penetrating peptides bearing hydrophilic proline-based lysine or arginine mimetics and hydrophobic proline-based leucine or tryptophan mimetics were investigated by Chmielewski and co-workers for mitochondrial targeting (Fig. 15). [133, 139] They exhibited uptake in MCF-7 breast cancer cells, in which the guanidinium functionalized peptides showed a generally higher uptake compared to their ammonium containing counterparts. The cell penetration efficiency increased with increasing number of cationic groups, consistent with the reported behavior of peptoids and oligoarginines tested on Jurkat cells and miniature proteins.[98b, 100]
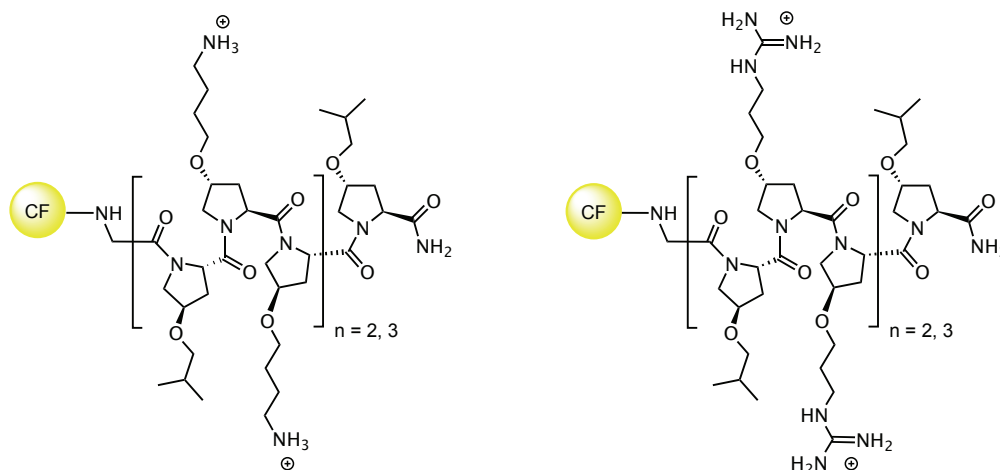
Figure 15: Structures of 5(6)-carboxyfluorescein-labeled amphiphatic polyproline oligomers with ammonium and guanidinium groups as cationic moieties and isobutyl groups as hydrophobic moieties; counterions not specified. [133] [139a]

1.3.4   Mechanisms of internalization

Research is still ongoing to analyze how CPPs can pass the cell membrane. This question represents a major challenge, since CPPs are a very divergent family of vectors[88] and it became clear that some CPPs may use more than just a single mechanism of internalization.[140] It has been established that cellular uptake pathways are depending on several parameters, such as a) the nature and secondary structure of the CPP; b) its ability to interact with the cell surface and membrane lipid components; c) the nature, type and active concentration of the cargo and its attachment to the CPP, and d) the cell type and membrane composition.[85] Classical uptake mechanisms like, for example, receptor-mediated internalization or uptake *via* an active transporter seem not to be involved, since D-analogs of CPPs show similar uptake efficiencies as the natural L-amino acid sequences.[98b] It is generally proposed that CPPs are able to enter cells by two distinct pathways: *via* an energy-dependent vesicular mechanisms, generally referred to as endocytosis (see 1.3.4.3), or *via* direct translocation through the cell membrane (see 1.3.4.2).[86]

1.3.4.1 Interactions with the extracellular matrix

It has been proposed that the translocation of CPPs starts by their adsorption on the cell surface. This occurs by an electrostatic interaction between the cationic guanidinium and/or ammonium moieties of the CPPs and the anionic counterparts on the cell surface,

such as heparan sulfate proteoglycans (HSPGs)[141] and phospholipids.[90b, 142] HSPGs are sulfated polysaccharides, anchored to cell surface polypeptides. They are present at the surface of most eukaryotic cells. *In vitro* experiments with enzymatic removal of extracellular HSPGs, competition with exogenous HSPG chains, and HSPG-deficient mutants indicated that they are involved in the uptake mechanism.[141a, 141b, 143]

Besides the electrostatic interaction as an initial contact, it is also likely that hydrogen bond formation is involved, due to the ability of the guanidinium group to form hydrogen bonds with sulfate, carboxylate, or phosphate groups of the cell surface HSPGs (Fig. 16). HSPGs themselves enter the cell by endocytosis and are subsequently degraded within lysosomes as a turnover route. It was therefore speculated that the internalization of CPPs is related to cell membrane recycling, which occurs frequently.[144] It has been reported that liposome-based delivery agents, like Lipofectamine, also require proteoglycans on the cell surface for efficient delivery.[145]
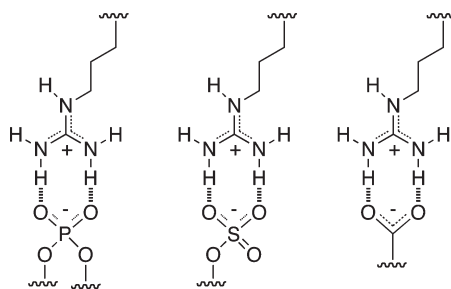
Figure 16: Hydrogen bond formation between guanidinium moieties and membrane-associated phosphate, sulfate, and carboxylate groups.[146]

1.3.4.2 Passive translocation

The energy-independent process of passive translocation was proposed for CPPs that are compatible with the lipid bilayer or sufficiently perturb the structural integrity of the membrane, similar to antimicrobial peptides.[147] Changes in the membrane potential and membrane structure perturbation, in the context of CPP exposure, have been intensively studied and several conceivable models for the uptake have been described, like the carpet model or the barrel-stave model (Scheme 3).[86] In the carpet model CPPs accumulate on the cell membrane until the membrane integrity is weakened and pores are formed. In the barrel-stave model a limited number of CPPs first assembles on the membrane and then inserts into the lipid bilayer.[148] Additional studies concentrating

on the role of the extracellular counterions of CPPs support these direct uptake mechanisms.[149]
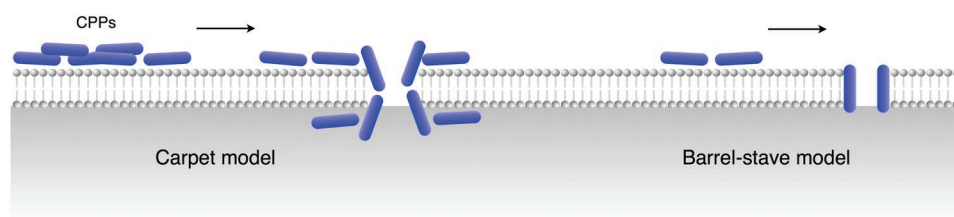
Scheme 3: Model of direct translocation mechanisms for CPPs (adapted from ref. [86] [148]).

Another model for direct translocation is proposed for penetratin. [90b, 150] Anionic moieties on the surface of the plasma membrane, as discussed before, have been suggested to form a complex with the peptide leading to the formation of inverted micelles (not shown).

In earlier reports the hypothesis of passive translocation was favored over endocytosis,[90c, 106, 151] but became less popular, when the uptake mechanisms of Tat and polyarginines had to be revised, due to cell fixation artifacts during the preparation of the cells for microscopy. It could be clearly demonstrated that chemical fixation of the cells influences the localization of the CPPs within the cell and consequently further studies have been performed with living non-fixed cells.[88] Additionally, quantification experiments *via* flow cytometry were affected by artifacts generated during the preparation of the cells, as this method does not discriminate between membrane-adsorbed and internalized CPPs. Therefore, a trypsin treatment of the cells was suggested to remove surface-bound peptides, in order to avoid overestimation of the uptake.[89c] Ever since, the mechanisms of many CPPs were re-evaluated and it was reported for the majority of the peptides that endocytosis is one of the pathways of cellular uptake.[152] For example re-evaluations of the uptake mechanisms of Tat(48-60) and polyarginine strongly supported the involvement of endocytosis as a major route for internalization, but the possibility that a small fraction of the peptides translocates the cells by an endocytosis-independent pathway could not be excluded.[89c] The observation that polyarginins and Tat(44-57) are not able to cross lipid bilayers or liposomal membranes may speak against passive diffusion.[141d, 144a, 152b, 153] However, there are also studies reporting the passive translocation of polyarginins through the cell membrane in the direction of the membrane potential.[154]

1.3.4.3 Endocytosis

In contrast to passive diffusion, endocytosis is a regulated process of the cell to internalize extracellular nutrients.[155] It also serves for other important cellular functions, such as the regulation of the expression of receptors on the cell surface or antigen representation. [155] Endocytosis is also utilized by viruses, toxins, and symbiotic microorganisms to enter cells.[155] Generally there are two main types of endocytosis: phagocytosis and pinocytosis. Phagocytosis occurs only in macrophages, monocytes and neutrophils to engulf and eliminate large particles, such as pathogens and infected or apoptotic cells. Pinocytosis, takes place in all cell types and is responsible for taking up fluids, solutes, and membrane components. Pinocytotic pathways can be further subdivided into four groups: macropinocytosis, clathrin-mediated endocytosis, caveolae/lipid raft-mediated, and clathrin- and caveolin-independent endocytosis (Scheme 4).[156] [86]
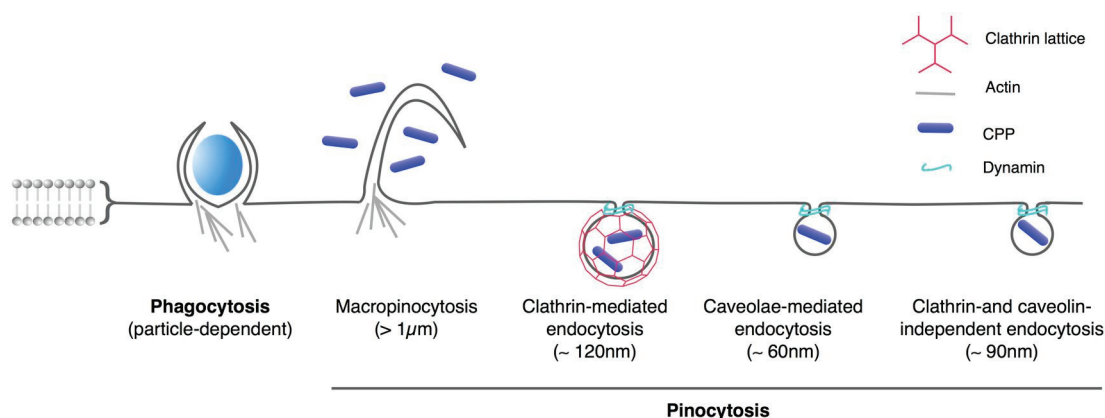
Scheme 4: Models for the mechanisms of the cellular uptake of CPPs (adapted from ref. [156] [86])

While the four pathways differ in their mechanistic details and machineries, they all have in common to encapsulate extracellular molecules into lipid vesicles, which are then internalized. After the internalization they can be either trafficked back to the plasma membrane for exocytosis or fused with lysosomes for degradation and further processing. This step marks a crucial point for cargo delivery *via* CPPs, since it might prevent the cargo from reaching the desired intracellular target. It is therefore important for CPP-cargo constructs to escape from the vesicles, before getting externalized or digested by the cell.[86] The endocytotic mechanism that a particular CPP will take, strongly depends on its cargo. For example it has been reported that Tat is using a lipid raft-mediated endocytosis when conjugated to a protein,[152c] but a clathrin-dependent pathway when a fluorophore is attached.[89b] Also the subtype

macropinocytosis has been reported to be a mechanism for the uptake of many CPP-cargo conjugates.[98a, 143a, 157]

1.3.4.4 Self-assembly of CPPs

Another interesting aspect, which is considered to be involved in the cellular uptake of CPPs, is their self-assembly.[131] This mode of action was proposed for certain amphiphilic CPPs that have a high tendency to aggregate in water or hydrophilic solvents. It suggests that they can enter cells as monomers and/or aggregates, but it is still unknown how the self-assembly is related to the cellular internalization pathways (Scheme 5).[131] For example concentration dependent CD analysis of the Sweet Arrow Peptide (SAP) showed an aggregation tendency and additionally fibrils were observed by atomic force microscopy (AFM) and transmission electron microscopy (TEM).[101a, 101b, 144a] Studies of Pep-1 or MAPs also revealed the formation of aggregates in aqueous solution.[158]
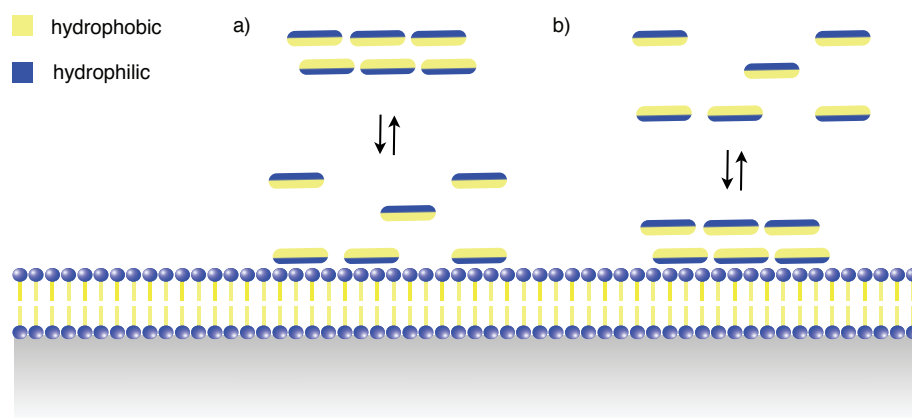
Scheme 5: Proposed model for the cellular uptake of certain amphiphilic CPPs a) *via* monomers and b) *via* aggregates (adapted from ref. [144a]).

Cellular uptake mechanisms still need to be confirmed for a variety of CPPs. The comparison of in particular mechanistic results has to be handled with care since the methods used for the studies often vary from lab to lab. For example, different peptide concentrations may trigger different endocytotic pathways, but also the cargo attached to the CPPs may alter their behavior.[86]

1.3.5 Applications and current state of research

In recent years a number of applications using CPPs *in vitro* and *in vivo* has been reported. CPPs as molecular transporters offer several advantages over other delivery systems, such as their low cytotoxicity and nonviral origin that decreases the risk of sidereactions.[159] An additional factor, representing one of the major advantages of CPPs in drug delivery, is that there is no limitation for the type of cargo. The size and nature of cargo molecules varies greatly and ranges from small molecules, oligonucleotides, plasmid DNA, peptides, proteins, nanoparticles to quantum dots and much more (Scheme 6) for a range of different applications.[160] Additionally CPPs constitute a valuable tool for the investigation of biological processes *in vitro* and *in vivo*. Since the delivery efficiency for different types of cargo molecules is strongly dependent on the specific CPP, which is used for delivery, there is still a need to develop novel systems with unique properties to broaden the spectrum of tracktable cargos and enhance their uptake into cells.
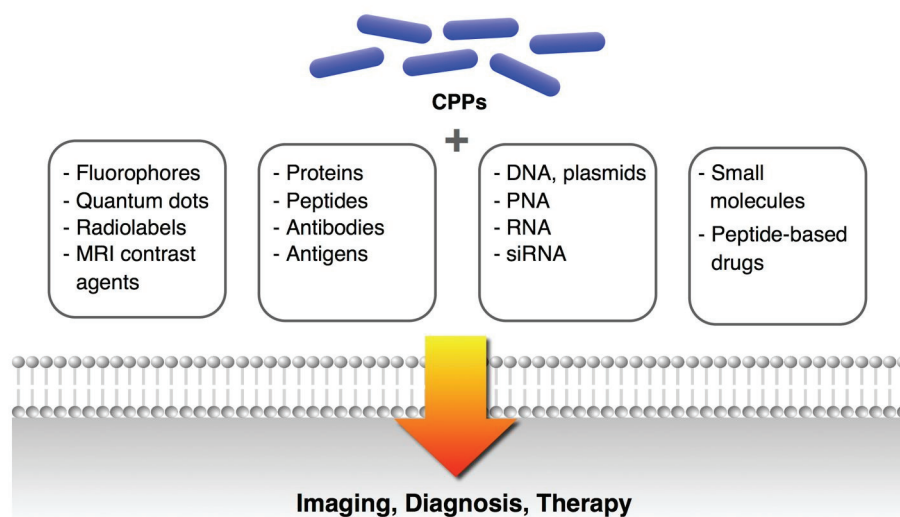
Scheme 6: Overview of cargo molecules and application types for CPPs (adapted from [86]).

1.3.5.1 Delivery strategies

Different delivery strategies for CPP-cargo constructs have been explored.[113, 161] They rely either on the covalent or non-covalent attachment of the cargo molecules to the CPPs (Scheme 7). A covalent linkage is employed, for example, frequently for peptidic cargo *via* a tandem peptide synthesis, but also for proteins that are fused to a specific CPP.[162] If the molecule of interest is a small molecule, the method of choice is usually

conjugation *via* a cleavable chemical linker. Many examples of linker systems are based on a disulfide bond that is cleaved off by intracellular glutathione (GSH) to release the cargo molecule within the cell.[163] But also pH-dependent[164] or photo-cleavable linker[165] systems were successfully applied. Non-covalent strategies rely on the complexation of the polycationic CPPs with negatively charged cargo molecules, such as oligonucleotides.[160]
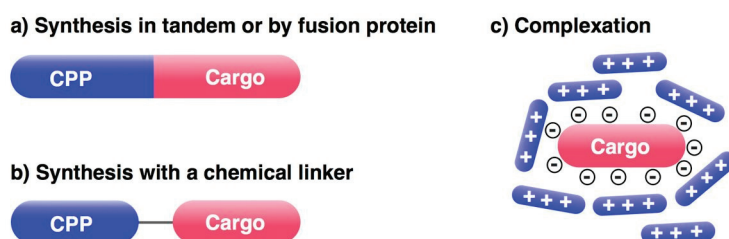
Scheme 7: Possible conjugation methods for CPPs with cargo molecules (adapted from [113]).

1.3.5.2 CPPs for imaging, diagnostics, and therapeutic applications

CPPs were applied for imaging and diagnostics to deliver fluorophores, nanoparticles, quantum dots, radiolabels, or MRI contrast agents.[166] For example Tat-conjugated CdS:Mn/ZnS quantum dots even crossed the blood brain barrier (BBB),[167] radiolabeled antibodies were targeted to intracellular sites[168] and viral infections could be visualized in real time.[169] Another promising study focused on the detection of apoptosis-associated caspase activity, with the aim to fluorescently monitor neuronal loss *in vivo*.[170] To improve the success rate for surgery a selective staining of tumorous tissue was achieved by delivering fluorophores with oligoarginines *in vivo*.[115]

The discovery of CPPs also opens up fascinating perspectives for therapeutic applications.[86, 113] For example, the efficacy of several small-molecule drugs has been improved by conjugation with CPPs. It was reported that covalent conjugation of the hydrophobic drugs Taxol or Paclitaxel to polyarginines improves the water solubility and cellular uptake. [171] [172] CPP conjugates with the anti-inflammatory molecule cyclosporine A showed increased potency for the treatment of skin diseases.[164] Additionally, CPPs were exploited to overcome cancer-resistance in cells. Doxorubicin was coupled to the peptides Tat or transferrin and caused cytotoxic effects in doxorubicin-resistant cell lines.[93b, 173] Also methotrexate was successfully delivered to chemotherapy resistant cells, when conjugated to CPPs.[174] Furthermore, CPPs are not

only able to deliver small hydrophobic molecules to cells, but also large hydrophilic cargos, such as biologically active peptides and proteins to interfere with diverse cellular mechanisms.[23b, 23c, 175] Penetratin, for instance, was employed to deliver fragments of protein-inhibiting cyclin-dependent kinase (Cdk), which is involved in the regulation of the cell cycle and inhibited human cancer cell growth.[176] Tat could also enhance the uptake of Cdk-inhibiting peptides and led to an arrest of cell proliferation.[177] Also the potency of several apoptosis inducing peptides could be enhanced by conjugation with CPPs as anti-cancer agents.[178] Whole proteins delivered by Tat *in vivo* are for example β-galactosidase, which also successfully crossed the BBB[179] and Bcl-xL, a death-suppressing molecule of the Bcl-2 family, which is supposed to play a crucial role in the prevention of neuronal apoptosis and ischemic brain injury.[180] Another application of CPPs is the delivery of intact antigens to improve vaccine efficacy.[181]

The delivery of anionic biomolecules, like oligonucleotides, into cells is very challenging, due to the low permeability of the plasma membrane to nucleic acids. Furthermore, often it results in endosomal entrapment or degradation by nucleases.[182] It has been reported that CPPs are able to complex and therefore protect plasmid DNA while delivering it into mammalian cells.[183] The study showed that complexes containing eight molecules of the Tat peptide per DNA strand efficiently entered different cell lines.[184] A major area of interest is currently the delivery of small interfering RNA (siRNA). RNA interference is not only a powerful biomedical tool, but is also valuable as a therapeutic strategy for the specific blocking of the translation of a gene into a functional protein following the antisense strategy. However, the strategy suffers from poor cellular uptake and biodistribution, since siRNA itself is not able to enter cells and needs to be delivered.[88] Tat and penetratin were conjugated *via* a disulfide bond to siRNA, successfully delivered into lung tissue and exhibited a silencing response.[185] But also non-covalent strategies have been applied, [108, 186] for example using Tat[187] and transportan.[188] The cell-penetrating peptide MPG has been used to deliver siRNA *in vivo* through intravenous administration and revealed efficient blocking of tumor growth in mice.[189]

1.3.5.3 Limitations of CPPs and possible solutions

Although CPPs often show a high efficiency *in vitro* their lack of specificity towards the cell type is a major drawback *in vivo*. This results in a distribution of the CPP-cargo constructs all over the body, independent from the way of administration.[190] In particular when CPPs are conjugated to cytotoxic molecules, such as anti-cancer drugs, side effects due to this non-specificity are a limiting factor.[88] Efforts were made in order to improve specificity for instance by adding a cell-targeting peptide (CTP) or a homing peptide to CPPs. [190-191] CTPs, like for example the RGD peptide,[192] interact with specific receptors that are overexpressed only by a certain cell type. Homing peptides have been identified for example for tumor blood and lymph vasculature by screening of phage display peptide libraries.[193] But also other strategies have been developed to target specific organs or cell types, exploiting the microenvironment, such as the peritumoral acidic pH,[194] or the metabolism of the target cells. The first targeting system used as activatable CPP is taking advantage of the metalloproteases of tumor cells.[115] In this system polyarginine is masked with a polyanionic counterpart, to avoid unspecific binding. Both parts were linked together *via* a matrix metalloprotease (MMP) cleavage site. The construct showed to be stable in the blood stream and was just cleaved around tumor cells, secreting MMP, to release the CPP-cargo moiety for selective cellular uptake.[115] Besides the generation of those chimeric molecules, it is also possible to create a CPP-loaded device with nanocapsules or liposomal structures, which allows for a local administration, for example in solid tumors or directly accessible organs, like the ocular cavity.[190] The second major challenge in the field of CPP-cargo delivery is their intracellular localization profile. In many cases CPP-cargo constructs suffer from endosomal entrapment, as briefly mentioned in in the previous chapter 1.3.4.3. In these cases the cargo molecule does not reach its target site and is digested or externalized by the cell. To improve endosomal escape, chemical agents, such as chloroquine,[195] calcium[196] or sucrose[197] are utilized, but they are restricted to *in vitro* experiments. Another approach is based on the attachment of polyhistidine to act as a proton sponge in acidic endosomes, which leads to an osmotic swelling and subsequent bursting of the vesicles.[198] Photo-induced endosomal escape has been also studied and led to promising results.[199] A further limitation for many naturally derived CPPs is their susceptibility towards proteolytic degradation, which is a disadvantage for *in vivo* applications. This drawback can be circumvented by using peptides composed of D-amino acids or other molecular transporters with modified backbones, such as foldamers. However, differences in the behavior towards the cells were observed for

peptides bearing D-amino acids in comparison to their L-analogs.[140a] In addition, the highly cationic character of certain CPPs, leading to interactions with the cellular membrane, can cause transmembrane pore formation and membrane leakage.[200] In general, CPPs with a pronounced amphiphilic character show a higher degree of cytotoxicity, caused by the formation of these pores.[201] A main reason that prevents intravenous delivery of certain amphiphatic CPPs is their potential to induce hemolysis, a leakage of the red blood cells.[202]

1.3.5.4 CPPs in preclinical and clinical trials

Considering future applications of CPP-cargo constructs for clinical use in humans, pharmacokinetic and biodistribution profiles will play a major role. An ideal CPP should have the potential to enhance the uptake, but also increase the systemic bioavailability of the cargo molecule in the blood plasma. Additionally it should be easy to manufacture on a large scale and be cost-effective.[113] Numerous pre-clinical and clinical trials of CPP delivery are currently under investigation. Already in 2004, over 200 pre-clinical studies in different therapeutic fields like neurology, cardiology, oncology, and much more were reported. [203] The first clinical trial was initiated by Cell Gate Inc. for topical delivery of cyclosporine A attached to oligoarginine and entered phase II in 2003, but was discontinued meanwhile.[204] Ever since, several companies are working on the clinical development on CPPs for a variety of diseases.[85] Further examples are given in Table 5.

Table 5: Clinical development status of a selection of CPP-conjugated compounds (from [88]).

Company	Compound	Target/Action	CPP	Indication	Status (2011)
Capstone Therapeutics	AZX100	HSP20	PTD4	Keloid scarring	Phase 2
KAI Pharmaceuticals	KAI-9803	Protein kinase Cδ inhibitor	TAT PTD	Myocardial infarction	Phase 2b
	Kai-1678	Protein kinase Cε inhibitor	TAT PTD	Pain	Phase 2a
	Kai-1455	Protein kinase Cε activator	TAT PTD	Cytoprotection/ ischemia	Phase 1
Xigen	XG-102	c-Jun-N-terminal kinases	TAT PTD	Hearing loss	Phase 2
				Stroke	Phase 1
Revance Therapeutics	RT001	Transdermal delivery of Botulinium toxin type A	TAT PTD	Wrinkles	Phase 2b
				Excessive sweating	Phase 1
Diatos SA	DTS-108	Nuclear delivery of cytotoxin	Anti-DNA anibody	Cancer	Preclinical
Cell Gate Inc.	PsorBan	Transdermal delivery of cyclosporin A	R8	Psoriasis	Phase 2 discontinued

2.   OBJECTIVES

The delivery of diagnostics, therapeutic molecules, and imaging agents into mammalian cells is challenging, since the passage of those molecules across the plasma membrane is highly restricted. This cellular barrier is often associated with a loss of pharmaceutical potency or the requirement for high doses, which increase the risk of undesired side effects. The low import presents a major limitation for the development of therapeutics against a growing variety of targets in different disease areas, such as oncology, neurobiology, and cardiology.[88, 160] In the past decade much effort has been made for the development of delivery systems, such as viral-mediated vectors[64] and liposomes,[69-70] but safety issues[65-67] and low efficacy *in vivo*[70] prevented those methods from becoming efficient means of delivery. CPPs constitute a very promising tool for non-invasive cargo delivery with a beneficial toxicity profile. They have been successfully used *in vitro* and *in vivo* to deliver a variety of different molecules.[88, 160] Despite the progress that has been made, there is still a need for the development of new CPPs, with superior physicochemical properties, enhanced uptake efficiency, intracellular targeting, and proteolytic stability.

The aim of this thesis was the design, synthesis, and biological evaluation of a novel type of CPPs based on an oligoproline scaffold. The well-defined and functionalizable polyproline type II (PPII) helix of Azp-containing oligoprolines was envisioned as the backbone. The Azp residues were anticipated to allow for functionalization of the oligoprolines with cationic moieties directly at the peptidic backbone, without a spacing unit. Thereby the charge density of the constructs would be increased in comparison to already existing systems, comprising oligoarginines or oligomers of proline-based arginine mimetics.[122] For the detection of the uptake and intracellular fate of the CPPs a fluorescent dye should be attached at the N-terminus of each peptide. With this novel type of CPPs, the question should be addressed how the geometrical arrangement of the functional groups along the helical backbone influences the cellular uptake of the peptides. We therefore envisioned to compare peptides with an alternating pattern of positively charged guanidino prolines (Gup) and unfunctionalized prolines (Pro) (Scheme 7a) with peptides, in which the Gup and Pro residues are directly connected to each other in a row (Scheme 7b). In this *en bloc* system, the effect of the cationic charges, located either at the N-terminus or the C-terminus of the peptides should be as well examined. Furthermore, we were interested to explore the influence of ammonium versus guanidinium functions on the cellular uptake, as well as different chain lengths of

the peptides. To analyze whether the absolute configuration at C(4) of the functionalized proline residues might influence the cellular uptake, peptides bearing (4*R*)- and (4*S*)Gup residues were planned to be evaluated.
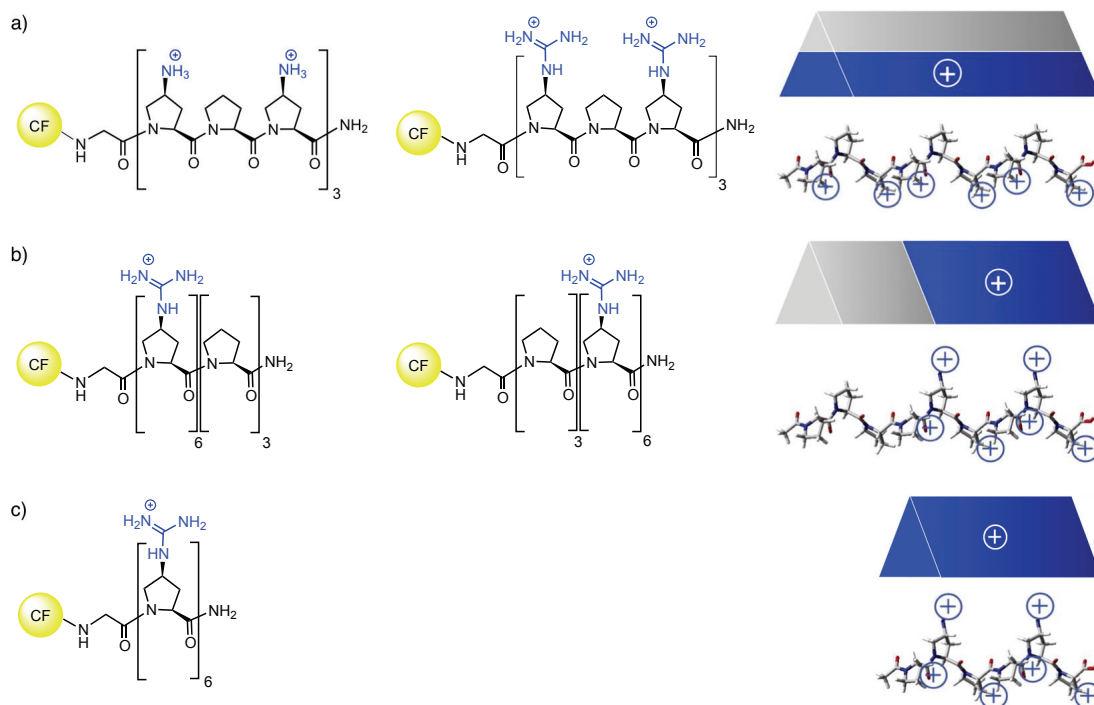
Scheme 7: Design and representative examples of different series of oligoproline-based CPPs with a) an alternating pattern and b) an *en bloc* arrangement of cationic moieties (blue) and unfunctionalized prolines (grey) along the helical axis; c) Oligoproline-based CPPs entirely composed of positively charged guanidino proline derivatives (blue); counterions are $CF_3CO_2^-$.

Since we were furthermore interested in the cellular uptake in the absence of additional unfunctionalized prolines, thus a series of peptides was created consisting entirely of Gup residues (Scheme 7c). In order to examine whether the cell-penetrating properties of our CPPs are associated with a specific receptor on the cellular membrane, which would suggest an effect of the chirality of the PPII helix, we envisaged the respective D-analogs of a selection of the L-oligoproline-based CPPs. The relative cellular uptake of the oligoproline-based CPPs should be compared with the uptake of reference peptides, such as oligoarginines, Tat(48-60) and penetratin. To investigate whether our CPPs show specificity towards different cell lines, the internalization in a selection of human tumor cell lines (HeLa, MCF-7, PC-3, and HT-29) should be tested. Furthermore, we were interested to study the effect of the described designs on the intracellular localization by confocal microscopy. Finally, the stability of the oligoproline-based CPPs towards proteases and their toxicity profile, in comparison to already established CPPs was as well in the focus of this thesis.

In addition, a second goal of this work was to investigate structure directing properties of electron-withdrawing groups (EWGs) derived from an azide at the C(4) position of proline. Towards this goal, methyl esters of both the (4*R*)- and (4*S*)-isomers of *N*-acetylated prolines should be used as model systems. Of special interest was the examination of the effect of *tert*-butyl carbamate (**8R**, **8S**) and ammonium (**9R**, **9S**, **10R**, **10S**) groups on the *cis/trans* conformer ratio around the tertiary prolyl amide bond and the pyrrolidine ring pucker (Fig. 17). To allow for a comparison to other previously examined proline derivatives, the azido proline models **7R** and **7S**, investigated by L.-S. Sonntag *et al.*,[22, 26a] were included as references in these studies. Furthermore, guanidinylated proline derivatives were in the focus of our interest, to explore the conformational properties of the cationic proline derivatives used for our oligoproline-based CPPs. Thus, proline derivatives bearing di-*tert*-butyl oxycarbonyl guanidino (**11R**, **11S**) and guanidinium (**12R**, **12S**, **13R**, **13S**) moieties were envisioned for analyses. *Ab initio* calculations, to examine the lowest energy structures of the proline derivatives, were planned in cooperation with S. Schweizer and C. Ochsenfeld. In addition, the effect of (4*R*)- and (4*S*)-configured ammonium groups on the PPII helix stability of oligoproline derivatives (**14S**, **14R**, Fig. 18) should be investigated and discussed in this thesis.
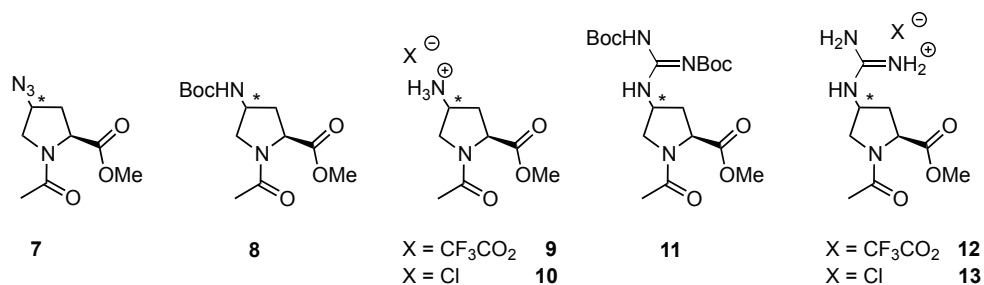
Figure 17: Monomer models bearing different electron withdrawing substituents at C(4) of proline, * = *R* or *S*.
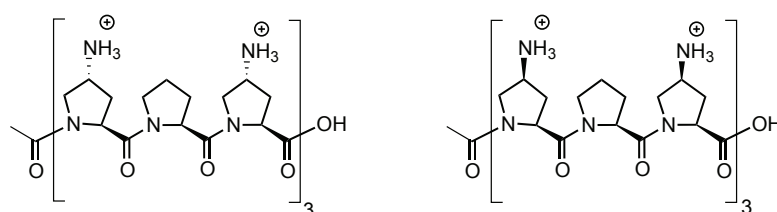
Figure 18: Oligoproline derivatives **14R** and **14S**, bearing (4*R*)- or (4*S*)-configured amino proline residues at every first and third position of the repeating unit; Counterions are $CF_3CO_2^-$.

3. RESULTS AND DISCUSSION

3.1 Identification and optimization of novel oligoproline-based CPPs

In this thesis a novel type of cationic oligoproline-based CPPs is presented, that was designed with the aim to enter eukaryotic cells and act as molecular transporter for cargo molecules. In the first section of this chapter (3.1.1) the focus is on the general design that provided the basis to create variations of different oligoproline-based CPPs. The subtypes of our CPPs, constructed to address different questions regarding their cell-penetrating properties, will be introduced. Secondly, the synthesis strategies for these peptides are discussed, as well as the syntheses of according Fmoc-protected building blocks for solid phase peptide synthesis (SPPS) (3.1.2). After the analysis of the secondary structure of the peptides *via* circular dichroism (CD) spectroscopy (3.1.3), the investigation of the cellular uptake will be presented and compared to established reference peptides (3.1.4). The efficiency of the cellular uptake was evaluated *via* flow cytometry and intracellular localization of the CPPs within the cells was analyzed by confocal microscopy. For further characterization of the CPPs, their stability towards trypsin and fresh human blood serum was analyzed (3.1.5). To address the question of potential cytotoxicity, MTT assays and hemolysis assays were performed (3.1.6). As a preliminary experiment to test the delivery potential of the oligoproline-based CPPs *in vitro*, the peptides were used to deliver siRNA into HeLa cells (human cervix carcinoma) and evaluated using a dual luciferase assay (3.1.7).

3.1.1 Design

The cationic character is a crucial requirement for cell-penetration and is considered to facilitate the cellular uptake through interactions with the negatively charged extracellular plasma membrane. In peptides composed of natural amino acids, the cationic charges at physiological pH are introduced through the basic residues lysine and arginine. In contrast to those CPPs, whose secondary structures are less defined, the Azp containing oligoprolines allow for a functionalization with cationic groups (ammonium or guanidinium) in a precise arrangement along the well-defined PPII helical scaffold (see Fig. 18 and 1.2.2). In contrast to naturally derived CPPs and other proline-based approaches (1.3.3), the direct attachment of the moieties on the peptidic backbone without a spacing unit, was considered to potentially enhance the cellular uptake and alter the intracellular localization. To detect the uptake and intracellular fate of the peptides 5(6)-carboxyfluorescein (abbreviated as 5(6)-CF or CF), a commonly used fluorophore for imaging, was attached to the N-terminus of the peptides *via* a glycine spacer.
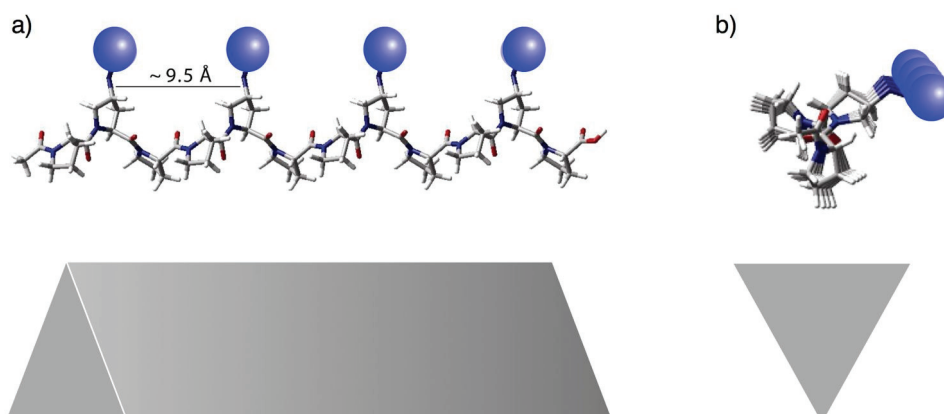
Figure 18: Example of a functionalization pattern of an oligoproline scaffold, bearing functional moieties at C(4) of proline at every third position: a) Side view; b) View along the helical axis.

First, we were interested to investigate whether the geometrical arrangement of the cationic residues along the helical backbone and therefore the local charge density of our oligoproline-based CPPs influences the cellular uptake, as it was observed for certain foldamers.[205] Thus, we created two sets of oligoproline-based CPPs with a different design: one with an alternating pattern of guanidinium moieties on an oligoproline scaffold and the other one consisting of a row of guanidino proline (Gup) and a row of unfunctionalized prolines (Pro) (Fig. 19). The alternating system with cationic moieties at every first and third position of the repeating unit and unfunctionalized proline residues at every second position is illustrated as a prism, with two positively charged edges (Fig. 19a, blue) and one edge displaying the rather hydrophobic part of the pyrollidine ring (grey). In contrast, the peptides of the *en bloc* system are illustrated as a prism with one polycationic part (Fig. 19b, blue) and another part of unfunctionalized proline residues (grey). To introduce a pronounced polycationic character in the alternating system we decided to start directly with two functionalized edges.
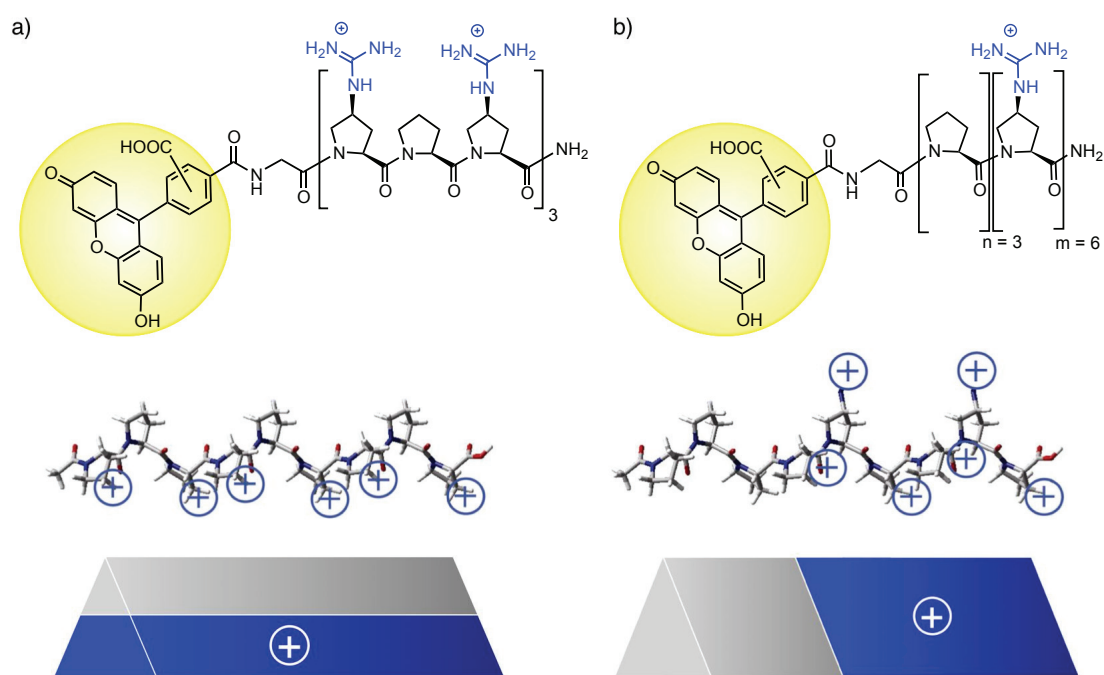
Figure 19: Oligoproline-based CPPs with different charge distributions along the helical axis: a) System with an alternating pattern and b) an *en bloc* arrangement of guanidino prolines (blue) and unfunctionalized prolines (grey); Counterions are $CF_3CO_2^-$.

Furthermore, we were interested to exploit the effect of ammonium versus guanidinium groups on the cellular uptake of our oligoproline-based CPPs, as well as the effect of different chain lengths of the peptides. We therefore envisioned a series of six peptides, bearing either (4*S*)-configured amino proline (4*S*)Amp or guanidine proline (4*S*)Gup (Fig. 20).
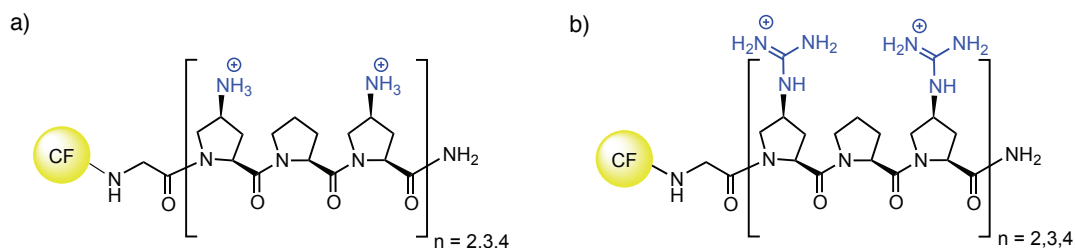
Figure 20: Molecular structure of CPPs with an alternating pattern of cationic moieties on an oligoproline scaffold, bearing (4*S*)Amp (a) or (4*S*)Gup (b) at every first and third position of the repeating unit and unfunctionalized proline residues at every second position; Counterions are $CF_3CO_2^-$.

Additionally, we aimed to explore whether the absolute configuration at C(4) of proline might influence the cellular uptake. Peptides with an alternating and an *en bloc* arrangement bearing either (4*R*)- or (4*S*)Gup were designed as illustrated (Fig. 21). In the case of the *en bloc* system, it was additionally examined whether the position of the blocs of cationic moieties either at the N- or C-terminus of the peptides and the close proximity of the cationic charges to the attached fluorophore affects their cell-penetrating properties (Fig. 21c-f).
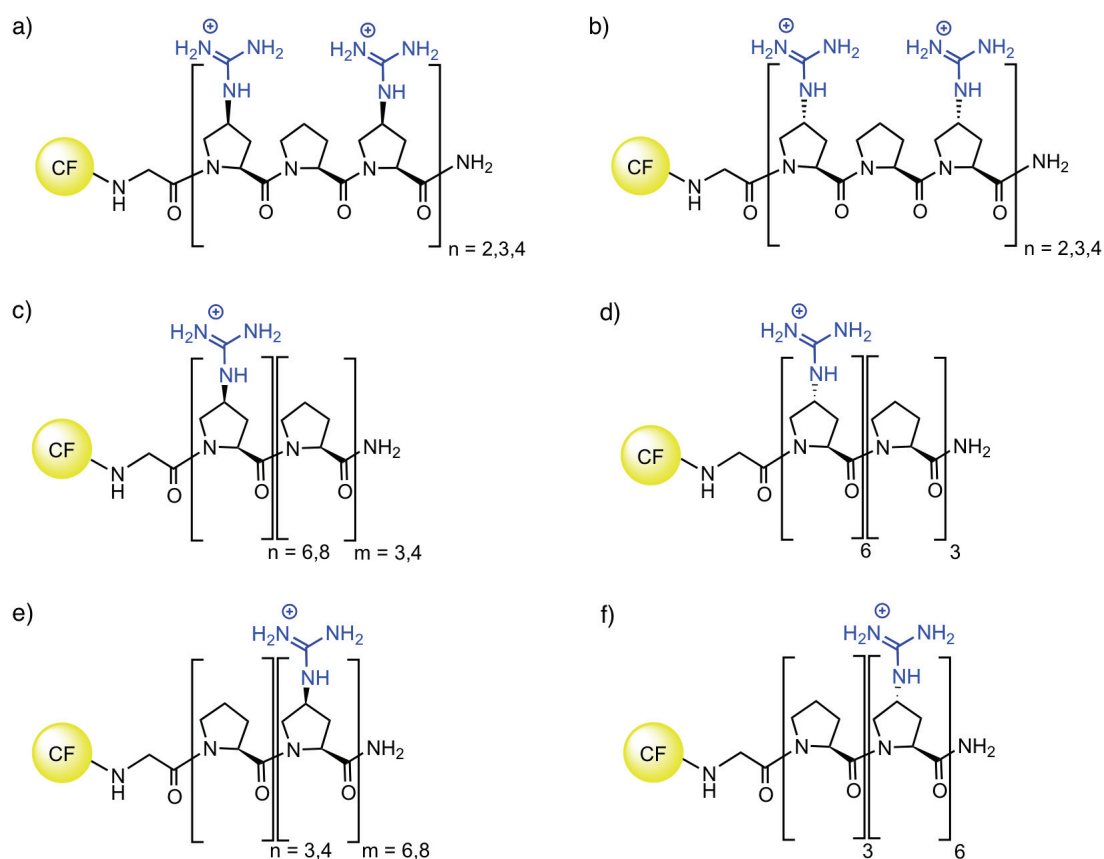
Figure 21: Functionalized oligoprolines of the alternating system bearing either (4*S*)Gup (a) or (4*R*)Gup residues (b); CPPs of the *en bloc* system with cationic moieties located either at the N- or C-terminus, bearing either (4*S*)Gup or (4*R*)Gup residues (c-f); Counterions are $CF_3CO_2^-$.

Since we were furthermore interested in the cellular uptake of the oligoproline-based CPPs in the absence of additional unfunctionalized proline residues, peptides were designed consisting entirely of (4*S*)Gup (Fig. 22). The influence of the chain length on the cellular uptake was as well evaluated for the peptides of this series.
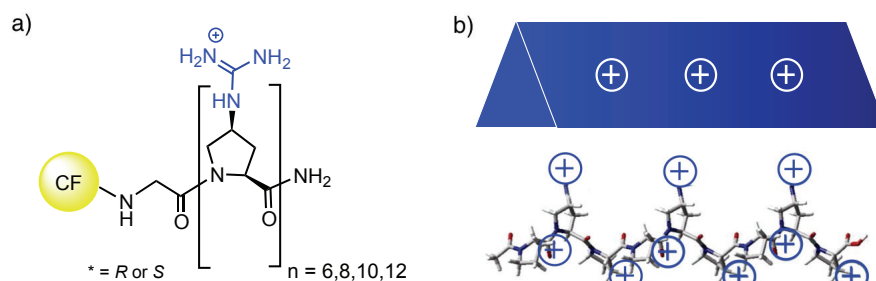
Figure 22: a) Molecular structure of peptides with an *en bloc* arrangement, consisting entirely of (4*S*)-Gup; b) Functionalized PPII helix consisting only of (4*S*)Gup residues, illustrated as a prism; Counterions are $CF_3CO_2^-$.

In order to examine, whether the cell-penetrating properties of our CPPs are associated with a specific receptor on the cell membrane, which would suggest an effect of the chirality of the PPII helix, we evaluated according D-analogs of a collection of oligoproline-based CPPs during the master thesis of P. Raschle.[206] Peptides with an alternating pattern of moieties and with an *en bloc* arrangement, bearing D-(4*S*)Gup and D-(4*R*)Gup, were synthesized (Fig. 23) and compared to the L-oligoproline derivatives of this thesis.

Figure 23: a) D-oligoproline-based CPPs with an alternating pattern of residues; b) D-oligoproline-based CPPs with an *en bloc* arrangement of cationic moieties either at the N-terminus or c) on the C-terminus; Counterions are $CF_3CO_2^-$.

A complete list of all synthesized peptides is given in the appendix 6.4. (4*S*)Gup will be abbreviated in the course of this thesis with the one-letter code Z, whereas (4*R*)Gup will be termed as X. The according small letters will represent the D-amino acid derivatives. (4*S*)Amp will be abbreviated as U.

3.1.2 Syntheses of CPPs

3.1.2.1 General peptide synthesis strategies for oligoproline-based CPPs

The cationic oligoprolines were synthesized by three different strategies (A, B and C in scheme 9). For each synthetic route standard SPPS procedures, following the Fmoc/*t*Bu protocol, were used to assemble the peptides (see chapter 5.1.4). The introduction of the ammonium and guanidinium groups in the γ-position of proline, respectively, proved to be the key reactions for the synthesis. The cationic moieties were either introduced after assembly of the Azp containing peptides using the building block Fmoc-Azp-OH (**16**) for SPPS (strategies A or B) or by using Fmoc-Gup(Boc)$_2$-OH (**17**) (strategy C).
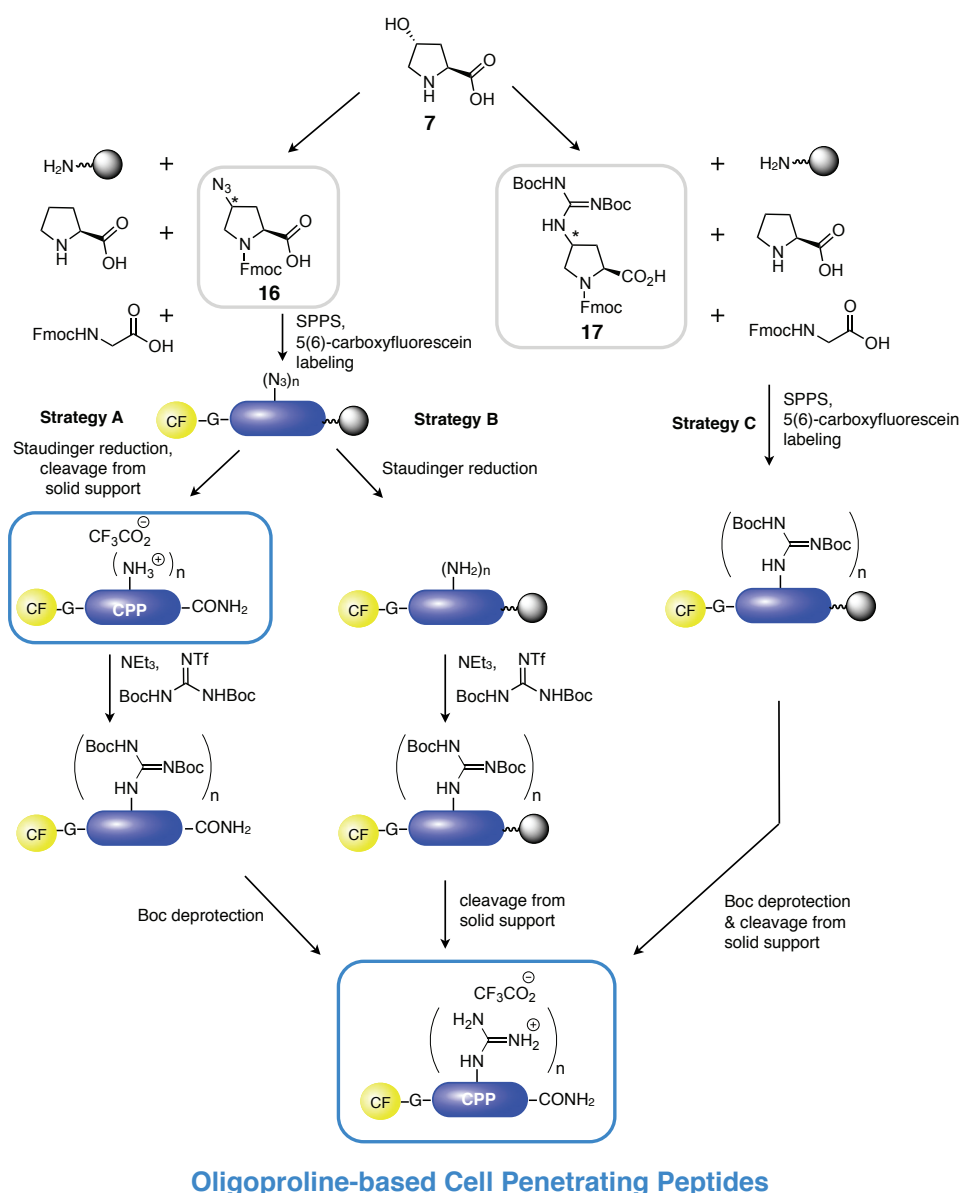
Scheme 9: Overview of different synthesis strategies towards oligoproline-based CPPs.

All CPPs were synthesized on ChemMatrix Rink amide resin to obtain the C-terminal carboxamide after cleavage from the solid support. The carboxamide was chosen for C-terminal capping of the peptides instead of the free carboxylic acid and to avoid a negative charge on the peptides. Furthermore, it was shown that the stability of the PPII helical structure is enhanced with a carboxamide compared to a carboxylic acid at the C-terminus of oligoprolines.[207] For peptides with an alternating pattern of functionalized prolines, the full loading of the resin (0.64 mmol/g) was exploited, whereas the loading was decreased to 0.3 mmol/g for the syntheses of peptides containing more than six modified residues in a row, in order to reduce the steric hindrance between the peptides on the beads. The automated peptide syntheses were conducted with a 0.5 M solution of Fmoc-Xaa-OH (4.0 eq) in DMF (chapter 5.1.4.1). As standard coupling reagent HCTU (0.5 M, 4.0 eq) in DMF was used and Hünig's base (3.0 M, 12.0 eq) was added. The mixture was shaken for 1 h and washed with DMF. After every coupling step Fmoc-deprotection with 40% piperidine in DMF was performed and the resin was washed with DMF. For peptides longer than eight amino acids 2% DBU in DMF was used for Fmoc-deprotection. Potential free amino functionalities on the N-termini after coupling were caped by acetylation with Ac_2O (1.0 eq) and Hünig's base (1.0 eq) in DMF and the mixture was washed with DMF afterwards. After complete synthesis a washing step with DCM was carried out.

3.1.2.1.1   Strategy A

In this strategy azido proline (Azp) containing oligoprolines were prepared and further modified in solution after cleavage from the resin (Scheme 10). Fmoc-(4*R*)Azp-OH (**16R**) and Fmoc-(4*S*)Azp-OH (**16S**), respectively, as well as the commercially available building blocks Fmoc-Pro-OH and Fmoc-Gly-OH served for SPPS. The labeling of the N-terminus with 5(6)-carboxyfluorescein, for the detection of the cellular uptake, was accomplished either by coupling of activated 5(6)-carboxyfluorescein *N*-succinimidylester or coupling of 5(6)-carboxyfluorescein with DIC and HOBt. The fluorophore was labeled *via* a glycine spacer, since direct attachment to the secondary amine of proline proved to be difficult. The peptides were cleaved from the solid support directly afterwards and the azides were subsequently converted into amines by Staudinger reduction in solution. A fraction of the obtained amino functionalized oligoprolines was directly purified by preparative RP-HPLC and evaluated for the cell-penetrating properties. For CPPs containing guanidinium moieties, a guanidinylation

step in solution using *N,N'*-di-Boc-*N''*-trifluoromethane sulfonylguanidine (**18**) followed. After deprotection of the Boc groups, the crude peptides were purified to obtain the desired guanidino proline containing peptides. This synthesis strategy was previously tested by F. Monnard during his Master thesis.[208]
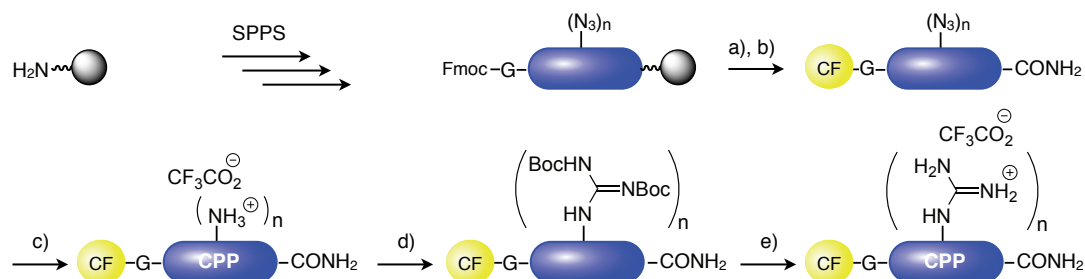
Scheme 10: Synthesis strategy A: Modifications steps after automated peptide synthesis: a) i) 40% piperidine in DMF, rt, 5 min; ii) 20% piperidine in DMF, rt, 10 min; b) 5(6)-carboxyfluorescein *N*-succinimidyl ester (1.1 eq), Hünig's base (3.0 eq), DMF, rt, 2.0 h or 5(6)-carboxyfluorescein (10 eq), DIC (10 eq), HOBt (10 eq), DMF, 2h, rt; c) PMe$_3$ (1 M in THF, 3.3 eq per azido group), H$_2$O (12 eq per azido group), rt, 22 h; d) *N,N'*-di-Boc-*N''*-trifluoromethane sulfonylguanidine (**18**) in MeOH (2.3 eq per amino group), NEt$_3$ (3.3 eq per amino group), dioxane, rt, 4 d; e) 95% TFA, 2.5% H$_2$O, 2.5% TIS, rt, 30 min.

Strategy A was applied to synthesize oligoprolines with an alternating pattern of cationic moieties, but did not show satisfying results for the synthesis of peptides with larger blocks of cationic residues. The synthesis of the Fmoc-protected building blocks Fmoc-(4*R*)Azp-OH (**16R**) and Fmoc-(4*S*)Azp-OH (**16S**) as well as the guanidinylation reagent *N,N'*-di-Boc-*N''*-trifluoromethane sulfonylguanidine (**18**) will be described in section 3.1.2.3.

3.1.2.1.2 *Strategy B*

The assembly of the Azp-containing peptides and the labeling of the fluorophore were performed according to strategy A, with the difference that the further modifications of the azides towards guanidinium groups were performed on solid support and not in solution (Scheme 11). The azido functions were converted to amines by Staudinger reduction on resin and the resulting amino prolines further transformed into guanidino prolines by nucleophilic substitution using *N,N'*-di-Boc-*N''*-trifluoromethane sulfonylguanidine (**18**). The Staudinger reduction of the azides was performed

according to established procedures in the Wennemers group and further optimized in the course of this thesis.[31] After cleavage from the resin, the crude peptides were purified *via* RP-HPLC.
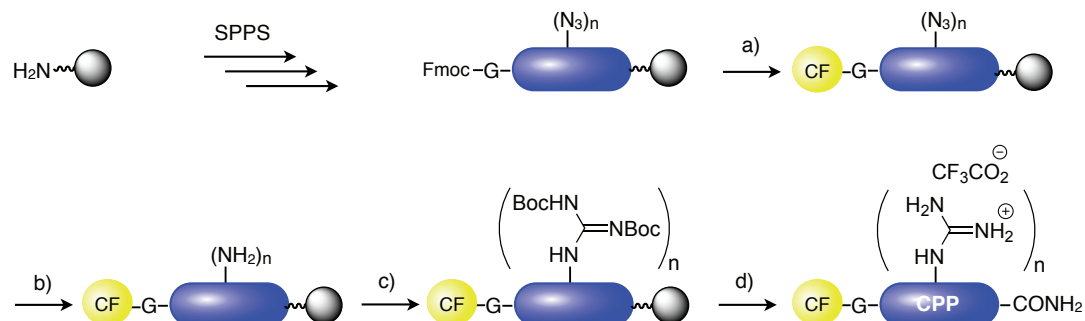
Scheme 11: Synthesis strategy B: Modifications steps after automated peptide synthesis: a) i) 40% piperidine in DMF, rt, 5 min; ii) 20% piperidine in DMF, rt, 10 min; iii) 5(6)-carboxyfluorescein *N*-succinimidyl ester (1.1 eq), Hünig's base (3.0 eq), DMF, rt, 2.0 h or 5(6)-carboxyfluorescein (10 eq), DIC (10 eq), HOBt (10 eq), DMF, 2h, rt; b) PMe_3 (1 M in THF, 5.0 eq per azido group), H_2O (22.0 eq per azido group), rt, 2.0 h; c) *N,N'*-di-Boc-*N"*-trifluoromethane sulfonylguanidine (**18**) in MeOH (3.5 eq per amino group), NEt_3 (4.2 eq per amino group), dioxane, rt, 4 d; d) 95% TFA, 2.5% H_2O, 2.5% TIS, rt, 2 x 1.5 h.

The advantage of this strategy in comparison to strategy A is that it does not require a solvent- and time-consuming purification. Peptides can be easily washed on resin by filtration, due to the performance of the reduction and guanidinylation reaction on solid support. Overall, this strategy proved to be more practical compared to strategy A. It was applied to synthesize oligoprolines with an alternating pattern of cationic moieties and oligoprolines containing up to six cationic moieties in a row, but was not suitable for the synthesis of peptides with larger blocks of cationic residues.

3.1.2.1.3   *Strategy C*

The third and most straightforward synthesis route to generate guanidino proline-rich CPPs represents strategy C (Scheme 12). Fmoc-(4*S*)Gup(Boc)$_2$-OH (**17**) and the unmodified amino acid building blocks Fmoc-Pro-OH and D-Fmoc-Pro-OH were used for SPPS. For according D-oligoprolines the building block D-Fmoc-(4*R*)Gup(Boc)$_2$-OH (**19**) was synthesized by P. Raschle.[206] Afterwards the glycine spacer was introduced and 5(6)-carboxyfluorescein was coupled to the N-terminus.
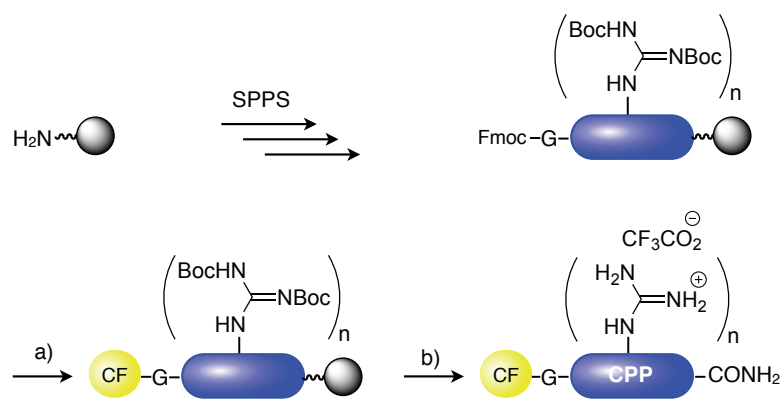
Scheme 12: Synthesis strategy C: Modifications steps after automated peptide synthesis: a) i) 40% piperidine in DMF, rt, 5 min; ii) 20% piperidine in DMF, rt, 10 min; iii) 5(6)-carboxyfluorescein *N*-succinimidyl ester (1.1 eq), Hünig's base (3.0 eq), DMF, rt, 2.0 h or 5(6)-carboxyfluorescein (10 eq), DIC (10 eq), HOBt (10 eq), DMF, 2 h, rt; b) 95% TFA, 2.5% H_2O, 2.5% TIS, rt, 2 x 1.5 h.

A clear advantage of strategy C is the possibility to perform a fully automated SPPS towards the final products, which cannot be performed with the previous strategies. The fast and direct route of this strategy saves two manual modification steps of the full length peptides in comparison to strategies A and B. Furthermore the synthesis of peptides with up to eight neighboring cationic moieties was accomplished with this strategy. A drawback is the need of the building blocks Fmoc-(4*S*)Gup(Boc)$_2$-OH (**17**) and D-Fmoc-(4*R*)Gup(Boc)$_2$-OH (**19**) that are not easily accessible in a large scale syntheses (for **17** see 3.1.2.3.3, for **19** see reference [206]). Furthermore **17** and **19** had to be freshly dissolved in DMF for automated SPPS and should not stand longer than 12 h, since the formation of an insoluble gel was observed. To prevent this formation 3 eq. of Hünig's base were added prior to automated peptides synthesis. The building block syntheses will be discussed in more detail in section 3.1.2.3.

Comparison of the different strategies revealed that all of them can be used as routes to obtain oligoprolines with an alternating pattern of cationic moieties up to an all over chain length of twelve residues and oligoprolines containing up to six cationic moieties in a row. The Staudinger reduction, as well as the guanidinylation reaction in solution and on solid support, were proceeding well in both strategies A and B. The coupling efficiencies of the guanidinylated building blocks for strategy C was acceptable and provided peptides with up to eight neighboring cationic residues. Thus, yields and purities were comparable for the respective peptides, when synthesized by one of the according strategies as described. However, the yields differed depending on the

subtype of the CPPs independent from the synthesis strategy. The yields after purification were good for oligoprolines with an alternating pattern of ammonium groups (18-29%, purities 97-100%) and moderate for oligoprolines with an alternating pattern of guanidinium groups (8-21%, purities 80-100%). For oligoprolines containing up to eight cationic moieties in a row as well moderate yields were obtained (5-19%, purities 94-100%). The slightly higher yields of the amino proline containing peptides might be explained by the shorter synthesis route compared to the guanidino proline containing peptides.[3] Usually, the obtained crude peptides did not show major impurities, unless it was generally observed that couplings of modified building blocks after each other are not as efficient than unmodified ones under the same standard conditions (e.g. unfunctionalized oligoprolines gave a yield of 23-40% and a purity of 99-100%). Impurities in the crude modified peptides could be assigned to acetylated peptide fragments *via* LC-MS, which were generated by capping of unreacted N-termial amines during the automated SPPS. Those fragments have different retention times, according to their indicidual chain length, and could be removed by preparative RP-HPLC The appearance of double peaks in the RP-HPLC chromatograms was assigned to the mixture of the isomers of 5- and 6-carboxyfluorescein *via* LC-MS analysis (Fig. 24). The masses of peptides, which contained several guanidino functions, were detected as multiple charged species when analyzed *via* LC-MS. In many cases the corresponding TFA adducts were observed.[3]
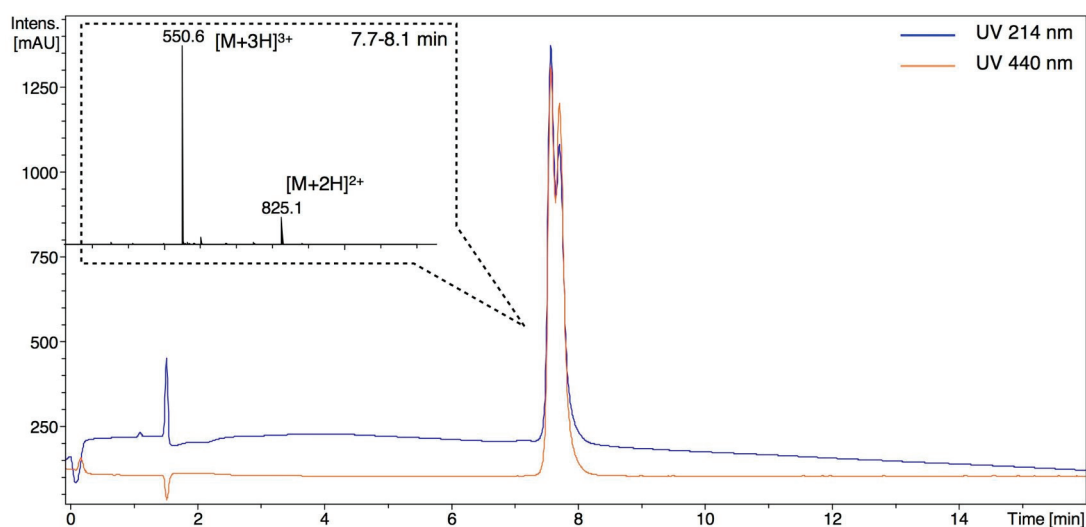
Figure 24: Representative LC-MS of a purified oligoproline-based CPP, the peptide CF-G-Z_6P_3-$CONH_2$ (**30**), showing a double set of peaks (R_t = 7.7 and 7.8 min), which were both identified as the main product (m/z = 1647.8) according to the two isomers of 5(6)-carboxyfluoresein.

---

[3] For a complete list of the yields and purities of all peptides see appendix 6.4.

The following oligoproline-based CPPs were successfully synthesized according to the described strategies:[4]

Alternating system:

20	CF-G-UPU-UPU-CONH$_2$	**23**	CF-G-ZPZ-ZPZ-CONH$_2$
21	CF-G-UPU-UPU-UPU-CONH$_2$	**24**	CF-G-ZPZ-ZPZ-ZPZ-CONH$_2$
22	CF-G-UPU-UPU-UPU-UPU-CONH$_2$	**25**	CF-G-ZPZ-ZPZ-ZPZ-ZPZ-CONH$_2$

26   CF-G-XPX-XPX-XPX-CONH$_2$

27   CF-G-zpz-zpz-zpz-CONH$_2$

28   CF-G-xpx-xpx-xpx-CONH$_2$

En bloc system:

29	CF-G-PPP-ZZZ-ZZZ-CONH$_2$	**32**	CF-G-ppp-zzz-zzz-CONH$_2$
30	CF-G-ZZZ-ZZZ-PPP-CONH$_2$	**33**	CF-G-zzz-zzz-ppp-CONH$_2$
31	CF-G-ZZZ-ZZZ-ZZP-PPP-CONH$_2$		

34	CF-G-PPP-XXX-XXX-CONH$_2$	**36**	CF-G-ppp-xxx-xxx-CONH$_2$
35	CF-G-XXX-XXX-PPP-CONH$_2$	**37**	CF-G-xxx-xxx-ppp-CONH$_2$

38   CF-G-ZZZ-ZZZ-CONH$_2$

39   CF-G-ZZZ-ZZZ-ZZ-CONH$_2$

In summary, it emerge that strategy C was the most straightforward route and provided the broadest scope of peptides, considering the restrictions of strategy A and B to serve only for the syntheses of certain types of oligoproline-based CPPs. A drawback of strategy C was the synthesis of the required building blocks Fmoc-(4*S*)Gup(Boc)$_2$-OH (**17**) and D-Fmoc-(4*R*)Gup(Boc)$_2$-OH (**19**), which did not lead to satisfying yields in a large scale. The synthesis of the longer chained peptides with more than eight neighboring guandino prolines, CF-G-Z$_n$-CONH$_2$ with n = 10 and 12 (**40** and **41**), proved to be difficult with all three strategies and could not be completed to obtain entirely pure products. The problems occurring during synthesis and attempts which were made to cap sideproducts are discussed in the following section.

---

[4] With the abbreviations: 5(6)-carboxyfluorescein (CF), Gly (G), (4*S*)Amp (U), (4*S*)Gup (Z), (4*R*)Gup (X), D-(4*S*)Gup (z), D-(4*R*)Gup (x), Pro (P), D-Pro (p).

3.1.2.1.4   *Synthesis towards longer chained oligoproline-based CPPs*

The synthesis of the peptides with more than eight neighboring guandino prolines, CF-G-Z_n-$CONH_2$ with n = 10 and 12 (**40** and **41**), were attempted with all three strategies A, B and C. Factors preventing the successful synthesis will be discussed for CF-G-Z_{10}-$CONH_2$ (**40**) as a representative example.

The syntheses according to strategies A and B did not lead to the pure product, since the Staudinger reduction of the azides, as well as the following guanidinylation reaction could neither be brought to completion in solution, nor on solid support as illustrated for strategy B (Fig. 25). The LC-MS analysis of the intermediate CF-G-U_{10}-$CONH_2$ (**53**) after Staudinger reduction revealed that the main peak contained sideproducts with a mass corresponding to a peptide with up to two azides instead of amino groups, next to the product mass. Other methods to reduce the azides, for example with palladium on charcoal, did not succeed without affecting the fluorophore. The LC-MS analysis of the main peak after the guanidinylation reaction showed the product as well as additional masses, corresponding to peptides with up to three remaining amines instead of guanidino groups within the peptide and their corresponding TFA adducts (Fig. 26). Variation of reaction parameters, such as equivalents, solvents, dilution, temperature, reaction time, and microwave assistance did not lead to entirely converted functionalities of the peptides for both reactions.
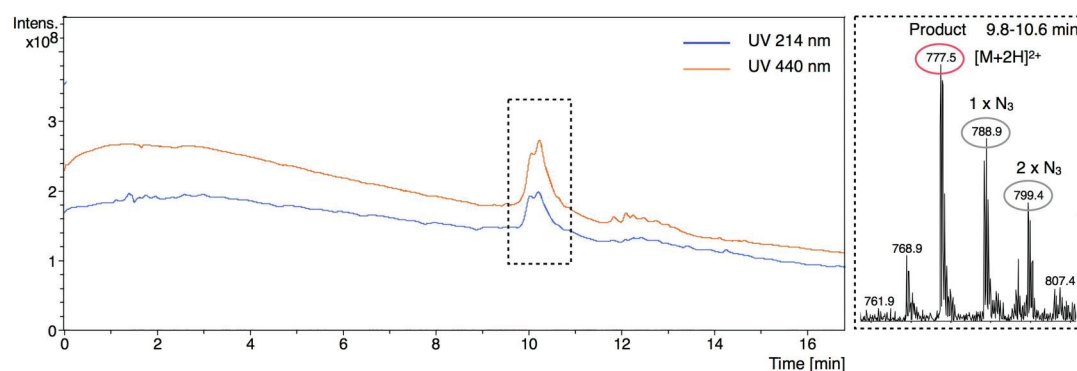
Figure 25: LC-MS of the intermediate CF-G-U_{10}-$CONH_2$ (**53**) showing the main product (R_t = 10.2 and 10.3 min, m/z = 1552.7; double peak corresponding to 5(6)-CF isomers) and additional sideproducts containing up to two remaining azido functions instead of amines within the peptide.
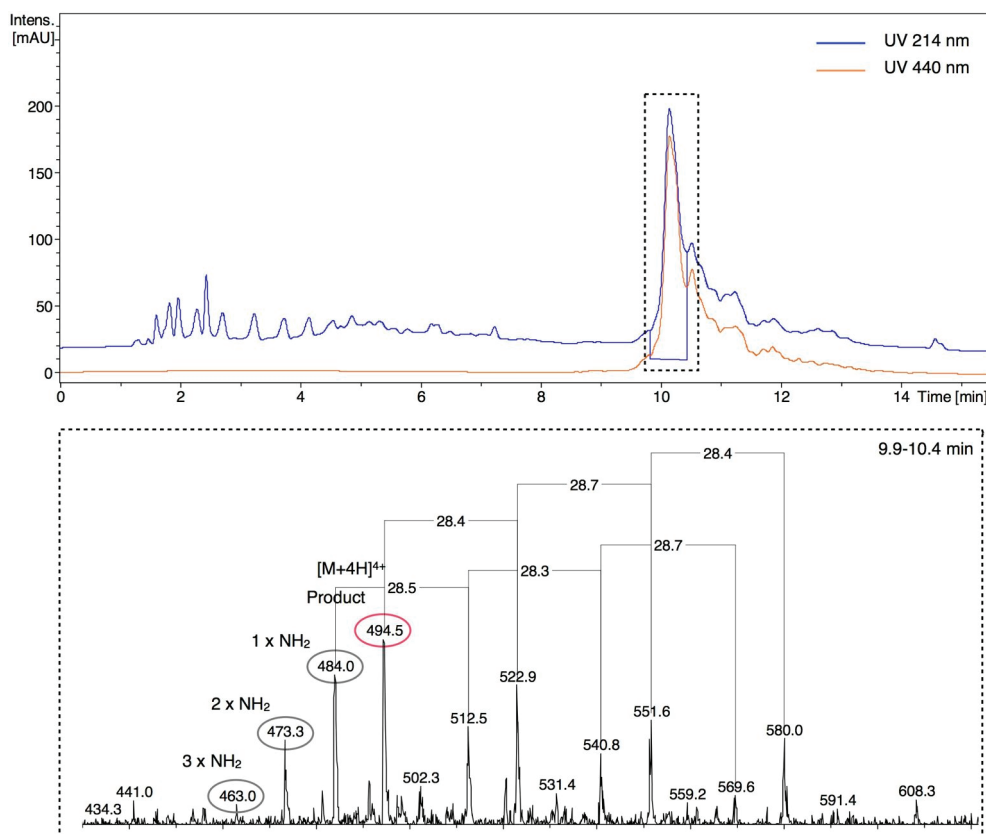
Figure 26: LC-MS of CF-G-Z_{10}-CONH$_2$ (**40**, m/z = 1973.0) showing the main product (R_t = 10.3 min) with the correct mass and additional peptides containing up to three remaining amino functions (the corresponding TFA adducts were detected as well, forming a characteristic pattern of mass peaks; TFA/4 = 28.3).

The remaining amines were tried to be capped with acetic anhydride and pivaloyl anhydride, respectively, to shift the retention times of the sideproducts away from the retention time of the product, enabling purification *via* RP-HPLC. Unfortunately, both reactions could not occur without affecting the 5(6)-carboxyfluorescein leading to a decrease in fluorescence detected by UV. Since the peptides with remaining azido functions significantly differ in the retention time from the guandinylated endproduct, they could be removed by preparative RP-HPLC. However, not all amino proline containing sideproducts could be removed. The resulting peptide CF-G-Z_{10}-CONH$_2$ (**40**) still showed a sideproduct containing one amino instead of a guanidino proline after purification (Fig. 27). The exact ratio of product and sideproduct could not be determined due to their similar retention time, shown in Fig. 27 with the overlaying extracted ion chromatograms (EIC) of the product ([M+4H]$^{4+}$, m/z = 494, red) and sideproduct ([M+4H]$^{4+}$, m/z = 484, green). Nevertheless, since amino groups are as well positively charged at physiological pH and are prone to enhance cell penetration, we were interested in testing them in our biological assays.
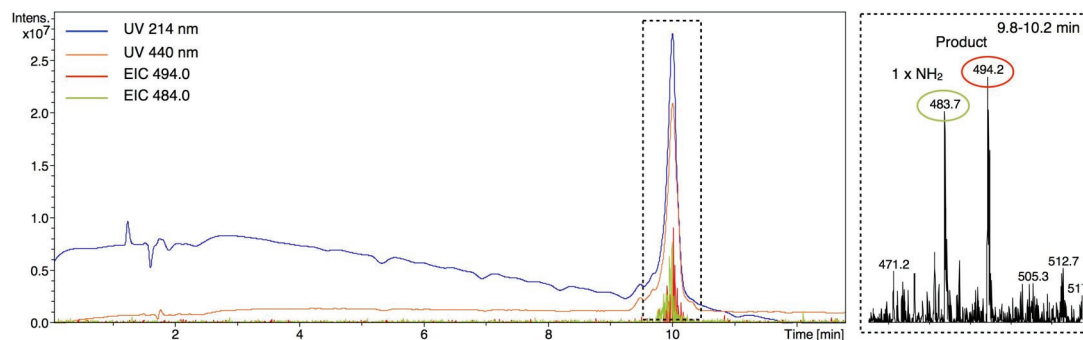
Figure 27: LC-MS of CF-G-Z$_{10}$-CONH$_2$ (**40**) after purification *via* preparative RP-HPLC.

Also synthesis strategy C did not provide the product, since the coupling efficiency of Fmoc-(4*S*)Gup(Boc)$_2$-OH (**17**) decreased with increasing chain length of the peptide. The change of the coupling reagent from HCTU to HATU, which provided the most efficient coupling for this type of building block in our hands and the use of NMP as solvent instead of DMF, could as well not improve the success of the synthesis. Peptides containing eight and nine guanidinylated moieties in a row as well as a small fraction of the product were detected, however it was not possible to isolate enough of the product *via* preparative HPLC for evaluations. Manual coupling of the modified building block (5.1.4.2) did as well not lead to success. A possible reason for the decrease of the coupling efficiency with increasing chain length could be the steric hindrance of the di-Boc-protected guanidino groups of the growing peptides on the resin. Furthermore, a diminished coupling efficiency associated with decreased nucleophilicity of the secondary amine due to the electron withdrawing properties of the substituents in the γ-position of the pyrroldine ring (Fig. 28) could affect the peptide synthesis.
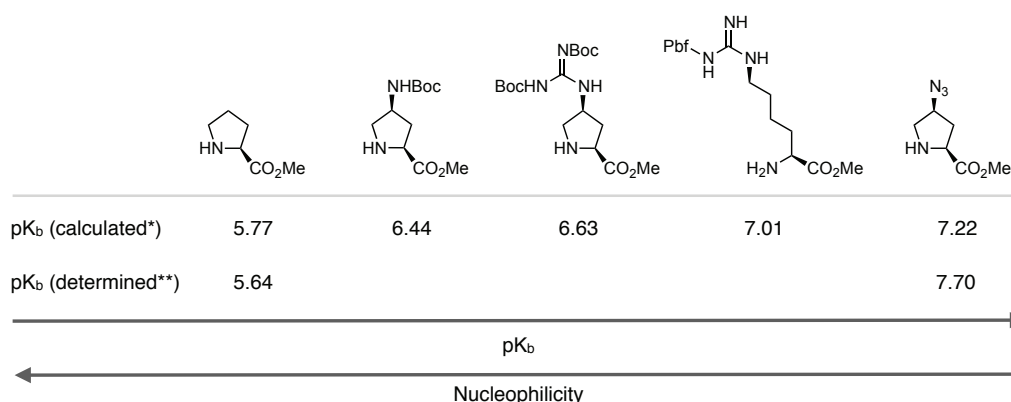
Figure 28: pK$_b$ values and nucleophilicity trends of secondary amines of different proline derivatives and arginine used as Fmoc-protected building blocks for SPPS (*according pK$_a$ values were calculated with ACD/pK$_a$ DB software and **titrated against 0.1 M NaOH at 25°C, at the Microelemental Analytics Laboratory, ETH Zürich).

To accomplish the challenging synthesis of longer chained functionalized oligoproline derivatives in the future, different possibilities can be tested. Currently members of the Wennemers group are working on the synthesis of a new guanidinylated proline building block with a less sterically hindered protecting group for the guanidino moiety, which might improve the coupling efficiency of this amino acid derivative. Additionally double couplings could be tested or the use of more than 4 eq. of the building block for coupling. A further decrease of the resin loading might as well support a more efficient synthesis.

3.1.2.2 Syntheses of the reference CPPs

The reference peptides containing natural amino acids were synthesized using standard SPPS and commercially available Fmoc-protected amino acids as building blocks (5.1.4.15). The reference peptides were as well equipped with a N-terminal glycine spacer and labeled with 5(6)-carboxyfluorescein according to the described procedures. The yield and purities were in a moderate to good range, depending on the specific sequences (yield 6-40%, purities 95-100%).[5]

| 42 | CF-G-RKK-RRQ-RRR-PPQ-CONH$_2$ | | |
| 43 | CF-G-RQI-KIW-FQN-RRM-KWK-K-CONH$_2$ | | |

44	CF-G-RRR-RRR-CONH$_2$	48	CF-G-rrr-rrr-CONH$_2$
45	CF-G-RRR-RRR-RR-CONH$_2$		
46	CF-G-RRR-RRR-RRR-R-CONH$_2$		
47	CF-G-RRR-RRR-RRR-RRR-CONH$_2$		

| 49 | CF-G-PPP-PPP-CONH$_2$ | 51 | CF-G-ppp-ppp-CONH$_2$ |
| 50 | CF-G-PPP-PPP-PPP-CONH$_2$ | 52 | CF-G-ppp-ppp-ppp-CONH$_2$ |

---

[5] For a complete list of the yields and purities of all peptides see appendix 6.4.

3.1.2.3 Syntheses of Fmoc-protected building blocks

The building blocks Fmoc-(4*R*)Azp-OH (**16R**) and Fmoc-(4*S*)Azp-OH (**16S**) were synthesized according to established routes in the Wennemers group.[22, 35a] The synthesis of Fmoc-(4*S*)Gup(Boc)$_2$-OH (**17**) was first described by Hruby *et al.*[209] and further improved in the course of this project. The according enantiomeric building block D-Fmoc-(4*R*)Gup(Boc)$_2$-OH (**19**) was synthesized by P. Raschle during his Master thesis affiliated with this project.[206]

3.1.2.3.1   Synthesis of Fmoc-(4S)Azp-OH (16S)
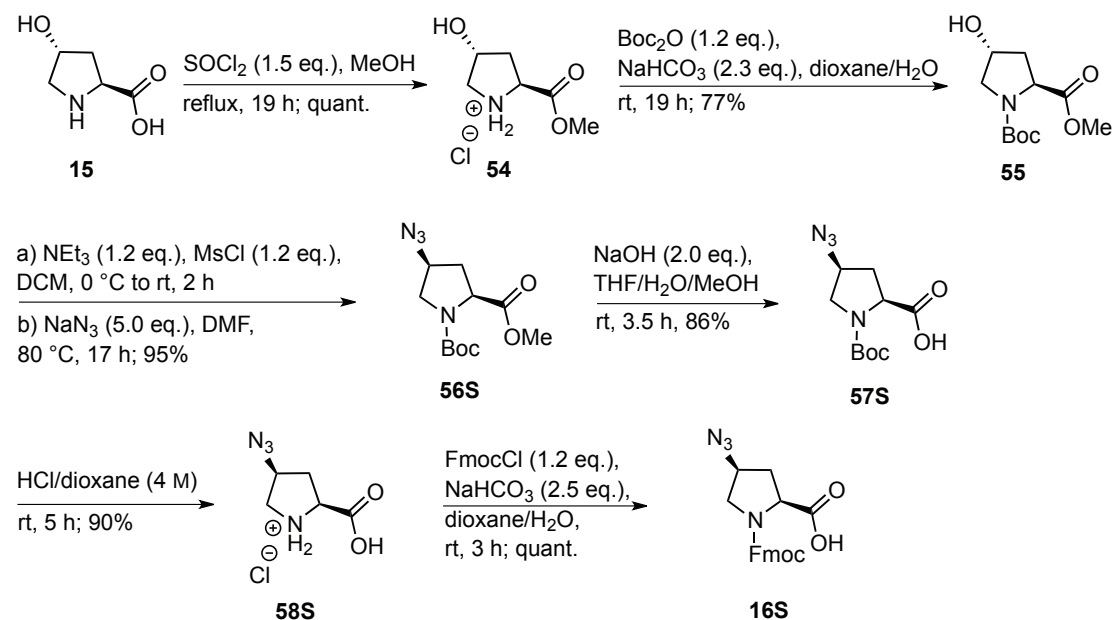
Scheme 13: Synthesis of the building block Fmoc-(4*S*)Azp-OH (**16S**).

The synthesis of Fmoc-(4*S*)Azp-OH (**16S**) (Scheme 13) started by esterification of (4*R*)-hydroxy proline, H-(4*R*)Hyp-OH (**15**), with thionyl chloride in methanol, followed by *tert*-butyl oxycarbonyl (Boc) protection of the secondary amine. The resulting Boc-(4*R*)Hyp-OMe (**55**) was activated as a mesylate and S$_N$2 substitution with sodium azide provided the azido proline derivative Boc-(4*S*)Azp-OMe (**56S**) with inversion of the configuration at C(4). After hydrolysis of the methyl ester and removal of the Boc protecting group the amine was re-protected using Fmoc chloride under Schotten-Baumann conditions to yield the desired building block Fmoc-(4*S*)Azp-OH (**16S**). All reactions provided the desired products in good yields in a range from 77% to quantitative. The overall yield after seven reaction steps was 57%.

3.1.2.3.2   Synthesis of Fmoc-(4R)Azp-OH (16R)
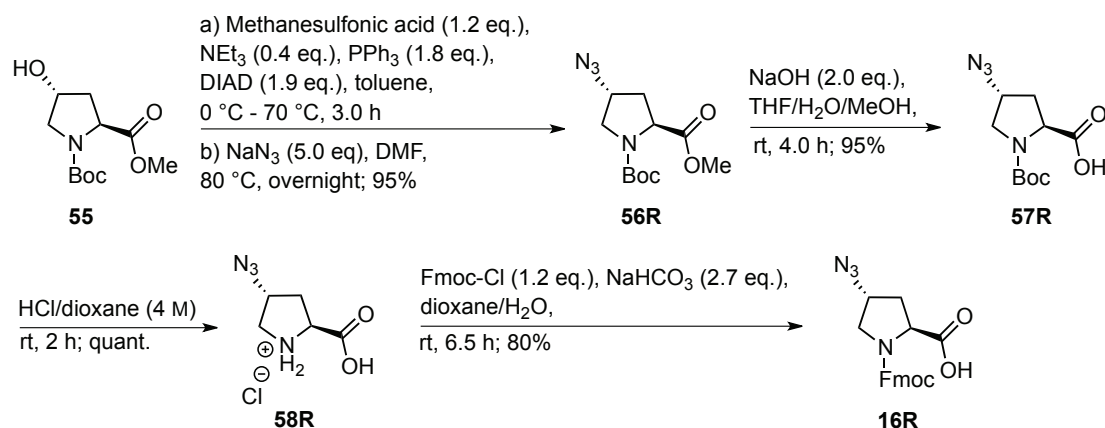
Scheme 14: Synthesis of the building block Fmoc-(4*R*)Azp-OH (**16R**).

To obtain the according (4*R*)-substituted diastereoisomer Fmoc-(4*R*)Azp-OH (**16R**) (Scheme 14), a fraction of the already synthesized (4*R*)-hydroxy proline derivative (**55**) was converted to a mesylate by a Mitsunobu reaction with methanesulfonic acid under inversion of the absolute configuration at C(4). A following S_N2 substitution with sodium azide, again under inversion of the configuration at the stereogenic center at C(4), led to Boc-(4*R*)Azp-OMe (**56R**) and an, all over retention of the configuration. The methyl ester was hydrolyzed under basic conditions, providing Boc-(4*R*)Azp-OH (**57R**). The following Boc-deprotected using 4 M HCl in dioxane led to H-(4*R*)-Azp-OH*HCl (**58R**). The last step was the Fmoc-protection of the secondary amine under Schotten-Baumann conditions, using Fmoc chloride to obtain the building block Fmoc-(4*R*)Azp-OH (**16R**). The yields of the single reactions ranged from 77% to quantitative yield. The overall yield after seven reaction steps (including the two steps to **55**) was 56%.

3.1.2.3.3   Synthesis of Fmoc-(4S)Gup(Boc)₂-OH (17)

The synthesis of the di-Boc-protected building block Fmoc-(4*S*)Gup(Boc)$_2$-OH (**17**) (Scheme 15) goes back to the protocol developed by Hruby *et al.* in 2001.[209] They describe the orthogonal protection of the guanidino group, attached at C(4) of proline, with two Boc groups. Therefore *N,N'*-di-Boc-*N"*-trifluoromethane sulfonylguanidine (**18**), was used as the guanidinylation reagent, developed by Feichtinger *et al.*[210] In earlier reports the use of 4-Methoxy-2,3,6-trimethylbenzenesulphonyl (Mtr)[211] or 2,2,5,7,8-pentamethyl-chroman-6-sulphonyl (Pmc)[212] was described to protect the guanidino group of arginine. Due to side reactions during the cleavage of Mtr and Pmc

groups, they have been often replaced by 2,2,4,6,7-pentamethyl-dihydrobenzofuran-5-sulfonyl (Pbf), which proved to be the better guanidino protection group for arginine.[213] Since the double Boc protection showed as well a beneficial behavior under cleavage conditions and in favor for the easy and cost effective accessibility of the guanidinylation reagent *N,N'*-di-Boc-*N''*-trifluoromethane sulfonylguanidine (**18**) in comparison to Pbf chloride or Pbf anhydride, we decided to apply this method to our synthesis. To keep both Boc groups intact during the synthesis of the building block, orthogonal protecting groups that could be cleaved under neutral conditions were required. Thus, the benzyloxy carbonyl (Cbz) and benzyl (Bn) groups were chosen. Base-sensitive groups could not be used, because they would be deprotected during the guanidinylation reaction. Thus the synthesis of the Fmoc-protected guanidinylated amino acid **17** started from H-(4*R*)Hyp-OH (**15**), which was protected at the secondary amine with the Cbz group using benzyl chloroformate under basic conditions, to give Cbz-(4*R*)-Hyp-OH (**59**).
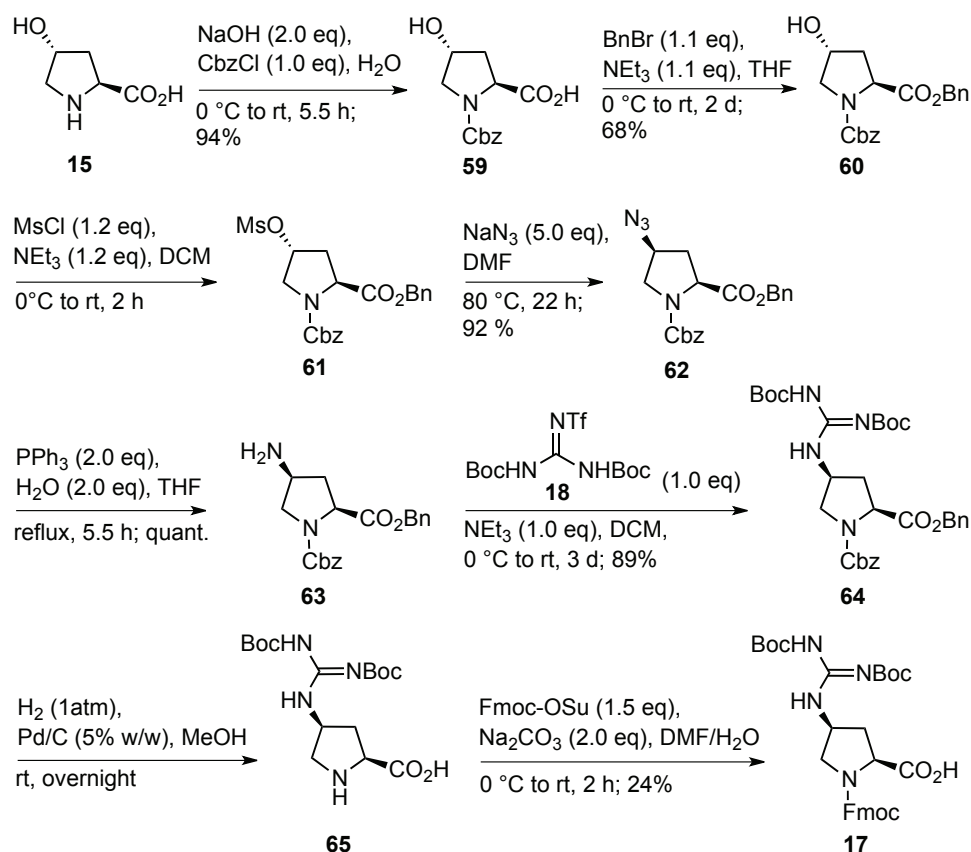
Scheme 15: Synthesis of the building block Fmoc-(4*S*)Gup(Boc)$_2$-OH (**17**).

After protection of the carboxylic acid with benzyl bromide, the resulting Cbz-(4*R*)Hyp-OBn (**60**) was directly activated as a mesylate using methanesulfonyl

chloride under basic conditions. In contrast, the protocol of Hruby *et al.* is using 4-toluenesulfonyl chloride (tosyl chloride) for activation of the hydroxy function. However, we observed a better conversion *via* the mesylate. The following S_N2 substitution with sodium azide provided the protected azido proline derivative Cbz-(4*S*)Azp-OBn (**62**) under inversion of the configuration. A Staudinger reduction of the azido moiety led to the amino functionalized derivative Cbz-(4*S*)Amp-OBn (**63**), which was further guanidinylated *via* a S_N2 substitution reaction of the amine at C(4) of the proline derivative with *N,N'*-di-Boc-*N"*-trifluoromethane sulfonylguanidine (**18**). The benzoyl oxycarbonyl and benzyl protecting groups of the resulting intermediate Cbz-(4*S*)Gup(Boc)$_2$-OBn (**64**) were catalytically hydrated with palladium on charcoal (5% (w/w)). A major problem in this step was the sticky consistence of the product H-(4*S*)Gup(Boc)$_2$-OH (**65**), which complicated an efficient purification at a large scale. Remaining palladium on charcoal could not be entirely removed by filtration and was present in the following re-protection of the secondary amine with Fmoc succinimide, towards the final building block Fmoc-(4*S*)Gup(Boc)$_2$-OH (**17**).

Generally the reactions proceeded with good yields between 89% and quantitative yields in our hands. Exceptions were the protection of the carboxylic acid with benzyl bromide with a yield of 68% and the mentioned final steps of Cbz and Bn deprotection and Fmoc-protection of the secondary amine, reported with yields of 75% and 77%, respectively, for a 1.34 mmol scale. In particular the Fmoc protection proved to be difficult in the larger scale (69 mmol), where only 24% yield was obtained. This last step significantly lowered the overall yield to 13%. To improve the overall yield, we are planning to adjust these last steps of the synthesis by changing the protecting group strategy. An obvious approach would be to introduce the Pbf protecting group instead of two Boc groups in order to change the consistence of H-(4*S*)Gup(Boc)$_2$-OH (**65**), enabling a proper purification and subsequent conversion to the desired building block Fmoc-(4*S*)Gup(Boc)$_2$-OH (**17**). This strategy is currently investigated by P. Raschle. The change in protecting group strategy towards less sterically hindered groups might as well have a positive impact on the coupling efficiency of the modified amino acid.

*Synthesis of N,N'-di-Boc-N''-trifluoromethane sulfonylguanidine (**18**)*
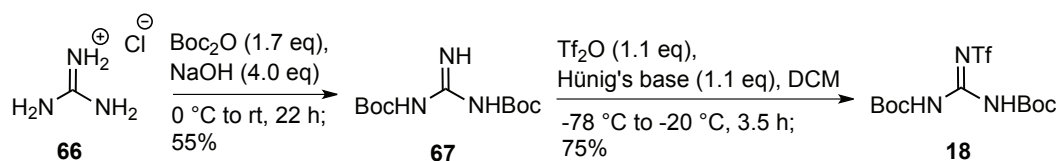
Scheme 16: Synthesis of *N,N'*-di-Boc-*N"*-trifluoromethane sulfonylguanidine (**18**).

The reagent for guanidinylation, *N,N'*-di-Boc-*N"*-trifluoromethane sulfonylguanidine (**18**), is commercially available, but can be easily accessed by a two step synthesis using the inexpensive starting material guanidinium hydrochloride (**66**). First, the Boc protection of the amino functions of **66** were conducted using Boc anhydride under basic conditions to give *N,N'*-di-Boc-guanidine (**67**). In a second step the imino group was activated with triflyl anhydride to obtain the product **18** in a moderate overall yield of 41%.

3.1.3   Conformational analyses of CPPs

To examine the conformational properties of the functionalized oligoprolines, CD spectra were recorded in aqueous phosphate buffer (PBS) at pH 7.4 and 37°C, reflecting the physiological conditions of the following cell experiments. The spectra of all oligoproline-based CPPs showed a minimum at ~ 206 nm and a less pronounced maximum at ~ 226 nm and are thus indicative for the left-handed PPII helix (see 1.2.1).[33a, 36] Thus the cationic moieties attached directly to the oligoproline backbone, without a spacing unit, do not affect the position of the characteristic bands for a PPII helical conformation. It was additionally noted that the CD spectra of peptides with an alternating or an *en bloc* arrangement of cationic moieties are comparable (Fig. 29). These results suggest that the basic scaffold maintains its structure even when cationic moieties are arranged in close proximity (helical pitch of ~ 9.5 Å) along the same side of the helix. The measurements were carried out using the full length CPPs, including the glycine spacer at the N-terminal site and the attached 5(6)-carboxyfluoresein, showing that these modifications do not affect the scaffold as well.[6]
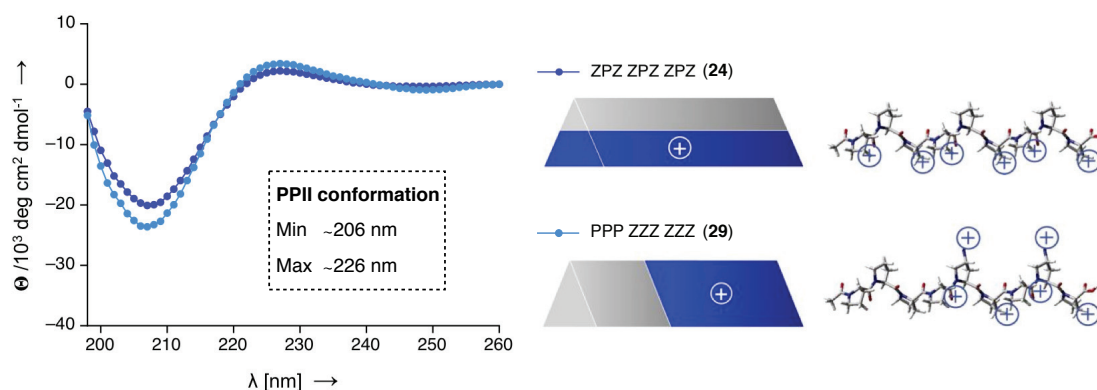
Figure 29: Circular dichroism spectra of CF-G-ZPZ-ZPZ-ZPZ-CONH$_2$ (**24**) and CF-G-PPP-ZZZ-ZZZ-CONH$_2$ (**29**). Spectra were recorded in PBS at pH 7.4, at concentrations of 70 µM and at 37°C.

However, the CD spectra of the modified oligoprolines show in general slightly weaker negative bands and more pronounced positive bands than unmodified oligoprolines. A possible reason for this effect might be the contribution of the substituents at C(4) of proline as chromophores to the CD signal. For example, it was observed that the oligoproline **24** bearing guanidinium groups shows a weaker minimum, (around -20 kdeg cm^2 dmol^{-1}) than the unfunctionalized oligoproline **50** under the same conditions (around -45 kdeg cm^2 dmol^{-1}) (Fig. 30, left). The oligoproline **21**, bearing

---

[6] The complete set of CD spectra of all synthesized CPPs is shown in the appendix (see 6.5).

ammonium groups, is in a medium range of -28 kdeg cm^2 dmol^{-1}. The ammonium groups of **21** are expected to contribute less to the CD signal, since they are weaker chromophores than the guanidinium groups. A second reason for the less pronounced minima of the functionalized oligoprolines **21** and **24** might be a potential intramolecular H-bond formation in the (4*S*)Amp and (4*S*)Gup containing peptides (see also chapter 3.2.3), which could influence the electronic structure of the amide chromophores of the helical backbone.[214]
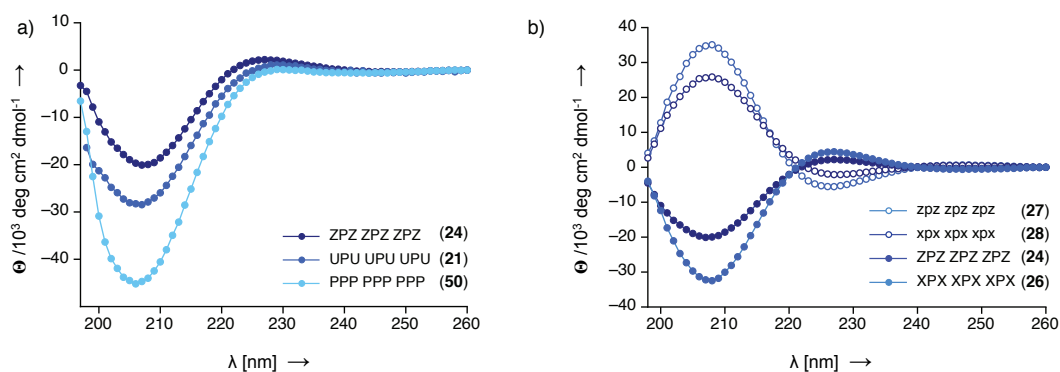
Figure 30: a) CD spectra of functionalized oligoprolines (**21** and **24**) compared to unfunctionalized oligoproline (**50**); b) CD spectra of L- and D-oligoproline based CPPs; Spectra were recorded in PBS at pH 7.4, at concentrations of 70 μM and at 37°C.

Since the D-oligoprolines exhibit the opposite stereoconfiguration at C$_\alpha$ of proline, the resulting CD spectra are mirror images of the spectra of the according functionalized L-analogs. They have a weak negative band at ~ 226 nm and a pronounced positive band at ~ 206 nm. The D-analogs of a selection of our CPPs were synthesized by P. Raschle during his Master thesis and confirmed these characteristics (Fig. 30, right).

An interesting observation is that the peptide CF-G-ZPZ-ZPZ-ZPZ-CONH$_2$ (**24**), bearing (4*S*)Gup that might be prone to intramolcular H-bond formation, shows a less pronounced minimum and maximum in comparison to its diastereoisomer CF-G-XPX-XPX-XPX-CONH$_2$ (**26**) bearing (4*R*)Gup. The conformational requirements to form intramolecular H-bonds were predicted for the according monomer model of (4*S*)Gup by *ab initio* calculations (see discussion in chapter 3.2.2.2). The enantiomers of **24** and **26**, CF-G-xpx-xpx-xpx-CONH$_2$ (**28**) and CF-G-zpz-zpz-zpz-CONH$_2$ (**27**), which bear D-(4*R*)Gup and D-(4*S*)Gup, show a similar behavior relative to each other in their CD spectra.

In contrast, the reference peptides CF-G-R_8-CONH$_2$ (**45**), CF-G-RKK-RRQ-RRR-PPQ-CONH$_2$ (Tat(48-60), **42**) and CF-G-RQI-KIW-FQN-RRM-KWK-K-CONH$_2$ (penetratin, **43**) did not show a defined secondary structure. Their minima and maxima are shifted towards shorter wavelengths, indicating that the peptides rather adopt a random coil structure (Fig. 31, left), a polymer, in which at least some of the bonds exist in more than one rotational state. The CD spectra of such statistically averaged conformations are characterized by a negative band at ~ 195 nm and a positive band at ~ 212 nm (Fig. 31, right).[215]
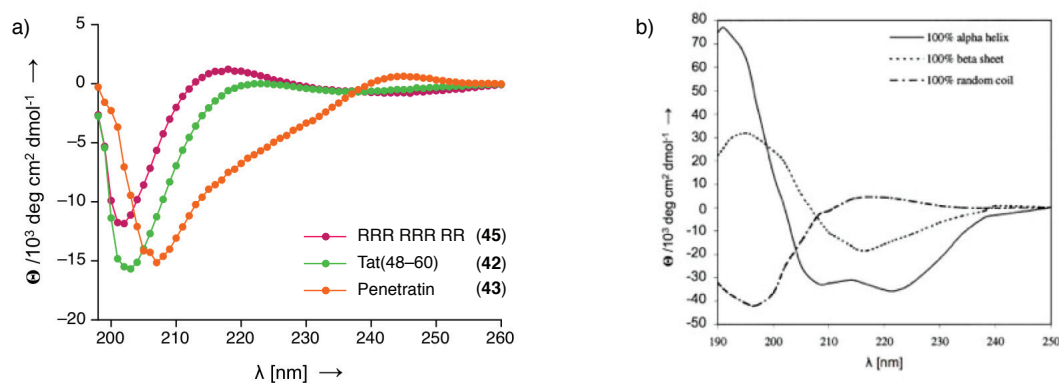
Figure 31: a) CD spectra of CF-G-R_8-CONH$_2$ (**45**), CF-G-Tat(48-60)-CONH$_2$ (**42**) and CF-G-RQI-KIW-FQN-RRM-KWK-K-CONH$_2$ (**43**) recorded in PBS at pH 7.4, at concentrations of 70 µM and at 37°C; b) CD spectra of poly-L-lysine in the α-helix, β-sheet and random coil conformations (from reference [215a]).

3.1.4 Evaluation of the cellular uptake

To investigate the cell-penetrating properties of the cationic oligoprolines, biological studies with human cancer cell lines were performed. The relative uptake of the CPPs was determined by flow cytometry (3.1.4.1). In the first biological experiments, HeLa cells (human cervical adenocarcinoma) were mainly used, due to the robustness and easy handling of this cell line. In addition, flow cytometry experiments were accomplished with HT-29 (human colon adenocarcinoma), PC-3 (human prostate adenocarcinoma), and MCF-7 (human breast adenocarcinoma) cells (Fig. 32). The cell lines used in our studies are well-known adherent cell lines, which were early identified, characterized and are routinely cultivated in laboratories worldwide (see 5.2.1.1).
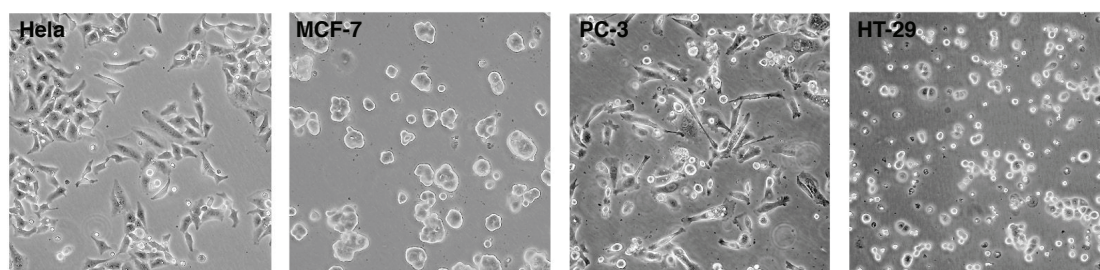
Figure 32: Microscopy images of the four different cell lines used in the flow cytometry studies (images released by the American Type Culture Collection (ATCC)).[216]

Confocal microscopy with non-fixed HeLa cells was used to analyze the intracellular localization of the oligoproline-based CPPs (e.g. Fig. 33) (3.1.4.2). In all biological experiments a sample with non-treated cells was used as a negative control, as well as cells that were incubated with 5(6)-carboxyfluorescein. Tat(48-60) (**42**), penetratin (**43**), and several oligoarginines (**44**, **45**, **46**, **47** and **48**) were used as reference CPPs.
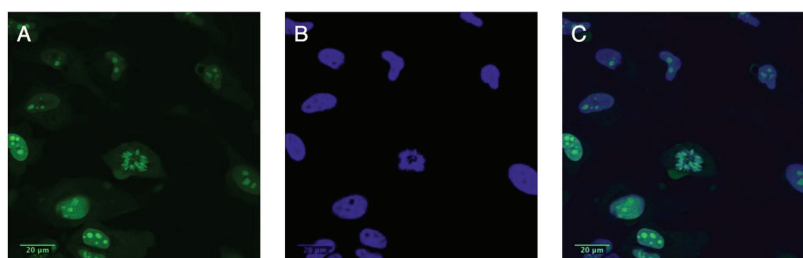
Figure 33: Confocal images of HeLa cells incubated with CF-G-PPP-ZZZ-ZZZ-CONH$_2$ (**29**) at a peptide concentration of 15 μM for 1 h at 37°C (A); Counter-staining with the nucleus marker Hoechst33342 (B) and overlay (C).

3.1.4.1 Quantification of the cellular uptake *via* flow cytometry

Flow cytometry is a method that allows to identify and count cells.[217] It is routinely used to purify and differentiate between different types of white blood cells (leukocytes) for the diagnosis of diseases such as leukemia.[217] Monochromatic light from a laser beam is directed to a hydrodynamically focused cell suspension. The light passing through the cell suspension, in line with the laser beam, is detected and gives information about the relative size of the cells (forward scatter or FSC), whereas the light reflected in a 90° angle to the original laser beam is used to gain information about the granularity of the cells (side scatter or SSC). Thus, cell populations can be identified and analyzed. Events corresponding to cellular debris can be removed by gating on FSC and SSC. Additionally, cells can be detected by their fluorescence and counted. In our experiments CPPs labeled with 5(6)-carboxyfluorescein were detected by excitation at 488 nm. A total of three times 10 000 cells per sample was counted. Each sample was run in triplicate and was repeated three times within one week. Non-treated control cells were analyzed to determine background and auto-fluorescence levels of the cells. To distinguish between living and dead cells propidium iodide (PI), a dye to stain dead cells, was used. Results are illustrated as the mean cellular fluorescence and errors are indicated as standard deviation (SD) of the three days of experiments.

One day before the experiment 100 000 cells, suspended in 10% DMEM, were seeded into 24-well plates and allow to adhere overnight. After 24 h culture medium was removed, cells were washed with PBS and incubated with the CPP solutions in 1% DMEM at different concentrations (5, 10 and 25 μM) and incubation times (1 and 1.5 h). Afterwards cells were washed several times with Ca^{2+}- and Mg^{2+}-deficient PBS and incubated with trypsin-EDTA. Cells were washed again and re-suspended in a solution of PI and ethylenediaminetetraacetic acid (EDTA) in PBS, respectively, at 4 °C. EDTA was added to avoid aggregation of the cells, since it complexes Ca^{2+} ions that are necessary for cell adhesion. The cell suspensions were placed in FACS tubes and kept on ice prior to analysis.

Initially a control experiment was performed, to prove that the fluorophore 5(6)-carboxyfluorescein is actually delivered by the CPPs and an influx mediated through membrane disruption or pore formation associated with the peptide treatment can be excluded. Towards this goal, HeLa cells were incubated with 5(6)-CF alone, 5(6)-CF covalently attached to a CPP at the N-terminus *via* a glycine spacer, CF-G-PPP-ZZZ-ZZZ-CONH$_2$ (**29**), and the acetylated peptide Ac-PPP-ZZZ-ZZZ-CONH$_2$ (**68**) in a mixture with 5(6)-CF (Fig. 34).
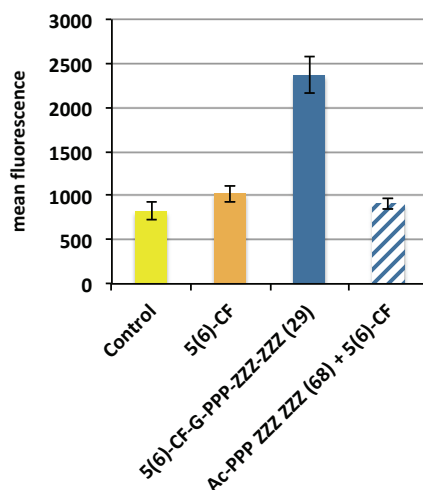
Figure 34: HeLa cell uptake of 5(6)-CF (orange), CF-G-PPP-ZZZ-ZZZ-CONH$_2$ (**29,** blue) and Ac-PPP-ZZZ-ZZZ-CONH$_2$ (**68**) together with 5(6)-CF (blue, shaded) at 25 µM for 1.5 h at 37°C. Control cells (yellow) were not treated with compounds.

The obtained quantification of the cellular uptake *via* flow cytometry revealed a significant mean fluorescence of the CF-G-PPP-ZZZ-ZZZ-CONH$_2$ (**29**) treated cells compared to the non-treated control cells, as well as to the cells treated with fluorophore alone and the ones incubated with control Ac-PPP-ZZZ-ZZZ-CONH$_2$ (**68**) and 5(6)-CF. This experiment clearly demonstrates that the detected fluorescence is not an artifact caused by an influx of the dye due to membrane disruption or pore formation through the CPPs.

In the following sections, the results of our flow cytometry experiments with different subtypes of the oligoproline-based CPPs are presented. Uptake into cells was observed with all oligoproline-based CPPs. The peptides with an alternating arrangement of functionalized proline residues, bearing either (4*S*)Amp (U) or (4*S*)Gup (Z) and unfunctionalized proline residues (Pro, P), will be presented first and the influence of ammonium versus guanidinium moieties on our system will be discussed. The aspect of chain lengths will be initially addressed in this section (3.1.4.1.1), but further investigated with the peptides of the following sections. Secondly, the results of the peptides carrying an *en bloc* arrangement of (4*S*)Gup, (4*R*)Gup (X) and Pro are given and compared to the alternating system (3.1.4.1.2), followed by the investigation of oligoproline-based CPPs entirely consisting of (4*S*)Gup residues (3.1.4.1.3). A brief overview of the results obtained with P. Raschle during his master thesis on D-oligoproline-based CPPs in comparison to the according L-analogs of this thesis, are given in section 3.1.4.1.4. Finally, the cellular uptake of the CPPs in different cells lines is illustrated (3.1.4.1.5).

3.1.4.1.1 *Influence of the ammonium versus the guandidinium groups*

A series of six peptides with an alternating pattern of cationic moieties directly attached to the backbone of the PPII helix was investigated, to address the effect of ammonium versus guanidinium groups on the cellular uptake of our system. The peptides were bearing either (4*S*)Amp (U) or (4*S*)Gup (Z) at every first and third position and unfunctionalized proline residues Pro (P) at every second position of the repeating unit. Furthermore, the influence of the chain length on the cellular uptake was addressed. The peptides were synthesized as 7-, 10- and 13-mers (including the glycine spacer):

20	CF-G-UPU-UPU-CONH$_2$	**23**	CF-G-ZPZ-ZPZ-CONH$_2$
21	CF-G-UPU-UPU-UPU-CONH$_2$	**24**	CF-G-ZPZ-ZPZ-ZPZ-CONH$_2$
22	CF-G-UPU-UPU-UPU-UPU-CONH$_2$	**25**	CF-G-ZPZ-ZPZ-ZPZ-ZPZ-CONH$_2$

The obtained data revealed that the CPPs bearing amino proline residues are less effective in cell penetration compared to those bearing guanidino proline (Fig. 35). An increase of cellular uptake with increasing chain length, and thus cationic moieties, was observed for both sets of peptides. These general trends observed for our system are consistent with literature and were also observed for CPPs consisting of arginine (Arg, R) or lysine (Lys, K), but also for other proline-based systems.[114, 139a]
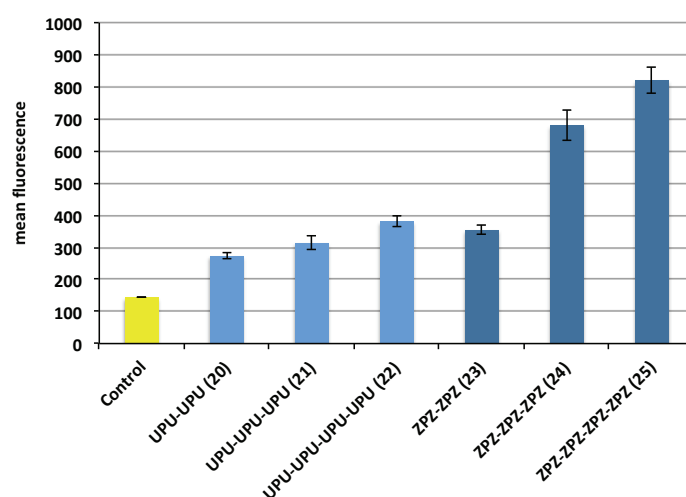
Figure 35: HeLa cells treated with CPPs of different chain length, containing (4*S*)Amp (U, light blue) and (4*S*)Gup (Z, dark blue), respectively. Cells were incubated at 5 μM for 1.5 h at 37°C. Control cells (yellow) were not treated with peptides.

The successive increase in cellular uptake for the amino proline-rich peptides **20**, **21**, and **22** with increasing chain length shows relatively small relative differences and is in the range of 1.2-fold steps. In the case of the guanidino proline containing CPPs **23**, **24**, and **25** we observed also a 1.2-fold increase in the cellular uptake from the 10-mer to the 13-mer, but a more significant 1.9-fold increase from the 7-mer to the 10-mer, indicating a non-linear behavior and suggesting a certain bottom limit of cationic moieties for an efficient uptake. Inspired by these results, we continued our further investigations only with guanidino proline-rich peptides, focusing on peptides containing at least six guanidinium moieties. Another aspect we were interested in was the influence of the geometrical positioning of the guanidinium moieties along the helical scaffold. The influence of the absolute configuration at C(4) was envisioned to be explored as well. To address these questions, CPPs with an *en bloc* arrangement of cationic moieties in contrast to the alternating system were synthesized and are presented in the following section.

3.1.4.1.2 *Influence of the arrangement of cationic moieties along the helical scaffold*

The influence of the geometrical arrangement of the cationic residues along the PPII helix as well as the change in all over charge density was investigated by comparison of peptides of the alternating system (**24**, **25**, and **26**) with peptides bearing a row of neighboring guanidino prolines and a row of unfunctionalized prolines (**29**, **30**, **31**, **34**, and **35**). Within this experiment the influence of the absolute configuration at C(4) was also investigated by insertion of either (4*S*)- or (4*R*)-configured Gup (Z and X, respectively) into the peptides:

24	CF-G-ZPZ-ZPZ-ZPZ-CONH$_2$	**26**	CF-G-XPX-XPX-XPX-CONH$_2$
29	CF-G-PPP-ZZZ-ZZZ-CONH$_2$	**34**	CF-G-PPP-XXX-XXX-CONH$_2$
30	CF-G-ZZZ-ZZZ-PPP-CONH$_2$	**35**	CF-G-XXX-XXX-PPP-CONH$_2$

25	CF-G-ZPZ-ZPZ-ZPZ-ZPZ-CONH$_2$
31	CF-G-ZZZ-ZZZ-ZZP-PPP-CONH$_2$

Furthermore, we were interested in the relative uptake of our CPPs in comparison to the well-established Tat(48-60) peptide (**42**). A fully unfunctionalized oligoproline **50** was also examined, to explore the uptake of the blank backbone itself and estimate the influence of the cationic charges:

42   CF-G-RKK-RRQ-RRR-PPQ-CONH$_2$

50   CF-G-PPP-PPP-PPP-CONH$_2$

The obtained data showed a similar degree of cell penetration for the four examined peptides with an *en bloc* arrangement (**29**, **30**, **34**, and **35**) and both peptides with an alternating pattern (**24** and **26**) (Fig. 36). Only the peptide CF-G-PPP-ZZZ-ZZZ-CONH$_2$ (**29**) showed a slightly higher uptake compared to the other oligoproline-based CPPs with the same chain length, which is considered to be in the range of the deviation. The uptake of the unfunctionalized oligoproline is in the range of the fluorophore 5(6)-CF. The reference peptide Tat (48-60) (**42**) showed a clearly higher uptake than the oligoproline-based peptides with six cationic moieties. This higher uptake is presumably due to the additional two positively charged amino acids of the 13-mer **42**, bearing six arginines and two lysines.
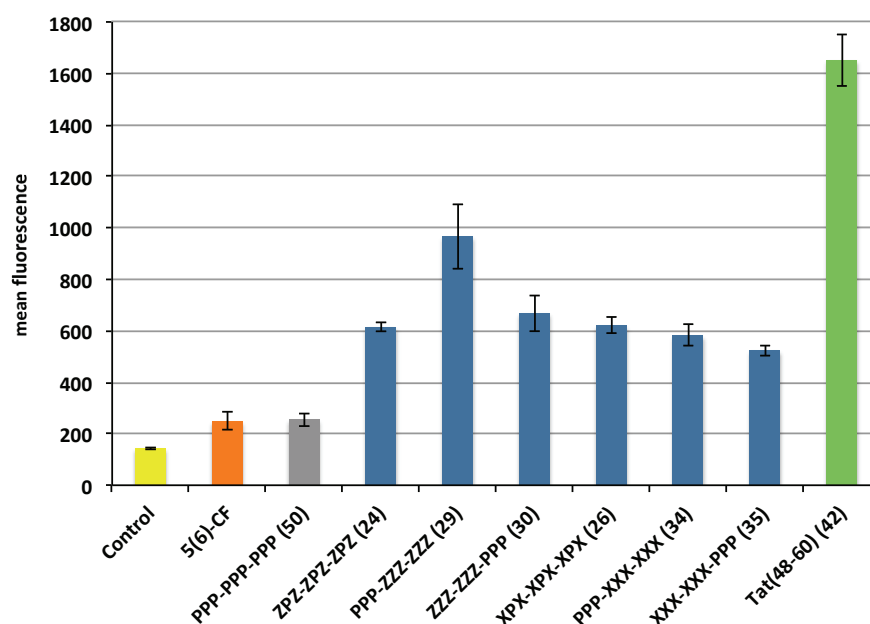
Figure 36: HeLa cells treated with oligoproline-based CPPs, containing (4*S*)Gup and (4*R*)Gup (Z and X, respectively, dark blue). The fully unfunctionalized oligoproline (grey) and the reference peptide Tat(48-60) (green) were measured for comparison. Cells were incubated at 5 µM for 1 h at 37°C. Control cells (yellow) were non-treated or incubated with 5(6)-CF (orange).

A comparison of CF-G-ZPZ-ZPZ-ZPZ-CONH$_2$ (**24**) and CF-G-ZZZ-ZZZ-PPP-CONH$_2$ (**30**) with the longer chained peptides CF-G-ZPZ-ZPZ-ZPZ-ZPZ-CONH$_2$ (**25**) and CF-G-ZZZ-ZZZ-ZZP-PPP-CONH$_2$ (**31**) at a higher peptide concentration of 10 µM showed again a comparable uptake for peptides with the same chain length and the same amount of

cationic moieties along the helical backbone (Fig. 37). The higher peptide concentration was chosen for this experiment, to test whether the differences in the cellular uptake are more evident at 10 μM. Generally, the previously observed enhancement of the cellular uptake with increasing chain lengths at 5 μM was observed in a greater extend than for the concentration of 10 μM. The difference for the 13-mers is estimated to be less significant in consideration of the biological deviations of the experiment with CF-G-ZPZ-ZPZ-ZPZ-ZPZ-CONH$_2$ (**25**). The other two 13-mers CF-G-ZZZ-ZZZ-ZZP-PPP-CONH$_2$ (**31**) and Tat (48-60) (**42**), bearing eight positively charged residues each, showed a comparable uptake.
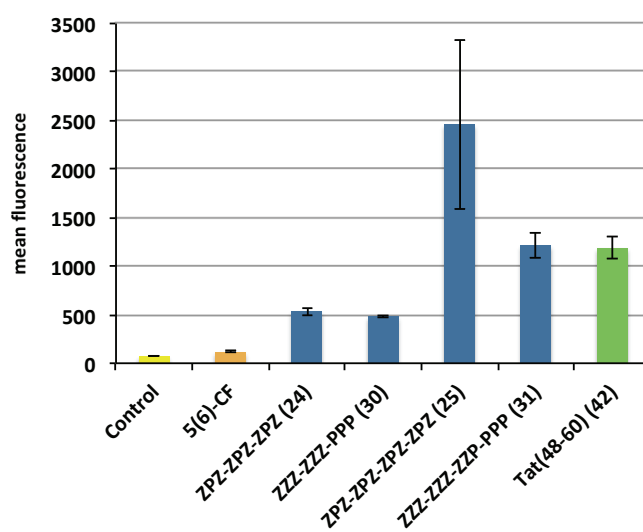
Figure 37: HeLa cells treated with CPPs with an alternating or an *en bloc* pattern of functionalized moieties in direct comparison. Cells were incubated at 10 μM for 1 h at 37°C.

These findings suggest that the exact geometrical arrangement of the cationic moieties along the helical scaffold does not influence the cellular uptake of our system as it was observed for certain foldamers.[144a, 205a] Furthermore, the absolute configuration at C(4) as well as the positioning of the cationic charges either at the C- or the N-terminus of the peptides do not influence the internalization (Fig. 36). The similar uptake of peptides bearing the block of cationic charges, either at the N-terminus or the C-terminus further suggests that the close proximity of the charges to the N-terminally attached fluorophore does not affect the cell-penetrating properties of the according peptides or alter the fluorescence intensity of 5(6)-carboxyfluorescein.

3.1.4.1.3   *Uptake of peptides entirely composed of (4S)Gup*

Since the cellular uptake of the oligoproline-based CPPs proved to be unaffected by the exact positioning of the unfunctionalized proline moieties, we were interested to test the properties of peptides, consisting only of guanidino proline residues. In addition the effect of the chain length was also examined within this series of CPPs (**38**, **39**, **40**, and **41**). As references we used the according oligoarginines (**44**, **45**, **46**, and **47**), Tat(48-60) (**42**), and penetratin (**43**):

38	CF-G-ZZZ-ZZZ-CONH$_2$	**44**	CF-G-RRR-RRR-CONH$_2$
39	CF-G-ZZZ-ZZZ-ZZ-CONH$_2$	**45**	CF-G-RRR-RRR-RR-CONH$_2$
40	CF-G-ZZZ-ZZZ-ZZZ-Z-CONH$_2$	**46**	CF-G-RRR-RRR-RRR-R-CONH$_2$
41	CF-G-ZZZ-ZZZ-ZZZ-ZZZ-CONH$_2$	**47**	CF-G-RRR-RRR-RRR-RRR-CONH$_2$

42	CF-G-RKK-RRQ-RRR-PPQ-CONH$_2$
43	CF-G-RQI-KIW-FQN-RRM-KWK-K-CONH$_2$

Our studies revealed a similar degree of uptake for the peptides CF-G-Z$_6$-CONH$_2$ (**38**) and CF-G-R$_6$-CONH$_2$ (**44**), which were both slightly lower compared to Tat(48-60) (**42**), containing two more cationic charges at lysines (Fig. 38). A dramatic increase was observed for the longer peptides CF-G-Z$_8$-CONH$_2$ (**39**) and CF-G-R$_8$-CONH$_2$ (**45**). Peptide **39** showed the highest cellular uptake in this experiment. A 1.6-fold higher uptake compared to its more flexible counterpart CF-G-R$_8$-CONH$_2$ (**45**), a 2-fold higher uptake compared to penetratin (**43**), and an 11-fold higher uptake compared to Tat(48-60) (**42**) was detected in these first studies. Although there was a noticeable deviation in the experiment for **39**, these results demonstrate the potential of our guanidino proline-based CPPs for efficient penetration of HeLa cells at least in the range of the according oligoarginines, the most potent encodable CPPs reported.[98b]
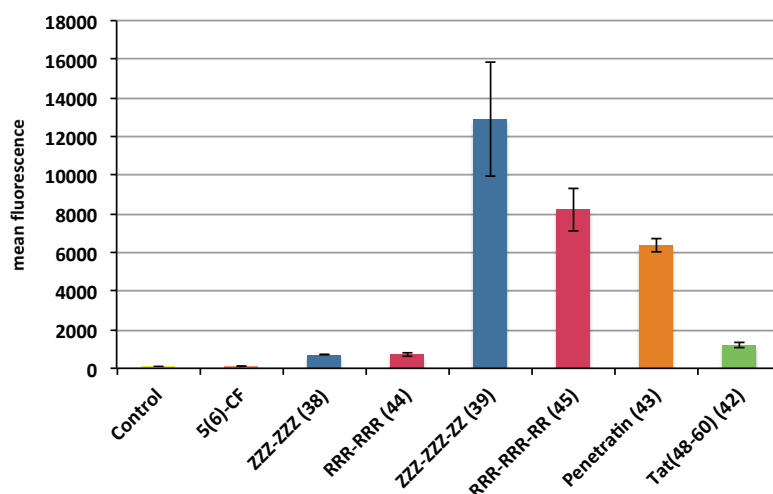
Figure 38: HeLa cells were treated with oligoproline-based CPPs composed of (4*S*)Gup (Z, blue) and according oligoarginines (red) of different chain lengths, compared with the reference peptides penetratin (orange) and Tat(48-60) (green). Cells were incubated at 10 μM for 1 h at 37°C.

The cellular uptake of the reference peptides relative to each other, obtained in our studies, are in good agreement with literature. According relative uptakes of the reference peptides Tat(48-60), octaarginine, and penetratin on HeLa cells were reported by Schepartz *et al.*[100, 135] A similar enhancement for the uptake of hexaarginine compared to octaarginine, was reported by Wender *et al.* using Jurkat cells.[98b, 114] However, comparisons should be taken with care, since differences in variables, related to the experimental procedures used by different groups, can influence the cellular uptake. These variables can include the attached fluorophore or cargo, the concentration of CPPs, cell-type, cell density, stage of cell cycle, incubation time, and final end point or readout of the applied method.

With these results in hands, the question arises whether longer peptides entirely consisting of (4*S*)Gup (Z) will have an even higher cellular uptake. Unfortunately, the syntheses of $CF-G-Z_n-CONH_2$ with n = 10 and 12 (**40** and **41**) proved to be difficult and both compounds were only isolated as mixtures with the according sideproduct containing one ammonium instead of a guanidinium moiety within the peptides (3.1.2.1.4). Thus a comparison with the according oligoarginines **46** and **47** is difficult. The results from the flow cytometry experiments showed a lower uptake for both functionalized oligoprolines **40** and **41** in comparison to **46** and **47** (Fig. 39). Since the enhancement of the cellular uptake is especially dramatic with increasing chain length,

starting from six up to twelve guanidino moieties, the peptides **40** and **41** suffer from the lack of full functionalization.
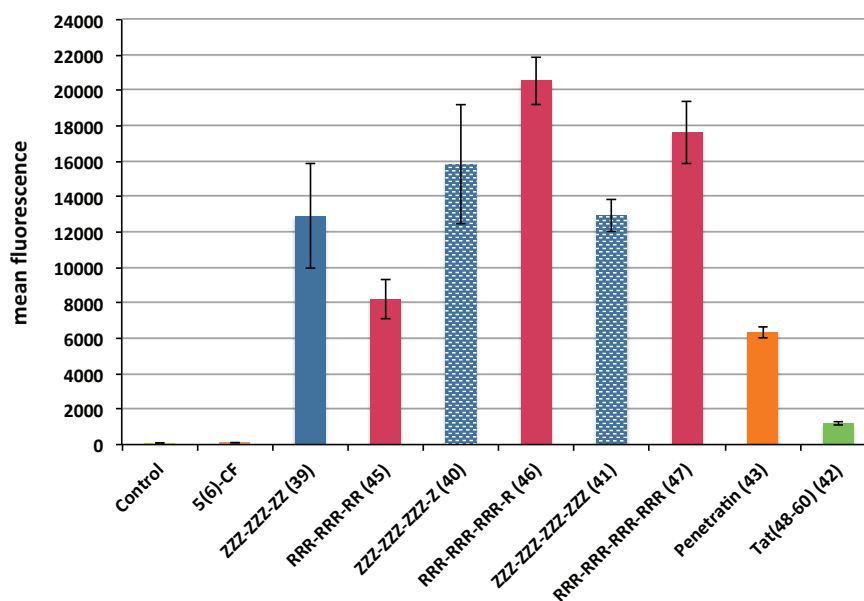
Figure 39: HeLa cells treated with guanidine proline-based CPPs (blue) compared to according oligoarginines (red) at different chain lengths. Cells were incubated at 10 μM for 1 h at 37°C.

In our experiment the uptake of the oligoarginines rises from R_8 (**45**) to R_{10} (**46**), whereas the uptake of R_{10} and is more than doubled compared to R_8. This observation is consistent with investigations on these peptides reported by Schepartz *et al.* on HeLa cells. Only a very minor increase was detected by Schepartz and co-workers for the cellular uptake of R_{10} (**46**) compared to R_{12} (**47**) which is not reflected in our studies.[100] However, considering the variance of the biological experiment, the uptake of the oligoarginines **46** and **47** relative to each other can be interpreted at least to be in a similar range.

For the syntheses of the longer chained guanidino proline-based CPPs in future, a guanidino proline building block with a sterically less demanding protecting group could lead to success by improving the coupling efficiency of this amino acid derivative in SPPS (see discussion in chapter 3.1.2.1.4). Currently members of the Wennemers group are working on the synthesis of such a building block. With the pure cationic oligoprolines, a re-evaluation of the cellular uptake of the peptides **40** and **41** compared to the according oligoarginines **46** and **47** can be performed.

3.1.4.1.4   Influence of the helix chirality

With the aim to address the question, if chirality plays a role in the cellular uptake of our CPPs we envisioned a series of cationic D-oligoprolines. Since D-oligoprolines differ in the absolute configuration at Cα from their L-oligoproline counterparts, they exhibit an inverted helix chirality as demonstrated by CD spectroscopic analysis (3.1.3). In this regard we created peptides bearing either D-(4*S*)Gup (z) or D-(4*R*)Gup (x), being the enantiomers of according cationic L-oligoprolines. As a platform to test the influence of chirality we chose to examine a series of 10-mers. The D-analogs have been synthesized and evaluated during the master thesis of P. Raschle, affiliated with this project:[206]

27	CF-G-zpz-zpz-zpz-CONH$_2$		**28**	CF-G-xpx-xpx-xpx-CONH$_2$
32	CF-G-ppp-zzz-zzz-CONH$_2$		**36**	CF-G-ppp-xxx-xxx-CONH$_2$
33	CF-G-zzz-zzz-ppp-CONH$_2$		**37**	CF-G-xxx-xxx-ppp-CONH$_2$

The cationic D-oligoprolines were compared with the according L-analogs (**24**, **26**, **29**, **30**, **34**, and **35**). Furthermore, a comparison with the following unfunctionalized D- and L-oligoprolines and reference CPPs was made:

51	CF-G-ppp-ppp-CONH$_2$		**49**	CF-G-PPP-PPP-CONH$_2$
52	CF-G-ppp-ppp-ppp-CONH$_2$		**50**	CF-G-PPP-PPP-PPP-CONH$_2$
48	CF-G-rrr-rrr-CONH$_2$		**44**	CF-G-RRR-RRR-CONH$_2$

42	CF-G-RKK-RRQ-RRR-PPQ-CONH$_2$
43	CF-G-RQI-KIW-FQN-RRM-KWK-K-CONH$_2$

The flow cytometry studies revealed that all investigated cationic D-oligoprolines penetrate into HeLa cells with an enhanced efficiency compared to unfunctionalized L-and D-oligoprolines **49, 50, 51** and **52**, whose uptakes were in the range of the control cells treated with 5(6)-CF (Fig. 40).
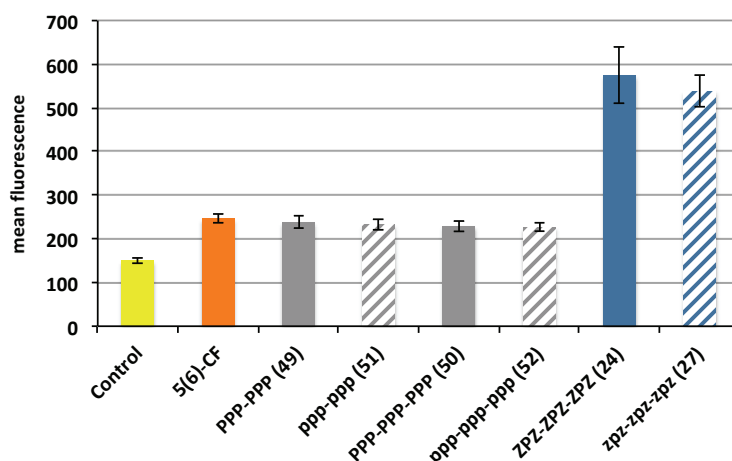
Figure 40: HeLa cells treated with unfunctionalized L- and D-oligoprolines of different chain lengths (P and p, grey and grey shaded) in comparison to cationic L- and D- oligoprolines of the alternating system (dark blue and dark blue shaded). Cells were incubated at 5 µM for 1 h at 37°C.

Interestingly the examined cationic D-oligoprolines showed a similar cellular uptake as their L-oligoproline counterparts (Fig. 41). This observation gives a valuable hint towards their way of entering cells. For a receptor-mediated pathway a respond to a binding site of a specific receptor is required, which would occur just for one enantiomer of a certain CPP due to the individual geometry of the binding pocket. The binding of this specific enantiomer to the receptor would alter its cellular uptake compared to the other enantiomer. Such a difference in the cellular uptake of enantiomeric peptides was not observed in our studies. This suggests an internalization of the peptides *via* a receptor independent pathway. Furthermore it can be assumed that for the majority of the peptides investigated in this series, no significant differences in binding towards heparan sulfate proteoglycans (HSPGs) on the surface of HeLa cells is occurring. Only the enantiomers CF-G-PPP-ZZZ-ZZZ-CONH$_2$ (**29**) and CF-G-ppp-xxx-xxx-CONH$_2$ (**36**) show a slightly enhanced uptake compared to the other peptides, which is considered to be due to the biological deviation of the experiement. To clarify if this observation is due to the biological error of the experiment or caused by association of the peptides with components on the extracellular membrane, binding affinity studies

could be performed. The involvement of a receptor is in this case excluded, since the peptides with the slightly enhanced uptake are enantiomers to each other.
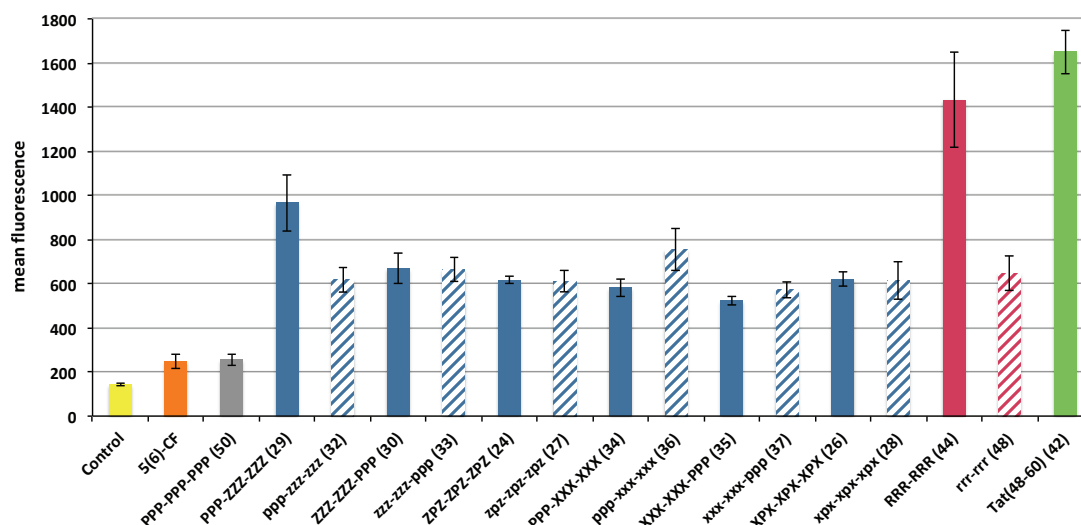
Figure 41: HeLa cells treated with L- and according D-oligoproline-based CPPs, containing (4*S*)Gup and D-(4*S*)Gup (Z and z, blue and blue shaded), (4*R*)Gup and D-(4*R*)Gup (X and x, blue and blue shaded) and only unfunctionalized proline (P, grey) respectively. Cells were incubated at 5 μM for 1 h at 37°C.

In addition, it was observed also in the case of the D-oligoproline-derived CPPs that peptides displaying an alternating pattern of cationic moieties show similar uptake as peptides with an *en bloc* arrangement, further supporting that the geometrical arrangement of the cationic moieties does not influence the internalization.

The Tat (48-60) peptide (**42**) showed a higher uptake than the examined L- and D-oligoproline-based CPPs, as it has been described in the previous section, presumably due to the additional two positive charges of Tat(48-60) bearing six arginines and two lysines. The analyzed D-hexaarginine (**48**) shows a similar uptake as the functionalized L- and D-oligoprolines. Remarkably, the L-hexaarginine (**44**) exhibited a dramatically higher cellular uptake than its D-analog (**48**). A possible explanation might be differences in the binding affinities of the peptides towards HSPGs on the cell surface of HeLa cells. This hypothesis is supported by investigations of the cellular uptake of R_9 and r_9 in HeLa cells, performed by Brock *et al*.[140a] They show a 21% higher uptake of R_9 compared to r_9 in HeLa cells, demonstrating a more efficient uptake for a L- compared to a D-oligoarginine. However, a comparison has to be taken with care, since the methodology of uptake detection differs. To quantify the intracellular fluorescence, Brock and co-workers developed a technique based on fluorescence-correlation (FSC) in

cell lysate. Differences in the uptake of the L- and D- oligoarginines were furthermore rationalized by ITC studies, showing an increased binding affinity of r_9 towards HSPGs on the cell surface than R_9, for cells containing significant amounts of HSPGs on the plasma membrane such as HeLa cells.[140a]

In contrast, investigations by Wender showed an inverted behavior of the L- and D-oligoarginines.[98b] However, direct comparison is also in this case difficult since the uptake was evaluated using a different cell type (Jurkat cells, human T-cell line), which can significantly alter the relative uptake of the CPPs, as will be demonstrated in the following section. Furthermore, the Jurkat cells were incubated at a higher level of fetal calf serum (FCS, 2%) in PBS, in contrast to the conditions used for our experiment with FCS (1%) in DMEM. A higher amount of FCS means also a higher degree of serum proteins, which are capable of degrading L-oligoarginines, as it will be shown in chapter 3.1.5 for human blood serum, whereas D-oligoarginines can be expected to be stable. Thus the influence of FCS in the culture medium during peptide incubation might alter the uptake of the CPPs and makes a comparison difficult as well. It also has been shown that intracellular degradation[152e, 218] and re-export[97b] affects the intracellular retention time of CPPs. These differences in the uptake of CPPs composed of natural amino acids can be excluded for our L- and D-oligoproline based CPPs, since no stability differences between the L-and D-analogs of our system are evident (see 3.1.5).

3.1.4.1.5 *Cell line dependency*

Since it has been generally shown that the cell-penetrating properties of CPPs vary for different cell lines,[133a, 219] we next tested the cell line specificity of our oligoproline-based CPPs. Thus we performed flow cytometry experiments with a selection of representative cationic oligoprolines, including peptides with an alternating and an *en bloc* pattern of (4*S*)- or (4*R*)Gup residues, as well as peptides with different chain lengths and D-analogs (**23**, **24**, **25**, **29**, **30**, **32**, **34**, **36**, **38**, and **39**). The unfunctionalized oligoproline **50** was as well tested. Furthermore, we examined several oligoarginines (**44**, **45**, and **48**) as reference peptides, as well as Tat(48-60) (**42**) and penetratin (**43**). For the investigations we used four different human cancer cell lines: cervical cancer (HeLa), breast cancer (MCF-7), prostate cancer (PC-3) and colon cancer (HT-29). Experiments were performed as described before for all cell lines.
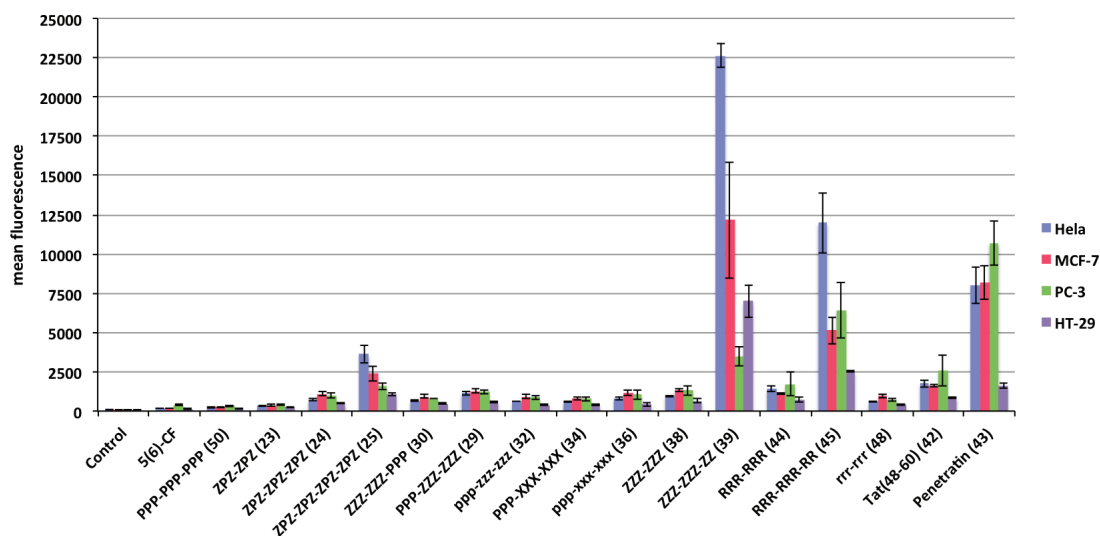
Figure 42: Overview of the cellular uptake of a selection of oligoproline-based CPPs, including L- and D-analogs as well as reference peptides in different cell lines. Cells were incubated at 10 µM 37°C for 1 h.
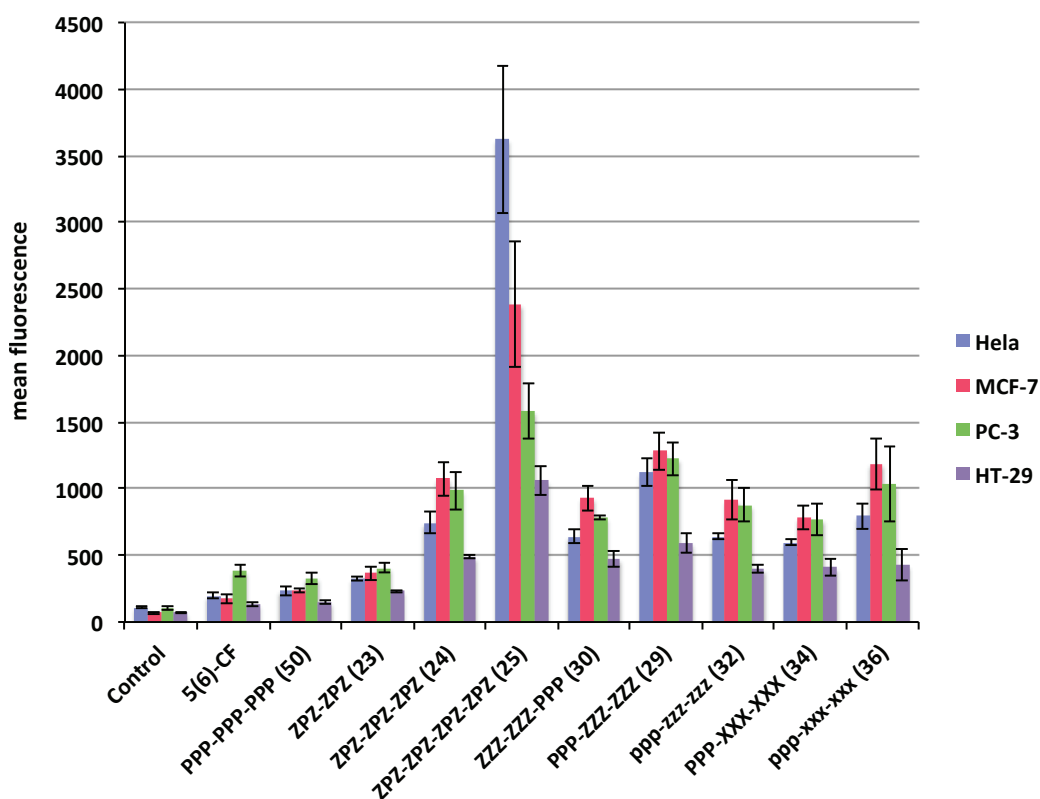
Figure 43: Zoom on the cellular uptake of a selection of oligoproline-based CPPs, including L-and D- analogs. Cells were incubated at 10 µM 37°C for 1 h.
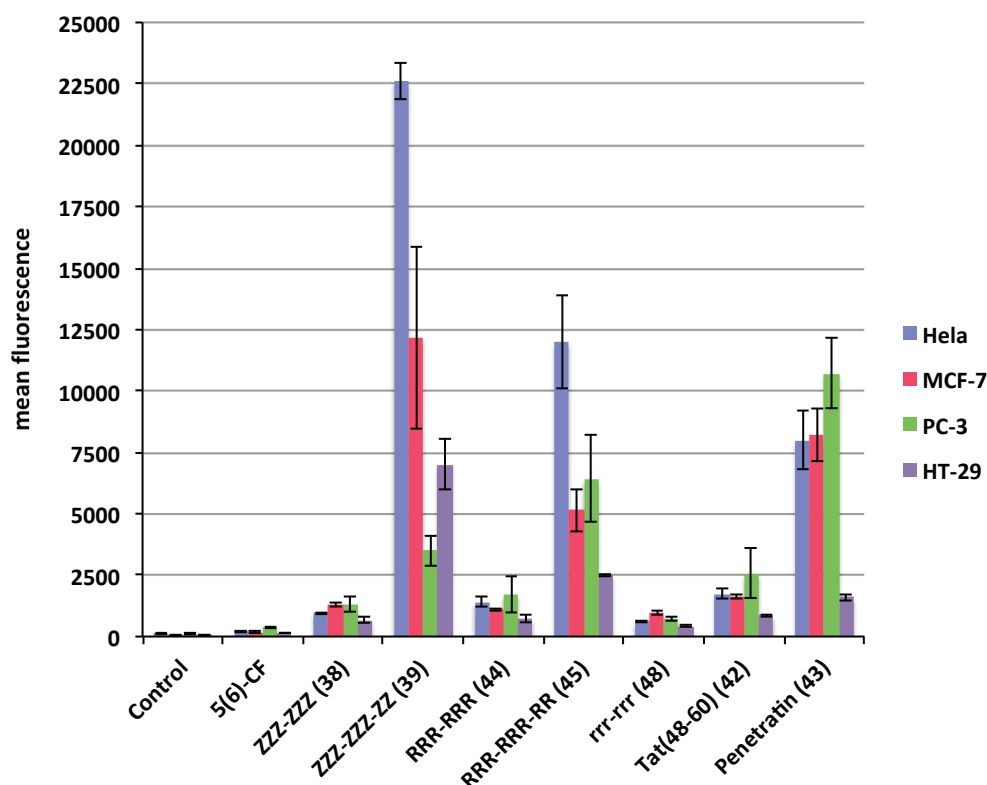
Figure 44: Zoom on the cellular uptake of oligoproline-based CPPs with an *en bloc* arrangement of cationic moieties and reference peptides. Cells were incubated at 10 μM 37°C for 1 h.

The obtained data showed a significantly different cellular uptake of the CPPs for the investigated four cell lines (Fig. 42), whereas the relative distribution of the uptake showed a similar tendency for HeLa, MCF-7 and HT-29, but differed for PC-3 cells. Generally, oligoproline-based CPPs are most efficiently internalized into HeLa cells and to a less extend into MCF-7 and HT-29 cells. The most potent CPPs in these three cell lines were CF-G-Z_8-$CONH_2$ (**39**), followed by CF-G-R_8-$CONH_2$ (**45**) and penetratin (**43**). In PC-3 cells penetratin showed the highest uptake, followed by octaarginine **45** and the guanidino proline containing CPP **39**, showing a reversed tendency in comparison to the other cell lines. The results of our study suggest a dependency of the internalization on the unique characteristics of the cell lines, such as membrane composition or potential. These differences in the uptake behavior could be exploited in future investigations to support a selective targeting of a certain cell type. For example cell specificity in contrast to non-cancerous cells could be explored.

In summary, the flow cytometry studies in this chapter demonstrated that CPPs bearing amino proline residues proved to be less effective in cell penetration compared to those containing guanidino proline, tested on HeLa cells. As expected, the cellular uptake is rising with increased chain lengths, and thus cationic moieties of the peptides. Comparisons made with oligoproline-based CPPs with an *en bloc* arrangement to those with an alternating pattern of cationic residues of the same chain lengths revealed that the exact geometrical positioning of the moieties does not influence the cellular uptake of our system. Investigations on functionalized D-oligoprolines compared to their L-analogs showed a similar cellular uptake for the enantiomers, which suggests an internalization of the peptides *via* a receptor independent pathway. Comparison to reference peptides showed an enhanced uptake of the peptides CF-G-ZPZ-ZPZ-ZPZ-ZPZ-CONH$_2$ (**25**) and CF-G-Z$_8$-CONH$_2$ (**39**) compared to Tat(48-60) (**42**). **39** is even surpassing the level of internalization of CF-G-R$_8$-CONH$_2$ (**45**) and penetratin (**43**) in HeLa, MCF-7 and HT-29 cells. In contrast, the relative distribution of the cellular uptake proved to be different in PC-3 cells. In this cell line the highest uptake was detected for penetratin (**43**), followed by octaarginine **45** and the eight guanidino proline containing peptide **39**. These results revealed a clear specificity of the oligoproline-based CPPs towards the tested cell lines. The high levels of cellular uptake of cationic oligoprolines, especially of the peptide **39**, constitute a promising basis for future applications as delivery vectors. As a next important step to characterize our oligoproline-based CPPs, we aimed to explore their intracellular localization.

3.1.4.2 Intracellular localization

To analyze where the CPPs are located after passing the cell membrane, we examined the cells after incubation with the peptides by confocal microscopy. In contrast to flow cytometry studies (3.1.4.1), confocal microscopy is not a quantitative method, but supplements the information gained from flow cytometry experiments. The intracellular localization of the CPPs generally depends on the specific nature of the CPP, but also on factors like concentration, incubation time, the cell line, and the experimental setup. HeLa cells were used for imaging, since the flow cytometry experiments in this thesis were mainly performed with this cell line.

We performed the imaging with live, non-fixed cells, since chemical fixation was shown to affect the intracellular distribution of the CPPs.[140c] Therefore a collection of oligoproline-based CPPs (**20**, **21**, **22**, **23**, **24**, **25**, **29**, **30**, **32**, **34**, **35**, **36**, **38**, **39**, and **50**) was examined. For the experiments 10,000 HeLa cells were seeded in 8-well plates and allowed to adhere overnight. The CPPs were incubated to the cells at different concentrations (5 and 15 µM) and incubation times (1 and 1.5 h) at 37°C. Then the cells were washed and incubated with Hoechst33342 for visualizing the nucleus. After several washing steps to assure that all membrane bound peptides were removed, the intracellular distribution was examined under an inverted confocal microscope. Non-treated cells and cells incubated with 5(6)-carboxyfluorescein at the same concentration as the peptides were used as negative controls in each experiment. Confocal images were taken at identical microscope settings. The images of a selection of representative CPPs (**24**, **29**, **32**, and **39**), including a peptide with an alternating pattern of cationic moieties, as well as an *en bloc* arrangement, bearing (4*S*)- or (4*R*)-configured guanidino proline and a D-analog, are presented and discussed in the course of this chapter. In addition, we will show images of two representative references Tat(48-69) (**42**) and R$_6$ (**44**). Furthermore, the intracellular localization of the reference peptides within literature will be discussed. However, also in the case of microscopy experiments, the comparison of results obtained by different laboratories is difficult and has to be taken with care.

The images obtained from the excitation at 488 nm (A) show the localization of the fluorescein-labeled peptides. Excitation at 543 nm (B) shows the nucleus marker Hoechst33342 within HeLa cells, whereas C represents the differential interference contrast (DIC) image, and D is the digital overlay. A punctuated pattern of fluorescence within the cytoplasm was observed for the reference peptide Tat(48-60) (**42**, Fig. 45), as well as for R_6 (**44**, Fig. 46), incubated to HeLa cells at 37°C and a peptide concentration of 5 μM for 1.5 h. Punctuated fluorescence can be an indication for endosomal localization, suggesting an endocytotic pathway, or a partial endosomal entrapment of the peptide. For Tat(48-60) (**42**) a weak nuclear localization was visible as well. However, the localization of Tat(47-57) at 5 μM and 30 min of incubation time, reported by Brock *et al.* showed no nucleus localization within HeLa cells, but only a punctuated pattern of fluorescence.[140a] 7 For R_9 and penetratin also a punctuated fluorescence was observed in their study.[140a] A similar behavior was found for octaarginine (R_8) incubated at 37°C and 10 μM to HeLa cells for 1 h by Futaki *et al.*, which also showed no uptake in the nucleus, but a punctuated fluorescence into the cytosol.[140c]
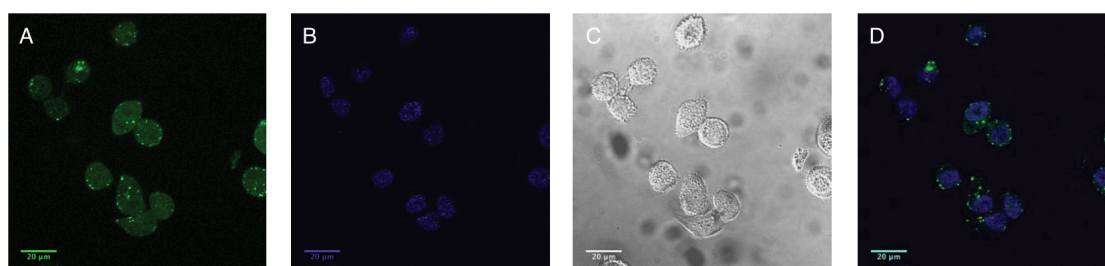
Figure 45: Confocal images showing HeLa cells incubated with CF-G-Tat(48-60)-CONH$_2$ (**42**) at 5 μM for 1.5 h at 37°C (A); Counter-staining with Hoechst33342 (B), DIC image (C) and overlay (D).
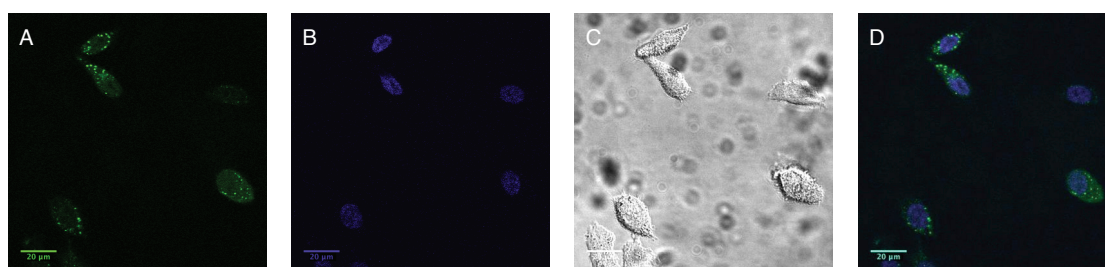
Figure 46: Confocal images showing HeLa cells incubated with CF-G-R$_6$-CONH$_2$ (**44**) at 5 μM for 1.5 h at 37°C (A); Counter-staining with Hoechst33342 (B), DIC image (C) and overlay (D).

---

7 Images of HeLa cells from literature are given in the appendix 6.7.

The oligoproline-based CPPs, investigated by Chmielewski and co-workers showed as well a punctuated cytoplasmic staining for each of the compounds in HeLa cells. Punctuated fluorescence can not only be an indication for endosomal localization,[220] but can also arise from the localization within mitochondria.[133b] In fact, the peptides developed by Chmielewski *et al.* demonstrated a high level of co-localization with the mitochondrial marker Mitotracker in HeLa cells at 5 µM. The mitochondrial targeting shows consistence with the structural and functional properties of these peptides, since the cationic charges drive them towards the mitochondria, as a response to the negative transmembrane potential. The hydrophobic leucine mimetics may facilitate the insertion of the peptides into the lipophilic mitochondrial inner membrane.[139c]

In contrast, the confocal microscopy images of our oligoproline-based CPPs revealed that all of them preferentially localize in the cell nucleus. The images of Fig. 47 and Fig. 48 show HeLa cells incubated with the peptides CF-G-ZPZ-ZPZ-ZPZ-CONH$_2$ (**24**) and CF-G-PPP-ZZZ-ZZZ-CONH$_2$ (**29**) at 5 µM concentration after 1.5 h of incubation time. The overlay (D) demonstrates clearly a nuclear localization of both peptides **24** and **29**. No punctuated fluorescence in the cytosol was observed under these conditions. In addition, the images show no difference in the intracellular distribution of the oligoproline-based CPPs with an alternating or an *en bloc* arrangement of the cationic moieties along the helical backbone.
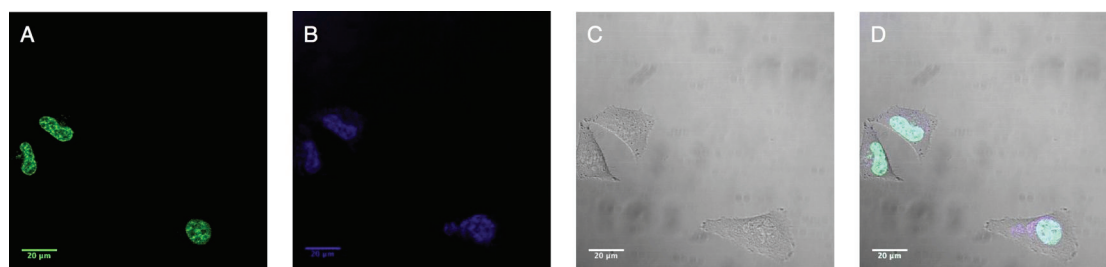
Figure 47: Confocal images of HeLa cells incubated with CF-G-ZPZ-ZPZ-ZPZ-CONH$_2$ (**24**) at 5 µM for 1.5 h at 37°C (A), Counter-staining Hoechst33342 (B), DIC image (C) and overlay (D).
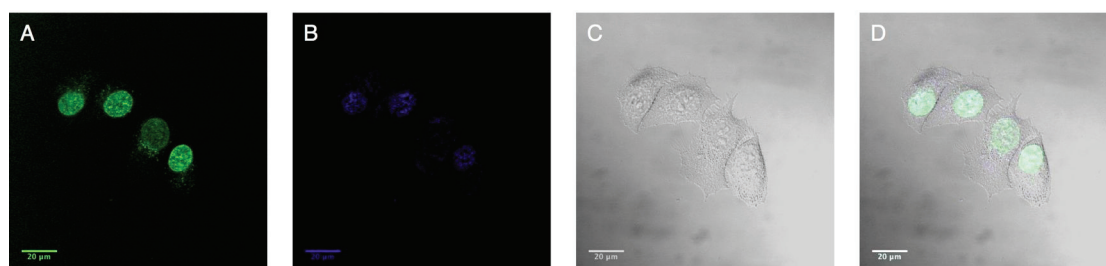
Figure 48: Confocal images of HeLa cells incubated with CF-G-PPP-ZZZ-ZZZ-CONH$_2$ (**29**) at 5 µM for 1.5 h at 37°C (A), Counter-staining Hoechst33342 (B), DIC (C) and overlay (D).

At a higher peptide concentration of 15 µM the peptides **24** and **29** are also localized in the nucleus. Remarkably, a particularly intensive staining of the nucleoli was observed under these conditions (Fig. 49 and Fig 50). CPPs composed of amino prolines showed a generally lower cellular uptake than their guanidinium functionalized counterparts (as it was also observed in flow cytometry studies, 3.1.4.1.1) and localization was hardly visible at the tested concentrations of 5 to 15 µM (not shown).
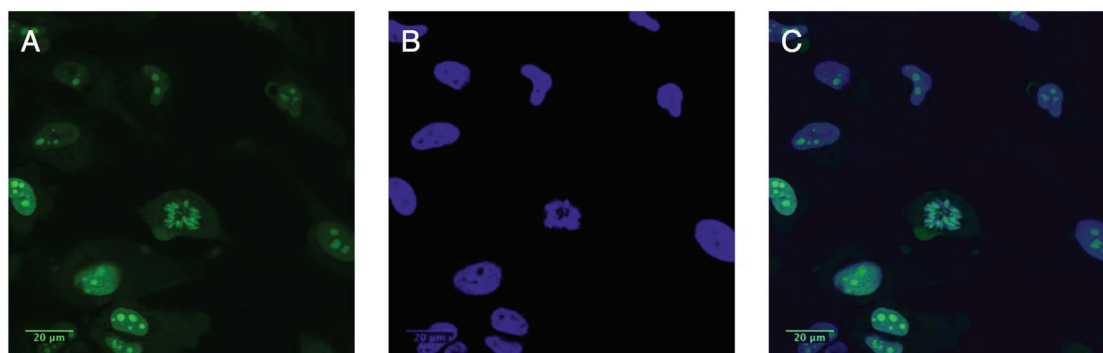
Figure 49: Confocal images of HeLa cells incubated with CF-G-ZPZ-ZPZ-ZPZ-CONH$_2$ (**24**) at 15 µM for 1 h at 37°C (A); Counter-staining with Hoechst33342 (B) and overlay (C).
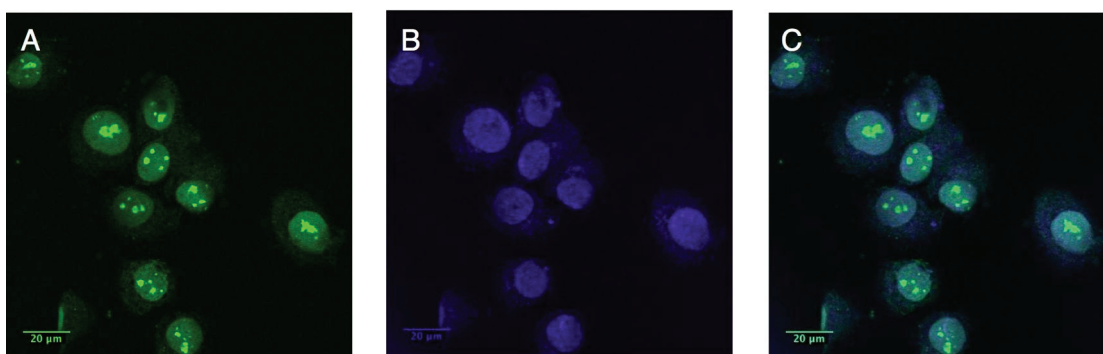
Figure 50: Confocal images of HeLa cells incubated with CF-G-PPP-ZZZ-ZZZ-CONH$_2$ (**29**) at 15 µM for 1 h at 37°C (A); Counter-staining with Hoechst33342 (B) and overlay (C).
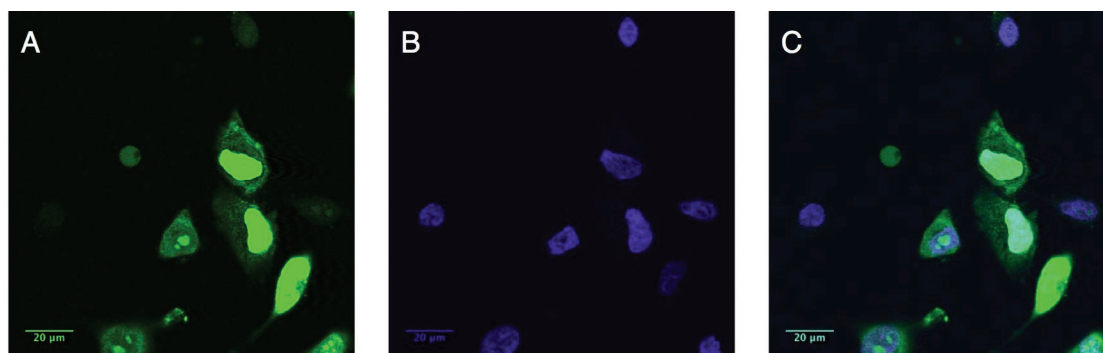
Figure 51: Confocal images of HeLa cells incubated with CF-G-Z$_8$-CONH$_2$ (**39**) at 15 µM and 1 h for 37°C (A); Counter-staining with Hoechst33342 (B) and overlay (C).

In the case of the peptide CF-G-Z_8-CONH$_2$ (**39**), which is entirely composed of guanidino proline, a slightly diffuse staining of the cytoplasm was visible, which might suggest passive diffusion as an additional pathway or release from endosomes (Fig. 51). The fluorescence intensities of the presented images (Fig. 49, 50, and 51) at the same conditions imply qualitatively a similar degree of cellular uptake for **24** and **29**, but an increase for **39**. In fact, quantification experiments *via* flow cytometry exhibited the same trend (3.1.4.1). The same intracellular localization observed for the cationic L-oligoprolines was examined for the D-analogs at 15 µM concentration after an incubation time of 1 h (Fig. 52).[206]
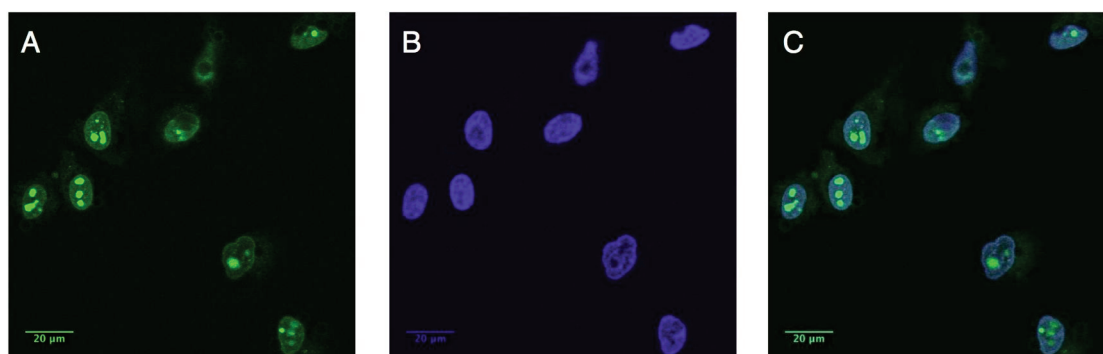
Figure 52: Confocal images of HeLa cells incubated with CF-G-ppp-zzz-zzz-CONH$_2$ (**32**) at 15 µM for 1 h at 37°C (A); Counter-staining with Hoechst33342 (B) and overlay (C).

Nuclear localization is not only depending on the cellular uptake through the plasma membrane, but also requires a sufficient endosomal escape or an alternative non-endosomal pathway for the uptake. Furthermore, the peptides need to have a certain enzymatic stability to diffuse towards the nucleus without degradation. Thus, the fact that our oligoproline-based CPP are able to diffuse within the cell to the nucleus, suggests that they have a high stability towards intracellular proteases (for stability assays see 3.1.5). A further reason for the nuclear localization of our CPPs might be the affinity of the high positive charge density of the peptides to the high density of negative charges in the nucleus. Similar accumulation in the nucleus of mammalian cells was observed for other enzymatically stable CPPs such as β-peptides by Seebach *et al.*,[118a, 221] as well as by Raines and Gellman and co-workers.[222] [8] Unfortunately, in the latter case cells were fixed and therefore cannot be compared to our images. However, the authors report that similar results were obtained when fixation was omitted.

---

[8] Images of HeLa cells from literature are given in the appendix 6.7.

Furthermore, our cationic oligoprolines seem not to suffer from endosomal entrapment under the examined conditions, since they reach the cell nucleus, which provides a further beneficial characteristic for future applications as delivery vectors. The nuclear affinity of our CPPs could be of particular interest for intracellular targeting applications. For example, the fusion with tumor-targeting radiolabeled peptides for therapy could provide a possibility to transport high energy and short range emitting radioactivity to the nucleus of cancer cells and would additionally provide selectivity of the CPPs towards the targeted tumor cells.

In conclusion, the results obtained from the confocal microscopy studies clearly demonstrated the nuclear localization of our oligoproline-based CPPs. A possible scenario could be the internalization *via* endocytosis, followed by an endosomal escape within the incubation time of 1 h to 1.5 h, and migration to the nucleus. In addition, a partially direct translocation of the peptides through the cellular membrane at higher concentrations cannot be excluded. To investigate this process in more detail, future experiments could be carried out at shorter incubation times and different intervals to monitor the translocation of the CPPs within the cells. To investigate the involvement of passive diffusion and the energy-dependence of the uptake, incubation could be carried out at 4°C or cells could be treated with NaN_3 and deoxyglucose for ATP depletion prior to peptide incubation. To test the strength of the nucleus association, an additional incubation time could be added after removing the peptide solution from the cells and adding fresh culture medium. Confocal microscopy studies could then be performed after different time intervals to test how long the CPPs stay in the nucleus and when elimination by exocytosis starts. Further interesting studies could be conducted with other fluorophores to explore if they show an effect on the subcellular distribution.

3.1.5   Enzymatic stability

Enzymatic stability tests of CPPs are crucial to get a hint of the behavior of the peptides for future applications *in vivo*. It is of great importance to provide an adequate stability of the molecular transporters in order to deliver the cargo molecules into the cell. We therefore conducted stability assays of the oligoproline-based CPPs and the reference CPPs towards trypsin (bovine pancreas) and fresh human blood serum under physiological conditions. The stability of the peptides in general depends on their sequence and the absolute configuration of the amino acids, enabling proteases to recognize them and cleave between specific residues. The assays were carried out using the full length CPPs including the glycine spacer and the 5(6)-carboxyfluorescein. Thus, the N-terminal cap of the peptides might be considered as a stabilizing factor. The 5(6)-CF labeled peptides were used, because the fluorophore allows for a facile detection of the degradation products. The CPPs were incubated at 37°C with trypsin or human blood serum and the degradation process was monitored at different time points (0 min, 30 min, 1 h, 2 h, 6 h, 12 h, 24 h and 48 h), *via* RP-HPLC at 214 nm and 440 nm. The time point "0 min" describes the moment of the first contact of the peptides with trypsin or blood serum and subsequent analyses of the samples. Metabolites were identified *via* LC-MS. Representative examples of the examined CPPs are given in the next chapters, showing their HPLC chromatograms at the time points 0 min, 1 h, and 48 h. To illustrate the successive degradation of the peptides with a better signal to noise ratio and to visualize the last remaining metabolite, 5(6)-carboxyfluorescein-glycine-OH, the figures in this chapter present the HPLC chromatograms at 440 nm.

3.1.5.1 Stability of the CPPs towards trypsin

To get an initial hint of the relative stabilities of the oligoproline-based CPPs we conducted a standard stability assay towards the protease trypsin[132a, 223] with a representative selection of peptides (**26, 28, 30, 33, 38, 39, 50**, and **52**) in comparison to the reference peptides Tat(48-60) (**42**), penetratin (**43**), octaarginine (**45**), and D-hexaarginine (**48**). Trypsin belongs to the family of serine proteases and is found in the digestive organs of many vertebrates. It recognizes specific amino acid sequences and catalytically cleaves peptides mainly at the C-terminal site of arginine and lysine, except when they are coupled to proline.[118e]

Enzymatic degradation of the peptides towards trypsin was carried out by incubation of the peptides with trypsin in 100mM Tris-HCl at pH 8.0, since the optimal conditions for trypsin activity are at a pH of 7 – 8. The trypsin to peptide ratio was 1:500, using a final peptide concentration of 125 μM. Samples were incubated at 37 °C up to 48 h. Aliquots were taken periodically and quenched with 1M HCl at precise time points, starting from the addition of the trypsin (0 min) and continuing after 30 min, 1 h, 2 h, 6 h, 12 h, 24 h, and 48 h to analyze their proteolytic stability. The samples were cooled on ice for 30 min and centrifuged. Degradation was monitored by HPLC and LC-MS of the supernatant. Pure PBS instead of a trypsin solution was added to the peptides as a negative control.

The comparison of the HPLC chromatograms before and after trypsin incubation demonstrated a high susceptibility of the reference CPPs, composed of natural amino acids, towards degradation through trypsin. A complete degradation of the peptides CF-G-Tat(48-60)-CONH$_2$ (**42**), CF-G-RQI-KIW-FQN-RRM-KWK-K-CONH$_2$ (penetratin, **43**), and CF-G-R$_8$-CONH$_2$ (**45**) was observed within 48 h as illustrated in Fig. 53 for the examples **42** and **45**. Since the degradation of **42** and **45** occurred already at the first contact with trypsin, the HPLC chromatograms of the non-treated peptides were added to Fig. 53 as controls. It was observed that even after 30 min the detected amount of intact peptide had decreased significantly (not shown). The last resulting peak was traced back to the last remaining metabolite in the degradation process, 5(6)-carboxyfluorescein-glycine-OH, *via* LC-MS. In comparison, the D-hexaarginine (**48**) showed full stability up to 48 h.[206]
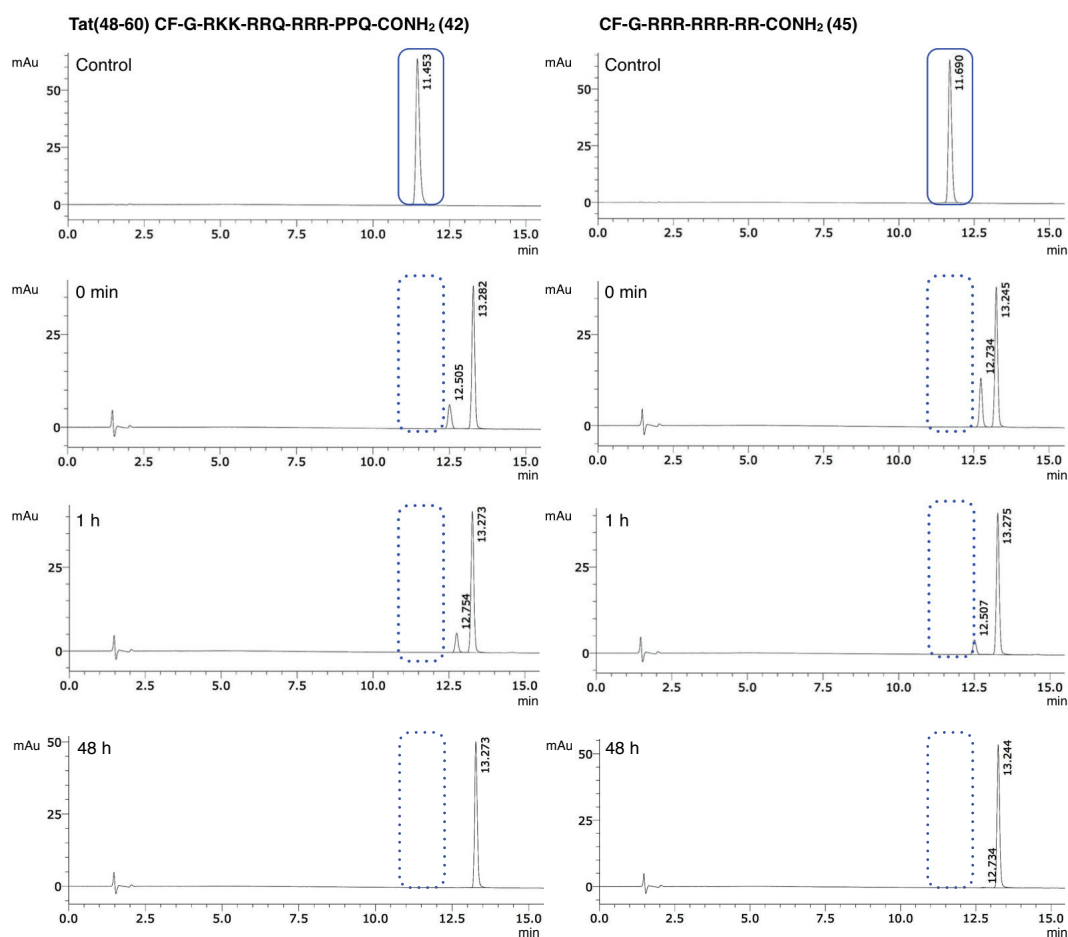
Figure 53: RP-HPLC chromatograms of the reference peptides CF-G-Tat(48-60)-CONH$_2$ (**42**, left) and CF-G-R$_8$-CONH$_2$ (**45**, right) treated with tryspin and analyzed after different time intervals.

In contrast, both the L- and D-oligoproline-based CPPs did not show any sign of degradation in the presence of the protease and remained stable up to 48 h (for D-analogs see [206]). Additionally, no difference in stability was observed for oligoproline-based CPPs with an alternating or an *en bloc* arrangement of the functionalized and unfunctionalized proline residues. Examples for stable L-oligoproline-based CPPs are given for the peptides CF-G-Z_6P_3-$CONH_2$ (**30**) and CF-G-Z_8-$CONH_2$ (**39**) (Fig. 53).
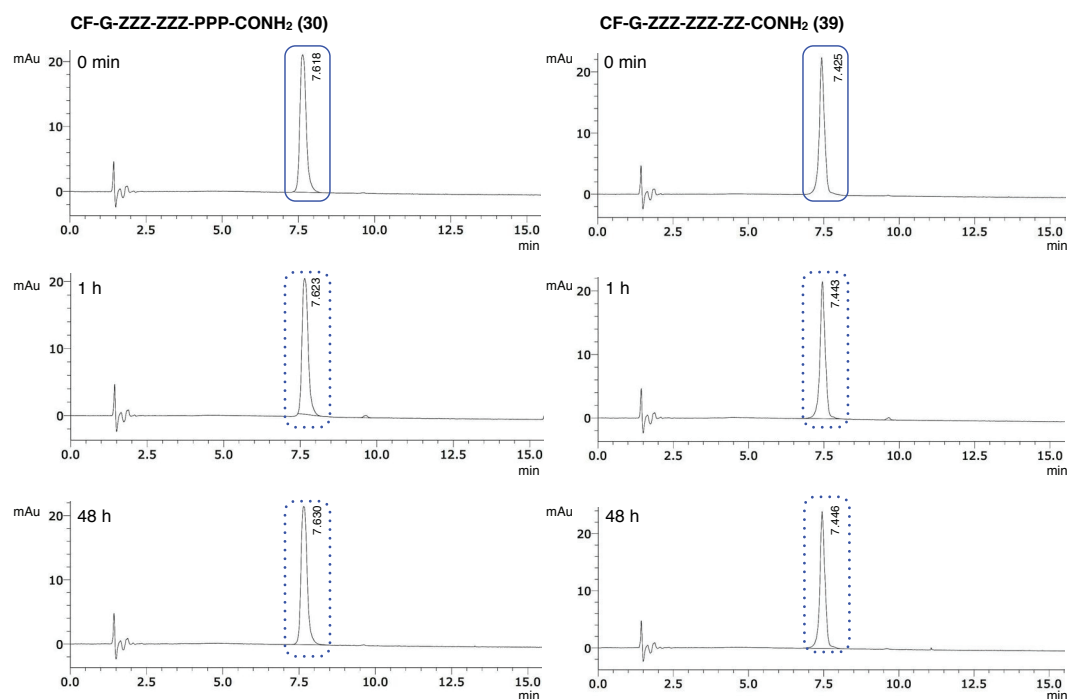
Figure 53: RP-HPLC chromatograms of CF-G-Z_6P_3-$CONH_2$ (**30**, left) and CF-G-Z_8-$CONH_2$ (**39**, right) treated with trypsin and analyzed after different time intervals.

As expected, also the entirely unfunctionalized L- and D-oligoprolines CF-G-P_9-$CONH_2$ (**50**) and CF-G-p_9-$CONH_2$ (**52**) remained stable in the presence of trypsin (Fig. 54). The appearance of double peaks in the RP-HPLC chromatograms of several peptides was closer investigated and LC-MS analysis revealed that both peaks show the same mass and correspond to the mixture of the two isomers of 5(6)-carboxyfluorescein, coupled to the peptides.
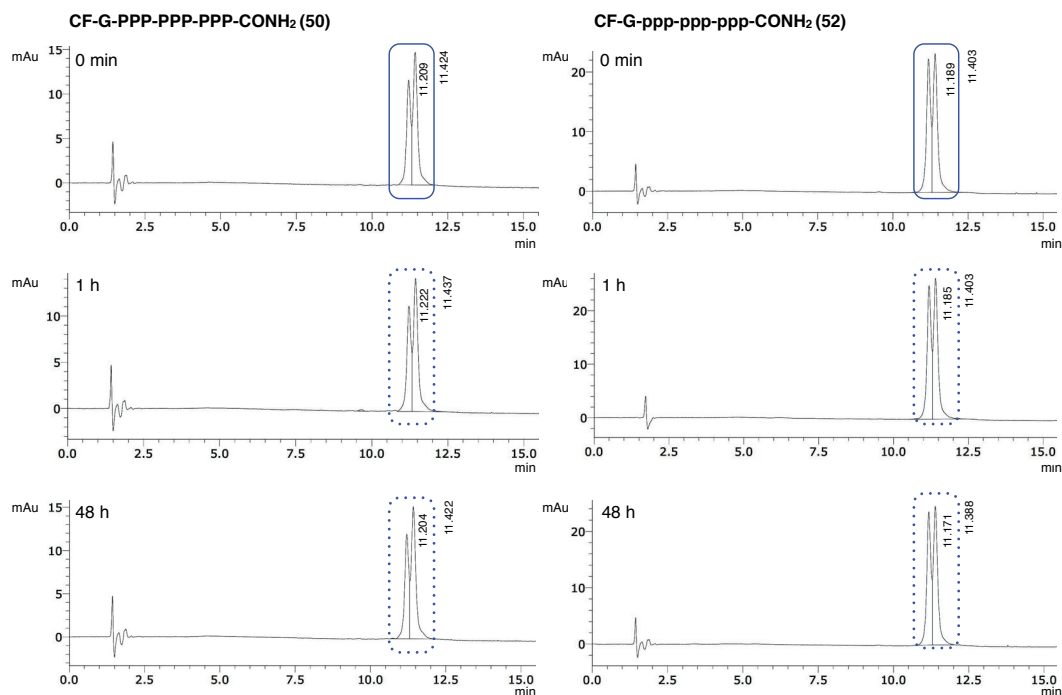
Figure 54: RP-HPLC chromatograms of CF-G-P_9-CONH$_2$ (**50**, left) and CF-G-p_9-CONH$_2$ (**52**, right) treated with trypsin and analyzed after different time intervals.

Thus the L-oligoproline-based CPPs are significantly more stable towards trypsin compared to the references Tat(48-60) (**42**), penetratin (**43**), and octaarginine (**45**). The D-oligoproline-based CPPs proved also to be resistant against trypsin, as well as D-hexaarginine (**48**). To further analyze the stability of our oligoproline-based CPPs we next examined their behavior towards a cocktail of diverse proteases and incubated them in human blood serum.

3.1.5.2 Stability of the CPPs towards human blood serum

Serum, derived from human blood without clotting factors, contains 60 – 80 mg of protein/mL and a variety of small molecules including salts, lipids, amino acids, and sugars. An estimation suggested that up to 10,000 different proteins may be commonly present in human blood serum.[224] It is therefore essential for delivery vectors to have a robust stability profile in order to transport their cargo through the plasma to the target cells, when administered in the blood stream.

Due to the unique structure of proline amongst the natural amino acids, there is only a limited number of peptidases capable of hydrolyzing oligoproline motifs.[225] An enzyme that was found in a wide range of organs and tissues of mammals, and was reported to

cleave Pro-Pro amide bonds, is Aminopeptidase P (APP).[226] APP was also found in human serum and was reported to specifically cleave Pro-Pro bonds.[227] It was isolated from the cytosol of human leukocytes and found to cleave in particular peptides with N-terminal Xaa-Pro sequences, whereas oligoproline was not hydrolyzed.[225] In contrast, APP isolated from the homogenate of bovine brain hydrolyzes even longer chained substrates such as Pro-Pro-Pro-Pro and cleaves N-terminal amino acids from peptides containing penultimate prolines such as neuropeptide Y.[226]

The well-known family of prolyl endopeptidases consists of cytosolic enzymes found in mammals that cleave peptide bonds on the C-terminal site of prolyl residues within peptides, but not Pro-Pro bonds.[228] Dipeptidyl peptidases II and IV remove Xaa-Pro dipeptides from the N-terminus of peptides.[225] The serum enzyme aminopeptidase B (APB) is a Zn^{2+}-dependent exopeptidase, which selectively removes arginine and lysine from the N-terminus of peptides.[229] Another metallopeptidase, which is found in human blood serum, is carboxypeptidase R (CPR), is known to hydrolyze peptide bonds C-terminal to arginine and lysine.[230]

To analyze the relative stability of our oligoproline-based CPPs towards this collection of enzymes in fresh human blood serum, stability tests were conducted with a representative selection of peptides (**26**, **28**, **30**, **25**, **30**, **31**, **50**, and **52**) at physiological conditions in comparison to the reference peptides Tat(48-60) (**42**), penetratin (**43**), octaarginine (**45**), and D-hexaarginine (**48**) in a time range up to 48 h. For the experiment, human blood was freshly taken into EDTA-containing tubes at the University Hospital Basel, to obtain the serum after coagulation of the blood within 15 min. Probes were centrifuged and the supernatant was taken and directly used for stability assays. The peptides were added as stock solutions in sterile PBS to the serum to reach a final peptide concentration of 125 µM. Samples were incubated at 37 °C for up to 48 h. Aliquots were taken periodically, starting from the addition of the the serum (0 min) and continuing after 30 min, 1 h, 2 h, 6 h, 12 h, 24 h up to 48 h. Aliquots were poured into a 1:1 mixture of acetonitrile/water to precipitate the proteins. The samples were cooled on ice for 30 min, centrifuged and the supernatant was analyzed by RP-HPLC. As negative controls, pure PBS instead of blood serum was added to the peptide solutions.

All three reference peptides, CF-G-Tat(48-60)-$CONH_2$ (**42**), penetratin (**43**), and CF-G-R_8-$CONH_2$ (**45**), composed of natural amino acids, were rapidly degraded under identical conditions, as illustrated in Fig. 55 for **42** and **45,** whereas the degradation of

the Tat(48-60) proceeded a little slower. This effect might be due to glutamine and proline residues, which are included in the sequence, and may lead to a partial protection of the peptide towards certain proteases present in the serum. Even at this early stage of the experiment degradation was visible for octaarginine (**45**). After 1 h the reference peptides showed a considerable degradation and after 48 h no trace of the intact peptides was detected anymore. The resulting peak eluting at 14.8 min was as well found to correspond with the last remaining metabolite in the degradation process, 5(6)-carboxyfluorescein-glycine-OH. Similar observations concerning the degradation of the reference peptides were reported by Trehin *et al.* and Hällbring *et al.* for stability assays with Tat(47-57) and penetratin in contact with different cell lines.[231] The D-hexa-arginine (**41**) in contrast showed full stability up to 48 h.[206]
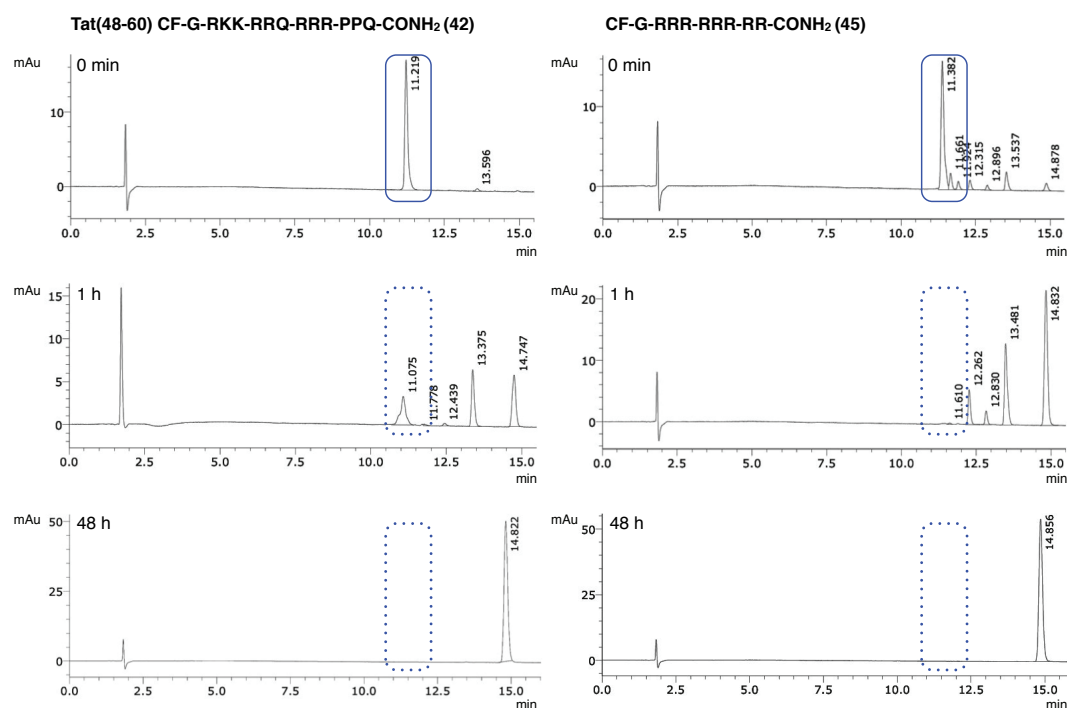
Figure 55: RP-HPLC chromatograms of the reference peptides CF-G-Tat(48-60)-CONH$_2$ (**42**, left) and CF-G-R$_8$-CONH$_2$ (**45**, right) treated with human blood serum and analyzed after several time intervals.

Analysis of the HPLC chromatograms of the L-oligoproline-based CPPs, recorded at different time points revealed that they are stable up to 48 h, as illustrated in Fig. 56 for the examples CF-G-ZZZ-ZZZ-PPP-CONH$_2$ (**30**) and CF-G-Z$_8$-CONH$_2$ (**39**). Furthermore, no difference in stability was observed for oligoproline-based CPPs with an alternating or an *en bloc* arrangement of their guanidino proline and proline residues. The

D-oligoproline-based CPPs showed as well full resistance against the enzymes in human blood serum.[206]
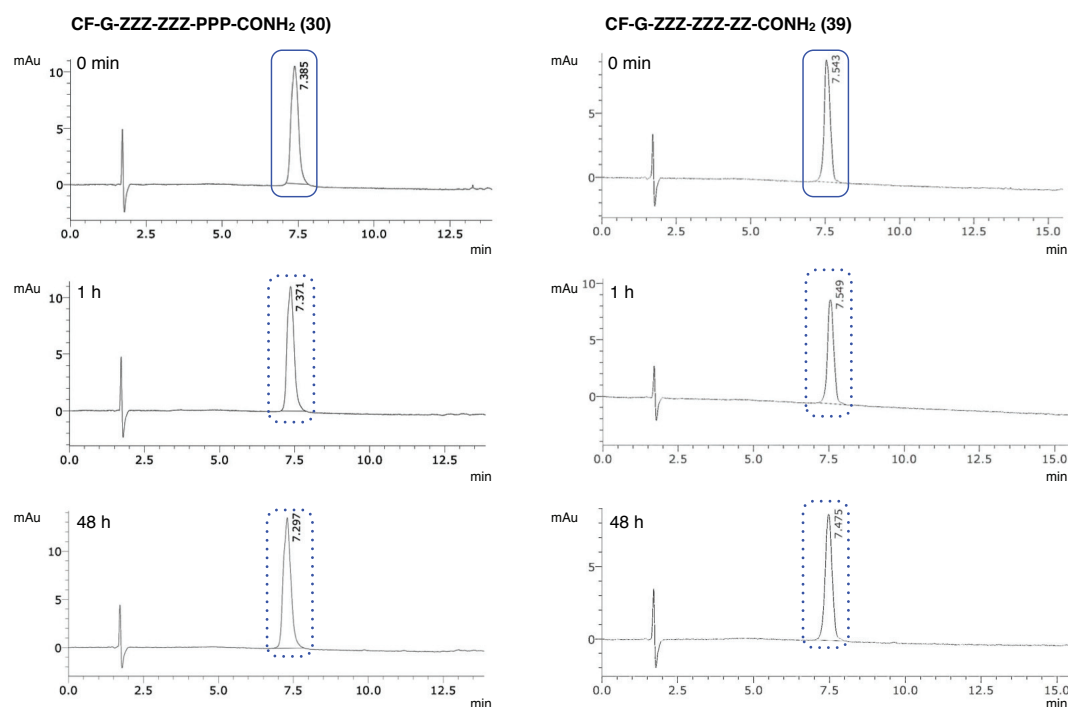
Figure 56: RP-HPLC chromatograms of CF-G-Z_6P_3-$CONH_2$ (**30**, left) and CF-G-Z_8-$CONH_2$ (**39**, right) treated with human blood serum and analyzed after several time intervals.

Analysis of the unfunctionalized peptide CF-G-P_9-$CONH_2$ (**50**) and its D-analog CF-G-p_9-$CONH_2$ (**52**) revealed the same stability as that observed for the functionalized oligoprolines (Fig. 57). In line with this, the stability of functionalized L-oligoprolines proved to be the same as those of their D-analogs.[206] This data demonstrates the stability of oligoproline-based CPPs in fresh human blood serum. Furthermore, it suggests that proteases that are able to cleave prolyl amide bonds do not prevalently occur in human blood serum. Our observations showed that the oligoproline-based CPPs are stable, independent of the arrangement of functionalized and unfunctionalized proline residues in the primary structure. Thus, alternating structures showed the same results than *en bloc* structures. The appearance of double peaks in the RP-HPLC chromatograms is again due to the mixture of the isomers of 5- and 6-carboxyfluorescein.
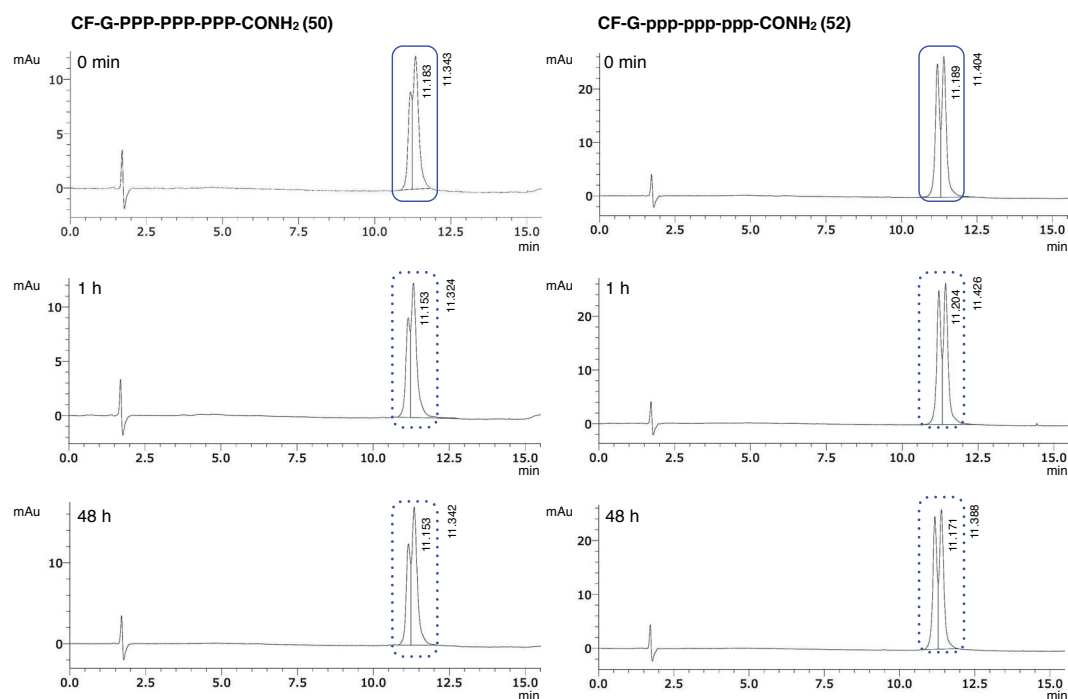
Figure 57: RP-HPLC chromatograms of CF-G-P$_9$-CONH$_2$ (**50**, left) and CF-G-p$_9$-CONH$_2$ (**52**, right) treated with human blood serum and analyzed after several time intervals.

As expected from the known susceptibility of the reference peptides CF-G-Tat(48-60)-CONH$_2$ (**42**), penetratin (**43**), and CF-G-R$_8$-CONH$_2$ (**45**) towards degradation through proteases present in human blood serum, a rapid degradation was detected. In contrast, the oligoproline-based CPPs proved to be stable under identical conditions, as well as D-hexaarginine (**48**). This feature represents a major advantage of oligoproline-based CPPs over proteolytically labile CPPs, which are limited in a great extend for biomedical applications. The usage of according D-analogs of the naturally derived CPPs to enhance stability, might lead to a different behavior of the peptides towards the cell, in particular the binding affinity of the peptides to the cellular membrane, as reported by Brock *et al.*[117] As demonstrated by flow cytometry experiments this is not the case for our oligoproline-based CPPs, where a similar uptake of both L- and D-analogs was observed (see 3.1.4.1.4).

An ideal transporter molecule should also be cleavable after a certain time span and/or be eliminated from the cells by exocytosis after cargo delivery. A balance between proteolytic stability and clearance from the organism is considered to be beneficial to avoid long-term toxicity effects. Thus, for future investigations it is planned to test the stability of the oligoproline-based CPPs towards the potent serine protease proteinase K, which is known to exhibit a lack of selectivity toward peptide substrates, and in cell

lysate, containing a mixture of effective intracellular proteases. The introduction of an intracellular cleavage site into the oligoproline sequence could be as well considered to balance stability and degradation of the peptides within the cells. In this respect it is as well of great importance to investigate the exocytotic removal of the oligoproline-based CPPs, which was already observed in preliminary microscopy studies, but needs to be confirmed and investigated in more detail. Based on this initial observation the peptides are expected to be washed out of the cells within hours.

3.1.6 Toxicity

Since various CPPs were used in recent years for *in vivo* applications and are in clinical trials at the current state, it becomes increasingly important to investigate toxicity effects associated with these delivery vectors. A thorough initial study of potential cytotoxicity *in vitro* is a first step towards the further development of CPPs for clinical applications. Most toxicity studies of CPPs *in vitro* are focused on membrane integrity (e. g. leakage assays) and cell viability (e.g. MTT assays).[88, 232] The present chapter is focused on the examination of cell viability *via* MTT assays and the hemolytic activity of our CPPs, which is an important parameter for experiments *in vivo*. A decrease in cell viability at higher peptide concentrations[219] and an induction of hemolysis[200a] was observed for certain amphiphilic CPPs. However, the cytotoxicity of most CPPs is low, considering the low doses required for efficient cargo delivery in most cases.[88]

3.1.6.1 MTT assays

The so-called MTT assay is the most frequently used method to monitor cell viability in association with cell proliferation and cytotoxicity.[88] The basic process examined by MTT assays takes place within the mitochondria of healthy cells. The activity of the mitochondria is observed by monitoring the activity of the mitochondrial dehydrogenase, which catalyzes the NAD(P)H-dependent reduction of the pale yellow tetrazolium dye 3-(4,5-Dimethylthiazol-2-yl)-2,5-diphenyltetrazolium bromide (MTT) to insoluble, purple formazan. The amount of the resulting formazan is then colorimetrically determined and reflects the amount of viable cells in the probe (Scheme 17). Modified variants of the MTT assay use tetrazolium dyes like 2,3-bis-(2-methoxy-4-nitro-5-sulfophenyl)-2H-tetrazolium-5-carboxanilide (XTT), 3-(4,5-dimethylthiazol-2-yl)-5-(3-carboxymethoxy-phenyl)-2-(4-sulfophenyl)-2H-tetrazolium (MTS), or water

soluble tetrazolium salts (WST) that facilitate the experimental procedure by forming soluble dyes.[87] A disadvantage is their relatively high cost (e. g. XTT, 100 mg ~ 470 CHF)[233] in comparison to usual MTT (100 mg ~ 25 CHF)[234] that works very well in established assay procedures.
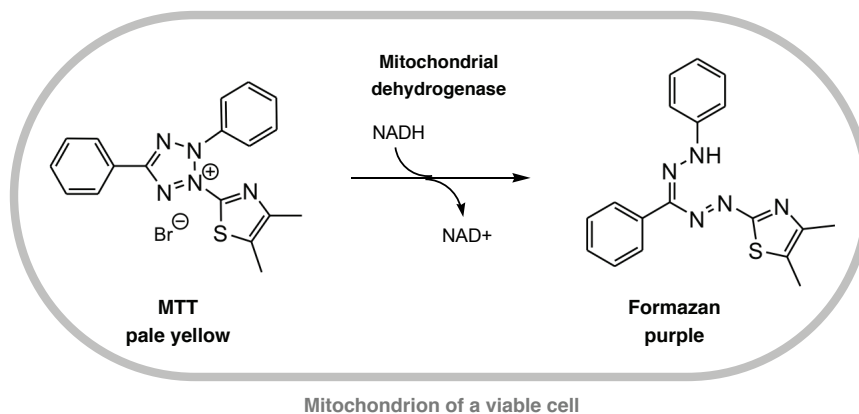
Scheme 17: Principle of the MTT assay: The mitochondrial dehydrogenase activity of healthy cells is monitored by colorimetric measurement.

To determine whether the oligoproline-based CPPs exhibit cytotoxicity *in vitro*, MTT assays were performed with HeLa cells at different peptide concentrations (5, 10, 25, and 50 µM) and incubation times (1.5 and 3 h). The measurements were carried out with a selection of representative CPPs using the full length peptides, including the 5(6)-carboxyfluoresein at the N-terminal site. For the experiment 5000 cells were seeded into 96-well plates and allowed to adhere overnight. Afterwards the cells were washed with PBS and incubated with 150 µL of the peptide solution at the defined concentrations in 1% DMEM and incubated at 37°C for 1.5 or 3 h. The cells were washed with PBS, 150 µL MTT solution (1.2 mM) was added and they were incubated for 3 h at 37 °C. The supernatant was discarded and the detergent reagent Triton X-100 (10% v/v in 0.1 N HCl in *i*PrOH) was added to lyse the cells. Samples were mixed and allowed to stand for 30 min until the measurement. Plates were analyzed in a microplate reader at 570 nm and the background fluorescence was substracted. Each measurement was repeated twice and assays were carried out in triplicate within one week. Cell viability was calculated relative to non-treated cells, which were used as controls for 100% viability.

The obtained data for a selected series of oligoproline-based CPPs (**20**, **21**, **22**, **23**, **24**, **25**, and **30**) of different chain lengths, including the modified proline residues (4*S*)Amp (U) and (4*S*)Gup (Z), revealed, that all of them exhibit a minimal cytotoxicity towards HeLa cells at 1.5 h of incubation time over the range of tested concentrations (Fig 58). Especially at the low concentration of 5 μM and 1.5 h of incubation time, the exact conditions used for flow cytometry experiments, high viability values (92 - 99%) were observed. Even at the highest concentration of 50 μM and at 1.5 h of incubation time, our CPPs still show a low cytotoxicity (78 - 90% viability). All values are comparable with the well-established Tat(48-60) (**42**) peptide, one of the most widely used CPPs for the development of clinical applications.
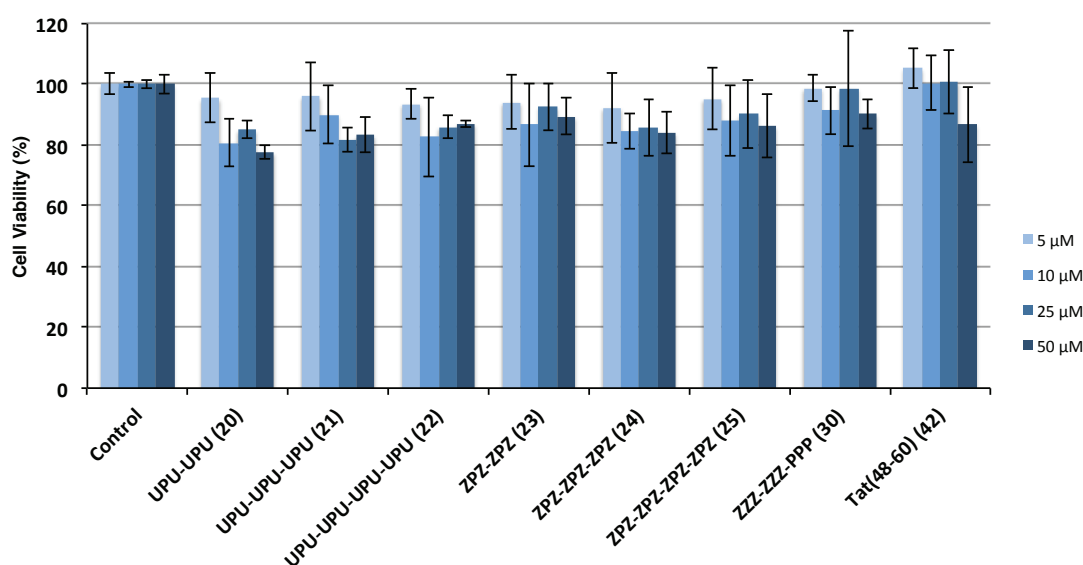
Figure 58: Viabilities of HeLa cells after incubation with CPPs at different concentrations for 1.5 h at 37°C.

Additionally, the cytotoxicity of a selection of CPPs (**24**, **25**, **27**, **29**, **30**, **31**, **33**, **39**, **40**, and **41**) including alternating and *en bloc* structures as well as D-analogs towards HeLa cells was examined for an increased incubation time of 3 h at 5 μM and at 37°C (Fig. 59). The unfunctionalized oligoprolines **50** and **52** and reference peptides (**42**, **43**, **45**, **46**, and **47**) were tested as well for their cytotoxicity under identical conditions. Generally, the cytotoxicity of the oligoproline-based CPPs increased only slightly under these conditions (73 - 100% viability). Exceptions were peptides bearing more than eight neighboring guanidinylated residues. The peptides CF-G-Z_{10}-$CONH_2$ (**40**) and CF-G-Z_{12}-$CONH_2$ (**41**) composed entirely of guanidino proline, exhibited a higher toxicity (76% and 66% viability). This observation might be due to their strong cell-penetrating properties, able to disrupt the membrane while entering the cells. The same loss in cell

viability was observed for the longer chained oligoarginines CF-G-R$_{10}$-CONH$_2$ (**46**) and CF-G-R$_{12}$-CONH$_2$ (**47**) (90% and 69% viability) and might be caused by the same effects. The Tat(48-60) peptide (**42**, 82%) and penetratin (**43**, 96%) proved to be not cytotoxic under the chosen conditions. The lower viability rates of the alternating peptides CF-G-ZPZ-ZPZ-ZPZ-CONH$_2$ (**24**) and CF-G-zpz-zpz-zpz-CONH$_2$ (**27**) in comparison especially to the longer peptide CF-G-ZPZ-ZPZ-ZPZ-ZPZ-CONH$_2$ (**25**) cannot be explained and might be attributed to the variance in the biological assay. The examined D-analogs showed similar viability rates, within the margin of error, as the according L-oligoprolines. The unfunctionalized L- and D-oligoprolines, CF-G-P$_9$-CONH$_2$ (**50**) and CF-G-p$_9$-CONH$_2$ (**52**) exhibited a low cytotoxicity as well.
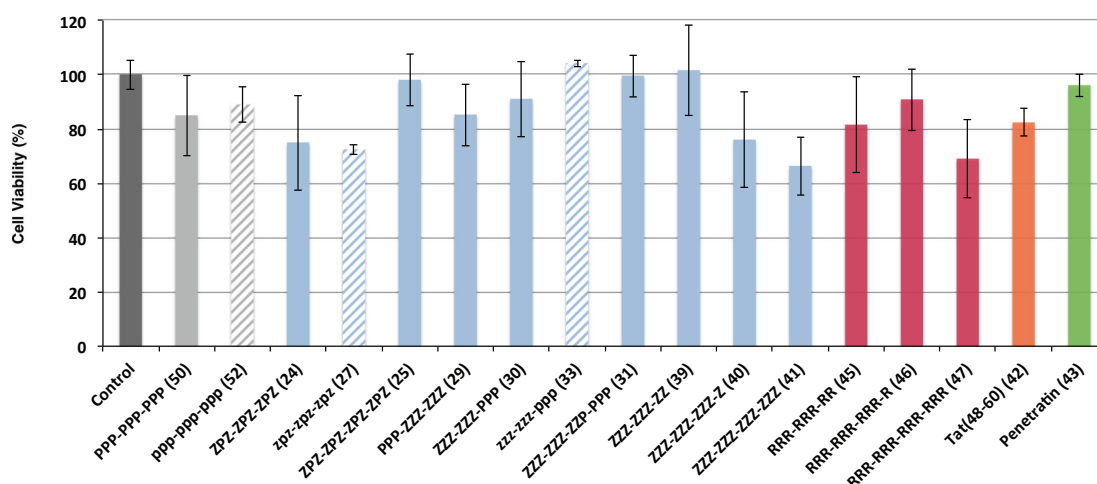
Figure 59: Viabilities of HeLa cells after incubation with oligoproline-based and reference CPPs at 5 µM for 3 h at 37°C (with P. Raschle).

In summary, we demonstrated a minimal cytotoxicity of the oligoproline-based CPPs towards HeLa cells at 1.5 h and 3 h of incubation time up to 50 µM of peptide concentration, whereas in particular at the low concentration of 5 µM, high viability values (92 - 99%) were observed. The reference peptides showed as well a low cytotoxicity towards HeLa cells. Since experiments for applications, as for example siRNA delivery (see 3.1.7), mostly take place in a nM concentration range and with longer incubation times, future investigations on this project include MTT assay at lower concentrations (0.1, 1 and 5 µM) for up to 12 h of incubation time. A preliminary hint of the behavior of the oligoproline-based CPPs is given by the observation that the incubation time of 24 h in the siRNA delivery experiment did not show a negative effect on cell viability, judged by the amount of detected counts per sample in the

measurement of the experiment and the morphology of the cells after treatment with the peptides in comparison with the non-treated control cells.

3.1.6.2 Hemolysis assays

A main reason that prevents intravenous delivery of cationic amphiphatic CPPs, next to proteolytic instability, is their potential hemolytic activity. In addition, a hemolytic activity often enhances the toxicity of CPP-cargo constructs when administered by other routes.[202] Hemolysis is the rupture of the red blood cells (erythrocytes) (Scheme 18a) and the efflux of their content, including hemoglobin (Hb) (Scheme 18b).[235] Thus, hemolysis assays are of great importance for the development of CPPs as delivery vectors.
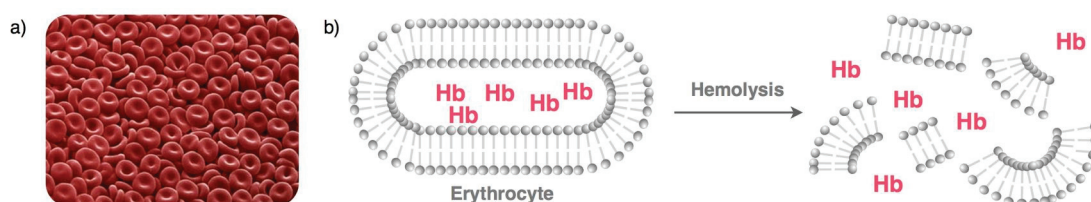
Scheme 18: a) A carpet of red blood cells (erythrocytes, color-enhanced scanning electron micrograph from reference [236]); b) Schematic representation of hemolysis of erythrocytes, releasing hemoglobin (Hb) (adapted from reference [88]).

To investigate the influence of the CPPs towards human erythrocytes, hemolysis assays with an incubation time of 4 h at 37°C were carried out using a selection of representative oligoproline-based CPPs (**30**, **33**, **37**, **38**, and **39**). Reference peptides (**42**, **43**, **44**, and **45**) were tested for their hemolytic activity under identical conditions as well. Therefore, again the full length CPPs were used. Hemolysis assays were performed using human blood, freshly taken at the University Hospital Basel. The erythrocytes were collected by centrifugation and washed with PBS. They were re-suspended in PBS to 4 % (v/v) and 100 µL per well were placed into a 96-well plate. 100 µL of the peptide solution was added to each well. Plates were incubated for 4 h at 37 °C, transferred to Eppendorf tubes and centrifuged. Aliquots of 100 µL of the supernatants were transferred to a 96-well plate and the release of hemoglobin was determined using a microplate reader at 540 nm (Hb). PBS and 0.1 % Triton X-100 in PBS were used as agents for 0% and 100% hemolysis, respectively. All hemolysis data points were presented as the percentage of the complete hemolysis.

The obtained data shows, that all tested oligoproline-based CPPs exhibit no hemolytic activity up to a 20 µM peptide concentration after 4 h of incubation (≤ 8.1±1.2 %). Tat(48-69) (**42**) and the oligoarginines (**44**, **45**) showed as well no significant hemolysis (up to 7.9±0.6 %) at these conditions. The reference peptide penetratin (**43**) exhibited increasing levels of hemolysis with increasing peptide concentrations up to 20 µM (10.6±0.5 %), which might be due to a pore formation of the amphiphatic peptide and subsequent leakage of the red blood cells. The results of the hemolysis assays are in agreement with the observed low cytotoxicity profile in the cell viability studies, discussed in the previous section.
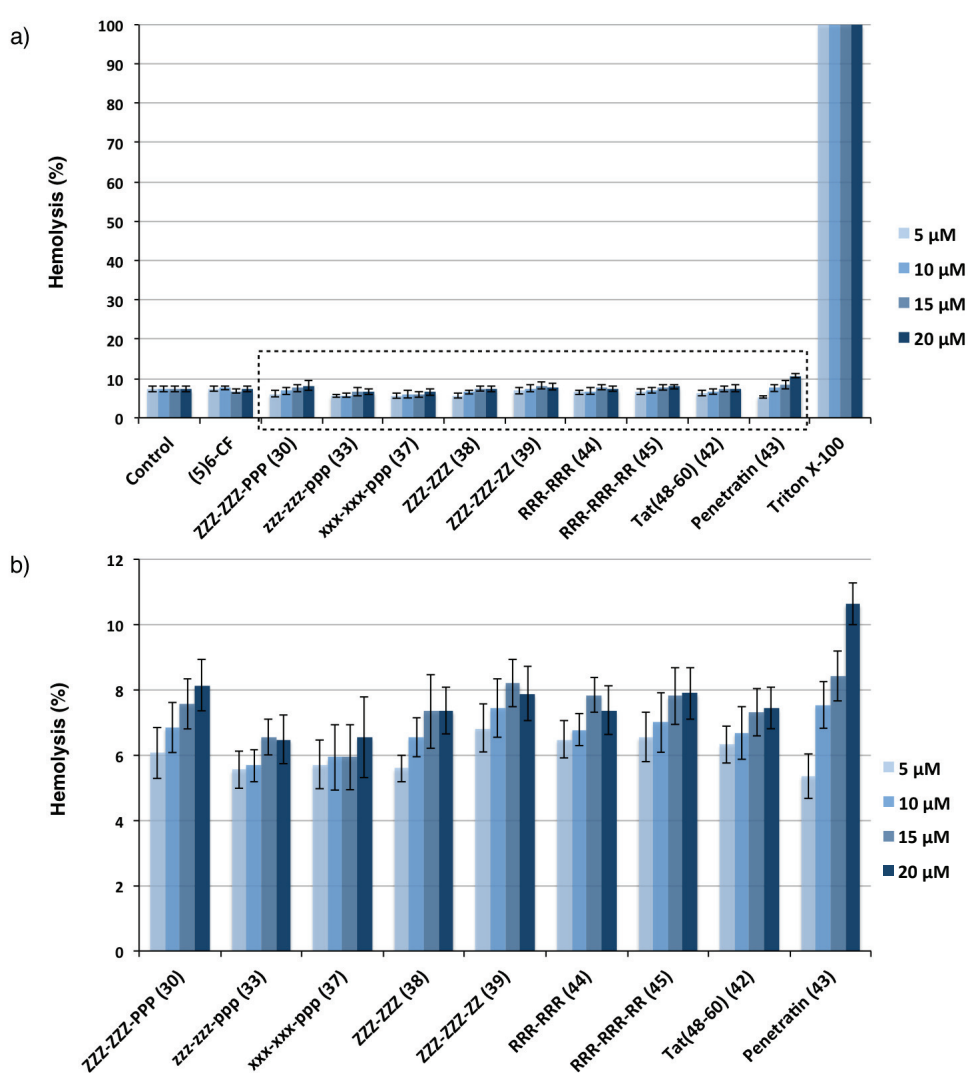
Figure 60: a) Hemolysis of erythrocytes after 4 h incubation at 37°C with a collection of CPPs at different concentrations and b) zoom on the examined CPPs.

Due to their highly cationic character CPPs might interact with the cellular membrane and lead to transmembrane pore formation and membrane leakage.[200] In general, CPPs

with a pronounced amphiphilic character show a higher degree of cytotoxicity, caused by the formation of pores.[201] To test these effects, leakage assays can be carried out, based on the efflux of fluorophores or radiolabels through an artificial membrane. Leakage assays might be interesting for future studies to further characterize the oligoproline-based CPPs.

The data obtained by the MTT and hemolysis studies revealed that the oligoproline-based CPPs have the potential to be safely applied for cargo delivery. As an initial delivery experiment we used our peptides as molecular transporters for siRNA, as described in the following chapter. For future investigations it will be interesting to extend our studies to *in vivo* experiments, in order to investigate the effect of CPP treatment in the living organism and examine whether immunological responses are associated.

3.1.7 Preliminary experiments for the delivery of siRNA

Potential cargos for CPP mediated delivery are wide ranging, amongst them are small molecule drugs, fluorophores, radiolabels, peptides and proteins, oligonucleotides, and many more. A special focus in the community has emerged in recent years in the field of small interfering RNA (siRNAs) delivery.[88] RNA interference (RNAi) constitutes a powerful tool for pharmaceutical research and became a method of choice to identify and validate the role of target genes in disease models.[237] RNAi is mediated through short double-stranded nuclei acids, siRNAs, which are capable of knocking down genes with extremely high selectivity.[237-238] The most intractable issue in the application of RNAi therapeutics *in vitro* and *in vivo* is associated with the delivery to their target. The negative charges in their backbone prevents the translocation through the cellular membrane.[187] Additional hurdles for delivery within the human body is the susceptibility to nuclease-mediated degradation of RNA, endosomal entrapment, and poor nuclear targeting.[87] To overcome these limitations, vectors such as viruses and liposomes have been developed. Viruses have been shown to be more efficient than non-viral vectors, but are potentially immunogenic *in vivo*.[87] Nowadays the delivery method of choice for most therapeutics in development is mediated by liposome-based formulations. However, the problem of delivery is not satisfying solved yet, since also the liposomes are in many cases not efficient enough or are too toxic for *in vivo* applications.[87] Despite the high potential of antisense techniques, many companies in the pharmaceutical industry canceled RNAi research in recent years, because of delivery problems.[239] Furthermore, the transfection of so-called difficult cells lines, such as stem cells, still remains a challenge. Due to their efficient cellular uptake, CPPs offer an attractive alternative for the delivery of siRNAs. However, only few studies on this topic have been reported.[187] The complexation of the cationic peptides with the negatively charged oligonucleotides (ONs) represents an elegant and fast way of preparation in comparison to covalent approaches and additionally offers a degree of protection against degradation of the cargo. Thereby the delivery efficiency is depending on the charge ratio for polycationic CPPs and the molar ratio for amphiphatic CPPs towards the siRNA. Delivery of siRNA *in vitro* and *in vivo* has been achieved so far with different CPPs, for example with transportan and penetratin using a disulfide linker strategy or CADY by complex formation with the cargo siRNA.[240] [187, 241] A non-covalent approach was explored for example with cholesteryl D-oligoarginines delivering vascular endothelial growth factor siRNA.[242] Since the success of delivery for a specific siRNA depends on several factors such as the characteristics of the CPP that is used, in

combination with the properties of the cargo siRNA itself, it is important to broaden the range of potential carriers to address different siRNAs in different cell lines and tissues.

3.1.7.1 Delivery of siRNA into HeLa cells

As an initial experiment to investigate the potency of our oligoproline-based CPPs as delivery vectors, we explored the uptake of siRNA into HeLa cells in cooperation with Prof. Dr. Jonathan Hall and Boris Guennewig from the Department of Pharmaceutical Chemistry at ETH Zürich. To monitor the associated biological response of the siRNA delivery, a dual luciferase assay was applied.[243] In this assay the transfection efficiencies of the CPPs were examined in correlation with the silencing potential of *Renilla* siRNA (5' GAGCGAAGAGGGCGAGAAAUU, siRen). Therefore we used the oligoproline-based CPP CF-G-Z_8-CONH$_2$ (**39**) in comparison to the references Tat(48-60) (**42**) and CF-G-R_8-CONH$_2$ (**45**). All three peptides showed cellular uptake into HeLa cells, previously determined by flow cytometry (see 3.1.4.1). As a negative control regarding the CPP mediated delivery the unfunctionalized oligoproline CF-G-P_9-CONH$_2$ (**50**) was tested, since it showed no significant uptake into HeLa cells (see 3.1.4.1.2). The transfection reagent Oligofectamine was used as a positive control. Oligofectamine is a liposome-based formulation, similar to Lipofectamine, and created to efficiently transfect siRNA or plasmid DNA *in vitro*.[244] Due to the lack of knowledge about the exact composition and concentration of Oligofectamine it is difficult to directly compare this transfection reagent with the CPPs. However, to have a benchmark of the maximal delivery of siRen, achievable with an optimized delivery reagent, we included the Oligofectamine-mediated transfection in our experiment. The target gene in our experiment was the mRNA of Renilla luciferase from a dual luciferase expression plasmid, transfected into HeLa cells. All transfections were performed in triplicate.

For the experiment we chose to test the delivery of siRen in different charge ratios (1:1, 3:1, 9:1)[9] with respect to the positive moieties of the CPPs and the negative charged RNA backbone. Additionally, four different siRNA concentrations (36, 9, 2.25, and 0 nM as negative control) were examined to evaluate the dose dependency of the response. Therefore 5000 HeLa cells were seeded in a 96-well plate and allowed to adhere for 8 h. Afterwards the pre-incubated CPP-siRNA and Oligofectamine-siRNA probes were

---

[9] Due to the experimental setup one more sample could be measured within the well-plate, so we decided to add the peptide Z_8 (**39**) in a ratio of 6:1 to the experiment.

incubated to the cells for 24 h at 37°C (Scheme 19, step a). Then the cells were transfected with a DNA plasmid (psi-CHECK-2), containing the gene for firefly luciferase as well as for *Renilla* luciferase. The plasmid was previously supplemented with the target mRNA, a validated microRNA site of the miR-106a family derived from the 3' untranslated region of CDKN1A (p21).[245] The transfections were performed using jetPEI, a polymer-based transfection reagent, mainly composed of linear polyethylenimine. (Scheme 19, step b).[74a]
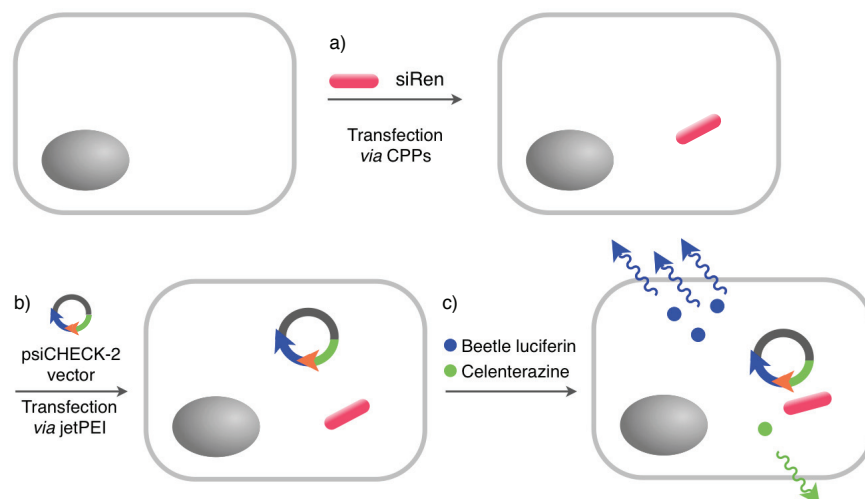
Scheme 19: Principle of the dual luciferase assay to monitor siRNA transfection efficiencies with CPPs: a) siRNA (siRen) delivery to the cells *via* CPPs or Oligofectamine; b) Transfection of a DNA plasmid encoding for firefly luciferase (blue) and *Renilla* luciferase (green) in fusion with the target gene (orange) using jetPEI; c) Addition of the substrates for both luciferases and subsequent measurement of bioluminescence.

After transfection of the plasmid into the cells a fusion of the *Renilla* gene and the target gene is transcribed and a functional *Renilla* luciferase is translated from the intact construct. If siRen was successfully delivered, it initiates a RNAi process on the target mRNA, the fused sequence will be degraded, which results in a decrease in *Renilla* luciferase activity.[246] After 48 h of incubation at 37°C the cells were washed and the substrates (beetle luciferin and coelenterazine) were successively added. The appearing bioluminescence, induced by the conversion of the substrates *via* the according luciferase, was measured (Scheme 19, step c and Fig. 61). Samples with transfected siRen were expected to show a difference in the normalized values for firefly and *Renilla* luciferase activity, whereas in the negative controls both luciferases were anticipated to be expressed to the full extend.
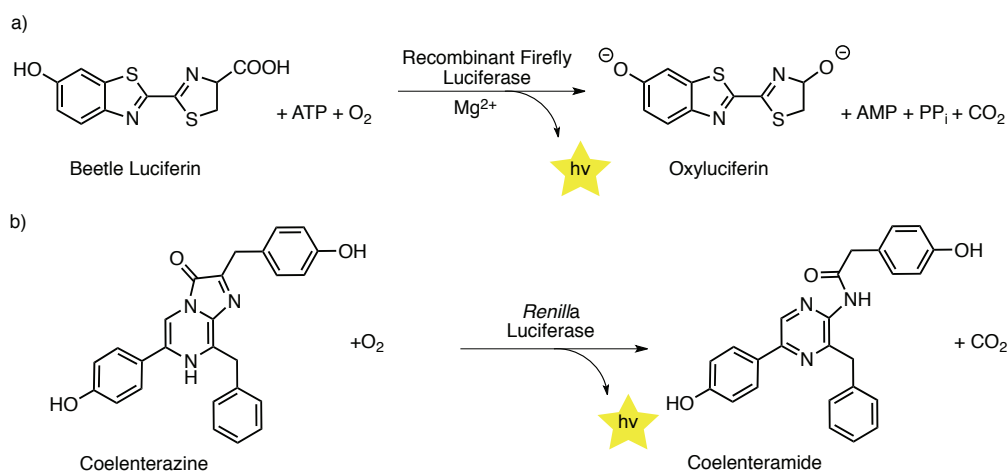
Figure 61: Bioluminescent reactions catalyzed by firefly (a) and *Renilla* luciferases (b); (adapted from [243a]).

The advantage of this assay, in contrast to a common luciferase assay, is the possibility to discriminate between cell death and cellular down-regulation.[243a] This can be accomplished by normalizing the expression of the experimental reporter (*Renilla* luciferase) to the control reporter (firefly luciferase).[243a] *Renilla* and firefly luciferase are both monomeric proteins, which do not require a post-translational modification and can be thus applied as genetic reporters directly after translation.[247] The results of our experiment are given as normalized signals against the unaffected firefly luciferase, which were in addition normalized to the value obtained for the lowest concentration of siRNA (2.25 nM).

The obtained data showed a silencing of 52% for 36 nM siRNA with the positive control Oligofectamine. The negative control peptide P_9 (**50**) did not show a statistically relevant down-regulation at all tested charge ratios and concentrations. The decrease in the normalized luciferase signals for P_9 at the ratio of 1:1 are expected to be due to the biological variance of the experiment. The obtained data revealed no significant down-regulation in the case of R_8 (**45**). In contrast, the CPPs Tat(48-60) (**42**), and Z_8 (**39**) revealed an increased silencing effect with increasing charge ratio and increasing siRNA concentration for the peptides. Tat(48-60) (**42**) exhibited just an effect at the siRNA concentration of 36 nM for all tested ratios, whereas Z_8 (**39**) already showed a slight effect at 9 nM, which intensified at 36 nM. The stepwise down-regulation with increasing charge ratio, and thus more cationic charges per molecule siRNA, was observed for both peptides. The highest silencing of the tested CPPs exhibited Z_8 (**39**) with 24% at a concentration of 36 nM and a charge ratio of 9:1. Tat(48-60) (**42**) displayed 13% at the same conditions. Reasons that no silencing effect was observed for

R_8 (**45**) in this experiment might be due to an endosomal entrapment of the CPP-cargo complex or that the CPP remained bound to the siRNA, which then could not exert its effect. To clarify this question, confocal microscopy studies with fluorophore labeled siRen could be performed in future to examine the intracellular localization of the CPP-cargo complex.
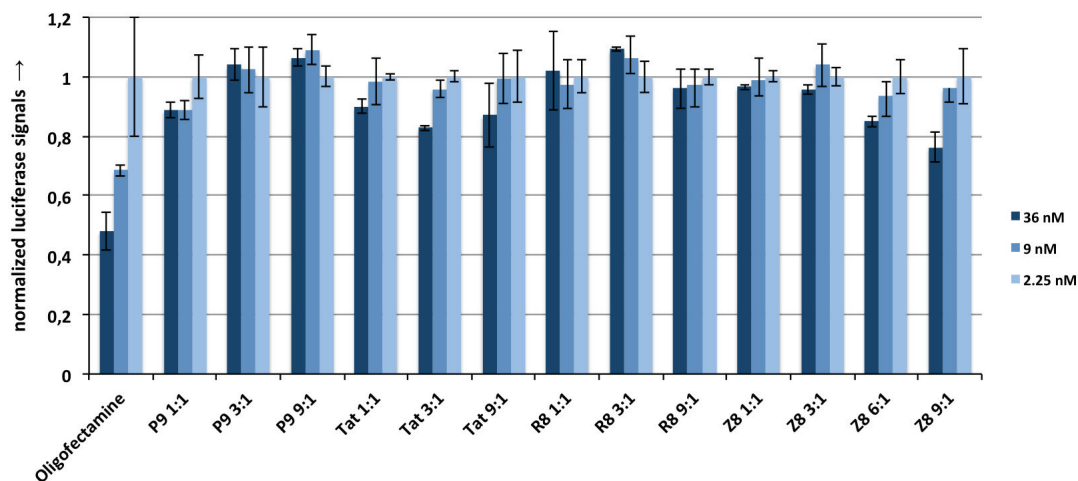
Figure 62: HeLa cells transfected with luciferase reporter plasmid and treated with increasing doses (36, 9, 2.25 nM) of siRen and CPPs in different charge ratios.
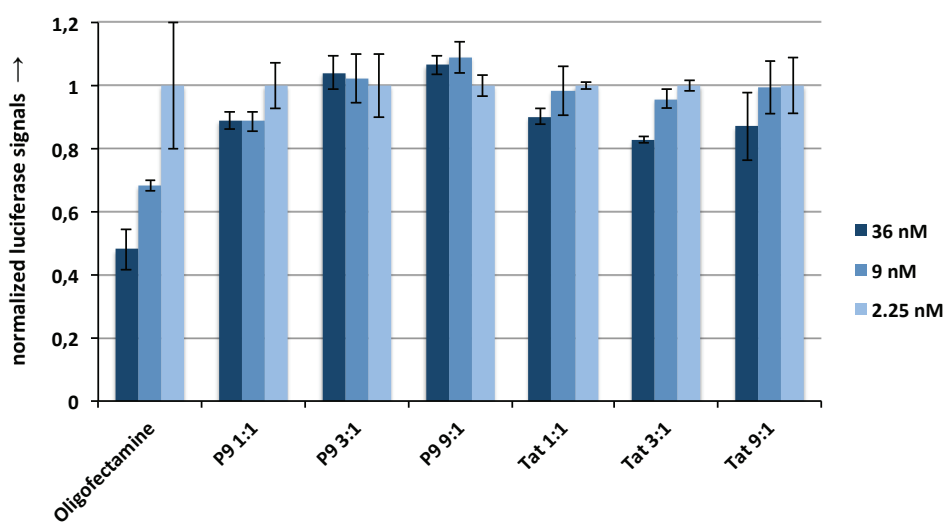
Figure 63: Zoom on the normalized luciferase signals of delivery using Oligofectamine, CF-G-P_9-$CONH_2$ (**50**) and CF-G-Tat(48-60)-$CONH_2$ (**42**) with increasing doses (36, 9, 2.25 nM) of siRen at different charge ratios.
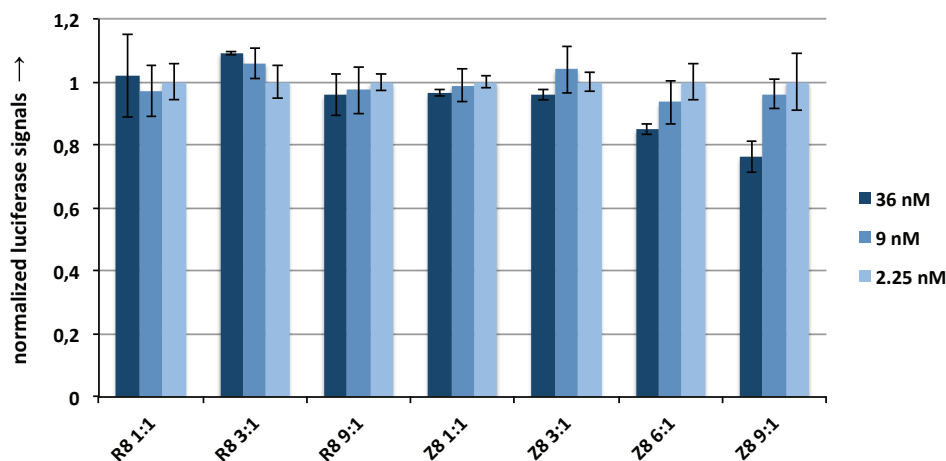
Figure 64: Zoom on the normalized luciferase signals of delivery with CF-G-R_8-$CONH_2$ (**45**) and CF-G-Z_8-$CONH_2$ (**39**) with increasing doses (36, 9, 2.25 nM) of siRen at different charge ratios.

This preliminary study showed a promising delivery potential of the examined oligoproline-based CPP Z_8 (**39**), but still leaves room for improvement for future investigations. To enhance the potency of the oligoproline-based CPPs, further experiments will be performed using the N-terminal acetylated peptides, lacking 5(6)-carboxyfluorescein. The fluorophore, originally attached for detection of the peptides in flow cytometry and microscopy experiments, presents an additional cargo in the delivery experiments. The efficiency of complexation of the CPPs with the siRNA as well as the intracellular delivery are considered to be influenced by this extra ballast. A further increase in silencing potency might also be achieved by enhancing the ratio of positive to negative charges or by increasing the chain length of the CPP to obtain the oligoproline derivative Z_9. A further extension of the chain length is currently not planed, since MTT assays revealed an increase in cytotoxicity for CPPs containing more than nine positive charged residues in a row at the tested concentrations and incubation times (3.1.6.1). An elegant way to further explore the potential of the oligoproline-based CPPs would be to examine siRNA and plasmid DNA delivery within the same assay. This could be accomplished by replacing the transfection agent jetPEI with a CPP. Other intriguing experiments could be to deliver other siRNAs or miRNA and finally to apply the assay to other cell lines, which are difficult or impossible to be transfected with established methods to date, such as stem cells.

3.2   Conformational analyses of proline derivatives

A second goal of this thesis was to investigate structure directing properties of electron-withdrawing groups (EWGs) derived from an azide at the C(4) position of proline. As a model system methyl esters of *N*-acetylated prolines were used. Monomer models of this kind are important for the understanding of the factors that determine the *cis*/*trans* ratio around the tertiary prolyl amide bond and serve therefore as valuable tools that allow for a tuning of the equilibrium within peptides (see also chapter 1.1).[22, 26a, 26b] The azido proline models **7R** and **7S** were investigated by L.-S. Sonntag *et al.* in the Wennemers group[22, 26a] and included as references to the studies in this thesis, conducted with M. Kümin. Thus, the proline derivatives bearing azido (**7R**, **7S**), *tert*-butyl carbamate (**8R**, **8S**) and ammonium (**9R**, **9S**, **10R**, **10S**) groups were synthesized and examined in regard of their *cis*/*trans* conformer ratio and their pyrrolidine ring pucker. Furthermore, guanidinylated proline derivatives were investigated, to explore the conformational properties of the cationic proline derivatives used for our oligoproline-based CPPs. Thus, proline derivatives bearing di-*tert*-butyl oxycarbonyl guanidino (**11R**, **11S**) and guanidinium (**12R**, **12S**, **13R**, **13S**) moieties, have been synthesized and analyzed by ^{1}H NMR studies:[10]
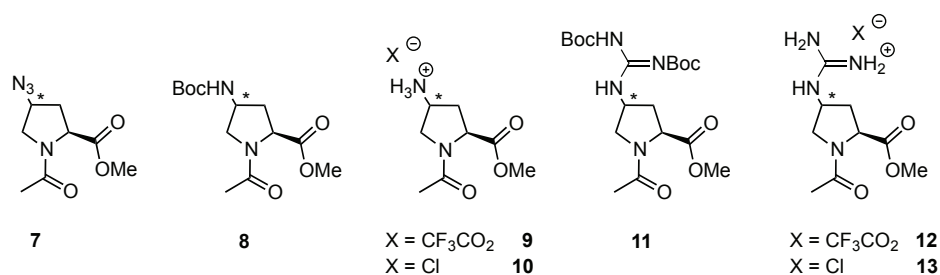
Figure 65: Monomer models bearing electron withdrawing substituents at C(4) of proline, synthesized and analyzed *via* ^{1}H NMR studies in this thesis. All compounds were synthesized as (4*R*)- and (4*S*)-isomers; * = *R* or *S*.

They were compared with amino proline derivatives **70R** and **70S**,[214] and hydroxy prolines **71R** and **71S** investigated by Raines and co-workers.[15b, 248] The investigation of the model compounds **8**-**10** provided deeper insight into the effects that determine the *cis*/*trans* conformer ratio of proline derivatives and has been published.[26b] Finally unpublished results obtained for the guanidino proline derivatives **11**-**13** will be presented and discussed.

---

[10] The syntheses and analyses of the monomer models **11**, **12** an **13** were supported by an internship performed by C. Hugelshofer with this project.

In addition the stability of all-*trans* configured PPII conformation of functionalized oligoprolines bearing (4*R*)- and (4*S*)-configured amino proline residues at every first and third position of the repeating unit was examined. We therefore synthesized the peptides Ac-[(4*R*)Amp-Pro-(4*R*)Amp]$_3$-OH (**14R**) and Ac-[(4*S*)Amp-Pro-(4*S*)Amp]$_3$-OH (**14S**) as acetylated 9-mers with a free carboxylic acid at the C-terminus (Fig. 66). Peptides with these termini were shown to be adequate systems for CD spectroscopic studies to analyze the relative stability of the PPII conformation by the switch towards the PPI conformation in different ratios of phosphate buffer and *n*-PrOH.[26a, 207]
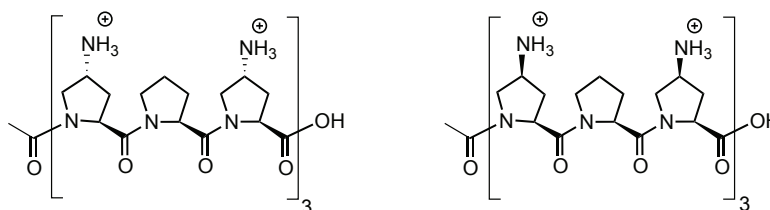
Figure 66: Oligoproline derivatives **14R** and **14S** bearing (4*R*) or (4*S*)-configured amino proline residues at every first and third position of the repeating unit; * = *R* or *S*.

In the following chapter, the syntheses of the monomer models as well as the according oligoproline derivatives are described (3.2.1). Subsequently the results of the conformational studies by ^{1}H NMR analysis and CD spectroscopy are presented (3.2.2).

3.2.1 Synthesis

3.2.1.1 Synthesis of the monomer models for ^{1}H NMR analysis

As precursors for the syntheses of the desired model compounds, the (4*R*)- and (4*S*)-configured Boc-protected azido proline methyl esters (**56R** and **56S**) were synthesized. Boc-(4*S*)Azp-OMe (**56S**) was obtained by activation of the hydroxy function of (4*R*)-hydroxy proline methyl ester (**55**) as a mesylate and S$_N$2 substitution with sodium azide under inversion of the configuration at C(4). Boc-(4*R*)Azp-OMe (**56R**) was synthesized by conversion of **55** to a mesylate by a Mitsunobu reaction with methanesulfonic acid under inversion of the absolute configuration at C(4). A following S$_N$2 substitution with sodium azide, again under inversion of the configuration at the stereogenic center at C(4), led to the product **56R** with a resulting retention of the configuration (Scheme 20). Compound **55** was prepared as described in chapter 3.1.2.3.1 from commercially available (4*R*)-hydroxy proline **15**.
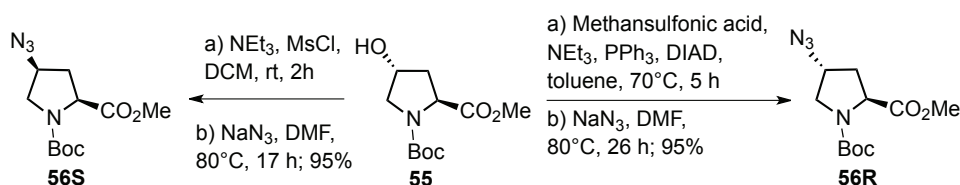
Scheme 20: Synthesis of the precursors Boc-(4*S*)Azp-OMe (**56S**) and Boc-(4*R*)Azp-OMe (**56R**).

All model compounds were obtained by the synthetic route shown in Scheme 21. Starting either from Boc-(4*R*)Azp-OMe (**56R**) or Boc-(4*S*)Azp-OMe (**56S**) the acid labile Boc protecting group was cleaved by treatment with HCl in dioxane (4 M). To prepare the azido proline derivatives **7R** and **7S**, the resulting secondary amine was acetylated with acetic anhydride under weakly basic conditions. The azido functions were subsequently reduced using Lindlar's catalyst (30% (w/w)) under a hydrogen atmosphere and the resulting amino groups were protected with Boc anhydride *in situ* to obtain the desired products Ac-(4*R*)Amp(Boc)-OMe (**8R**) and Ac-(4*S*)Amp(Boc)-OMe (**8S**). Depending on the acid used for the following Boc deprotection, the trifluoroacetic acid (TFA) salts Ac-(4*R*)Amp-OMe*TFA (**9R**) and Ac-(4*S*)Amp-OMe*TFA (**9S**) or chloride salts Ac-(4*R*)Amp-OMe*HCl (**10R**) and Ac-(4*S*)Amp-OMe*HCl (**10S**) were generated. To obtain a chloride as the counterion, the deprotection of the Boc group was achieved using HCl in dioxane (4 M), whereas the TFA salt was generated by treatment with TFA in dichloromethane in a ratio of 3:2. To prepare the guanidinylated proline derivatives **11R** and **11S**, a S$_N$2 reaction of the free amine with *N,N'*-di-Boc-*N''*-trifluoromethane sulfonylguanidine (**18**) was performed. Finally Boc deprotection using either TFA in dichloromethane in a ratio of 1:1 or HCl in dioxane (4 M), led to the according TFA salts **12R** and **12S** or chloride salts **13R** and **13S**.
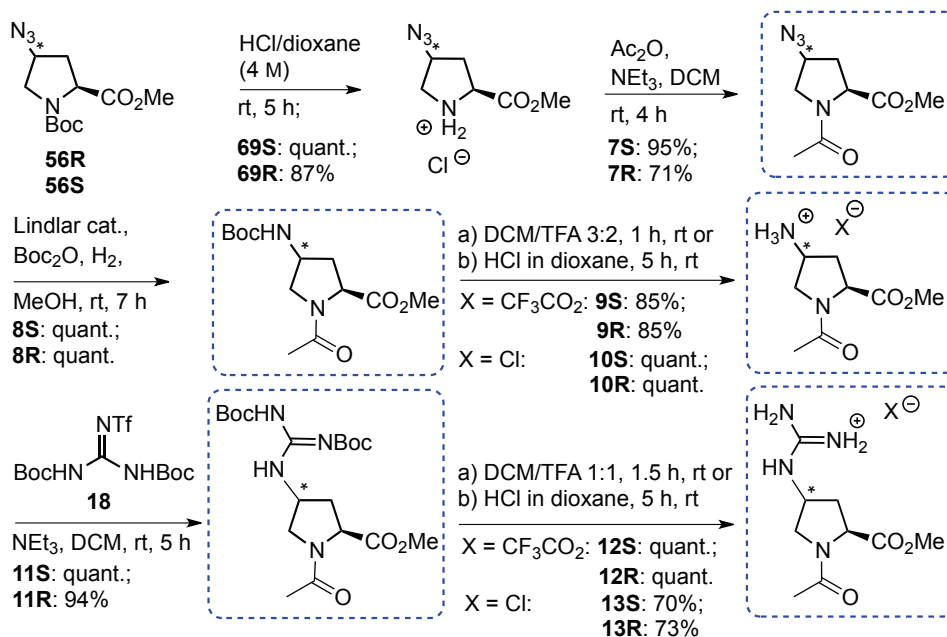
Scheme 21: Overview of the synthetic route leading to the desired acetylated proline methyl ester derivatives; * = *R* or *S*.

The guanidino proline derivatives **11R** and **11S** are also accessible directly from azido proline derivatives **3R** and **3S** by *in situ* hydrogenation and guanidinylation. This alternative route was tested for the synthesis of **11R**. The reactions were performed using *N,N'*-di-Boc-*N''*-trifluoromethane sulfonylguanidine (**18**), NEt₃ and Lindlar's catalyst (37% (w/w)), suspended in abs. MeOH and under a hydrogen atmosphere (see 5.1.3.15). This method provided the product **11R** in only one step with 98% yield after purification, compared to a 94% yield for the conventional three step synthesis and can be applied as a faster route, when the Boc-protected amino prolines **8R** and **8S** and amino proline salts **9R**, **9S**, **10R** and **10S** are not required as products on the way towards **11R** and **11S**.

3.2.1.2 Synthesis of oligoproline derivatives for CD spectroscopy

The peptides Ac-[(4*R*)Amp-Pro-(4*R*)Amp]₃-OH (**14R**) and Ac-[(4*S*)Amp-Pro-(4*S*)Amp]₃-OH (**14S**) were synthesized from their azido proline containing precursors Ac-[(4*R*)Azp-Pro-(4*R*)Azp]₃-OH (**72R**) and Ac-[(4*S*)Azp-Pro-(4*S*)Azp]₃-OH (**72S**) *via* Staudinger reduction on solid support. **72R** and **72S** were synthesized using standard SPPS (chapter 5.1.4). The coupling of the first amino acid, Fmoc-(4*R*)Azp-OH (**16R**) and Fmoc-(4*S*)Azp-OH (**16S**), respectively, on 2-chlorotrityl chloride resin was performed using the described procedure (chapter 5.1.4.3). After the initial coupling onto the resin

and capping of unreacted sites, a quantitative Fmoc test was performed to determine the loading of the amino acid on the resin. The following synthesis steps using Fmoc-(4*R*)Azp-OH (**16R**) or Fmoc-(4*S*)Azp-OH (**16S**), and Fmoc-Pro-OH were performed according to the general procedures. After cleavage from the solid support, the crude peptides were purified by preparative HPLC and solutions in different ratios of phosphate buffer and *n*-PrOH were prepared for the CD spectroscopic analyses.

3.2.2   The *cis/trans* ratio of the monomer models

As reported by L.-S. Sonntag *et al.*, the analyses of the monomers Ac-(4*R*)Azp-OMe (**7R**) and Ac-(4*S*)Azp-OMe (**7S**) revealed a significantly higher content of the *trans* conformer for the (4*R*)-substituted derivative ($K_{trans/cis}$ = 6.1 in D_2O) in comparison to the corresponding (4*S*)-configured compound ($K_{trans/cis}$ = 2.6 in D_2O). [22, 26b] [11] These findings were rationalized by a gauche effect in both (4*S*)- and (4*R*)-configured derivatives bearing electron withdrawing substituents at C(4) (see also chapter 1.1.2.3). An additional n→π* interaction between the oxygen of the acetyl group (O_{i-1}) and the carbonyl group of the methyl ester ($C_i=O_i$) is occurring in the (4*R*)-configured compounds adopting a C(4)-*exo* ring pucker and leads to a stabilization of the *trans* conformer, which is not the case in the (4*S*)-configured compounds adopting a C(4)-*endo* ring pucker (see chapter 1.1.2.1). Thus, proline derivatives with electron withdrawing substituents such as (4*R*)-configured azido proline are used as tools to stabilize the *trans* conformer of Xaa-Pro bonds in which the pyrrolidine ring adopts a C(4)-*exo* pucker. However, within many peptides and proteins the preferred ring pucker of proline with *trans* amide bonds is not C(4)*exo* but C(4)-*endo*. Thus, proline derivatives that adopt preferentially the C(4)-*endo* ring pucker and favor the *trans* conformer are valuable probes that have not been developed so far.

A n→π* interaction, stabilizing the *trans* conformation, requires a dihedral angle between O_{i-1} and $C_i=O_i$ close to the Bürgi-Dunitz trajectory, which is realized when the methyl ester is pointing inwards (ψ ≈ 145°) and a short distance is observed between O_{i-1} and C_i, as illustrated for the C(4)-*exo* puckered (4*R*)-configured proline derivatives with electron withdrawing substituents (Scheme 22a).[26b] We hypothesized that an inward orientation of the methyl ester is disfavored in proline derivatives adopting an

---

[11] The ^1H ^1H vicinal coupling constants and $K_{trans/cis}$ values obtained for **7R** and **7S** in this thesis agreed with the reported data by L.-S. Sonntag *et al*.

endo ring pucker, because of steric repulsion between the substituent at C(4) and the oxygen of the methyl ester (Scheme 22b).
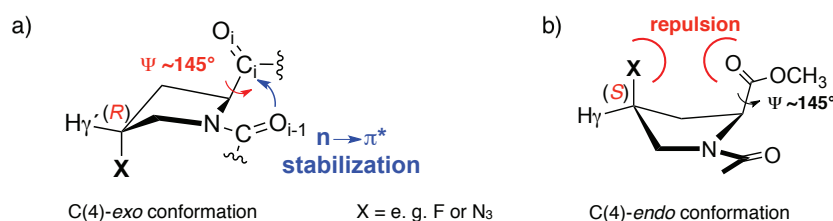
Scheme 22: a) C(4)-*exo* conformation of (4*R*)-configured proline derivatives and b) C(4)-*endo* conformation of (4*S*)-configured proline derivatives with electron-withdrawing substituents such as F or N_3. [26b]

However, the ideal orientation of the methyl ester for a n→π* interaction should be also possible in *endo* ring puckered derivatives, supported by attractive interactions between the substituent at C(4) and the carbonyl group of the methyl ester, such as a hydrogen bond or electrostatic interactions. In that case, the stabilizing n→π* interaction should lead to a favoring of the *trans* conformation. To test this hypothesis, we analyzed the conformation of (4*S*)-configured proline derivatives (**8S**-**13S**) bearing H-bond donors at C(4) and compared them to the (4*R*)- and (4*S*)-configured azido proline derivatives **7R** and **7S**. The NMR spectroscopic analyses were performed in both protic and aprotic solvents such as $CDCl_3$, in which the attractive interaction was expected to be more pronounced since solvation of the H-bond donor cannot occur and compete with the intramolecular H-bonding.

3.2.2.1 Analyses of the amino proline derivatives

Analysis of the ring pucker of the proline derivatives **8**-**10** *via* the ¹H ¹H vicinal coupling constants in correlation with the Karplus curve, revealed that all (4*S*)-configured derivatives preferentially adopt a C(4)-*endo* conformation, whereas the (4*R*)-configured ones prefer a C(4)-*exo* ring pucker.[12] By integration of the spectra a double set of signals was found, corresponding to the *cis* and *trans* conformers of the molecules. The *trans* conformer proved to be the major conformer in all cases, however the values of $K_{trans/cis}$ differ significantly between derivatives with different absolute configuration and substituents at C(4) in $CDCl_3$ and D_2O (Table 6).

---

[12] For the complete set of coupling constants, see appendix 6.6.

Table 6: Equilibrium constants $K_{trans/cis}$ of the monomer models **7-10** and **70-71** in CDCl$_3$ and D$_2$O determined *via* ^{1}H NMR analysis at 25°C.
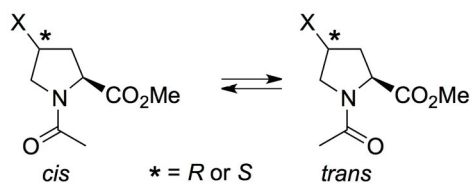
entry	Subst. X	abs. conf. at C(4)	$K_{trans/cis}$ (CDCl$_3$)	$K_{trans/cis}$ (D$_2$O)
1	N$_3$	**7S**	1.9[c]	2.6[c]
2		**7R**	3.9[c]	6.1[c]
3	NHBoc	**8S**	5.5	3.8
4		**8R**	3.5	5.2
5	NH$_3$*TFA	**9S**	n. d.[a]	5.7[b]
6		**9R**	n. d.[a]	3.5[b]
7	NH$_3$*HCl	**10S**	n. d.[a]	5.7[b]
8		**10R**	n. d.[a]	3.5[b]
9	NHAc	**70S**	5.8	4.3
10		**70R**	5.2	5.8
11	OH	**71S**	4.7	2.4[d]
12		**71R**	4.2	6.1[d]

[a] Not determined because of poor solubility, [b] Spectra recorded in 1 M TFA were identical to those of the Cl$^-$ and the CF$_3$CO$_2^-$ salts in D$_2$O [c] In agreement with reference [22, 26a]; [d] From reference [15b].

Remarkably, analysis of the ammonium-functionalized monomers **9R** and **9S** showed a higher content of the *trans* conformer around the prolyl amide bond for the (4*S*)-configured compound **9S** adopting a C(4)-*endo* ring pucker in D$_2$O (entry 5, $K_{trans/cis}$ = 5.7) in comparison to **9R** adopting a C(4)-*exo* ring pucker (entry 6, $K_{trans/cis}$ = 3.5).[13] This preference for the *trans* conformer in *endo* ring puckers compared to *exo* ring puckers was as well observed for other proline derivatives with H-bond donating substituents at C(4) in CDCl$_3$ (entries 3-4 and 9-12). Considering the differences in the *trans*/*cis* conformer ratios of the compounds relative to each other, the (4*S*)-ammonium substituent showed the most pronounced effect in D$_2$O, followed by the amide (**70S**, entry 9, $K_{trans/cis}$ = 4.3), carbamate (**8S**, entry 3, $K_{trans/cis}$ = 3.8) and hydroxyl group (**71S**, entry 11, $K_{trans/cis}$ = 2.4).

---

[13] Since spectra recorded in 1 M TFA were identical to those of the Cl$^-$ and the CF$_3$CO$_2^-$ salts in D$_2$O the following discussion will be made for compounds **9R** and **9S**.

Ab initio calculations further supported the hypothesis, since the lowest-energy conformation of Ac-[(4*S*)NHAc-Pro]-OMe (**70S**) allows for a H-bond which directs the methyl ester inwards, forming an angle of 104° between O_{i-1} and $C_i=O_i$, thus supporting an n→π* interaction and stabilization of the *trans* conformer.
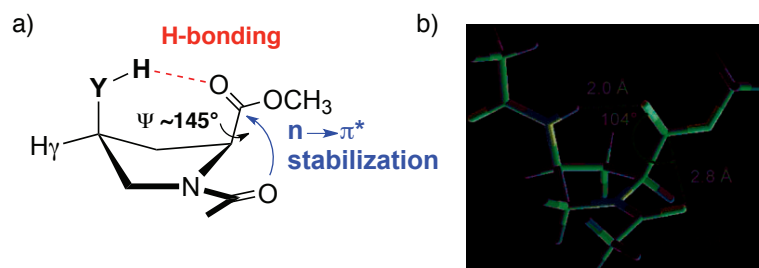
Scheme 23: a) C(4)-*endo* conformations of (4*S*)-configured derivatives with H-bond donating substituents; b) Lowest-energy conformation of Ac-[(4*S*)NHAc-Pro]-OMe (**70S**) obtained from *ab initio* calculations, performed by S. Schweizer.[26b]

These results demonstrate that the *trans* amide conformer in Xaa-Pro bonds can be populated to a significant extent in proline derivatives with a C(4)-*endo* ring pucker. IR-spectroscopic studies further supported this findings.[26b]

3.2.2.2 Analyses of the guanidino proline derivatives

The guanidinium moieties of the compounds **11-13** can be considered as EWGs, although a weaker electron withdrawing effect would be expected compared to the azido group. Furthermore they could act as well as hydrogen bond donors and lead to the preference of the *trans* conformer for C(4)-*endo* ring puckered (4*S*)-configured derivatives, as previously described for the compounds **8-10** and **70-71**. However, the bulkiness of the guanidinium group compared to the other investigated substituents might cause steric repulsions in the pseudoaxial position of this conformation and could direct the moiety towards a pseudoequatorial position. This would lead to a reversed effect in regard of the ring pucker, namely a C(4)-*exo* ring pucker for the (4*S*)-configured derivatives and a C(4)-*endo* pucker for the (4*R*)-configured compounds.

To investigate the preference of the (4*R*)- and (4*S*)-configured guanidino proline derivatives in regard of the ring pucker, the ¹H ¹H vicinal coupling constants were analyzed as described before. Tables 7 and 8 present a direct comparison of the values

for the (4*R*)- and (4*S*)-configured compounds Ac-Azp-OMe (**7**), Ac-Amp-OMe*TFA (**9**) and Ac-Gup-OMe*TFA (**12**) in D_2O.

Table 7: Values of the vicinal ^1H ^1H coupling constants of the (4*S*)-configured isomers of **7**, **9** and **12** in D_2O; Values for **7S** were taken from reference [22].

entry	$^3J_{(H,H)}$	7S		9S		12S	
		trans	*cis*	*trans*	*cis*	*trans*	*cis*
1	Hα-Hβ	9.6	7.2	9.1	9.4	9.2	9.1
2	**Hα-Hβ′**	**2.5**	**3.1**	**5.8**	**4.3**	**5.0**	**2.4**
3	Hβ-Hγ	5.2	n. d.	7.0	7.4	5.8	5.2
4	**Hβ′-Hγ**	**2.4**	**5.3**	**5.7**	**4.6**	**5.0**	**3.9**
5	Hγ-Hδ	5.3	<1	n. d.	n. d.	6.2	6.2
6	**Hγ-Hδ′**	**1.6**	**n. d.**	**n. d.**	**n. d.**	**4.4**	**1.0**

Table 8: Values of the vicinal ^1H ^1H coupling constants of the (4*R*)-configured isomers of **7**, **9** and **12** in D_2O; Values for **7R** were taken from reference [22].

entry	$^3J_{(H,H)}$	7R		9R		12R	
		trans	*cis*	*trans*	*cis*	*trans*	*cis*
1	Hα-Hβ	8.0	8.6	8.0	8.9	7.7	8.6
2	Hα-Hβ′	8.3	n. d.	7.0	4.2	7.7	6.0
3	**Hβ-Hγ′**	**3.3**	**n. d.**	**n. d.**	**6.8**	**4.9**	**6.7**
4	Hβ′-Hγ′	5.3	n. d.	n. d.	6.9	5.9	5.1
5	**Hγ′-Hδ**	**n. d.**	**n. d.**	**3.9**	**n. d.**	**3.9**	**n. d.**
6	Hγ′-Hδ′	5.9	5.5	6.3	n. d.	5.7	5.1

A similar trend of small coupling constants for Hα-Hβ′, Hβ′-Hγ′ and Hγ-Hδ′ (Table 7, entries 2, 4 and 6) of the (4*S*)-configured guanidino proline derivative **12S** was observed as for the compounds **7S** and **9S**, indicating a C(4)-*endo* pucker. Indicative for a C(4)-*exo* pucker, the coupling constants for Hβ-Hγ′ and Hγ′-Hδ (Table 8, entries 3 and 5) were small for **12R**, similar to **7R** and **9R**. Similar coupling constants were observed for according isomers of Ac-Gup(Boc)$_2$-OMe (**11**) and Ac-Gup-OMe*HCl (**13**) in D_2O.[14]

The *trans* conformer proved to be the major conformer for compounds **11**-**13** in D_2O, DMSO-d$_6$ and CD$_3$OD. However, the values of K$_{trans/cis}$ did not significantly differ between

---

[14] For the complete set of coupling constants of all compounds see appendix 6.6.

the diastereoisomers (Table 9). In D_2O **12R** showed a slightly higher $K_{trans/cis}$ equilibrium constant than **12S** (4.3 vs. 3.9). This could indicate a solvation of the guanidinium groups that compensates a hydrogen bonding effect. Due to the poor solubility in $CDCl_3$ and other aprotic solvents it was not possible to measure compounds **12** and **13** in an environment that would promote H-bonding. Attemps were made to exchange the counterions against weakly coordinating anions (WCAs), such as BArF[-]. An advantage of salt of these WCAs is that they are usually better soluble in organic solvents.[175] However, the complete exchange of all counterions in the sample could not be achieved and ^{1}H NMR spectra showed multiple species due to a partial hydrolysis of the methyl ester. Ac-Gup(Boc)$_2$-OMe (**11**) showed as well similar *trans* conformer content for both diastereoisomers in $CDCl_3$, which might be caused by steric effects due to the two Boc protection groups on the guanidyl moiety and cannot be further explained *via* ^{1}H NMR analysis.

Table 9: Equilibrium constants $K_{trans/cis}$ of the monomer models **11-13** in different solvents determined *via* ^{1}H NMR analysis at 25°C.

entry	Subst.	abs. conf.	$K_{trans/cis}$	$K_{trans/cis}$	$K_{trans/cis}$	$K_{trans/cis}$
	X	at C(4)	($CDCl_3$)	(D_2O)	(DMSO-d_6)	(CD_3OD)
1	(Boc)$_2$Gup	**11S**	3.6	n. d.[a]	2.5	n. d.[a]
2		**11R**	4.4	n. d.[a]	3.6	n. d.[a]
3	Gup*TFA	**12S**	n. d.[a]	3.9	3.3	3.0
4		**12R**	n. d.[a]	4.3	2.9	2.9
5	Gup*HCl	**13S**	n. d.[a]	3.4	3.4	n. d.
6		**13R**	n. d.[a]	4.1	3.2	n. d.

[a] Not determined because of poor solubility.

However, to further investigate if a hydrogen bond as well as a gauche effect combined with an n→π* interaction and stabilization of the *trans* conformer is possible in (4*S*)-configured derivatives bearing a guanidinium moiety at C(4), *ab initio* calculations were performed, as before in cooperation with S. Schweizer and C. Ochsenfeld. The lowest energy structures were obtained by optimizing possible conformations in the gas phase at the B3LYP/6-31G** level as previously for Ac-[(4*S*)NHAc-Pro]-OMe (**70S**, chapter 3.2.2.1). In the lowest energy conformation Ac-(4*S*)Gup-OMe (**12S**, b) adopts a C(4)-*endo*

ring pucker as observed by the analysis of the vicinal coupling constants of the ¹H NMR. Furthermore a H-bond between the substituent at C(4) and the methyl ester is predicted. As assumed, the hydrogen bond leads to an inward orientation of the methyl ester allowing for an n→π* interaction due to the favorable angle of 106° between the oxygen of the acetyl group and the carbonyl of the methyl ester, stabilizing the *trans* conformation.
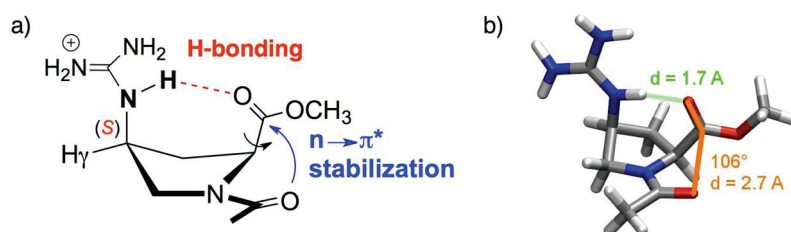
Scheme 24: a) C(4)-*endo* conformation of Ac-(4*S*)Gup-OMe (**12S**); b) B3LYP/6-31G** optimized structure of **12S**; *Ab initio* calculations were performed by S. Schweizer.

Calculated energy differences of the *trans* and *cis* conformers (ΔE*trans-cis*) further support a preference of the *trans* conformer for **12S,** although to a slightly lower extend in comparison to the compounds **70S** and **71S**, but stronger than the *trans* preference predicted for **7R** (Table 10). For the (4*R*)-configured diastereoisomer Ac-(4*R*)Gup-OMe (**12R**) a preference for the C(4)-*exo* ring pucker was observed in the lowest energy conformer as observed by the analysis of the vicinal coupling constants of the ¹H NMR. However, no preference concerning the *trans*/*cis* conformers around the tertiary amide bond could be determined according to ΔE*trans-cis* (Table 10). A possible reason is the neglected solvent interaction in the gas phase calculation, leading in this case to a similar energy level for the lowest energy conformers adopting *trans* and *cis* conformations, respectively.

Table 10: Calculated energy differences ΔE$_{trans-cis}$ between the lowest energy *trans* and *cis* conformers at the RI-MP2/TZVP//B3LYP/6-31G** level, performed by S. Schweizer.

abs. conf.	ΔE*trans-cis* [kJ mol⁻¹]			
at C(4)	N₃ (**7**)	NHAc (**70**)	OH (**71**)	Gup (**12**)
(4*S*)	1.1[a]	-11.2[b]	-15.5[b]	-9.5
(4*R*)	-6.7[a]	-4.0[b]	-6.6[b]	0.6

[a] From reference [22]; [b] From reference [26b].

3.2.3 Effects on PPII helix stability

Since a stabilization of the *trans* conformer around the prolyl amide bond was observed for the C(4)-*endo* ring puckered compound Ac-(4*S*)Amp-OMe*TFA (**9S**) due to an intramolecular H-bonding, we were interested whether this amino acid derivative can be used to tune the *cis*/*trans* amide bond ratio in a peptide. Thus, a stabilization of the all *trans* configured PPII helix would be expected. To test this hypothesis, we investigated the influence of the solvent-induced switch between the PPII and PPI helices of the oligoprolines Ac-[(4*R*)Amp-Pro-(4*R*)Amp]₃-OH (**14R**) and Ac-[(4*S*)Amp-Pro-(4*S*)Amp]₃-OH (**14S**) (Fig. 67). While the PPII conformation is preferentially adopted in aqueous environments, the all-*cis* configured PPI helix is favored in more hydrophobic solvents such as *n*-PrOH (see chapter 1.2.1). Thus the relative conformational stability of the PPII helix can be measured by the amount of *n*-PrOH necessary to induce the switch to PPI.[26a, 26b, 33a, 207, 249] To evaluate the relative PPII helix stability the peptides were acetylated at the N-terminus and the C-terminus was chosen as a carboxylic acid, which has been shown to be an adequate system for CD spectroscopic studies to analyze the relative stability of the PPII conformation by the switch towards the PPI conformation in different ratios of phosphate buffer and *n*-PrOH.[26a, 207] To ensure that the amino functions were protonated, the studies were performed in an aqueous phosphate buffer with pH 2. In fact, the CD spectroscopic studies of the oligoprolines **14R** and **14S** demonstrated a stabilization of the PPII helix by (4*S*)Amp residues (Fig. 67b). The characteristic signals for a PPII helix (minimum at 206 nm, maximum at 226 nm)[33a, 36] are present even in pure *n*-PrOH. The observed effect goes in line with the low content of the *cis* conformer of the monomer Ac-(4*S*)Amp-OMe (**9S**).[26b] However, the diastereoisomer **14R** containing (4*R*)Amp showed a switch to a PPI conformation (minimum at 215 nm, maximum at 232 nm)[33a, 36] starting from approximately 90% *n*-PrOH (Fig. 67a). The data suggest that one of both conformers or an equilibrium is adopted by oligoprolines containing (4*R*)Amp, depending on the solvent. Generally the minimum at 206 nm for **14S** is less intensive than for **14R**. Possible reasons are the positive charges or the intramolecular H-bond formation in the (4*S*)Amp containing oligoproline **14S**, which could influence the electronic structure of the amide chromophore.[214] A similar effect was observed for guanidino proline containing CPPs such as CF-G-[(4*R*)Gup-Pro-(4*R*)Gup]-CONH₂ (**26**) and CF-G-[(4*S*)Gup-Pro-(4*S*)Gup]-CONH₂ (**24**), where the (4*S*)Gup containing peptide **24** showed a less intensive minimum than **26** bearing (4*R*)Gup (see chapter 3.1.3).
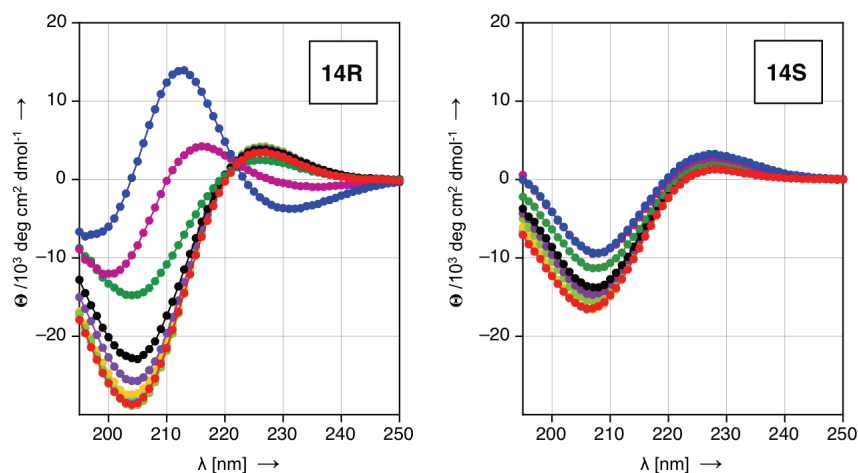
Figure 67: CD spectra of **14R** (left) and **14S** (right) in aqueous phosphate buffer (10 mM, pH 2) (•), 25% v/v *n*-PrOH in buffer (•), 50% v/v *n*-PrOH in buffer (•), 75% v/v *n*-PrOH in buffer (•), 85% v/v *n*-PrOH in buffer (•), 90% v/v *n*-PrOH in buffer (•), 95 % v/v *n*-PrOH in buffer (•), 99% v/v *n*-PrOH in buffer (•) and *n*-PrOH in buffer (•). Spectra were recorded at concentrations of 70 µM at 25 °C.

In contrast, previous studies with oligoprolines bearing (4*R*)Azp (**73R**) and (4*S*)Azp (**73S**) showed a stabilization of the PPII helix by (4*R*)Azp (Fig. 68), consistent with the reported azido gauche effect (see 1.1.2.3).[22, 26a]
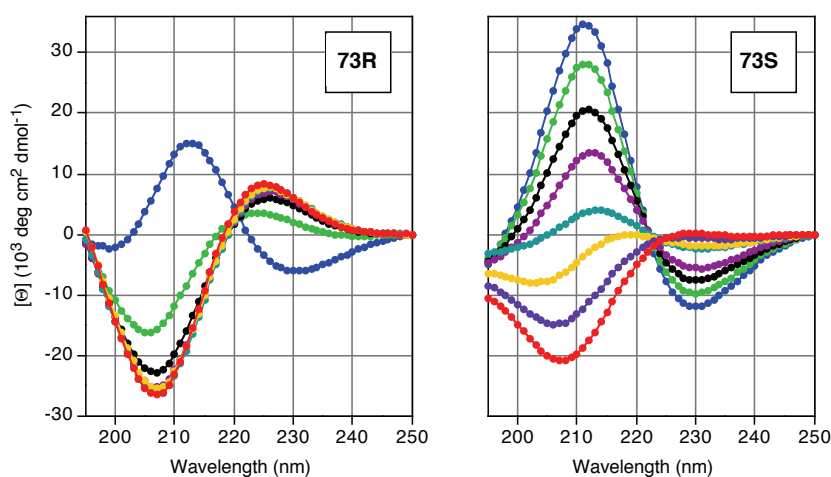
Figure 68: CD spectra of Ac-[(4*R*)Azp]₉-OH (**73R**, left) and Ac-[(4*S*)Azp]₉-OH (**73S**, right) in aqueous phosphate buffer (10 mM, pH 2) (•), 25% v/v *n*-PrOH in buffer (•), 50% v/v *n*-PrOH in buffer (•), 75% v/v *n*-PrOH in buffer (•), 85% v/v *n*-PrOH in buffer (•), 90% v/v *n*-PrOH in buffer (•), 95 % v/v *n*-PrOH in buffer (•) and *n*-PrOH in buffer (•). Spectra were recorded at concentrations of 70 µM at 25°C; From reference [26a].

In summary we observed conformational preferences for oligoproline (4*S*)-configured amino prolines, which reflects the preference of the according monomer model Ac-Amp-OMe (**9**). C(4)-endo puckered (4*S*)Amp introduced into oligoprolines leads to a higher amount of trans conformer, thus stabilizing the PPII structure, as it was possible for C(4)-exo puckered (4*R*)Azp. In contrast, C(4)-exo puckered (4*R*)Amp stabilizes the PPII conformation to a lesser extent, when introduced into oligoprolines and allows for a switch to a PPI conformation by changing the solvent from water to a more hydrophobic environment, as well as C(4)-endo puckered (4*S*)Azp. In case of the derivative Ac-Gup-OMe (**12**) a similar H-bonding and n→π* interaction for the (4*S*)-configured monomer model (**12S**) is proposed, stabilizing a *trans* conformation of a proline derivative adopting a C(4)-*endo* ring pucker, as reported for Ac-(4*S*)Amp-OMe (**9S**). For the (4*R*)-configured diastereoisomer **12R** adopting a C(4)-*exo* ring pucker a similar equilibrium constant K$_{trans/cis}$ was observed, preferring the *trans* confomer. Thus, it would be interesting for future investigations to study the relative stability of the PPII conformation in according (4*R*)- and (4*S*)-configured Gup-containing peptides. The results provide deeper insight into the factors that determine the conformation of proline residues and demonstrate that the ring pucker is not the only factor that influences the amide bond conformer ratio. We showed that a hydrogen bond between the substituent at C(4) and the amide backbone has a profound effect on the *cis/trans* conformer ratio around the tertiary amide bond. Thus, the presented proline derivatives are not only valuable monomer models as tools for understanding and investigating the factors that determine the *cis/trans* isomerization of prolyl amide bonds, but can also serve as prototypes for the development of novel tools.

4.   CONCLUSIONS AND OUTLOOK

Within this thesis we established a novel type of CPPs based on an oligoproline scaffold that shows a number of advantages over existing systems, such as an efficient uptake into different human tumor cell lines under physiological conditions, a defined intracellular localization in the nucleus, as well as low cytotoxicity and low hemolytic activity. Additional advantages are an easy functionalization of the scaffold and water solubility.

The relative cellular uptake of the developed CPPs in a selection of different human cancer cell lines revealed an enhanced uptake of the peptides $CF-G-(ZPZ)_4-CONH_2$ (**25**) and $CF-G-Z_8-CONH_2$ (**39**) in comparison to the established Tat(48-60) peptide (**42**), bearing the same amount of cationic residues, in HeLa, MCF-7, and HT-29 cells. Peptide **39** is even surpassing the level of internalization of $CF-G-R_8-CONH_2$ (**45**) and penetratin (**43**) in these cell lines under the same conditions. A different relative distribution of the uptake was found for PC-3 cells, indicating a certain cell line specificity of the CPPs. Investigations of the influence of the exact geometrical positioning of the cationic moieties along the helical backbone on the cellular uptake showed a similar internalization of the tested peptides. These findings suggest that the geometrical arrangement does not influence the internalization of our CPPs, as it was observed for certain foldamers. For these studies different subtypes of oligoproline-based CPPs were designed and evaluated, such as oligoprolines with an alternating pattern of cationic residues and unfunctionalized prolines and peptides with an *en bloc* arrangement. Peptides with the same chain lengths, but differences in the local charge distribution, bearing a row of neighboring guanidinium groups either on the N- or the C-terminus, were as well included.

The effect of the PPII helix chirality on the cellular uptake was tested with enantiomers of L- and D-oligoproline derivatives during the Master thesis of P. Raschle and showed no significant difference.[206] These findings gave a valuable hint towards the pathway by which the oligoproline-based CPPs enter cells and suggest an internalization *via* a receptor independent pathway. Further mechanistic studies could provide deeper insight into the question, how these peptides translocate the cell membrane. Towards this goal, studies at decreased temperatures (4 °C) or ATP depletion by incubation with

NaN_3 and deoxyglucose could be performed, to investigate whether the peptides prefer an energy-dependent or independent way of internalization. The investigation of the influence of the counterions of the cationic moieties on the cellular uptake might give further information for tuning the cell-penetrating properties of the peptides.

Studies with oligoproline-based CPPs containing amino or guanidino prolines revealed that the peptides bearing guanidinium groups internalize to a greater extend into cells, compared to those with ammonium groups. Furthermore, an increasing cellular uptake with increasing chain lengths and thereby cationic moieties was observed. These general trends are in line with the trends reported for arginine- versus lysine-rich CPPs.

Confocal microscopy studies of the oligoproline-based CPPs on live non-fixed HeLa cells showed a specific accumulation of the cationic oligoprolines in the nucleus. At a concentration of 15 µM and higher, a particularly intensive accumulation of the peptides within the nucleoli was observed. In contrast, a punctuated fluorescence in the cytosol of the cells was observed for the reference peptides Tat(48-60) (**42**) and CF-G-R_6-$CONH_2$ (**44**), indicative for an endosomal localization. Remarkably, no punctuated fluorescence was visible for our oligoproline-based CPPs under these conditions. This nucleus localization of the CPPs, combined with the ability to escape from endosomes, holds promise for future intracellular targeting applications.

The proteolytic stability of our CPPs proved to be very high. All L- and D-oligoproline-based CPPs exhibited a significantly higher stability towards trypsin up to 48 h compared to the reference peptides Tat(48-60) (**42**), CF-G-R_8-$CONH_2$ (**45**), and penetratin (**43**), which were completely degraded within hours. A further stability test was performed using fresh human blood serum, which led to the same results. These properties represent a major advantage of oligoproline-based CPPs over proteolytically labile CPPs that are limited to a great extend in their use for biomedical applications. The toxicity profile of the oligoproline derivatives was evaluated by MTT assays on HeLa cells and revealed a non-cytotoxic character of the oligoproline-based CPPs with up to eight neighboring guanidinium groups up to a peptide concentration of 50 µM and an incubation time of 1.5 h. Especially at a peptide concentration of 5 µM, the conditions used for flow cytometry experiments, high cell viability values (92 - 99%) were observed. The longer chained peptides CF-G-Z_{10}-$CONH_2$ (**40**) and CF-G-Z_{12}-$CONH_2$ (**41**) composed entirely of guanidino prolines, exhibited cytotoxicity, which might be due to their strong cell-penetrating properties by which the membrane could be disrupted

while entering the cells. The same loss in cell viability was observed for the longer chained references CF-G-R$_{10}$-CONH$_2$ (**46**) and CF-G-R$_{12}$-CONH$_2$ (**47**). Hemolysis assays of the CPPs on fresh human erythrocytes showed that the cationic oligoprolines do not harm the red blood cells up to a peptide concentration of 20 μM for 4 h of incubation. These are important findings, since they show that our CPPs have the potential to be applied safely for cargo delivery. A preliminary siRNA delivery experiment performed in cooperation with the group of Prof. J. Hall from the Pharmaceutical Chemistry at ETH Zürich, showed a promising delivery potential of the peptide CF-G-Z$_8$-CONH$_2$ (**39**) compared to Tat(48-60) (**42**) and CF-G-R$_8$-CONH$_2$ (**45**) in HeLa cells. These results demonstrate the potential of these novel oligoproline-based CPPs for delivery applications and will be continued in future. Currently members of the Wennemers group are working on further delivery experiments with the aim to expand the range of different cargoes. Those cargoes are envisioned to include other oligonucleotides such as plasmid DNA, but also peptides, proteins, and inorganic complexes, e.g. polyoxometalates (POMs) to target intracellular sites.

The oligoproline-based CPPs have been synthesized according to different synthesis strategies, developed during the course of this thesis. The strategy using a Fmoc-protected guanidinylated building block for SPPS emerged as the most straightforward route and provided most of the peptides. Limitations for the synthesis were the oligoproline-based CPPs bearing more than eight neighboring guanidinium moieties. This challenge will be tackled by the use of a guanidino proline building block with a sterically less demanding protecting group, to enhance the coupling efficiency of this amino acid derivative in SPPS. The synthesis of such a building block is currently developed in the Wennemers group.

Conformational studies using CD spectroscopy revealed that all oligoproline-based CPPs adopt a well-defined PPII helical structure in aqueous phosphate buffer at pH 7.4. In contrast, the reference peptides CF-G-R$_8$-CONH$_2$ (**45**), Tat(48-60), (**42**) and penetratin (**43**) do not adopt a defined secondary structure. More detailed studies on monomeric (4*S*)- and (4*R*)-configured guanidino proline derivatives have been performed in the course of a conformational analysis project, which was a second goal of this thesis.

We identified C(4)-*endo* puckered amino proline derivatives favoring a *trans* conformation around the tertiary prolyl amide bond. These derivatives can be used as tools to tune the *cis/trans* conformer ratio of Xaa-Pro bonds within peptides and thus stabilize the biologically relevant PPII conformation. Proline derivatives with a C(4)-*endo* pucker that favor *trans* amide bonds have not been developed to date. We showed that in these derivatives a hydrogen bond between the substituent at C(4) and the carbonyl group of the amide backbone is formed. This geometrical arrangement supports a n→π* interaction between the oxygen of the acetyl group and the carbonyl group of the methyl ester and stabilizes the *trans* conformer. These findings were further supported by *ab initio* calculations of the monomer models. Using the oligoprolines Ac-[(4*R*)Amp-Pro-(4*R*)Amp]$_3$-OH (**14R**) and Ac-[(4*S*)Amp-Pro-(4*S*)Amp]$_3$-OH (**14S**), we demonstrated a stabilization of the PPII conformation for peptides bearing (4*S*)Amp residues by measuring the solvent-induced conformational switch between the PPII and PPI conformation *via* CD spectroscopy.

The conformational properties of guanidinylated proline derivatives were also investigated. Attempts to analyze the *cis/trans* conformer ratios of the model compounds by ¹H NMR were not possible due to solubility issues. However, to get a hint of the conformational properties of the guanidino proline derivatives, *ab initio* calculations were performed and showed a C(4)-*endo* ring pucker for the lowest energy conformation of Ac-(4*S*)Gup-OMe (**12S**). Furthermore, a hydrogen bond combined with a n→π* interaction and subsequent stabilization of the *trans* conformer is predicted. The prospective analysis of the according oligoprolines Ac-[(4*R*)Gup-Pro-(4*R*)Gup]$_3$-OH and Ac-[(4*S*)Gup-Pro-(4*S*)Gup]$_3$-OH could provide valuable informations on the effect of guanidino proline introduced into oligoprolines.

These results provide deeper insight into the factors that determine the conformation of proline residues and demonstrate that the ring pucker is not the only factor that influences the amide bond conformer ratio. Also other non-covalent interactions such as the observed hydrogen bond have a profound effect on the *cis/trans* conformer ratio around the tertiary amide bond. Thus, the presented proline derivatives will not only be useful for the study of biological processes in which the *cis/trans* isomerization is involved, but also for the development of new probes.

5. EXPERIMENTAL PROCEDURES

5.1 Chemical synthesis

5.1.1 Materials and instruments

Solvents used for reactions corresponded to the quality puriss. for analytical and preparative Reversed Phase High Performance Liquid Chromatography (RP-HPLC), HPLC-grade solvents were used. The water used for reactions and HPLC was filtered using a Milli-Q system from Millipore, achieving resistivity above 18 ΩM at 25 °C. Solvents for column chromatography and extractions were distilled prior to use. Reagents were obtained from commercial sources and used without further purification.

Reactions were monitored by thin layer chromatography using Merck silica gel 60 F_{254} aluminium plates. Flash chromatography was performed using Fluka high purity grade silica gel 60, 230 – 400 mesh. Compounds were visualized by UV (254 nm), ninhydrin or $KMnO_4$ solutions.

Analytical RP-HPLC was performed on a Shimadzu instrument (Prominence) at the University of Basel and a Dionex UHPLC, Ultimate 3000 at ETH Zürich, respectively. Therefore the columns LiChrosphere 100 RP-18, 5 μm, Reprosil 100 C18, 150 x 4 mm, 5 μm and Reprosil gold 120 C18, 150 x 4 mm, 5 μm with a flow of 1 mL/min on the Shimadzu instrument and 0.7 mL/min on the Dionex UHPLC were used. Preparative RP-HPLC was conducted on a LC-10 system from Shimadzu at the University of Basel and a Dionex UHPLC, Ultimate 3000 at ETH Zürich, respectively, using a Reprosil 100 C18 column, 150 x 10 mm, 5 μm with a flow of 6 mL/min at 50°C. As solvent A pure acetonitrile was used, whereas solvent B was composed of 0.1% TFA and 1% acetonitrile in nanopure water.

^{1}H- and ^{13}C-NMR spectra were recorded on a Bruker DPX 400 spectrometer. Solvents for NMR were obtained from Cambridge Isotope Laboratories and chemical shifts are reported in ppm using trimethylsilane or the residual solvent peaks as a reference.

For MALDI-TOF spectra an applied Biosystems Voyager-DE PRO apparatus was used. 2,5-Dihydroxybenzoic acid (5 mg/mL in $CH_3CN/H_2O/EtOH$ 1:1:1), 4-nitroanilin (10 mg/mL in DCM/MeOH 9:1) and sinapic acid (10 mg/mL in CH_3CN/H_2O 3:7 with 0.1% TFA) were used as matrices. Sample desorption and ionization was induced by a

N_2-Laser. Data are given in mass groups per charge (m/z).

For electrospray ionization mass spectrometry (ESI-MS) a Bruker esquire 3000plus was used at the University of Basel and a Bruker Amazon speed at ETH Zürich, respectively. Liquid chromatography mass spectrometry (LC-MS) was conducted in combination with an Agilent 1100series HPLC at the University of Basel and a Dionex UHPLC, Ultimate 3000 at ETH Zürich. LC-MS was performed on a Reprosil gold C18 column, 125 x 3 mm, 3 μm with a flow of 0.5 mL/min at 50°C. Data are given in mass groups per charge (m/z).

Infrared spectra (IR) were measured on a Perkin Elmer 1600 Series FT-IR in KBr or neat between NaCl-plates. The signals were abbreviated as follows: vs = very strong, s = strong, m = medium, w = weak, vw = very weak.

UV-Vis spectroscopy was performed on a CARY 300 Bio from Varian.

Solid phase peptide synthesis was performed according to the Fmoc-Strategy. As resins for peptide synthesis 2-chlorotrityl chloride resin from Rapp Polymere and ChemMatrix from pcas BioMatrix and Biotage was used. The amino acids were purchased from Bachem and Iris Biotech.

Automated peptide synthesis was performed on a Syro I Peptide Synthesizer from MultiSynTech (Witten, Germany). Peptides were dried using an Eppendorf Concentrator plus or an Alpha 2-4 LD plus lyophilizor from Christ.

Circular dichroism (CD) spectra were recorded on a Chirascan apparatus from Applied Photophysics Ltd (United Kingdom).

5.1.2 Synthesis of building blocks for SPPS

5.1.2.1 Synthesis of Fmoc-(4*S*)Azp-OH (16*S*)

Synthesis of H-(4*R*)Hyp-OMe*HCl (**54**)
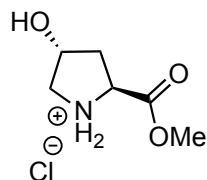
181.6 g/mol

50.0 g (381 mmol, 1.0 eq) of H-(4*R*)Hyp-OH (**15**) were dissolved in MeOH (700 mL). The solution was cooled in an ice bath and 40 mL (551 mmol, 1.5 eq) of thionyl chloride were added dropwise within 1 h. The solution was stirred at reflux for 19 h. The solvent was removed under reduced pressure to yield 69.2 g (381 mmol, quant.) of **54** as a colorless powder.

TLC (SiO$_2$, DCM/MeOH 9:1, ninhydrin): R$_f$ = 0.53

^{1}H NMR (400 MHz, DMSO-d$_6$): δ = 10.50 (s, 1H; NH2), 9.41 (s, 1H; NH), 5.36 (s, 1H; OH), 4.43 (dd, *J* = 10.8, 7.6, 1H, Hα), 4.38 (m, 1H, Hγ'), 3.72 (s, 3H; OMe), 3.36 (dd, *J* = 12.0, 4.3, 1H; Hδ), 3.04 (d, *J* = 12.0, 1H; Hδ), 2.17 (dd, *J* = 13.3, 7.3, 1H; Hβ), 2.06 (m, 1H; Hβ').

^{13}C NMR (100 MHz, DMSO-d$_6$): δ = 169.0 (Cq; CO$_2$), 68.4 (CH, Cγ), 57.3 (CH; Cα), 52.9 (CH$_3$; CH$_3$), 52.8 (CH$_2$, Cδ), 36.8 (CH$_2$; Cβ).

MS (ESI, pos.) m/z = 145.8 [M]$^+$, 146.6 [M+H]$^+$, 290.8 [2M]$^+$, (145.07 g/mol calculated for C$_6$H$_{11}$NO$_3$).

Synthesis of Boc-(4*R*)Hyp-OMe (**55**)
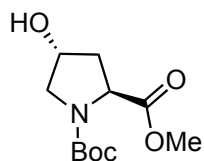
245.3 g/mol

70.0 g (385 mmol, 1.0 eq) of H-(4*R*)Hyp-OMe*HCl (**54**) were dissolved in a 1 M solution of NaHCO$_3$ (889 mL, 2.3 eq). A solution of 104.6 g (479 mmol, 1.2 eq) of Boc$_2$O in dioxane (210 mL) was slowly added under a N$_2$ atmosphere. The solution was stirred at rt for 19 h. The product was extracted with EtOAc and the organic layers were washed with a 1 M HCl solution and dried over MgSO$_4$. The solvent was removed to yield 73.1 g (298 mmol, 77%) of **55** as colorless crystals.

TLC (SiO$_2$, DCM/MeOH 9:1, ninhydrin): R$_f$ = 0.54

^{1}H and ^{13}C NMR show a double set of peaks due to *cis* and *trans* conformer around the tertiary carbamate in a ratio of 1:1.8.

^{1}H NMR (400 MHz, DMSO-d$_6$, *major conformer*): δ = 5.09 (d, *J* = 3.6, 1H; OH), 4.25 (m, 1H; Hγ'), 4.20 (m, 1H; Hα), 3.65 (s, 3H; CH3), 3.37 (dd, *J* = 11.2, 4.1, 1H; Hδ), 3.26 (m, 1H; Hδ'), 2.11 (m, 1H; Hβ), 1.88 (m, 1H; Hβ), 1.32 (s, 9H; *t*Bu).

^{1}H NMR (400 MHz, DMSO-d$_6$, *minor conformer*): δ = 3.65 (s, 3H; CH$_3$), 3.40 (dd, J = 11.1, 4.4, 1H; H$_\delta$), 1.39 (s, 9H; *t*Bu).

^{13}C NMR (100 MHz, DMSO-d$_6$, *major conformer*): δ = 174.2 (Cq; CO$_2$), 153.8 (Cq; *t*Bu), 79.8 (Cq; *t*Bu), 68.7 (CH; Cγ), 58.5 (CH; Cα), 55.3 (CH$_2$, Cδ), 52.6 (CH$_3$; CH$_3$), 40.5 (CH$_2$, Cβ), 28.7 (CH$_3$, *t*Bu).

^{13}C NMR (100 MHz, DMSO-d$_6$, *minor conformer*): 173.7 (Cq; CO$_2$), 154.6 (Cq; *t*Bu), 69.4 (CH; Cγ), 58.5 (CH; Cα), 55.3 (CH$_2$, Cδ), 52.7 (CH$_3$; CH$_3$).

MS (ESI, pos.) m/z = 146.1 [M+2Na]$^{2+}$, 268.0 [M+Na]$^+$, 513.1 [2M+Na]$^+$, (245.13 g/mol calculated for C$_{11}$H$_{19}$NO$_5$).

Synthesis of Boc-(4*S*)Azp-OMe (**56S**)
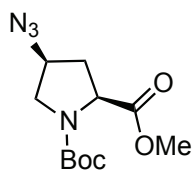
270.3 g/mol

40.0 g (163 mmol, 1.0 eq) of Boc-(4*R*)Hyp-OMe (**55**) were dissolved in DCM (310 mL) and 28 mL (196 mmol, 1.2 eq) of NEt$_3$ were added. After 15 min, the solution was cooled to 0 °C and 15 mL (196 mmol, 1.2 eq) of methanesulfonyl chloride were slowly added. The solution was stirred at rt for 2.0 h. The mixture was washed with a sat. solution of NaHCO$_3$ and the aqueous layer re-extracted with DCM. The combined organic layers were dried over MgSO$_4$ and the solvent was removed under reduced pressure. The product was dissolved in DMF (160 mL) and 53.0 g (815 mmol, 5.0 eq) NaN$_3$ were added. The solution was stirred at 80 °C for 17 h. The solvent was removed by distillation to yield 41.9 g (155 mmol, 95%) of **56S** as a yellow oil.

TLC (SiO$_2$, DCM/MeOH 9:1, ninhydrin): R$_f$ = 1.24

^{1}H and ^{13}C NMR show a double set of peaks due to *cis* and *trans* conformer around the tertiary carbamate in a ratio of 1:1.3.

^{1}H NMR (400 MHz, CDCl$_3$, *major conformer*): δ = 4.26 (dd, *J* = 8.8, 4.2, 1H, Hα), 4.11 (m, 1H, Hγ), 3.69 (s, 3H; CH$_3$), 3.63 (m, 1H; Hδ), 3.41 (m, 1H; Hδ'), 2.41 (m, 1H, Hβ), 2.10 (m, 1H; Hβ'), 1.35 (s, 9H; *t*Bu).

^{1}H NMR (400 MHz, CDCl$_3$, *minor conformer, separated signals*): 4.36 (dd, *J* = 8.9, 3.6, 1H; Hα), 1.40 (s, 9H; *t*Bu).

^{13}C NMR (100 MHz, CDCl$_3$, *major conformer*): δ = 172.6, 154.3, 80.8, 59.6, 58.0, 52.6, 51.2, 36.3, 28.5.

^{13}C NMR (100 MHz, CDCl$_3$, *minor conformer, separated signals*): δ = 172.3, 153.8, 58.6, 57.7, 52.7, 51.6, 35.4, 28.7.

MS (ESI, pos.) m/z (%) = 293.0 [M+Na]$^+$, (270.13 g/mol calculated for C$_{11}$H$_{18}$N$_4$O$_4$).

Synthesis of Boc-(4*S*)Azp-OH (**57S**)
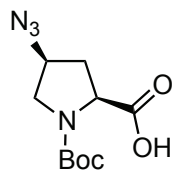
256.3 g/mol

39.8 g (147 mmol, 1.0 eq) of Boc-(4*S*)Azp-OMe (**56S**) were dissolved in THF (80 mL) and MeOH (80 mL) was added. A solution of 11.8 g (294 mmol, 2.0 eq) of NaOH in water (31 mL) were added. The mixture was stirred at rt for 3.5 h. The solution was acidified with 1 M HCl and extracted with EtOAc. The organic layers were dried over Na_2SO_4 and the solvent was removed to yield 32.2 g (126 mmol, 86%) of (**57S**) as a white powder.

TLC (SiO_2, DCM/MeOH 9:1, 254 nm): R_f = 0.51

^1H and ^{13}C NMR show a double set of peaks due to *cis* and *trans* conformer around the tertiary carbamate in a ratio of 1:1.

^1H NMR (400 MHz, CDCl$_3$, *major conformer*): δ = 10.66 (s, 1H; COOH), 4.40 (m, 1H; Hα), 4.13 (m, 1H; Hγ), 3.69 (m, 1H; Hδ), 3.45 (m, 1H; Hδ), 2.46 (m, 1H; Hβ), 2.36 (m, 1H; Hβ), 1.42 (s, 9H; *t*Bu).

^1H NMR (400 MHz, CDCl$_3$, *minor conformer*): δ = 10.66 (s, 1H; COOH), 4.30 (m, 1H; Hα), 4.13 (m, 1H; Hγ), 3.59 (m, 1H; Hδ), 3.38 (m, 1H; Hδ), 2.36 (m, 1H; Hβ), 2.18 (m, 1H; Hβ), 1.36 (s, 9H; *t*Bu).

^{13}C NMR (100 MHz, CDCl$_3$, *major conformer*): δ = 177.5, 155.8, 82.2, 59.6, 57.9, 52.1, 36.3, 28.7.

^{13}C NMR (100 MHz, CDCl$_3$, *minor conformer*): δ = 175.3, 154.1, 81.5, 59.6, 58.7, 51.3, 34.6, 28.6.

MS (ESI, pos.) m/z (%) = 255.7 [M]$^+$, 511.2 [2M]$^+$, (256.12 g/mol calculated for $C_{10}H_{16}N_4O_4$).

Synthesis of H-(4*S*)Azp-OH*HCl (**58S**)
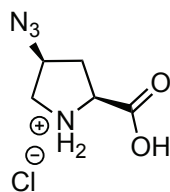
156.1 g/mol

30.0 g (117 mmol, 1.0 eq) of Boc-(4*S*)Azp-OH (**57S**) were dissolved in 4 M HCl in dioxane (173 mL). The mixture was stirred at rt for 5.0 h. The solvent was removed under reduced pressure. The solid residue was dissolved in a minimum of a 1:1 (v/v) solution of MeOH/DCM and precipitated with Et$_2$O. The solvent was removed to yield 20.2 g (105 mmol, 90%) of (**58S**) as a white powder.

TLC (SiO$_2$, CH$_3$CN/H$_2$O 4:1, ninhydrin): R$_f$ = 0.24

^{1}H NMR (400 MHz, D$_2$O): δ = 4.57 (m, 2H; Hα, Hγ), 3.49 (m, 2H; Hδ, Hδ), 2.60 (ddd, *J* = 15.3, 10.1, 5.3 Hz, 1H; Hβ), 2.45 (m, 1H; Hβ).

^{13}C NMR (100 MHz, CDCl$_3$): δ = 170.8, 60.7, 59.5, 52.0, 35.3.

MS (ESI, pos.) m/z (%) = 156.9 [M]$^+$, (156.06 g/mol calculated for C$_5$H$_8$N$_4$O$_2$).

Synthesis of Fmoc-(4*S*)Azp-OH (**16S**)
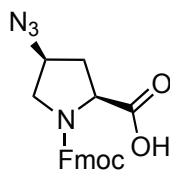
378.4 g/mol

20.0 g (104 mmol, 1.0 eq) of H-(4*S*)Azp-OH*HCl (**58S**) were dissolved in dioxane (50 mL). A solution of 22.0 g (262 mmol, 2.5 eq) of NaHCO$_3$ in water (200 mL) and dioxane (50 mL) was added. Afterwards a solution of 32.2 g (134 mmol, 1.2 eq) Fmoc chloride in dioxane (50 mL) was added to the reaction mixture. The solution was stirred at rt for 3.0 h. The organic solvent was removed and 250 mL of sat. NaHCO$_3$ solution was added to a basic pH around 8. The solution was washed with Et$_2$O and acidified with 1 M HCl to pH 1.5 and a white precipitate was formed. The suspension was extracted with EtOAc, dried over Na$_2$SO$_4$ and the solvent was removed *in vacuo.* The product **16S** was obtained as a colorless powder (39.2 g, 104 mmol, quant.).

TLC (SiO$_2$, MeOH/DCM 1:9, ninhydrin): R$_f$ = 0.42

Analytical HPLC: R$_t$ = 12.8 min, 70% to 10% B in 27 min, Reprosil gold, 1 mL/min, 254 nm.

^{1}H and ^{13}C NMR show a double set of peaks due to *cis* and *trans* conformer around the tertiary carbamate in a ratio of 1:1.

^{1}H NMR (400 MHz, CDCl$_3$/CH$_3$OD, *conformer a*): δ = 7.55 (d, *J* = 7.8 Hz, 2H; Fmoc), 7.38 (m, 2H; Fmoc), 7.18 (m, 2H; Fmoc), 7.10 (m, 2H; Fmoc), 3.97 – 4.28 (m, 5H, Fmoc, Hα, Hγ), 3.57 (dd, *J* = 11.8, 5.9 Hz, 1H; Hδ), 3.35 (dd, *J* = 12.7, 3.0 Hz, 1H; Hδ), 2.29 (m, 1H; Hβ), 2.09 (m, 1H; Hβ).

^{1}H NMR (400 MHz, CDCl$_3$/CH$_3$OD, *conformer b*): δ = 7.53 (d, *J* = 7.8 Hz, 2H; Fmoc), 7.38 (m, 2H; Fmoc), 7.18 (m, 2H; Fmoc), (m, 2H; Fmoc), 3.97 – 4.28 (m, 5H, Fmoc, Hα, Hγ), 3.49 (dd, *J* = 11.8, 5.9 Hz, 1H; Hδ), 3.32 (dd, *J* = 12.7, 3.0 Hz, 1H; Hδ), 2.29 (m, 1H; Hβ), 2.09 (m, 1H; Hβ).

^{13}C NMR (100 MHz, DMSO-d$_6$, both conformers): δ = 172.6, 172.0, 153.6, 153.6, 143.8, 143.6, 140.6, 140. 6, 127.4, 127.1, 125.0, 120.0, 66.8, 66.5, 58.8, 58.1, 57.4, 57.2, 51.4, 50.8, 46.7, 46.5, 35.5, 35.4.

MS (ESI, pos.) m/z (%) = 379.3 [M+H]$^+$, 401.2 [M+Na]$^+$, (378.13 g/mol calculated for C$_{20}$H$_{18}$N$_4$O$_4$).

5.1.2.2   Synthesis of Fmoc-(4*R*)Azp-OH (16R)

Synthesis of Boc-(4*R*)Azp-OMe (**56R**)
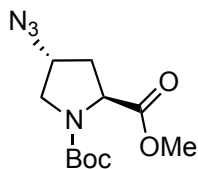
270.3 g/mol

4.80 mL (74 mmol, 1.2 eq) of methanesulfonic acid and 3.45 mL (25 mmol, 0.4 eq) of NEt$_3$ were added to a solution of 29.0 g (110 mmol, 1.8 eq) of PPh$_3$ in toluene (60 mL). The solution was cooled with an ice bath and a suspension of 15.0 g (61 mmol, 1.0 eq) of Boc-(4*R*)Hyp-OMe (**55**) in toluene (75 mL) was added. 23.7 mL (122 mmol, 1.9 eq) DIAD were slowly added. The ice bath was removed and the mixture stirred for 3.0 h at 70 °C. Afterwards the mixture was extracted with DCM. The organic layers were washed with a sat. NaHCO$_3$ solution, dried over Na$_2$SO$_4$ and the solvent was removed under reduced pressure. The resulting yellow oil was dissolved in DMF abs. (150 mL) and 20.3 g (312 mmol, 5.0 eq) of NaN$_3$ were added. The mixture was stirred overnight at 80 °C. After cooling, the solvent was removed. Et$_2$O (300 mL) was added and the mixture was extracted with sat. NaHCO$_3$. The aqueous layer was extracted with EtOAc. The combined organic layers were dried over Na$_2$SO$_4$ and the volume of the solution reduced *in vacuo*. After addition of pentane, crystals of triphenylphosphine oxide were removed by filtration. All volatiles were removed and the product was purified by flash chromatography (pentane/EtOAc, 4:1 to 3:1) to yield 15.6 g (58 mmol, 95%) of **56R** as an yellow oil.

TLC (SiO$_2$, pentane/EtOAc 4:1, ninhydrin): R$_f$ = 0.56

^{1}H and ^{13}C NMR show a double set of peaks due to *cis* and *trans* conformer around the tertiary carbamate in a ratio of 1:1.5.

^{1}H NMR (400 MHz, CDCl$_3$, *major conformer*): δ = 4.26 (t, *J* = 7.6 Hz, 1H; Hα), 4.17 – 4.13 (m, 1H; Hγ), 3.68 – 3.69 (m, 4H; OCH$_3$, Hδ), 3.64 (dd, *J* = 11.6, 3.3 Hz, 1H; Hδ), 2.32 – 2.21 (m, 1H; Hβ), 2.15 – 2.08 (m, 1H; Hβ), 1.35 (s, 9H; *t*Bu).

¹H NMR (400 MHz, CDCl₃, *minor conformer, separated signals*): δ = 4.35 (t, *J* = 7.3 Hz, 1H; Hα), 3.43 – 3.39 (d, *J* = 11.4, 3.4 Hz, 1H; Hδ), 1.40 (s, 9H, *t*Bu).

¹³C NMR (100 MHz, CDCl₃, *major conformer*): δ = 172.6, 153.1, 80.5, 58.5, 57.6, 52.0, 50.8, 36.0. 27.9.

¹³C NMR (100 MHz, CDCl₃, *minor conformer*): δ = 172.3, 153.7, 80.4, 59.0, 57.0, 52.1, 51.1, 35.1, 28.1.

MS (ESI, pos.) m/z (%) = 293.1 [M+Na]⁺, (270.13 g/mol calculated for C₁₁H₁₈N₄O₄)

Synthesis of Boc-(4*R*)Azp-OH (**57R**)
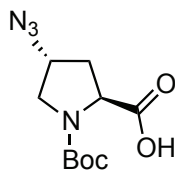
256.3 g/mol

10.9 g (40 mmol, 1.0 eq) of Boc-(4*R*)Azp-OMe (**56R**) were dissolved in THF (27 mL) and MeOH (27 mL) was added. A solution of NaOH (3.33 g, 80 mmol, 2.0 eq) in water (8 mL) was added. The mixture was stirred for 4.0 h at rt. The solution was acidified with 1 M HCl to pH 4-5 and extracted with EtOAc. The organic layers were dried over Na_2SO_4 and the solvent was removed to yield 9.74 g (38 mmol, 95%) of **57R** as a yellow powder.

TLC (SiO_2, MeOH/DCM 1:9, ninhydrin): R_f = 0.46

^{1}H and ^{13}C NMR show a double set of peaks due to *cis* and *trans* conformer around the tertiary carbamate in a ratio of 1:1.

^{1}H NMR (400 MHz, CDCl₃, *both conformers*): δ = 9.58 (bs, 2H, 2 x COOH), 4.44 (dd, *J* = 7.9, 6.3 Hz, 1H; Hα), 4.34 (dd, *J* = 7.6 Hz, 1H; Hα), 4.19 (m, 2H; Hγ), 3.70 (dd, *J* = 11.6, 5.2 Hz, 1H; Hδ), 3.62 (dd, *J* = 11.6, 5.4 Hz, 1H; Hδ), 3.58 (m, 1H; Hδ), 3.49 (m, 1H; Hδ), 2.38 – 2.44 (m, 2H; Hβ), 2.31 – 2.22 (m, 2H; Hβ), 1.47 (s, 9H; *t*Bu), 1.42 (s, 9H, *t*Bu).

^{13}C NMR (100 MHz, CDCl₃, *both conformers*): δ = 176.8, 174.5, 155.1, 153.3, 81.6, 81.0, 58.7, 58.5, 57.2, 57.1, 51.1, 50.9, 36.0, 34.2, 28.0 27.9.

MS (ESI, pos.) m/z (%) = 279.0 [M+Na]⁺, 293.1 [M+K]⁺, 535.2 [2M+Na]⁺, (256.12 g/mol calculated for $C_{10}H_{16}N_4O_4$).

Synthesis of H-(4*R*)Azp-OH*HCl (**58R**)
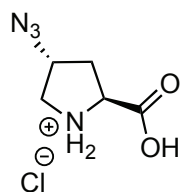
156.1 g/mol

6.20 g (24.2 mmol, 1.0 eq) of Boc-(4*R*)Azp-OH (**57R**) were dissolved in 4 M HCl in dioxane (80 mL). The mixture was stirred at rt for 2.0 h. The solvent was removed under reduced pressure. The solid residue was dissolved in a minimum of 1:1 (v/v) solution of DCM/MeOH. The product was obtained by precipitation with Et$_2$O. The solvent was removed to yield 4.68 g (24.2 mmol, quant.) of **58R** as a red powder.

TLC (SiO$_2$, CH$_3$CN/H$_2$O 4:1, ninhydrin): R$_f$ = 0.34

^{1}H NMR (400 MHz, D$_2$O): δ = 4.66 (m, 1H; Hγ), 4.51 (dd, *J* = 10.0, 8.0 Hz, 1H; Hα), 3.58 (dd, *J* = 12.8, 4.7 Hz, 1H; Hδ), 3.47 (ddd, *J* = 12.8, 2.2, 1.7 Hz, 1H; Hδ), 2.60 (dddd, *J* = 14.2, 7.9, 2.7, 1.6 Hz, 1H; Hβ), 2.37 (ddd, *J* = 14.2, 10.0, 5.2 Hz, 1H; Hβ).

^{13}C NMR (100 MHz, D$_2$O): δ = 172.2, 60.4, 59.0, 51.1, 34.8.

MS (ESI, pos.) m/z (%) = 157.5 [M+H]$^+$, (156.06 g/mol calculated for C$_5$H$_8$N$_4$O$_2$).

Synthesis of Fmoc-(4*R*)Azp-OH (**16R**)
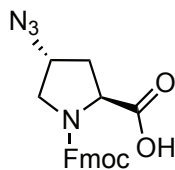
378.4 g/mol

4.68 g (24.3 mmol, 1.0 eq) of H-(4*R*)Azp-OH*HCl (**58R**) were dissolved in dioxane (12 mL). A solution of 5.39 g (64.3 mmol, 2.7 eq) of $NaHCO_3$ in water (45 mL) and dioxane (12 mL) was added. A solution of 7.50 g (29.0 mmol, 1.2 eq) Fmoc chloride in dioxane (12 mL) was added to the reaction mixture. The solution was stirred for 6.5 h at rt. The organic solvent was removed and a sat. $NaHCO_3$ solution was added to a basic pH around 8. The solution was washed with Et_2O and acidified with 1 M HCl to pH 1.5, where a white precipitate was formed. The suspension was extracted with EtOAc, dried over Na_2SO_4 and the solvent was removed *in vacuo.* The product **16R** was obtained as a pale brown powder (7.28 g, 19.2 mmol, 80%).

TLC (MeOH/DCM 1:9, ninhydrin): R_f = 0.66

Analytical HPLC: R_t = 14.8 min, 70% to 10% B in 20 min, Reprosil gold, 1 mL/min, 254 nm.

^{1}H NMR shows a double set of peaks due to *cis* and *trans* conformer around the tertiary carbamate in a ratio of 1:2.

^{1}H NMR (400 MHz, CDCl$_3$, *major conformer*): δ = 7.77 (d, *J* = 7.4 Hz, 2H; Fmoc), 7.55 (m, 2H; Fmoc), 7.43 – 7.29 (m, 4H; Fmoc), 4.52 – 4.09 (m, 5H; Fmoc, Hα, Hγ), 3.71 – 3.64 (m, 1H; Hδ), 3.55 (dd, *J* = 11.4, 3.5 Hz, 1H; Hδ), 2.45 – 2.29 (m, 2H; Hβ).

^{1}H NMR (400 MHz, CDCl$_3$, *minor conformer*): δ = 7.72 (d, *J* = 7.3 Hz, 2H; Fmoc), 7.55 (m, 2H; Fmoc), 7.43 – 7.29 (m, 4H; Fmoc), 4.52 – 4.09 (m, 5H; Fmoc, Hα, Hγ), 3.71 – 3.64 (m, 1H; Hδ), 2.45 – 2.29 (m, 2H; Hβ).

MS (ESI, pos.) m/z (%) = 401.1 [M+H]$^+$, (378.13 g/mol calculated for $C_{20}H_{18}N_4O_4$).

5.1.2.3   Synthesis of Fmoc-(4*S*)Gup(Boc)₂-OH (17)

Synthesis of Cbz-(4*R*)Hyp-OH (**59**)
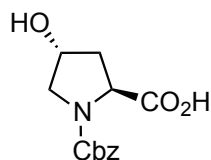
265.3 g/mol

H-(4*R*)-Hyp-OH (**15**, 30.0 g, 228 mmol, 1.0 eq) was added to a NaOH solution (18.3 g, 457 mmol, 2.0 eq) in 200 mL water. The mixture was cooled to 0 °C and benzyl chloroformate (32.7 mL, 228 mmol, 1.0 eq) was added. The reaction mixture was stirred for 5.5 h at rt and then adjusted to pH 2 with conc. HCl. The aqueous phase was extracted with EtOAc, the combined organic layers were washed with brine and dried over Na_2SO_4. The solvent was evaporated and 57.0 g (215 mmol, 94 %) of **59** were yielded as a white solid.

TLC (SiO_2, MeOH/DCM 1:9, 254 nm): R_f = 0.10

^{1}H NMR (400 MHz, $CDCl_3$): δ = 7.34-7.10 (m, 5H; Cbz), 5.02 (dd, *J* = 7.9 Hz, 2H; Cbz), 4.47-4.38 (m, 1H; Hα), 4.34 (dd, *J* = 3.80 Hz, 1H; Hγ), 3.58-3.40 (m, 2H; Hδ), 2.21 (ddt, *J* = 3.80 Hz, 11.1 Hz, 1H; Hβ), 2.06 (ddd, *J* = 4.50 Hz, 9.20 Hz, 1H; Hβ).

^{13}C NMR (400 MHz, $CDCl_3$): δ = 171.4, 152.1, 131.2, 130.4, 129.1, 128.9, 67.9, 65.6, 61.3, 59.1, 36.8.

Synthesis of Cbz-(4*R*)Hyp-OBn (**60**)
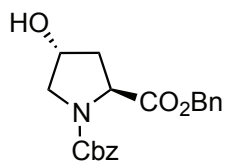
355.5 g/mol

Cbz-(4*R*)-Hyp-OH (**59**) (56.9 g, 215 mmol, 1.0 eq) was dissolved in THF (215 mL) and benzyl bromide (28.2 mL, 237 mmol, 1.1 eq) was dropwise added. The solution was cooled to 0 °C and NEt$_3$ (33.0 mL, 237 mmol, 1.1 eq) was added. The reaction mixture was stirred for 2 d at rt. Afterwards the solvent was evaporated. The obtained residue was purified by column chromatography (DCM/MeOH 20:1). The solvent was removed *in vacuo* to yield 52.3 g (147 mmol, 68%) of **60** as a colorless oil.

TLC (SiO$_2$, MeOH/DCM 1:20, 254 nm): R$_f$ = 0.43

^{1}H NMR (400 MHz, CDCl$_3$): 7.35-7.05 (m, 10H; Cbz, OBn), 5.25-4.85 (m, 4H; Cbz, OBn), 4.54-4.42 (m, 1H; Hα), 4.39 (t, *J* = 4.20 Hz, 1H; Hγ), 3.70-3.42 (m, 2H; Hδ), 2.30-2.08 (m, 1H; Hβ), 1.99 (ddd, *J* = 4.7, 7.9, 12.5 Hz; 1H, Hβ).

^{13}C NMR (400 MHz, CDCl$_3$): δ = 174.3, 154.1, 136.5, 135.8, 128.4, 128.7, 128.4, 128.2, 127.7, 127.4, 71.5, 67.3, 67.1, 58.2, 56.4, 38.9.

MS (ESI, pos.) m/z (%) = 378.1 [M+Na]$^+$, (355.14 g/mol calculated for C$_{20}$H$_{21}$NO$_5$).

Synthesis of Cbz-(4*S*)Hyp(OMs)-OBn (**61**)
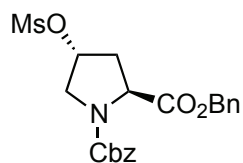
433.5 g/mol

Cbz-(4*R*)-Hyp-OBn (**60**) (52.3 g, 147 mmol, 1.0 eq) was dissolved in DCM (280 mL). NEt$_3$ (24.6 mL, 177 mmol, 1.2 eq.) was added and after stirring for 2 h the reaction mixture was cooled to 0 °C. MsCl (13.7 mL, 177 mmol, 1.2 eq) was added slowly and the mixture was stirred for another 30 min at 0 °C and further 2 h at rt. The suspension was washed with a sat. NaHCO$_3$ solution and the combined organic layers were dried over Na$_2$SO$_4$. After evaporation of the solvent a pale yellow oil was yielded. (No yield was determined because the product was directly used for the next reaction.)

TLC (SiO$_2$, EtOAc/CH 3:7, 254 nm): R$_f$ = 0.21

Synthesis of Cbz-(4*S*)Azp-OBn (**62**)
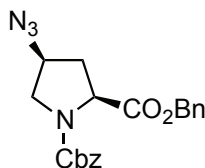
380.4 g/mol

Cbz-(4*R*)Hyp(OMs)-OBn (**61**) (52.2 g, 147 mmol, 1.0 eq) was dissolved in DMF (130 mL) and NaN$_3$ (47.8 g, 736 mmol, 5.0 eq) was added. The reaction mixture was stirred for 22 h at 80 °C. The solvent was removed *in vacuo*. The residue was dissolved in EtOAc (580 mL) and washed with H$_2$O and brine. The combined organic layers were dried over Na$_2$SO$_4$ and the solvent was evaporated. 51.2 g (135 mmol, 92%) of a **62** were obtained as a white solid.

TLC (SiO$_2$, CH/EtOAc 7:3, 254 nm): R$_f$ = 0.32

^{1}H and ^{13}C NMR show a double set of peaks due to *cis* and *trans* conformer around the tertiary carbamate in a ratio of 1:1.

^{1}H NMR (400 MHz, CDCl$_3$, *conformer a*): δ = 7.18 - 7.28 (m, 10H, Cbz), 4.95 - 5.15 (m, 4H, Cbz), 4.40 (dd, *J* = 8.9, 3.4 Hz, 1H, Hα), 4.11 (m, 1H, Hγ), 3.71 (m, 1H, Hδ), 3.50 (m, 1H, Hδ), 2.38 (m, 1H, Hβ), 2.17 (m, 1H, Hβ).

^{1}H NMR (400 MHz, CDCl$_3$, *conformer b*): 7.18 - 7.28 (m, 10H, Cbz), 4.95 - 5.15 (m, 4H, Cbz), 4.49 (dd, *J* = 9.0, 3.4 Hz, 1H, Hα), 4.11 (m, 1H, Hγ), 3.71 (m, 1H, Hδ), 3.50 (m, Hδ), 2.38 (m, 1H, Hβ), 2.17 (m, 1H, Hβ).

^{13}C NMR (100 MHz, DMSO-d$_6$, *conformer a*): δ = 171.2, 154.5, 136.3, 135.5, 128.6 - 128.3, 67.4, 67.3, 59.3, 57.9, 51.5, 36.0.

^{13}C NMR (100 MHz, DMSO-d$_6$, *conformer b*): 170.9, 154.1, 136.2, 135.3, 128.3 – 127.9, 67.4, 67.2, 58.4, 57.7, 51.2

MS (ESI, pos.) m/z (%) = 403.1 [M+Na]$^+$, 426.2 [M+2Na]$^+$ (380.15 g/mol calculated for C$_{20}$H$_{20}$N$_4$O$_4$).

Synthesis of Cbz-(4*S*)Amp-OBn (**63**)
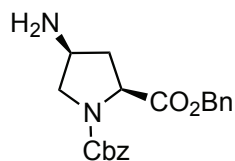
354.4 g/mol

Cbz-(4*S*)Azp-OBn (**62**) (22.8 g, 60.0 mmol, 1.0 eq) and PPh_3 (31.4 g, 120 mmol, 2.0 eq) were dissolved in THF abs. (208 mL) and H_2O (2.15 mL, 120 mmol, 2.0 eq) was added. The reaction mixture was heated for 5.5 h under reflux and afterwards the solvent was evaporated. The residue was dissolved in Et_2O (600 mL) and HCl (0.1 N, 500 mL). The aqueous phase was washed with Et_2O and the pH adjusted to 7 with an aqueous solution of Na_2CO_3 (10%). DCM was added and a white suspension formed. Afterwards Na_2CO_3 (150 mL) and brine (150 mL) were added. The aqueous phases were extracted with DCM and the combined organic layers were dried over Na_2SO_4. The solvent was evaporated and 20.9 g (59.0 mmol, quant.) of **63** were yielded as a colorless oil. The oil was used directly for further conversion.

TLC (SiO_2, MeOH/DCM 1:9, 254 nm): R_f = 0.50

MS (ESI, pos.) m/z (%) = 355.3 [M+H]+, 377.2 [M+Na]+, (354.16 g/mol calculated for $C_{20}H_{22}N_2O_4$).

Synthesis of Cbz-(4*S*)Gup(Boc)$_2$-OBn (**64**)
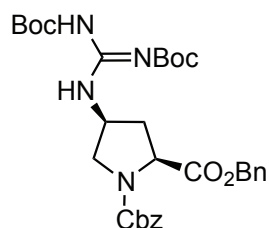
596.7 g/mol

Cbz-(4*S*)Amp-OBn (**63**) (10.4 g, 29.4 mmol, 1.0 eq) was dissolved in DCM (50 mL) and added to a solution of *N,N'*-di-Boc-*N"*-trifluoromethane sulfonylguanidine (**18**) (11.5 g, 29.4 mmol, 1.0 eq) and NEt$_3$ (4.10 mL, 29.4 mmol, 1.0 eq.) in DCM (180 mL) at 0 °C. The reaction mixture was stirred for 3 d at rt. The solvent was evaporated and the crude solid product purified by column chromatography (CH/EtOAc 7:3). The solvent was removed to yield **64** as colorless crystals (14.8 g, 24.8 mmol, 89%).

TLC (SiO$_2$, hexane/EtOAc, 254 nm): R$_f$ = 0.44

^{1}H and ^{13}C NMR show a double set of peaks due to *cis* and *trans* conformer around the tertiary carbamate in a ratio of 1:1.

^{1}H NMR (400 MHz, DMSO-d$_6$, *conformer a*): δ = 11.36 (bs, 1H; NHBoc), 8.64 (bs, 1H; NH), 7.28 - 7.19 (m, 5H; Hα, 2 x CH$_2$ (Cbz, Bn)), 4.42 (dd, *J* = 9.6, 4.6 Hz, 1H; Hδ), 3.91 – 3.84 (m, 1H; Hγ), 3.47 (dd, *J* = 11.5, 4.2 Hz, 1H; Hδ), 2.61 – 2.51 (m, 1H; Hβ), 2.03 – 1.93 (m, 1H; Hβ), 1.43 (s, 18H; 2 x *t*Bu).

^{1}H NMR (400 MHz, DMSO-d$_6$, *conformer b*): 11.36 (bs, 1H; NHBoc), 8.64 (bs, 1H; NH), 7.28 - 7.19 (m, 5H; Hα, 2 x CH$_2$ (Cbz, Bn)), 4.35 (dd, *J* = 9.2, 4.2 Hz, 1H; Hδ), 3.91 – 3.84 (m, 1H; Hγ), 3.40 (dd, *J* = 11.4, 4.6 Hz, 1H; Hδ), 2.61 – 2.51 (m, 1H; Hβ), 2.03 – 1.93 (m, 1H; Hβ), 1.41 (s, 18H; 2 x *t*Bu).

MS (ESI, pos.) m/z (%) = 619.3 [M+Na]$^+$, (596.28 g/mol calculated for C$_{31}$H$_{40}$N$_4$O$_8$).

Synthesis of H-(4*S*)Gup(Boc)$_2$-OH (**65**)
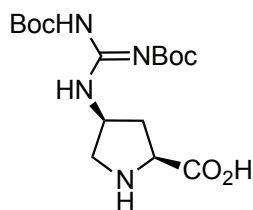
372.4 g/mol

Cbz-(4*S*)Gup(Boc)$_2$-OBn (**64**) (10.9 g, 18.3 mmol, 1.0 eq) was dissolved in MeOH (300 mL). The flask was purged three times with nitrogen. Pd/C (545 mg, 5% w/w) was added to the mixture. Nitrogen was removed and a balloon filled with hydrogen was placed at the flask. The reaction mixture was flushed three times with hydrogen. Finally a full balloon filled with hydrogen was placed again at the flask and the mixture was stirred overnight at rt. The solvent was removed and the crude residue was used directly for the next synthesis step.

TLC (SiO$_2$, EtOAc/CH 3:7, 254 nm): R$_f$ = 0.10

MS (ESI, pos.) m/z (%) = 373.2 [M+H]$^+$, 395.1 [M+Na]$^+$, (372.20 g/mol calculated for C$_{16}$H$_{28}$N$_4$O$_6$).

Synthesis of Fmoc-(4*S*)Gup(Boc)$_2$-OH (**17**)
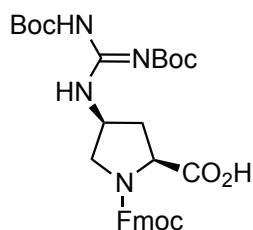
594.7 g/mol

H-(4*S*)Gup(Boc)$_2$-OH (**65**) (21.9 g, 58.7 mmol, 1.0 eq.) and Na$_2$CO$_3$ (12.4 g, 117 mmol, 2.0 eq) were dissolved in H$_2$O (500 mL) and cooled with an ice bath. A solution of Fmoc-OSu (29.7 g, 88.0 mmol, 1.5 eq) in DMF (20 mL) was added at 0 °C in one portion and the reaction mixture was stirred for 2 h at 0 °C. Water and DMF were removed and EtOAc was added to the residue. The organic layer was dried over Na$_2$SO$_4$ and the solvent was evaporated. The solid residue was recrystallized from EtOAc and further purified by column chromatography (MeOH/DCM 3:97) to yield 8.28 g (13.9 mmol, 24%) of **17** as a colorless solid.

TLC (SiO$_2$, DCM/EtOAc 1:1, 254 nm): R$_f$ = 0.25

^{1}H NMR (250 MHz, DMSO-d$_6$): δ = 11.4 (bs, 1H, OH), 8.45 (dd, *J* = 7.6, 13.0 Hz, 1H, NHBoc), 7.90 (dd, *J* = 3.7, 7.3 Hz, 2H, Fmoc), 7.66 (d, *J* = 7.4 Hz, 2H, Fmoc), 7.42 (t, *J* = 7.40 Hz, 2H, Fmoc), 7.34 (t, *J* = 6.8 Hz, 2H, Fmoc), 4.32-4.27 (m, 2H; Fmoc, CH$_2$), 4.21-4.15 (m, 2H, Hδ), 4.03 (q, *J* = 7.1 Hz, 1H; Fmoc, CH), 3.83-3.77 (m, 1H, Hα), 3.37 (ddd, *J* = 3.5, 10.9, 20.6 Hz, 1H, Hγ), 2.70-2.50 (m, 2H; Hβ), 1.47-1.41 (m, 18H; 2 x *t*Bu).

^{13}C NMR (100 MHz, DMSO-d$_6$): δ = 174.1, 173.7, 162.8, 154.8, 153.8, 151.7, 143.7, 143.6, 140.7, 140.6, 127.7, 127.2, 125.2, 120.1, 83.0, 78.4, 67.2, 66.8, 59.7, 57.7, 52.4, 51.8, 49.4, 48.5, 46.7, 46.5, 35.8, 34.6, 28.0, 27.6.

MS (ESI, pos.) m/z (%) = 595.3 [M+H]$^+$, (594.27 g/mol calculated for C$_{31}$H$_{38}$N$_4$O$_8$).

5.1.2.4   Synthesis of *N,N'*-di-Boc-*N''*-trifluoromethane sulfonylguanidine (18)

Synthesis of *N,N'*-di-Boc-guanidine (**67**)

$$BocHN \diagup NH$$
$$| $$
$$NHBoc$$
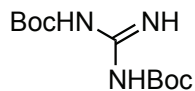
259.3 g/mol

NaOH (32.0 g, 800 mmol, 4.0 eq) was dissolved in H_2O (200 mL) and guanidinium hydrochloride (**66**) (19.2 g, 201 mmol, 1.0 eq) was added. Dioxane (400 mL) was added and the mixture was cooled to 0 °C. Afterwards Boc_2O (74.0 g, 340 mmol, 1.7 eq) was added and after removing of the ice bath the mixture was stirred for another 22 h at rt. The solvent was evaporated to one third of the original volume and the suspension was diluted with H_2O (200 mL) and extracted with DCM. The combined organic layers were washed with citric acid (10% in water), water and brine and finally dried over Na_2SO_4. The solvent was removed and the product purified by column chromatography (DCM to DCM/MeOH 9:1). **67** was obtained as colorless crystals (28.8 g, 111 mmol, 55%).

TLC (SiO_2, MeOH/DCM 3:97, 254 nm): R_f = 0.64

^{1}H NMR (400 MHz, CDCl$_3$): δ/ppm = 8.41 (s, 3H; NH), 1.47-1.37 (m, 18H; *t*Bu).

^{13}C NMR (100 MHz, CDCl$_3$): δ/ppm = 158.5 (carbamate), 50.42 (guanidine), 30.5 (*t*Bu), 22.9 (*t*Bu).

MS (ESI, pos.) m/z (%) = 282.0 [M+Na]$^+$ (259.15 g/mol calculated for $C_{11}H_{21}N_3O_4$).

Synthesis of *N,N'*-di-Boc-*N"*-trifluoromethane sulfonylguanidine (**18**)

$$\text{BocHN} \diagup \text{NTf}$$
$$\underset{\text{NHBoc}}{|}$$
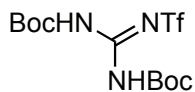
391.4 g/mol

N,N'-di-Boc-guanidine **67** (17.5 g, 67.6 mmol, 1.0 eq.) was dissolved in DCM abs. (180 mL) and DIPEA (12.2 mL, 71.0 mmol, 1.1 eq.) was added under a nitrogen atmosphere. Trifluoroacetic anhydride (11.9 mL, 71.0 mmol, 1.1 eq.) was added dropwise at -80 °C. Within 3.5 h the temperature was raised constantly to -20°C. A 2 M NaHSO$_4$-solution (120 mL) was added slowly to the mixture and it was stirred for 5 min. The layers were immediately separated. The aqueous phase was extracted with DCM. The combined organic layers were washed with 2 M NaHSO$_4$ solution and brine. Afterwards they were dried over Na$_2$SO$_4$. After evaporation of the solvent 19.9 g (50.8 mmol, 75%) of **18** was yielded as colorless crystals.

TLC (SiO$_2$, DCM, 254 nm): R$_f$ = 0.70

^{1}H NMR (400 MHz, CDCl$_3$): δ = 10.0 (s, 2H; NH), 1.47 (s, 18H; *t*Bu).

^{13}C NMR (100 MHz, CDCl$_3$): δ = 151.4 (carbamate), 120.9 (guanidine), 117.7 (CF$_3$), 86.0 (*t*Bu), 27.8 (*t*Bu).

MS (ESI, pos.) m/z (%) = 414.1 [M+Na]$^+$, (391.10 g/mol calculated for C$_{12}$H$_{20}$F$_3$N$_3$O$_6$S)

5.1.3 Synthesis of monomer models

5.1.3.1 Synthesis of Ac-(4*S*)Azp-OMe (7*S*)

Synthesis of H-(4*S*)Azp-OMe*HCl (**69S**)
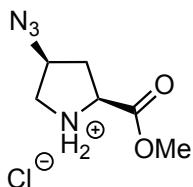
206.6 g/mol

1.00 g (3.70 mmol, 1.0 eq) of Boc-(4*S*)Azp-OMe (**56S**) was dissolved in 4 M HCl in dioxane (5.80 mL). The mixture was stirred at rt for 5.0 h. The solvent was removed under reduced pressure. The solid residue was dissolved in a minimum of a 1:1 (v/v) solution of MeOH/DCM and precipitated with Et_2O. The solvent was removed to yield 0.76 g (3.70 mmol, quant.) of **69S** as a white powder.

TLC (SiO$_2$, H$_2$O/CH$_3$CN 1:4, ninhydrin): R$_f$ = 0.55

^{1}H NMR (400 MHz, D$_2$O): δ = 4.57 (dd, *J* = 9.9, 3.8 Hz; Hα), 4.56 – 4.51 (m, 1H; Hγ), 3.76 (s, 3H; OCH$_3$), 3.44 – 3.43 (m, 2H; Hδ, Hδ), 2.55 (ddd, *J* = 15.2, 9.9, 5.4 Hz, 1H; Hβ), 2.43 – 2.38 (m, 1H; Hβ).

^{13}C NMR (100 MHz, MeOD): δ = 170.0, 60.6, 59.6, 54.2, 52.1, 35.2.

MS (ESI, pos.) m/z (%) = 171.0 [M+H]$^+$, 193.0 [M+Na]$^+$, 341.1 [2M+H]$^+$, 363.1 [2M+Na]$^+$, (170.08 g/mol calculated for C$_6$H$_{10}$N$_4$O$_2$).

Synthesis of Ac-(4*S*)Azp-OMe (**7S**)
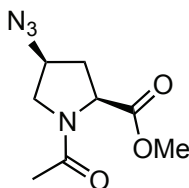
212.2 g/mol

H-(4*S*)Azp-OMe*HCl (**69S**) (3.84 g, 16.6 mmol, 1.0 eq) was dissolved in abs. DCM (20 ml). Ac$_2$O (3.2 ml, 33.2 mmol, 2.0 eq) and NEt$_3$ (6.9 ml, 49.8 mmol, 3.0 eq) were added and the suspension was stirred at rt for 3 h. 1 M HCl (8 ml) was added and the mixture was extracted with EtOAc (2 x 100 ml). The combined org. layers were dried over Na$_2$SO$_4$ and the solvent was evaporated. The yellow residue was purified by flash chromatography (SiO$_2$, 5% MeOH/DCM) to **7S** yield a light yellow oil (3.35 g, 15.8 mmol, 95 %).

TLC (SiO$_2$, MeOH/DCM 5:95, KMnO$_4$): R$_f$ = 0.31

^{1}H and ^{13}C NMR show a double set of peaks due to *cis* and *trans* conformer around the tertiary carbamate in a ratio of 1:1.9 in CDCl$_3$.

^{1}H NMR (400 MHz, CDCl$_3$, *major conformer*): δ = 4.54 (dd, *J* = 9.0, 4.2 Hz, 1H; Hα), 4.25-4.18 (m, 1H; Hγ), 3.74 (dd, *J* = 10.9, 6.1 Hz, 1H; Hδ), 3.68 (s, 3H; OCH$_3$), 3.50 (dd, *J* = 10.9, 4.0 Hz, 1H; Hδ), 2.41 (ddd, *J* = 13.5, 9.0, 6.0 Hz, 1H; Hβ), 2.14 (ddd, *J* = 13.5, 4.3, 4.2 Hz, 1H; Hβ), 2.04 (s 3H, Ac);

^{1}H NMR (400 MHz, CDCl$_3$, *minor conformer*): δ = 4.40 (dd, *J* = 5.3, 5.3 Hz, 1H; Hα), 4.25-4.18 (m, 1H; Hγ), 3.76 - 3.66 (m, 1 H, Hδ), 3.73 (s, 3H; OCH$_3$), 3.56 - 3.47 (m, 1H; Hδ), 2.44 - 2.37 (m, 1H; Hβ), 2.17 - 2.10 (m, 1H; Hβ), 1.97 (s, 3H; Ac).

^{13}C NMR (100 MHz, CDCl$_3$, *major conformer*): δ = 171.2, 169.5, 59.3, 57.1, 52.4, 52.3, 34.5, 22.1.

^{13}C NMR (100 MHz, CDCl$_3$, *minor conformer*): δ = 173.7, 170.2, 58.7, 58.1, 52.8, 51.3, 36.6, 21.9.

MS (ESI, pos.) m/z (%) = 235.0 [M+Na]⁺, (212.09 g/mol calculated for $C_8H_{12}N_4O_3$).

5.1.3.2   Synthesis of Ac-(4*R*)Azp-OMe (7R)

Synthesis of H-(4*R*)Azp-OMe*HCl (**69R**)
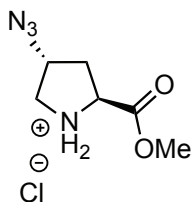
206.6 g/mol

1.00 g (3.7 mmol, 1.0 eq) of Boc-(4*R*)Azp-OMe (**56R**) was dissolved in 4 M HCl in dioxane (5.80 mL). The mixture was stirred at rt for 5.0 h. The solvent was removed under reduced pressure. The solid residue was dissolved in a minimum of a 1:1 (v/v) solution of MeOH/DCM and precipitated with Et₂O. The solvent was removed to yield 0.66 g (3.20 mmol, 87%) of **69R** as a white powder.

TLC (SiO₂, H₂O/CH₃CN 1:4, ninhydrin): R_f = 0.55

¹H NMR (400 MHz, D₂O): δ = 4.54 – 4.59 (m, 2H; Hα, Hγ), 3.73 (s, 3H; OCH₃), 3.49 (dd, *J* = 12.8, 4.7 Hz, 1H; Hδ), 3.39 (dd, *J* = 12.8, 1.4 Hz, 1H; Hδ), 2.52 (ddd, *J* = 14.3, 7.9, 1.4 Hz, 1H; Hβ), 2.35 – 2.27 (m, 1H; Hβ).

¹³C NMR (100 MHz, MeOD): δ = 169.8, 61.3, 59.4, 54.1, 52.1, 35.5.

MS (ESI, pos.) m/z (%) = 171.0 [M+H]⁺, 193.0 [M+Na]⁺, (170.08 g/mol calculated for $C_6H_{10}N_4O_2$).

Synthesis of Ac-(4*R*)Azp-OMe (**7R**)
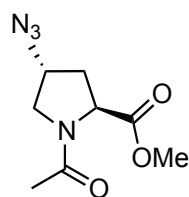
212.2 g/mol

Ac-(4*R*)Azp-OMe (**7R**) was synthesized according to the procedure described for Ac-(4*S*)Azp-OMe (**7S**). Starting from H-(4*R*)Azp-OMe*HCl (**69R**) (4.07 g, 19.7 mmol, 1.0 eq) **7R** was obtained as a yellow oil (2.97 g, 14.0 mmol, 71 %).

TLC (SiO$_2$, MeOH/DCM 5:95, KMnO$_4$): R$_f$ = 0.38

^{1}H and ^{13}C NMR show a double set of peaks due to *cis* and *trans* conformer around the tertiary carbamate in a ratio of 1:3.9 in CDCl$_3$.

^{1}H NMR (400 MHz, CDCl$_3$, *major conformer*): δ = 4.52 (dd, *J* = 8.0, 6.7 Hz, 1H, Hα), 4.32-4.27 (m, 1H, Hγ), 3.84 (dd, *J* = 10.8, 5.6 Hz, 1H, Hδ), 3.72 (s, 3H, OCH$_3$), 3.48 (ddd, J = 10.7, 3.8, 0.6 Hz, 1H, Hδ), 2.31 (dddd, J = 13.5 Hz, 8.2 Hz, 5.0 Hz, 0.9 Hz, 1 H, Hβ), 2.22-2.16 (m, 1 H, Hβ), 2.07 (s, 3H, Ac).

^{1}H NMR (400 MHz, CDCl$_3$, *minor conformer, separated signals*): δ = 4.47 (dd, *J* = 8.2, 5.9 Hz, 1H, Hα), 4.22-4.17 (m, 1 H, Hγ), 3.76 (s, 3H, OCH$_3$), 3.67 (dd, *J* = 12.5, 5.9 Hz, 1H, Hδ), 2.42 (dddd, J = 13.4 Hz, 8.2 Hz, 5.1 Hz, 1.2 Hz, 1H, Hβ), 1.96 (s, 3H, Ac).

^{13}C NMR (100 MHz, CDCl$_3$, *major conformer*): δ = 172.2, 169.5, 59.5, 57.3, 52.6, 52.5, 34.8, 22.2.

^{13}C NMR (100 MHz, CDCl$_3$, *minor conformer*): δ = 172.0, 170.0, 58.6, 58.0, 52.9, 51.0, 36.9, 21.6.

MS (ESI, pos.) m/z (%) = 235.0 [M+Na]$^+$, (212.09 g/mol calculated for C$_8$H$_{12}$N$_4$O$_3$).

5.1.3.3   Synthesis of Ac-(4*S*)Amp(Boc)-OMe (8S)
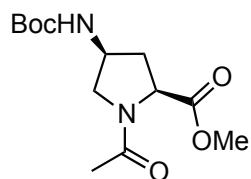
286.3 g/mol

Ac-(4*S*)Azp-OMe (**7S**) (1.10 g, 5.18 mmol, 1.0 eq) was dissolved in abs. MeOH (60 mL). Boc$_2$O (1.81 g, 8.29 mmol, 1.6 eq) and Lindlar catalyst (380 mg, 35 wt%) were added and the mixture was stirred under a hydrogen atmosphere at rt for 7 h. The mixture was filtered over celite and rinsed with MeOH. The solvent was removed *in vacuo* to yield **8S** as a colorless oil (1.48 g, 5.17 mmol, quant.).

TLC (SiO$_2$, MeOH/DCM 1:9, ninhydrin): R$_f$ = 0.58

^{1}H and ^{13}C NMR show a double set of peaks due to *cis* and *trans* conformer around the tertiary carbamate in a ratio of 1:3.8 in D$_2$O.

^{1}H NMR (400 MHz, D$_2$O, *major conformer*): δ = 4.52 (dd, *J* = 8.7, 5.8 Hz, 1H, Hα), 4.26-4.20 (m, 1H, Hγ), 3.95 (dd, *J* = 11.0, 6.5 Hz, 1H, Hδ), 3.78 (s, 3H, OCH$_3$), 3.54 (dd, *J* = 11.0, 5.4 Hz, 1H, Hδ), 2.60 (ddd, *J* = 13.5, 8.8, 6.1 Hz, 1H, Hβ), 2.13 (s, 3H, Ac), 2.16-2.03 (m, 1 H, Hβ), 1.45 (s, 9H, *t*Bu)

^{1}H NMR (400 MHz, CDCl$_3$, *minor conformer, separated signals*): δ = 4.11 (m$_c$, 1H, Hγ), 3.82 (s, 3H, OCH$_3$), 3.45 (dd, *J* = 12.7, 2.0 Hz, 1H, Hδ), 2.06 (s, 3H, Ac), 1.45 (s, 9H, *t*Bu).

^{13}C NMR (100 MHz, CDCl$_3$, *major conformer*): δ = 174.3, 173.1, 157.3, 81.4, 69.7, 57.6, 53.1, 52.7, 29.6, 27.6, 21.3

^{13}C NMR (100 MHz, CDCl$_3$, *minor conformer*): δ = 174.2, 173.9, 157.3, 81.4, 69.7, 59.0, 53.4, 51.4, 34.4, 27.6, 21.1.

MS (ESI, pos.) m/z (%) = 309 [M+Na]$^+$ (100), (286.15 g/mol calculated for C$_{13}$H$_{22}$N$_2$O$_5$).

5.1.3.4 Synthesis of Ac-(4*R*)Amp(Boc)-OMe (8R)
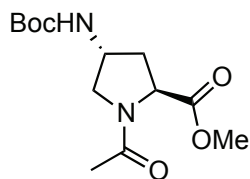
286.3 g/mol

Ac-(4*R*)Amp(Boc)-OMe (**8R**) was synthesized according to the procedure described for Ac-(4*S*)Amp(Boc)-OMe (**8S**). Starting from Ac-(4*R*)Azp-OMe (**7S**) (1.10 g, 5.18 mmol, 1.00 eq) **8R** was obtained as a light yellow oil (1.48 g, 7.70 mmol, quant.).

TLC (SiO$_2$, MeOH/DCM 1:9, ninhydrin): R$_f$ = 0.49

^{1}H and ^{13}C NMR show a double set of peaks due to *cis* and *trans* conformer around the tertiary carbamate in a ratio of 1:5.2 in D$_2$O.

^{1}H NMR (400 MHz, D$_2$O, *major conformer*): δ = 4.40 (dd, *J* = 8.6, 5.3 Hz, 1H, Hα), 4.14 (m$_c$, 1H, Hγ), 3.80 (dd, *J* = 11.0, 6.1 Hz, 1H, Hδ), 3.64 (s, 3H, OCH$_3$), 3.40 (dd, *J* = 11.0, 4.7 Hz, 1H, Hδ), 2.18-2.14 (m, 2H, Hβ), 1.99 (s, 3H, Ac), 1.30 (s, 9H, *t*Bu).

^{1}H NMR (400 MHz, D$_2$O, *minor conformer, separated signals*): δ = 4.06 (m$_c$, 1H, Hγ), 3.69 (s, 3H, OCH$_3$), 3.60-3.58 (m, 1H, Hδ), 3.30 (dd, *J* = 12.2, 6.0 Hz, 1H, Hδ), 2.36-2.20 (m, 2 H, Hβ), 1.88 (s, 3H, Ac), 1.11 (s, 9H, *t*Bu).

^{13}C NMR (100 MHz, CDCl$_3$, *major conformer*): δ = 174.2, 173.1, 157.5, 81.4, 69.7, 57.6, 53.1, 34.3, 29.6, 27.6, 21.2; (*minor conformer not detectable).

MS (ESI, pos.) m/z (%) = 309 [M+Na]$^+$ (90), 595 [2M+Na]$^+$ (100), (286.15 g/mol calculated for C$_{13}$H$_{22}$N$_2$O$_5$).

5.1.3.5 Synthesis of Ac-(4*S*)Amp-OMe*TFA (9S)
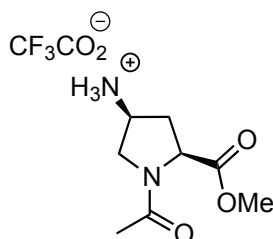
300.2 g/mol

Ac-(4*S*)Amp(Boc)-OMe (**8S**) (1.48 g, 5.17 mmol, 1.0 eq) was dissolved in abs. DCM (18 ml) and the mixture was cooled to 0°C. TFA (12.0 ml) was added dropwise, the cooling bath was removed and the mixture was stirred under Argon atmosphere at rt for 1 h. TFA and the solvent was removed *in vacuo*, the residue was dissolved in a minimum of DCM/MeOH 1:1 (v/v) and added dropwise to cool Et_2O. The white solid was filtered off and dried *in vacuo* to yield **9S** (1.31 g, 4.40 mmol, 85 %).

TLC (SiO_2, MeOH/DCM 1:9, ninhydrin): R_f = 0.2

^{1}H and ^{13}C NMR spectra of the HCl- and the TFA-salt are identical and show a double set of peaks in a ratio of 1:5.7 in D_2O due to *cis* and *trans* conformers around the tertiary amide.

^{1}H NMR (400 MHz, D_2O, *major conformer*): δ = 4.39 (dd, *J* = 9.1, 5.8 Hz, 1H; Hα), 4.01-3.94 (m, 2H; Hγ, Hδ), 3.71 (m, 1H; Hδ), 3.67 (s, 3H; OCH_3), 2.69 (ddd, *J* = 14.5, 9.0, 6.8 Hz, 1H; Hβ), 2.07 (dt, *J* = 14.3, 5.6 Hz, 1H; Hβ), 2.01 (s, 3H; Ac).

^{1}H NMR (400 MHz, D_2O, *minor conformer, separated signals*): δ = 4.71 (dd, *J* = 9.5, 4.4 Hz, 1H; Hα), 4.01-3.90 (m, 2H; Hγ, Hδ), 3.73 (s, 3H; OCH_3), 3.45 (dd, *J* = 12.4, 4.9 Hz, 1H; Hδ), 2.81 (ddd, *J* = 14.6, 9.5, 7.4 Hz, 1H; Hβ), 2.24 (dt, *J* = 14.6, 4.6 Hz, 1H; Hβ), 1.92 (s, 3H; Ac).

^{13}C NMR (100 MHz, D_2O, *major conformer*): δ = 174.4, 173.2, 57.7, 53.3, 50.9, 49.4, 32.2, 21.3.

^{13}C NMR (100 MHz, D_2O, *minor conformer*): δ = 174.0, 173.7, 58.8, 53.7, 49.6, 47.9, 33.6, 20.9.

MS (ESI, pos.) m/z (%) = 187.0 [M+H]$^+$ (100), 373.1 [2M+H]$^+$ (40), (186.10 g/mol calculated for $C_8H_{14}N_2O_3$).

5.1.3.6 Synthesis of Ac-(4*R*)Amp-OMe*TFA (9R)
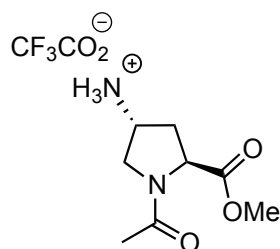
M = 300.2 g/mol

Ac-(4*R*)Amp(Boc)-OMe (**8R**) (1.48 g, 5.17 mmol, 1.0 eq) was dissolved in abs. DCM (20 mL) and the mixture was cooled to 0 °C. TFA (14.0 mL) was added dropwise, the cooling bath was removed and the mixture was stirred under an Argon atmosphere at rt for 1 h. TFA and the solvent were removed *in vacuo*, Et_2O was added, the mixture was sonicated and the solvent decanted. After repeating this procedure three times a brown solid was dried *in vacuo* to yield **9R** (1.32 g, 4.40 mmol, 85%).

TLC (SiO_2, MeOH/DCM 1:9, ninhydrin): R_f = 0.2

^1H and ^{13}C NMR spectra of the HCl- and the TFA-salt are identical and show a double set of peaks in a ratio of 1:3.5 in D_2O due to *cis* and *trans* conformers around the tertiary amide.

^1H NMR (400 MHz, D_2O, *major conformer*): δ = 4.53 (dd, *J* = 7.9, 7.2 Hz, 1H; Hα), 4.05-3.89 (m, 2H; Hγ, Hδ), 3.69 (m, 1H; Hδ), 3.65 (s, 3H; OCH_3), 2.33-2.42 (m, 2H; Hβ), 2.03 (s, 3H; Ac).

^1H NMR (400 MHz, D_2O, *minor conformer*): δ = 4.80 (dd, *J* = 8.9, 4.1 Hz, 1H; Hα), 4.05-3.89 (m, 2H; Hγ, Hδ), 3.70 (s, 3H; OCH_3), 3.73-3.66 (m, 1H; Hδ), 2.56 (ddd, *J* = 14.0, 6.8 Hz, 4.2 Hz, 1H; Hβ), 2.47 (ddd, *J* = 13.8, 8.8, 6.8 Hz, 1H; Hβ), 1.92 (s, 3H; Ac).

^{13}C NMR (100 MHz, D_2O, *major conformer*): δ = 173,7, 173.6, 57.6, 53.6, 51.3, 49.9, 32.8, 21.7.

^{13}C NMR (100 MHz, D_2O, *minor conformer*): δ = 173.7, 173.5, 59.1, 53.9, 49.4, 48.2, 34.2, 21.2.

MS (ESI, pos.) m/z (%) = 187.0 $[M+H]^+$ (100), 373.1 $[2M+H]^+$ (40), (186.10 g/mol calculated for $C_8H_{14}N_2O_3$).

5.1.3.7 Synthesis of Ac-(4*S*)Amp-OMe*HCl (10S)
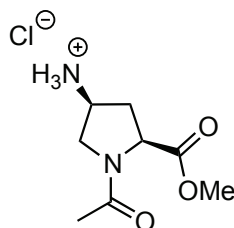
222.7 g/mol

Ac-(4*S*)Amp(Boc)-OMe (**8S**) (404 mg, 1.41 mmol, 1.0 eq) was dissolved in 4 M HCl in dioxane (2.1 mL) and stirred at rt for 5 h. The solvent was evaporated and the solid residue dissolved in a minimum of a solution of MeOH/DCM 1:1 (v/v) and precipitated from Et$_2$O. **10S** was yielded as a white powder (310 mg, 1.39 mmol, quant.).

^{1}H and ^{13}C NMR spectra of the HCl- and the TFA-salt are identical and show a double set of peaks in a ratio of 1:5.7 in D$_2$O due to *cis* and *trans* conformers around the tertiary amide.

^{1}H NMR (400 MHz, D$_2$O, *major conformer*): δ = 4.39 (dd, *J* = 9.1, 5.8 Hz, 1H; Hα), 4.01-3.94 (m, 2H; Hγ, Hδ), 3.71 (m, 1H; Hδ), 3.67 (s, 3H; OCH$_3$), 2.69 (ddd, *J* = 14.5, 9.0, 6.8 Hz, 1H; Hβ), 2.07 (dt, *J* = 14.3, 5.6 Hz, 1H; Hβ), 2.01 (s, 3H; Ac).

^{1}H NMR (400 MHz, D$_2$O, *minor conformer*): δ = 4.71 (dd, *J* = 9.5, 4.4 Hz, 1H; Hα), 4.01-3.90 (m, 2H; Hγ, Hδ), 3.73 (s, 3H; OCH$_3$), 3.45 (dd, *J* = 12.4, 4.9 Hz, 1H; Hδ), 2.81 (ddd, *J* = 14.6, 9.5, 7.4 Hz, 1H; Hβ), 2.24 (dt, *J* = 14.6, 4.6 Hz, 1H; Hβ), 1.92 (s, 3H; Ac).

^{13}C NMR (100 MHz, CDCl$_3$, *major conformer*): δ = 174.8, 173.6, 58.1, 53.7, 51.3, 49.8, 32.6, 21.6.

^{13}C NMR (100 MHz, CDCl$_3$, *minor conformer*): δ = 174.4, 175.0, 59.2, 54.1, 50.0, 48.3, 34.0, 21.3.

MS (ESI, pos.) m/z (%) = 187.0 [M+H]$^+$ (100), 373.1 [2M+H]$^+$ (20) (186.10 g/mol calculated for C$_8$H$_{14}$N$_2$O$_3$).

5.1.3.8   Synthesis of Ac-(4*R*)Amp-OMe*HCl (10R)
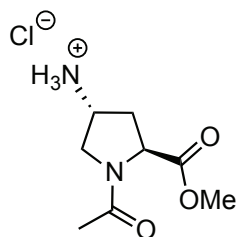
222.7 g/mol

Ac-(4*R*)Amp-OMe*HCl (**10R**) was synthesized according to the same procedure as described for Ac-(4*R*)Amp-OMe*HCl (**10S**). Starting from Ac-(4*R*)Amp(Boc)-OMe (**8R**) **10R** was obtained in quant. yield.

TLC (SiO$_2$, EtOAc/CH 3:7, 254 nm): R$_f$ = 0.2

^{1}H and ^{13}C NMR spectra of the HCl- and the TFA-salt are identical and show a double set of peaks in a ratio of 1:3.5 in D$_2$O due to *cis* and *trans* conformers around the tertiary amide.

^{1}H NMR (400 MHz, D$_2$O, *major conformer*): δ = 4.53 (dd, *J* = 7.9, 7.2 Hz, 1H; Hα), 4.05-3.89 (m, 2H; Hγ, Hδ), 3.69 (m, 1H; Hδ), 3.65 (s, 3H; OCH$_3$), 2.33-2.42 (m, 2H; Hβ), 2.03 (s, 3H; Ac).

^{1}H NMR (400 MHz, D$_2$O, *minor conformer*): δ = 4.80 (dd, *J* = 8.9, 4.1 Hz, 1H; Hα), 4.05-3.89 (m, 2H; Hγ, Hδ), 3.70 (s, 3H; OCH$_3$), 3.73-3.66 (m, 1H; Hδ), 2.56 (ddd, *J* = 14.0, 6.8 Hz, 4.2 Hz, 1H; Hβ), 2.47 (ddd, *J* = 13.8, 8.8, 6.8 Hz, 1H; Hβ), 1.92 (s, 3H; Ac).

^{13}C NMR (100 MHz, D$_2$O, *major conformer*): δ = 173,7, 173.6, 57.6, 53.6, 51.3, 49.9, 32.8, 21.7.

^{13}C NMR (100 MHz, D$_2$O, *minor conformer*): δ = 173.7, 173.5, 59.1, 53.9, 49.4, 48.2, 34.2, 21.2.

MS (ESI, pos.) m/z (%) = 187.0 [M+H]$^+$, 209.0 [M+Na]$^+$, 373.2 [2M+H]$^+$, 395.2 [2M+Na]$^+$, (186.10 g/mol calculated for C$_8$H$_{14}$N$_2$O$_3$).

5.1.3.9   Synthesis of Ac-(4*S*)Gup(Boc)₂-OMe (11S)
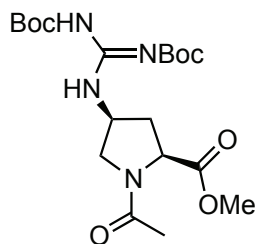
428.5 g/mol

Ac-(4*S*)Amp-OMe*TFA (**9S**) (0.60 g, 2.01 mmol, 1.0 eq) and *N,N'*-di-Boc-*N"*-trifluoromethane sulfonylguanidine (**18**, 1.22 g, 3.12 mmol, 1.6 eq) were dissolved in abs. DCM (30 mL). NEt₃ (0.4 mL, 2.92 mmol, 1.5 eq) was added and the solution was stirred under an Argon atmosphere at rt for 2 d. DCM (30 mL) was added, the mixture was washed with sat. Na₂CO₃ and brine and the combined aq. layers were extracted with DCM. The combined org. layers were dried over MgSO₄, the solvent was evaporated and the residue was purified by flash chromatography (SiO₂, MeOH/DCM 1:24) to yield **11S** as a colorless solid (0.84 g, 1.96 mmol, quant.).

TLC (SiO₂, MeOH/DCM 1:24, 254 nm): R_f = 0.25

¹H and ¹³C NMR spectra show a double set of peaks in a ratio of 1:3.6 in CDCl₃ due to *cis* and *trans* conformers around the tertiary amide.

¹H NMR (400 MHz, CDCl₃, *major conformer*): δ = 11.4 (bs, 1H, NH), 8.67 (d, *J* = 7.8 Hz, 1H, NH), 4.97-4.87 (m, 1H, Hγ), 4.48 (dd, *J* = 9.1, 5.2 Hz, 1H, Hα), 3.94 (dd, *J* = 10.7, 6.8 Hz, 1H, Hδ), 3.73 (s, 3H, OCH₃), 3.49 (dd, *J* = 10.7, 5.1 Hz, 1H, Hδ), 2.58 (ddd, *J* = 13.6, 9.1, 7.0 Hz, 1H, Hβ), 2.06 (s, 3H, Ac) 1.98 (ddd, *J* = 13.6, 5.3, 5.2 Hz, 1H, Hβ), 1.51-1.44 (m, 18H, *t*Bu).

¹H NMR (400 MHz, CDCl₃, *minor conformer*): δ = 11.4 (bs, 1H, NH), 8.59 (d, *J* = 7.1 Hz, 1H, NH), 4.87-4.79 (m, 1H, Hγ), 4.43 (dd, *J* = 9.4, 2.5 Hz, 1H, Hα), 3.98-3.89 (m, 1H, Hδ), 3.77 (s, 3H, OCH₃), 3.53 (dd, *J* = 13.1, 3.0 Hz, 1H, Hδ), 2.65 (ddd, *J* = 14.0, 9.4, 6.6 Hz, 1H, Hβ), 2.28 (dt, *J* = 14.0, 2.5 Hz, 1H, Hβ), 1.98 (s, 3H, Ac), 1.51-1.44 (m, 18H, *t*Bu).

¹³C NMR (100 MHz, D₂O, *major conformer*): δ = 172.5, 169.5, 163.0, 155.7, 153.0, 83.7, 80.1, 57.7, 53.5, 52.7, 49.7, 35.3, 28.3, 28.1, 22.4.

^{13}C NMR (100 MHz, D$_2$O, *minor conformer*): δ = 172.4, 169.9, 163.2, 155.3, 153.0, 83.6, 79.9, 59.3, 53.1, 52.6, 48.4, 37.8, 28.3, 28.1, 22.1.

MS (ESI, pos.) m/z (%) = 451.3 [M+Na]$^+$, (428.23 g/mol calculated for C$_{19}$H$_{32}$N$_4$O$_7$).

5.1.3.10   Synthesis of Ac-(4*R*)Gup(Boc)₂-OMe (11R)
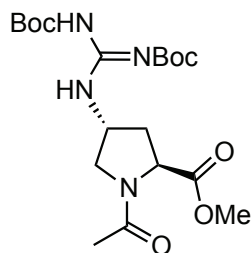
M = 428.5 g/mol

Ac-(4*R*)Gup(Boc)₂-OMe (**11R**) was synthesized according to the procedure described for Ac-(4*S*)Gup(Boc)₂-OMe (**11S**). Starting from Ac-(4*R*)Amp-OMe*TFA (**9R**) (0.67 g, 2.23 mmol, 1.0 eq) and 18 h reaction time a white solid (0.90 g, 2.09 mmol, 94 %) was obtained.

TLC (SiO₂, MeOH/DCM 5:95, 254 nm): R_f = 0.35

^{1}H and ^{13}C NMR spectra show a double set of peaks in a ratio of 1:4.4 in CDCl₃ due to *cis* and *trans* conformers around the tertiary amide.

^{1}H NMR (400 MHz, CDCl₃, *major conformer*): δ = 11.4 (bs, 1H, NH), 8.59 (bs, 1H, NH), 4.90-4.81 (m, 1H, Hγ), 4.57 (dd, *J* = 8.4, 6.0, 1H, Hα), 4.00 (dd, *J* = 10.6, 6.2, 1H, Hδ), 3.72 (s, 3H, OCH₃), 3.42 (dd, *J* = 10.6, 4.5, 1H, Hδ), 2.34-2.27 (m, 1H, Hβ), 2.23 (ddd, *J* = 13.7, 8.4, 6.3 Hz, 1H, Hβ), 2.08 (s, 3H, Ac), 1.49-1.47 (m, 18H, *t*Bu).

^{1}H NMR (400 MHz, CDCl₃, *minor conformer*): δ = 11.4 (bs, 1H, NH), 8.59 (bs, 1H, NH), 4.85-4.75 (m, 1H, Hγ), 4.48 (dd, *J* = 8.7, 4.4 Hz, 1H, Hα), 3.86 (dd, *J* = 12.4, 6.8 Hz, 1H, Hδ), 3.77 (s, 3H, OCH₃), 3.61 (dd, *J* = 12.4, 5.0 Hz, 1H, Hδ), 2.53 (ddd, *J* = 10.9, 6.3, 4.4 Hz, 1H, Hβ), 2.40-2.30 (m, 1H, Hβ), 1.97 (s, 3H, Ac), 1.49-1.47 (m, 18H, *t*Bu).

^{13}C NMR (100 MHz, CDCl₃, *major conformer*): δ = 172.1, 169.7, 155.7, 153.3, 84.1, 57.3, 53.6, 53.0, 52.6, 51.9, 50.0, 35.2, 28.3, 28.1, 22.4; *(minor conformer not detectable).*

MS (ESI, pos.) m/z (%) = 451.3 [M+Na]⁺, (428.23 g/mol calculated for C₁₉H₃₂N₄O₇).

5.1.3.11   Synthesis of Ac-(4*S*)Gup-OMe*TFA (12S)
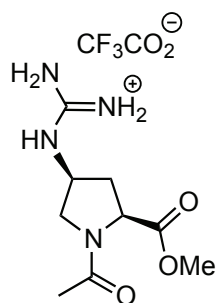
342.3 g/mol

M = 358.3 g/mol

Ac-(4*S*)Gup(Boc)$_2$-OMe (**11S**) (0.49 g, 1.14 mmol, 1.0 eq) was suspended in abs. DCM (30 mL) and cooled to 0 °C. TFA (30 ml) was added, the mixture was stirred under an Argon atmosphere at rt for 2 h and the solvent was removed *in vacuo*. Et$_2$O (ca. 15 mL) was added, the mixture was sonicated and the solvent was decanted. After repeating this procedure three times the residue was dried *in vacuo* to yield **12S** as a colorless solid (0.39 g, 1.14 mmol, quant.).

TLC (SiO$_2$, MeOH/DCM 5:95, ninhydrin): R$_f$ = 0.04

^{1}H and ^{13}C NMR spectra show a double set of peaks in a ratio of 1:3.9 in D$_2$O due to *cis* and *trans* conformers around the tertiary amide.

^{1}H NMR (400 MHz, D$_2$O, *major conformer*): δ = 4.52 (dd, *J* = 9.2, 5.0 Hz, 1H, Hα), 4.29-4.24 (m, 1H, Hγ), 4.00 (dd, *J* = 11.4, 6.2 Hz, 1H, Hδ), 3.75 (s, 3H, OCH$_3$), 3.67 (dd, *J* = 11.4, 4.4 Hz, 1H, Hδ), 2.64 (ddd, *J* = 13.9, 9.2, 5.8 Hz, 1H, Hβ), 2.17 (ddd, *J* = 13.8, 5.0, 0.7 Hz, 1H, Hβ), 2.10 (s, 3H, Ac).

^{1}H NMR (400 MHz, D$_2$O, *minor conformer*): δ = 4.81 (dd, *J* = 9.1, 2.4 Hz, 1H, Hα), 4.22-4.18 (m, 1H, Hγ), 3.85 (dd, *J* = 13.0, 6.2 Hz, 1H, Hδ), 3.79 (s, 3H, OCH$_3$), 3.56 (ddd, *J* = 13.0, 2.4, 1.6 Hz, 1H, Hδ), 2.62 (ddd, *J* = 14.0, 9.1, 5.2 Hz, 1H, Hβ), 2.50 (ddd, *J* = 14.0, 3.9, 2.4 Hz, 1H, Hβ), 2.03 (s, 3H, Ac).

^{13}C NMR (100 MHz, D$_2$O, *major conformer*): δ = 174.0, 173.2, 156.2, 57.5, 53.1, 52.5, 50.6, 34.0, 21.2.

^{13}C NMR (100 MHz, D$_2$O, *minor conformer*): δ = 163.0, 162.6, 156.2, 58.9, 53.5, 51.4, 49.4, 35.6, 21.1.

MS (ESI, pos.) m/z (%) = 229.0 [M+H]$^+$, 457.1 [2M+H]$^+$, (228.12 g/mol calculated for C$_9$H$_{16}$N$_4$O$_3$).

5.1.3.12 Synthesis of Ac-(4*R*)Gup-OMe*TFA (12R)
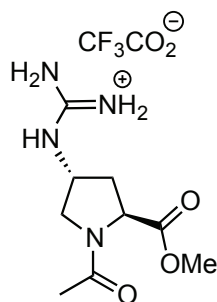
M = 358.3 g/mol

Ac-(4*R*)Gup-OMe*TFA (**12R**) was synthesized according to the procedure described for Ac-(4*S*)Gup-OMe*TFA (**12S**). Starting from Ac-(4*R*)Gup(Boc)$_2$-OMe (**11R**) (0.45 g, 1.05 mmol, 1.0 eq) a colorless solid (0.36 g, 1.05 mmol, quant.) was obtained.

TLC (SiO$_2$, MeOH/DCM 5:95, ninhydrin): R$_f$ = 0.04

^{1}H and ^{13}C NMR spectra show a double set of peaks in a ratio of 1:4.3 in D$_2$O due to *cis* and *trans* conformers around the tertiary amide.

^{1}H NMR (400 MHz, D$_2$O, *major conformer*): 4.52 (t, *J* = 7.7 Hz, 1H, Hα), 4.32-4.27 (m, 1H, Hγ), 3.97 (dd, *J* = 11.4, 5.7 Hz, 1H, Hδ), 3.73 (s, 3H, OCH$_3$), 3.64 (ddd, *J* = 11.4, 3.9, 0.7 Hz, 1H, Hδ), 2.41 (dddd, *J* = 13.6, 8.3, 4.9, 1.0 Hz, 1H, Hβ), 2.31 (ddd, *J* = 13.6, 6.9, 5.9 Hz, 1H, Hβ), 2.09 (s, 3H, Ac).

^{1}H NMR (400 MHz, D$_2$O, *minor conformer*): 4.83-4.79 (m, 1H, Hα), 4.24-4.19 (m, 1H, Hγ), 3.78 (s, 3H, OCH$_3$), 3.78-3.73 (m, 1H, Hδ), 3.56 (dd, *J* = 12.3, 5.2 Hz, 1H, Hδ), 2.56-2.46 (m, 2H, Hβ), 1.98 (s, 3H, Ac).

^{13}C NMR (100 MHz, CDCl$_3$, *major conformer*): δ = 173.9, 173.2, 156.3, 57.4, 53.1, 52.7, 50.5, 34.2, 21.3.

^{13}C NMR (100 MHz, CDCl$_3$, *minor conformer*): δ = 173.7, 173.5, 156.3, 58.8, 53.5, 50.7, 48.9, 34.6, 20.6.

MS (ESI, pos.) m/z (%) = 229.0 [M+H]$^+$, 251.0 [M+Na]$^+$, 457.1 [2M+H]$^+$, (228.12 g/mol calculated for C$_9$H$_{16}$N$_4$O$_3$).

5.1.3.13 Synthesis of Ac-(4*S*)Gup-OMe*HCl (13*S*)
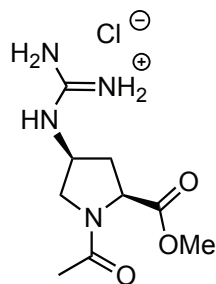
M = 264.7 g/mol

Ac-[(Boc)$_2$(4*S*)Gup]-OMe*HCl (**11S**) (0.10 g, 0.23 mmol, 1.0 eq) was dissolved in 4 M HCl in dioxane (0.7 mL) and stirred at rt under an Argon atmosphere for 3.5 h. A white solid precipitated. The solvent was removed *in vacuo*, Et$_2$O was added, the mixture was sonicated and the solvent was decanted. The residue was dried *in vacuo* to yield **13S** as a colorless solid (43.2 mg, 0.16 mmol, 70%).

^{1}H and ^{13}C NMR spectra show a double set of peaks in a ratio of 1:3.4 in D$_2$O due to *cis* and *trans* conformers around the tertiary amide.

^{1}H NMR (400 MHz, D$_2$O, *major conformer*): 4.57 (dd, *J* = 9.2, 5.0 Hz, 1H, Hα), 4.35-4.28 (m, 1H, Hγ), 4.05 (dd, *J* = 11.5, 6.2 Hz, 1H, Hδ), 3.80 (s, 3H, OCH$_3$), 3.72 (dd, *J* = 11.5, 4.4 Hz, 1H, Hδ), 2.69 (ddd, *J* = 13.8, 9.2, 6.0 Hz, 1H, Hβ), 2.22 (ddd, *J* = 13.8, 5.0, 4.8 Hz, 1H, Hβ), 2.15 (s, 3H, Ac).

^{1}H NMR (400 MHz, D$_2$O, *minor conformer*): 4.86 (dd, *J* = 9.1, 2.4 Hz, 1H, Hα), 4.28-4.22 (m, 1H, Hγ), 3.91 (dd, *J* = 13.0, 6.1 Hz, 1H, Hδ), 3.84 (s, 3H, OCH$_3$), 3.63-3.58 (m, 1H, Hδ), 2.55 (ddd, *J* = 14.1, 3.7, 2.4 Hz, 1H, Hβ), 2.34-2.27 (m, 1H, Hβ), 2.07 (s, 3H, Ac).

MS (ESI, pos.) m/z (%) = 229.0 [M+H]$^+$, 457.1 [2M+H]$^+$, (228.12 g/mol calculated for C$_9$H$_{16}$N$_4$O$_3$).

5.1.3.14   Synthesis of Ac-(4*R*)Gup-OMe*HCl (13R)
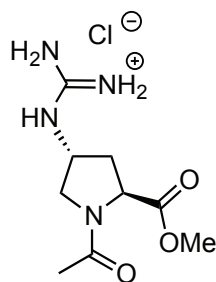
M = 264.7 g/mol

Ac-(4*R*)Gup-OMe*HCl (**13R**) was synthesized according to the procedure described for Ac-(4*S*)Gup-OMe*HCl (**13S**). Starting from Ac-(4*R*)Gup(Boc)$_2$-OMe*HCl (**11S**) (0.10 g, 0.23 mmol, 1.0 eq) a colorless solid (45.0 mg, 0.17 mmol, 73%) was obtained.

^{1}H and ^{13}C NMR spectra show a double set of peaks in a ratio of 1:4.1 in D$_2$O due to *cis* and *trans* conformers around the tertiary amide.

^{1}H NMR (400 MHz, D$_2$O, *major conformer*): 4.59 (t, *J* = 7.7 Hz, 1H, Hα), 4.40-4.32 (m, 1H, Hγ), 4.03 (dd, *J* = 11.4, 5.7 Hz, 1H, Hδ), 3.79 (s, 3H, OCH$_3$), 3.71 (dd, *J* = 11.4, 3.8 Hz, 1H, Hδ), 2.47 (ddd, *J* = 13.4, 8.2, 5.0 Hz, 1H, Hβ), 2.37 (m, 1H, Hβ), 2.15 (s, 3H, Ac).

^{1}H NMR (400 MHz, D$_2$O, *minor conformer*): 4.87 (dd, *J* = 8.4, 5.0 Hz, 1H, Hα), 4.31-4.24 (m, 1H, Hγ), 3.84 (s, 3H, OCH$_3$), 3.82-3.75 (m, 1H, Hδ), 3.62 (dd, *J* = 12.0, 4.8 Hz, 1H, Hδ), 2.64-2.51 (m, 2H, Hβ), 2.04 (s, 3H, Ac).

MS (ESI, pos.) m/z (%) = 229.0 [M+H]$^+$, 251.0 [M+Na]$^+$, 457.2 [2M+H]$^+$, 479.3 [2M+Na]$^+$, (228.12 g/mol calculated for C$_9$H$_{16}$N$_4$O$_3$).

5.1.3.15 Alternative synthetic routes to Ac-(4*R*)Gup(Boc)$_2$-OMe (11R)

Direct synthesis *via in situ* hydrogenation and guanidinylation

Ac-(4*R*)Azp-OMe (**8R**) (150 mg, 0.71 mmol, 1.0 eq), *N,N'*-di-Boc-*N''*-trifluoromethane sulfonylguanidine (360 mg, 0.92 mmol, 1.3 eq), NEt$_3$ (0.13 ml, 0.92 mmol, 1.3 eq) and Lindlar catalyst (55 mg, 37 wt%) were suspended in abs. MeOH (10 mL). The mixture was stirred under an H$_2$ atmosphere at rt for 6 h, filtered over celite and the solvent was removed *in vacuo*. The residue was dissolved in DCM (20 mL), washed with sat. Na$_2$CO$_3$, brine and the combined aq. layers were extracted with DCM. The combined org. layers were dried over MgSO$_4$, the solvent was evaporated and the residue was purified by flash chromatography (SiO$_2$, MeOH/DCM 1:24) to yield a colorless solid (296 mg, 0.69 mmol, 98%).

MS (ESI, pos.) m/z = 429.3 [M]$^+$, 451.2 [M+Na]$^+$, (428.23 g/mol calculated for C$_{19}$H$_{32}$N$_4$O$_7$).

Further analytical data is consistent with reported data for **11R**.

5.1.4 Solide Phase Peptide Synthesis (SPPS)

5.1.4.1 General procedures for the Syro I Peptide Synthesizer

A 0.5 M solution of Fmoc-Xaa-OH (4.0 eq) in DMF was added to amino-functionalized resin (ChemMatrix Rink Amide or 2-chlorotrityl chloride, the latter one already equipped with the first amino acid), with a loading of 0.3 – 0.64 mmol/g, depending on the peptide. As standard coupling reagent HCTU (0.5 M, 4.0 eq) in DMF was used, with Hünig's base (3.0 M, 12.0 eq) in NMP. The mixture was shaken for 1 h and washed with DMF (5 x). After every coupling step Fmoc-deprotection was performed with 40% piperidine in DMF and the resin was washed with DMF. For peptides longer than 8 amino acids 2% DBU in DMF was used for Fmoc-deprotection. Potentially free amino functionalities were capped by acetylation with Ac$_2$O (1.0 eq) and Hünig's base (1.0 eq) in DMF for 20 min and the mixture was washed with DMF (5 x) afterwards. The resin was washed After complete synthesis a washing with DCM was carried out.

5.1.4.2   General procedure for manual coupling

The manual coupling of amino acids was performed according to the following steps:

1. Swelling of the resin: DCM was added to the resin (8 mL / g, ChemMatrix Rink Amide resin), with a loading of 0.3 – 0.64 mmol/g (depending on the peptide) and the mixture was shaken for 30 min at rt.

2. Pre-activation: Hünig´s base (9.0 eq) was added to HCTU (0.5 M, 3.0 eq) and Fmoc-Xaa-OH (3.0 eq) in DMF (5 mL / g resin), and shaken for 3 min at rt.

3. Coupling: The pre-activated mixture was added to the resin and agitated for 1.5 h at rt.

4. Washing: The reaction mixture was removed and the resin was washed with DMF (5 x 2.5 mL) and DCM (5 x 2.5 mL).

5. Coupling test: To check the efficiency of the coupling a color test on bead was performed.

6. Fmoc-deprotection: 2 mL of 40% (v/v) piperidine in DMF were added to the resin and the mixture was shaken for 5 min. The procedure was repeated with 20% (v/v) piperidine in DMF for 10 min.

7. Washing: The resin was washed with DMF (5 x 2.5 mL) and DCM (5 x 2.5 mL).

8. Steps 2 to 7 were repeated until the desired peptide was completed.

5.1.4.3   General procedure for coupling of the first amino acid

For the first coupling on 2-chlorotrityl chloride resin Fmoc-Xaa-OH (1.0 eq) and Hünig´s base (4.0 eq) were dissolved in abs. DCM (5 mL / g resin) and added to pre-swollen resin, agitated for 1 h and washed with a mixture of DCM/MeOH/DIPEA (17:2:1, 3 x), DCM (3 x), DMF (3 x) and again DCM (5 x). The loading was determined with a quantitative Fmoc test. The first coupling on ChemMatrix rink amide resin was performed as described in 5.1.4.2.

5.1.4.4   General procedure for the quantitative Fmoc-test

To determine the loading of the resin, 3 mg of very well dried resin were weight into a 1 cm UV cuvette and 500 μL of 30% (v/v) piperidine in DMF was added and the mixture was shaken for 30 min. Afterwards 3 mL DMF were added and the UV absorption at 301 nm was measured with a dilution of 1:10 in DMF. As a blank 500 μL of 30% (v/v) piperidine in DMF dissolved with 3 mL DMF was used. The loading of the resin could be

calculated according to the following equation (valid in a linear range until an absorption of 0.8):

Loading [mmol / g] = $A_{301} \cdot V_{dilution}$ [mL] / $\varepsilon_{301} \cdot m_{resin}$ [mg]

With ε_{301} = 7.8

5.1.4.5   General procedure for acetylation

NEt_3 (20 eq) and Ac_2O (20 eq) in DCM ($\approx$ 120 mM) were added to the resin. The mixture was agitated for 1 h and washed with DCM (5 x). The reaction was monitored by qualitative color tests on bead.

5.1.4.6   Monitoring of coupling and deprotection

Kaiser test for primary amines:[250]

- − Solution 1:   5 g ninhydrin in 100 mL ethanol
- − Solution 2:   80 g phenol in 20 mL ethanol
- − Solution 3:   2 mL 0.001 M aqueous KCN in 98 mL pyridine

A few beads were placed in a small vial and 2 drops of each solution were added. The mixture was heated at 100°C for 5 min. In case of a positive test, indicating a free amino function, both the beads and the solution were stained blue. In case of a negative outcome the solution and the beads were colorless to yellowish. Although this test is less suitable for secondary amines, a brownish red color could be observed. Too long heating was avoided, since it might cause deprotection of side chains (Boc) or Fmoc removal by pyridine.

Acetaldehyde/Chloranil test for secondary amines:[251]

- − Solution 1:   2% acetaldehyde in DMF
- − Solution 2:   2% chloranil in DMF

A few beads were placed in a small vial and 2 drops of each solution were added. After a short mixing, the test tube was left at rt for 5 min, then the beads were inspected under a microscope. In case of a positive test only the beads should be dark blue to green. When the test is negative the beads should be colorless to yellowish. This test has been developed for secondary amines, but will also detect primary amino groups. Stock solutions should be stored at -20 °C. Instead of 2% acetaldehyde in DMF as solution 1 also pure acetone can be used alternatively.

TNBS test for secondary amines:[252]

- Solution 1: 10% DIPEA in DMF
- Solution 2: 1 M aqueous TNBS

A few beads were placed in a small vial and 2 drops of each solution were added. After a short mixing, the test tube was left at rt for 5 min, then the beads were inspected under a microscope. In case of a positive test only the beads should be orange to red. When the test is negative the beads should be colorless. Yellowish beads indicate a slightly positive test.

5.1.4.7   5(6)-Carboxyfluorescein labeling

Variant a):

The procedure for the coupling of 5(6)-carboxyfluorescein is similar to the manual coupling of amino acids. However, due to the use of an activated carboxyfluorescein derivative, no coupling reagent is needed. After swelling and Fmoc-deprotection, 5(6)-carboxyfluorescein *N*-succinimidylester (1.1 eq.) and Hünig's base (3.0 eq.) in DMF (8 mL/g resin) were added to the resin and the mixture was shaken for 2 h at rt. The reactions mixture was washed according to the usual procedures.

Variant b):

After swelling and Fmoc-deprotection, 5(6)-carboxyfluorescein (10 eq), DIC (10 eq) and HOBt (10 eq) dissolved in DMF (8mL/g resin) were added to the resin and the mixture was shaken for 2 h at rt. After reaction the resin was washed with DMF (5 x 2 mL) and CH_2Cl_2 (5 x 2 mL). To avoid double coupling and auto-quenching of fluorescence 2 mL of a solution of 20 % piperidine in DMF was added, shaken for 20 min and washed with

DMF (5 x 2 mL) and DCM (5 x 2 mL). This step was repeated until the supernatant was colorless.

5.1.4.8   Staudinger reduction in solution

The general procedure for the Staudinger reduction in solution will be described for the synthesis of CF-Gly-[(4S)Amp-Pro-(4S)Amp]$_3$-CONH$_2$ (**21**): 41.2 mg of CF-Gly-[(4S)Azp-Pro-(4S)Azp]$_3$-CONH$_2$ (26.5 μmol, 1.0 eq) were dissolved in a 200 μL of H$_2$O/THF (1:1 (v/v)). 530 μL (530 μmol, 20.0 eq) of a 1 M solution of PMe$_3$ in THF were added and the solution stirred for 22 h at rt. The solvent was removed *in vacuo* and the obtained crude peptide purified by preparative HPLC (98% to 70% B in 30 min) to yield 13.6 mg (9.9 μmol, 37%) of **21** as a yellow solid.

5.1.4.9   Staudinger reduction on solid support

After swelling of the resin in THF for 30 min, PMe$_3$ (1 M in THF, 5.0 eq per N$_3$), and H$_2$O (22.0 eq per N$_3$) were added and the reaction mixture was agitated for 2 h at rt. In case of the presence of the Fmoc-protecting group, the reaction time was reduced to 80 min, to prevent the cleavage of the Fmoc-group. After the reaction, the resin was washed with THF (5 x 2.5 mL), DMF (5 x 2.5 mL) and DCM (5 x 2.5 mL).

5.1.4.10   Guanidinylation in solution

The general procedure for guanidinylation in solution will be described for the synthesis of CF-Gly-[(4S)Gup-Pro-(4S)Gup]$_3$-CONH$_2$ (**24**): 4 mg of CF-Gly-[(4S)Amp-Pro-(4S)Amp]$_3$-CONH$_2$ (**21**, 2.9 μmol, 1.0 eq) were dissolved in MeOH (40 μL). 16.2 mg (42 μmol, 14.0 eq) of *N,N'*-di-Boc-*N"*-trifluoromethane sulfonylguanidine (**18**) in dioxane (200 μL) were added. After 5 min 8.0 μL (58 μmol, 20.0 eq) NEt$_3$ were added. The solution was stirred for 4 d at rt. Afterwards the solvent was removed *in vacuo* to yield the crude peptide CF-Gly-[(Boc)$_2$(4S)Gup-Pro-(Boc)$_2$(4S)Gup]$_3$-CONH$_2$ as a yellow solid, which was subsequently dissolved in a mixture of TFA (95%) and H$_2$O (5%) (200 μL). The mixture was stirred for 30 min at rt and the solvent evaporated. The resulting peptide was purified by preparative HPLC (98% to 70% B in 30 min) to yield 2.1 mg (1.3 μmol, 45%) of CF-Gly-[(4S)Gup-Pro-(4S)Gup]$_3$-CONH$_2$ **24.**

5.1.4.11   Guanidinylation on solid support

After swelling of the resin in DCM for 30 min, *N,N'*-di-Boc-*N"*-trifluoromethane sulfonylguanidine (**18**, 3.5 eq per NH_2) dissolved in MeOH was added and the mixture was shaken for 10 min at rt. Afterwards NEt_3 (4.2 eq per NH_2) was added. The mixture was shaken for 4 d at rt. After the reaction, the resin was washed following the usual procedures.

5.1.4.12   Cleavage from the resin and simultaneous side-chain deprotection

General procedure for peptide cleavage from ChemMatrix Rink amide resin

A solution of 95% TFA, 2.5% water and 2.5% TIS as a scavenger was added to the resin and the mixture was shaken at rt for 2 x 1.5 h. The combined filtrates were concentrated *in vacuo*, the remaining peptide was precipitated with Et_2O and dried.

General procedure for peptide cleavage from 2-chlorotrityl chloride resin

A mixture of DCM / AcOH / TFE (8:1:1) was added to the resin and it was agitated for 1 h. The cleavage cocktail was removed and stored. The resin was supplemented with a fresh amount of the cleavage mixture for 20 min. The combined filtrates were concentrated *in vacuo*, the remaining peptide was precipitated with Et_2O and dried.

5.1.4.13   Synthesis of CPPs of the alternating system

The peptides were synthesized according to strategy A or B on ChemMatrix Rink amide resin with a loading of 0.64 mmol/g using Fmoc-(4*S*)Azp-OH (**16S**), Fmoc-(4*R*)Azp-OH (**16R**), Fmoc-Pro-OH and Fmoc-Gly-OH on a Syro I Peptide Synthesizer according to the general procedures. N-terminal labeling with 5(6)-carboxyfluorescein was accomplished according to previously described procedures. The Staudinger reduction of the azido function was carried out either on solid support or in solution according to the described procedure, followed by guanidinylation as well either on solid support or in solution. After cleavage from solid support, the crude peptides were purified by preparative RP-HPLC using a Reprosil 100 C18, 150 x 10 mm, 5 μm column with a flow of 6 mL/min at 50°C. Preparative methods were used according to analytical methods. Analytical data, purities and yields are given in the appendix 6.4.

5.1.4.14   Synthesis of CPPs of the *en bloc* system

CPPs bearing up to six functionalized prolines in a row, were synthesized according to strategy B on ChemMatrix Rink amide resin with a loading of 0.30 – 0.64 mmol/g, depending on the peptide, using Fmoc-(4*S*)Azp-OH (**16S**), Fmoc-(4*R*)Azp-OH (**16R**), Fmoc-Pro-OH and Fmoc-Gly-OH on a Syro I Peptide Synthesizer according to the general procedures. Peptides bearing more than six functionalized prolines in a row, were synthesized following strategy C on ChemMatrix Rink amide resin with a loading of 0.30 - 0.64 mmol/g, depending on the peptide, using Fmoc-(4*S*)Gup(Boc)$_2$-OH (**17**), D-Fmoc-(4*R*)Gup(Boc)$_2$-OH (**19**), Fmoc-Pro-OH, D-Fmoc-Pro-OH and Fmoc-Gly-OH. N-terminal labeling with 5(6)-carboxyfluorescein was accomplished according to previously described procedures. After cleavage from the solid support, the crude peptides were purified by preparative RP-HPLC, using a Reprosil 100 C18, 150 x 10 mm, 5 μm column with a flow of 6 mL/min at 50°C. Preparative methods were used according to analytical methods. Analytical data, purities and yields are given in the appendix 6.4.

5.1.4.15   Synthesis of reference CPPs

The reference peptides were synthesized on ChemMatrix Rink amide resin with a loading of 0.64 mmol/g using Fmoc- and side-chain protected amino acids on a Syro I Peptide Synthesizer according to the general procedures. N-terminal labeling with 5(6)-carboxyfluorescein was accomplished according to previously described procedures. After cleavage from the solid support, the crude peptides were purified by preparative HPLC, using a Reprosil 100 C18, 150 x 10 mm, 5 μm column with a flow of 6 mL/min at 50°C. Preparative methods were used according to analytical methods. Analytical data, purities and yields are given in the appendix 6.4.

5.1.4.16   Synthesis of peptides for conformational analysis

Synthesis of Ac-[(4*S*)Amp-Pro-(4*S*)Amp]-OH (**14S**)

The coupling of the first amino acid, Fmoc-(4*S*)Azp-OH (**16S**), on 400 mg of 2-chlorotrityl chloride resin was performed according to the previously described procedure. After the initial coupling onto the resin and capping of unreacted sites, a

quantitative Fmoc test revealed a loading of 0.46 mmol / g to give a 184 µmol scale. The following synthesis steps using Fmoc-(4*S*)Azp-OH (**16S**) and Fmoc-Pro-OH were conducted on a Syro I Peptide Synthesizer according to the general procedures. The azido moieties of Ac-Gly-[(4*S*)Azp-Pro-(4*S*)Azp]-OH on resin were reduced *via* Staudinger reduction on solid support to obtain the amino moieties. Afterwards the peptides were cleaved from the 2-chlorotrityl chloride resin and purified by preparative HPLC to yield 14.1 mg of **14S.** Analytical data, purities and yields are given in the appendix 6.4.

Synthesis of Ac-[(4*R*)Amp-Pro-(4*R*)Amp]-OH (**14R**)

Synthesis of the precursor Ac-[(4*R*)Azp-Pro-(4*R*)Azp]-OH on resin was performed according to the synthesis of Ac-[(4*S*)Azp-Pro-(4*S*)Azp]-OH on 400 mg of 2-chlorotrityl chloride resin with a loading of 0.39 mmol / g to give a 156 µmol scale. The following steps leading to Ac-Gly-[(4*R*)Amp-Pro-(4*R*)Amp]-OH (**14R**) were conducted according to the synthesis of **14S**. After cleavage from the solid support, the crude peptide was purified by preparative HPLC to yield 11.5 mg of **14R.** Analytical data, purities and yields are given in the appendix 6.4.

5.1.4.17 Concentration determination

The concentrations of the 5(6)-carboxyfluorescein labeled peptide stock solutions in PBS at pH 7.4 were determined by measuring the absorption at 494 nm at rt and calculation according to Lambert-Beer´s law:

$$c = A_{494} / \varepsilon\, d$$

with c = conc. [mol/L]

            d = path length [cm]

            ε = extinction coefficient [L/(mol cm^{-1})]

5.1.5 CD spectroscopy

For all CD spectroscopic analyses, 70 µM solutions of the peptides in PBS were prepared and equilibrated for at least 12 h at rt before measurement. A quartz cell with a path length of 2 mm was used for all measurements. Spectra were recorded from 260-196 nm with a spectral bandwidth of 1 nm, at 25 °C with a time constant of 5 s and a step resolution of 1 nm. Before each measurement a background measurement with pure PBS was performed. CD data are given as mean residual molar ellipticities (θ_{MRW} in deg cm^2 dmol^{-1}). The formula includes the total ellipticity $[\theta]$, divided by the number of amino acids $[n]$, the concentration of the peptidic solution $[c]$ and the width of the cuvette $[w]$:

$$\theta_{MRW} = \theta \,/\, n \cdot c \cdot w$$

5.2 Biological investigations

5.2.1   Cell culture

5.2.1.1   Biosafety

The cell lines used in our studies (see Table 11) are well-known established cell lines. They were early identified, characterized and routinely cultivated in laboratories worldwide and were categorized to safety class 1. Cell lines were purchased from the Health Protection Agency (www.HPA.org.uk) and European Collection of Cell Cultures (ECCC).

Table 11: Human cancer cell lines cultivated and used for experiments.

Cell line	Type	ECACC/ATCC® number	Safety class
HeLa	Human cervical adenocarcinoma	CCL-2	1
PC-3	Human prostata adenocarcinoma	CRL-1435	1
MCF-7	Human breast adenocarcinoma	HTB-22	1
HT-29	Human colon adenocarcinoma	HTB-38	1

With adequate treatment and consideration of the according safety procedures a contamination of the laboratory and environment with the organism can be excluded. The safety risk is considered to be minimal, since cells were treated according to good laboratory practice (GLP) in cell culture and were autoclaved before discarded. Survival of the species outside the especially created milieu is unlikely.

For our studies an ECOGEN notification (A100837, Investigation of cell-penetrating peptides) was made at BAFU (Bundesamt für Umwelt), Switzerland. Generally our project is not subject to registration, but underlies the duty of care.

5.2.1.2   General aspects

The cell lines were cultured in the cell culture laboratory of the research group of Prof. H. Wennemers at the Department of Organic Chemistry at the University of Basel and the Laboratory of Organic Chemistry at ETH Zürich.

All cell lines were maintained under sterile conditions and were always treated inside a Herasafe HSP 12 Laminar-Airflow (LAF) bench, safety class II. Disinfection of all objects entering the LAF bench was accomplished by spraying with 80% (v/v) EtOH in sterile water. Water was prepared by reverse osmosis and resin cartridge purification using a Milli-Q system from Millipore, with a final resistance of 18 MΩ and was subsequently filter sterilized. For personal and cell culture protection sterile gloves, a laboratory coat, and glasses were used. The cells were grown in a humidified 5% CO_2 atmosphere to balance the required pH (7.0 – 7.4) with the HCO_3^-/CO_3^{2-} content of the culture medium at 37 °C. Therefore an incubator from Thermo, type 311, was used. To maintain water quality within the incubator 2 mL/1 L of Prothermal concentrate was added to the water reservoir. For centrifugation, an Eppendorf Concentrator plus was used. For cultivation, small, medium, and large culture flasks with sterile filter caps were used, with a bottom surface of 12.5 cm^2, 75 cm^2, and 150 cm^2, respectively. Dead cells and used media were removed with a vacuum aspirator IBS Vacusafe comfort plus from Integra and collected in a closed system, containing 300 mL EtOH for disinfection. Biological waste was decontaminated by using a Systec VX-75 autoclave before disposal. To visually check cell morphology, assess the degree of confluency, and confirm the absence of bacterial and fungal contaminations, an inverted microscope Zeiss Primo Vert, equipped with Plan-Achromat objective 4x and LD Plan-Achromat objectives 10x, 20x and 40x and a binocular tube for bright field and phase contrast was used.

Culture medium DMEM high glucose, L-glutamine (200 mM), penicillin (10.000 units/mL), streptomycin (10 mg/mL), and trypan blue solution was purchased from Sigma. Trypsin-EDTA (0.05%/0.02%) in PBS (1:250) were purchased from Amimed. PBS (pH 7.4) was purchased from Invitrogen. Freshly prepared medium, as well as PBS and trypsin-EDTA (0.05%/0.02%) in PBS (1:250), were aliquoted to 50 mL and 10 mL portions and stored at 4 °C, in order to diminish the risk of contaminations. They were pre-warmed to room temperature, before treatment of the cells. FCS superior was bought from Oxoid AG. It was heat deactivated at 50 °C for 30 min, sterile filtered, aliquoted to 50 mL portions to prevent contaminations, and stored at -20 °C until usage. Prothermal was bought from Lucerna-Chem AG. Cell culture flasks as well as serological pipettes were purchased from BD Biosciences and Sarstedt. For thawing of frozen cell aliquots, only a freshly prepared water bath was used, since a long-term standing water bath represents a main source of contaminations.

5.2.1.3   Procedures for cell culture

Adherent cell lines will grow *in vitro* until they have covered the available surface area or the medium is depleted of nutrients. At this point the cell lines should be sub-cultured (approximately 70-80% confluency) in order to prevent the culture dying. To subculture the cells they need to be brought into suspension in order to partition and transfer them to new cell culture flasks. The degree of adhesion varies from cell line to cell line and usually trypsin is used to release the cells from the flask to sub-cultivate them. The cells were split every two to three days, usually in a Monday-Wednesday-Friday rhythm, in order to introduce routine methods for cultivation. Cells were set in culture two weeks before experiments to control growth and sterility and were cultivated approximately up to passage 30, before discarding and setting fresh cells in culture.

Cells were cultured using DMEM high glucose (4.5 g/L, Sigma) supplemented with L-glutamine (200 mM), penicillin (10.000 units/mL), streptomycin (10 mg/mL), and 10% FCS superior (standardized). For cell experiments only 1% FCS superior was added to the medium, to prevent undesired side reactions of FCS with the investigated peptides during the assays, but also to avoid starving the cells. Since L-glutamine is degraded relatively fast in media, it is important to supplement media with L-glutamine prior to use.

Preparation of media

DMEM (10%) high glucose
- 435 mL DMEM
- 50 mL FCS
- 10 mL L-glutamine (200 mM)
- 5 mL of penicillin (10.000 units/mL) and streptomycin (10 mg/mL)

DMEM (1%) high glucose
- 480 mL DMEM
- 5mL FCS
- 10 mL L-glutamine
- 5 mL of penicillin (10.000 units/mL) and streptomycin (10 mg/mL)

To check the sterility of the freshly prepared medium, an aliquot of 5 mL was placed in a small culture flask and incubated at 37 °C and 5% CO_2. After two days the aliquot was examined under the microscope and controlled within the following two weeks.

General procedure for resuscitation of cell lines

A frozen cell pellet (stored in liquid nitrogen) was kept cool in a dry ice box during transport and subsequently quickly thawed (ca. 3 min), while fixed with tweezers and agitated it in a freshly prepared water bath at 37 °C until approximately 90% of the pellet was thawed. The cap is opened gently with a small rotation to prevent overpressure and it is recommended to wear safety glasses for this procedure, in case the cryo vial might explode. Afterwards the vial had to be sterilized properly. The cell suspension was transferred carefully into a 15 mL Falcon tube containing 10 mL PBS (at rt) using a 5 mL serological pipette. The Falcon tube was slowly turned up and down twice and centrifuged at 1500 rpm for 5 min. The supernatant was carefully aspirated and the pellet re-suspended in 10 mL DMEM (10%, at rt) and transferred in a medium size culture flask filled with 10 mL DMEM (10%), pre-warmed to 37°C. The flask was stored in the incubator and the medium exchanged after 24 h.

General procedure for medium exchange

In general, the quality of the medium and the need to replace it was controlled by the color, due to the pH indicator phenol red comprised in the DMEM. Usually the medium should be exchanged if the color turns yellow, indicating an acidic pH after consumption of nutrients and excretion by the cells. Then, used medium was aspirated. A fresh amount of 5 mL, 15 mL, and 30 mL medium was added to small, medium, and large cell culture flasks for culturing during the week and 5 mL, 25 mL, and 40 mL for culturing over the weekend, respectively. Afterwards the flasks were placed in the incubator.

General procedure for splitting cells

Used medium was aspirated carefully without damaging the cell layer on the bottom of the culture flask. Cells were washed twice (2 x 1.5 mL; 2 x 3 mL, 2 x 5 mL for small, medium, and large flasks, respectively) with PBS (w/o Ca^{2+}/Mg^{2+}) to remove traces of FCS that could deactivate the trypsin. Afterwards trypsin-EDTA (0.05%/0.02%) in PBS (1:250) was added (0.5 mL, 0.7 mL, 1.0 mL for small, medium, and large flasks,

respectively). The flask was slightly moved to allow the trypsin to cover the monolayer entirely. The excess of trypsin was carefully aspirated and the flask incubated for 4 min at 37 °C and 5% CO_2. Afterwards the flask was gently tapped to release remaining cells from the surface. Cells were examined under the microscope to ensure that all the cells were detached and floating. The cells were thoroughly re-suspended in 10 mL (10%) DMEM to inactivate the trypsin by pipetting up and down with a serological pipette. An aliquot of 100 μL was removed to perform a cell count. The required number of cells was transferred to a new labeled culture flask with an according volume of medium that was previously warmed to 37°C. For splitting 1:10, 1 mL of the 10 mL cell suspension was transferred to a new culture flask filled with pre-warmed medium. The cell culture flask was stored in the incubator.

General procedure for cell counting

For counting the cells a Neubauer chamber was used. Therefore a 100 μL aliquot of the cell suspension was thoroughly mixed with 200 μL of (0.4%) trypan blue (dilution factor = 3) and deposited on the chamber. By viewing under an inverted phase contrast microscope using x20 magnification, only living cells (seen as bright colorless cells) inside the four quadrants were counted. Blue stained cells (dead) were discarded. Taking the average number of the counted cells in all four quadrants, the total number of living cells in the entire cell suspension of 10 mL was calculated with the following formula:
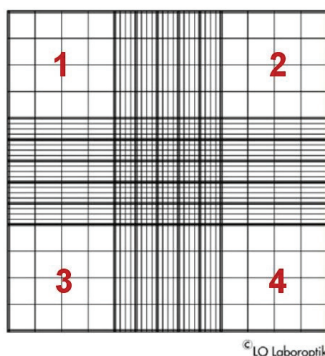
$$n(total) = n(average) \cdot V \cdot d \cdot 10^4$$

with

n = number of cells

V = volume of the total cell suspension in mL

d = dilution factor

10^4 = conversion factor due to chamber size

General procedure for cryopreservation of cell lines

Before freezing, the cells should be healthy with a viability >90% and no signs of microbial contamination. They should be in the logarithmic phase of growth, proliferating properly and be approximately 70% confluent. To cryopreserve cell lines, cells were treated with trypsin and counted as described before for cell splitting. Then they were centrifuged at 1500 rpm for 5 min and the supernatant was aspirated. The pellet was re-suspended in a defined volume of DMEM (1%) to give a ratio of 2 Mio cells/ mL. Previously labeled and sterilized cryo vials were placed in the bench and caps were opened. A calculated amount of DMSO (final ratio DMSO to DMEM (1%) should be 1:9) was added to the cell suspension to prevent cells from rupture by formation of ice crystals during the freezing process. The cell suspension was gently agitated and each cryo vial was filled with 1 mL using a 10 mL serological pipette. Properly closed cryo vials were transferred in a rate controlled freezing box that was filled with *n*-PrOH, and placed in a -80 °C freezer overnight. Afterwards pellets were transferred in liquid nitrogen for longer storage.

5.2.2   Cell experiments

5.2.2.1   Materials and instruments

Flow cytometry was carried out on a BD FACS Canto II, located in the group of Prof. D. Bumann, Biocenter Basel. Confocal microscopy was conducted on a Zeiss LSM 510/Confocor 2 located in the group of Prof. W. Meier at the Department of Chemistry, University Basel. Microplate readers were used in the group of Prof. T. Ward at the Department of Chemistry at the University of Basel and in the group of Prof. D. Hilvert, Laboratory of Organic Chemistry, ETH Zürich. Trypsin from bovine pancreas for stability assays was purchased from Sigma-Alrich. Enzymatic stability assays were monitored on a Shimadzu HPLC (Prominence) and ESI-MS system consisting of a Bruker esquire 3000plus and a Agilent 1100series HPLC at the University of Basel and a Dionex UPLC, Ultimate 3000 and a LC-MS system consisting of a Bruker, Amazon speed and a Dionex UHPLC, Ultimate 3000 at ETH Zürich, respectively. The column used for stability assays was a Reprosil gold 120 C18, 150 x 4 mm, 5 µm.

EDTA, PI, Triton X-100, trypsin and proteinase K were purchased from Sigma-Aldrich. Hoechst 33342 and Deep Red were purchased from Invitrogen, Life technologies. MTT was purchased from Merck.

5.2.2.2 Flow cytometry procedure

One day before the experiment 100,000 cells, suspended in 1 mL of 10% DMEM, were seeded into 24-well plates and allowed to adhere overnight. After 24 h culture medium was aspirated, cells were washed once with PBS (250 µL) and incubated with 250 µL peptide solution in 1% DMEM at different concentrations for 1 h. Afterwards cells were washed with Ca^{2+}- and Mg^{2+}-deficient PBS (3 x 250 µL) and incubated for 4 min with 100 µL trypsin-EDTA. Subsequently 300 µL PBS (4 °C) was added, cells were gently suspended and centrifuged at 1500 rpm for 5 min. The supernatant was carefully removed and the pellet resuspended in 400 µL of a solution of 1.5 µM PI and 2 mM EDTA in PBS or DMEM without phenolred, respectively, at 4 °C. The cell suspensions were placed in FACS tubes and kept on ice prior to analysis. Fluorescein and propidium iodide were excited at 488 nm and monitored with 530/30 bandpass and 650 longpass filters, respectively. Events corresponding to cellular debris were removed by gating on forward and side scatter. A total of 10,000 events per sample was counted. Each sample was run in triplicate and was repeated three times within one week. Control cells not treated with peptides were analyzed to determine background and auto-fluorescence levels. Mean fluorescence values FITC-A and FITC-H were determined from the histograms using FlowJo 7.6.3 software, while dead cells were removed by propidium iodide staining.

5.2.2.3 Confocal microscopy

One day before the experiment 10,000 cells, suspended in 200 µL of 10% DMEM, were seeded into 8-well plates and allowed to adhere overnight. After 24 h culture medium was aspirated, cells washed once with PBS (200 µL) and incubated with 200 µL peptide solution in 1% DMEM at different concentrations for 1 h. Cells were washed once with 1% DMEM (200 µL) and incubated with Hoechst 33342 (2 μM in 1% DMEM) for 10 min at 37 °C. Afterwards, cells were washed with PBS (3 x 200 µL) and a final amount of 200 µL 1% DMEM (w/o phenolred) was added. Non-fixed cells were immediately observed under the microscope. For detection of the Hoechst33342 nucleus marker a laser diode 405 nm and for 5,6-carboxyfluorescein an argon laser 458, 477, 488 &

514 nm was used. Pictures were taken using a C-Apochromat 63x/1.2W$_{corr}$ objective with water as immersion medium.

5.2.2.4 MTT assay

One day before the experiment 5000 cells, suspended in 100 µL of 10% DMEM, were seeded into 96-well plates and allowed to adhere overnight. After 24 h culture medium was aspirated, cells were washed once with PBS (100 µL) and incubated with 150 µL peptide solution in 1% DMEM at different concentrations for different incubation times. Afterwards, cells were washed with PBS (3 x 100 µL) and 150 µL MTT solution (1.2 mM in 1% DMEM w/o phenolred) was added. The cells were incubated for 3 h at 37 °C and 5% CO$_2$. The supernatant was discarded and 100 µL of detergent reagent (10% v/v Triton X-100 in 0.1 N HCl in *i*PrOH) was added. Samples were mixed by pipetting up and down, each 10 times and let stand for 30 min until measurement. Plates were analyzed in a microplate reader at 570 nm, background fluorescence was substracted. Each measurement was repeated twice and assays were carried out in triplicate within one week. Cell viability was calculated relative to PBS treated control cells, which were set to 100% viability according to the following formula:

$$\% \text{ cell viability} = A_{570} : A_{570} \text{ (control cells)} \cdot 100$$

5.2.2.5 Hemolysis assay

Hemolysis assays were performed using human blood, freshly taken at the University Hospital Basel. Probes were standing for 15 min and the erythrocytes were collected by centrifugation at 3000 rpm for 5 min and washed 3 times with PBS (pH 7.4, 3 x 5 mL) by centrifugation at 3000 rpm for 5 min. The erythrocytes were resuspended in PBS to 4 % (v/v) and 100 µL per well were placed into a 96-well plate. After a preincubation at 37°C for 10 min, 100 µL of the peptide solution in PBS was added to each well. Plates were incubated for 4 h at 37 °C, transferred to Eppendorf tubes and centrifuged at 3000 rpm for 5 min. Aliquots of 100 µL of the supernatants were transferred to a plane bottom 96-well plate and the release of hemoglobin was determined using a microplate reader at 540 nm (Hb). PBS and 0.1 % Triton X-100 in PBS were used as agents for 0% and 100% hemolysis, respectively. All hemolysis data points were presented as the percentage of the complete hemolysis.

5.2.2.6   Stability in trypsin

Enzymatic degradation of the peptides towards trypsin was carried out by incubation at 37 °C in 100mM Tris-HCl at pH 8.0. The trypsin to peptide ratio was 1:500, using a final peptide concentration of 125 μM and addition of a defined solution of trypsin from bovine pancreas in glycerol/water 1:1 (6.25 mg/mL). Samples were pipetted carefully up and down three times and incubated in a humidified 5% CO_2 atmosphere at 37 °C. Aliquots (50 μL) were taken periodically, starting from the addition of the trypsin (0 min) and continuing after 30 min, 1 h, 2 h, 6 h, 12 h, 24 h up to 48 h. To stop degradation and precipitate the enzyme, 150 μL of 1 N HCl were added. The samples were cooled on ice for 30 min and centrifuged at 4400 rpm for 10 min. Degradation was monitored by analytical RP-HPLC of the supernatant. As a negativ control pure PBS, without peptide, was added to the trypsin solution.

5.2.2.7   Stability in human blood serum

Human blood was freshly taken at the University Hospital Basel into EDTA-containing tubes to obtain the serum after coagulation of the blood after 15 min. Probes were centrifuged at 3000 rpm for 10 min and the supernatant was taken and directly used for stability assays. The peptides were added as stock solutions in sterile PBS to the serum to reach a final peptide concentration of 125 μM and a volume of 500 μL. Samples were pipetted carefully up and down three times and incubated in a humidified 5% CO_2 atmosphere at 37 °C. Aliquots of 50 μL were taken periodically, starting from the addition of the serum (0 min) and continuing after 30 min, 1 h, 2 h, 6 h, 12 h, 24 h up to 48 h. Aliquots were poured into 200 μL of a 1:1 mixture of acetonitrile/water to precipitate the proteins. The samples were cooled on ice for 30 min and centrifuged at 4400 rpm for 10 min. The supernatant was analyzed by RP-HPLC. As a negative control pure PBS, without peptide, was added to fresh blood serum.

5.2.2.8   siRNA delivery

The sequence of the siRNA against Renilla (siRen), which was delivered using CPPs, was 5' GAGCGAAGAGGGCGAGAAAUU (Dharmacon). Dual luciferase reporter plasmids containing the target site of miR-106a (CDKN1A; NM_000389.4; 3' UTR: 10511200) were cloned into the psiCHECK-2 Vector (No. C8021, Promega). The siRNA was delivered in different charge ratios (1:1, 3:1, 6:1, 9:1) in respect of the positive moieties

of the CPPs and the negative charged RNA backbone and in four different concentrations (36 nM, 9 nM, 2.25 nM, and 0 nM as negative control). As a positive control siRNA transfection with Oligofectamine (No. 12252-011; Invitrogen) according to manufacturer's instructions was applied.

For the dual luciferase assays, 5000 HeLa cells per well were seeded in white 96-well plates and RNAs were transfected after 8 hours. All transfections were performed in triplicate. DNA (20 ng of plasmid per well) was transfected using jetPEI (No. 101-10, Polyplus) according to manufacturer's protocol. After 48 hours, supernatants were removed and firefly substrate (15 mL; Dual-Glo® Luciferase Assay System, Promega) was added. Luminescence was measured on a microtiter plate reader (Mithras LB940, Berthold Technologies). After 30 min, 15 mL of renilla substrate per well was added and the measurement was repeated. Values were normalized against the firefly luciferase and the corresponding lowest concentration experiment, respectively.

6. APPENDIX

6.1 References

[1]   a) C. Schmuck, H. Wennemers, R. Breslow, in *Highlights in Bioorganic Chemistry: Methods and Applications*, John Wiley & Sons, **2006**, pp. 19-30; b) H. Reiersen, A. R. Rees, *Trends Biochem. Sci.* **2001**, *26*, 679-684; c) G. Vanhoof, F. Goossens, I. De Meester, D. Hendriks, S. Scharpe, *FASEB J..* **1995**, *9*, 736-744.

[2]   a) R. B. Corey, L. Pauling, *Proc. R. Soc. Lond. B. Biol. Sci.* **1953**, *141*, 10-20; b) W. J. Wedemeyer, E. Welker, H. A. Scheraga, *Biochemistry* **2002**, *41*, 14637-14644.

[3]   a) G. N. Ramachandran, V. Sasisekharan, *Adv. Protein Chem.* **1968**, *23*, 283-438; b) D. L. Nelson, M. M. Cox, in *Lehninger Principles of Biochemistry*, Worth, New York, **2000**, pp. 161-163; c) M. S. Weiss, A. Jabs, R. Hilgenfeld, *Nat. Struct. Biol.* **1998**, *5*, 676.

[4]   F. Schmid, in *Protein Folding Handbook, Vol. 5* (Ed.: B. J, T. Kiefhaber), WILEY-VCH, Weinheim, **2005**, pp. 916-945.

[5]   C. Grathwohl, K. Wuthrich, *Biopolymers* **1976**, *15*, 2043-2057.

[6]   a) J. F. Brandts, H. R. Halvorson, M. Brennan, *Biochemistry* **1975**, *14*, 4953-4963; b) G. Fischer, *Chem. Soc. Rev.* **2000**, *29*, 119-127; c) C. Dugave, L. Demange, *Chem. Rev.* **2003**, *103*, 2475-2532; d) A. Rath, A. R. Davidson, C. M. Deber, *Biopolymers* **2005**, *80*, 179-185; e) A. H. Andreotti, *Biochemistry* **2003**, *42*, 9515-9524; f) K. P. Lu, G. Finn, T. H. Lee, L. K. Nicholson, *Nat. Chem. Biol.* **2007**, *3*, 619-629.

[7]   a) G. Fischer, H. Bang, C. Mech, *Biomed. Biochim. Acta* **1984**, *43*, 1101-1111; b) J. Balbach, F. X. Schmid, *Mechanisms of protein folding,* 2nd ed., Oxford University Press, **2000**; c) G. Fischer, F. X. Schmid, *Biochemistry* **1990**, *29*, 2205-2212.

[8]   R. T. Raines, *Chem. Rev.* **1998**, *98*, 1045-1066.

[9]   a) T. Kiefhaber, H. P. Grunert, U. Hahn, F. X. Schmid, *Biochemistry* **1990**, *29*, 6475-6480; b) L. M. Mayr, F. X. Schmid, *J. Mol. Biol.* **1993**, *231*, 913-926.

[10]   Y. Wu, C. R. Matthews, *J. Mol. Biol.* **2002**, *322*, 7-13.

[11]   a) H. A. Schreuder, J. M. Rondeau, C. Tardif, A. Soffientini, E. Sarubbi, A. Akeson, T. L. Bowlin, S. Yanofsky, R. W. Barrett, *Eur. J. Biochem.* **1995**, *227*, 838-847; b) B. C. Finzel, L. L. Clancy, D. R. Holland, S. W. Muchmore, K. D. Watenpaugh, H. M. Einspahr, *J. Mol. Biol.* **1989**, *209*, 779-791; c) Y. Feng, W. F. Hood, R. W. Forgey, A. L. Abegg, M. H. Caparon, B. R. Thiele, R. M. Leimgruber, C. A. McWherter, *Protein Sci.* **1997**, *6*, 1777-1782.

[12]   A. Yaron, F. Naider, *Crit. Rev. Biochem. Mol. Biol.* **1993**, *28*, 31-81.

[13]   M. P. Hinderaker, R. T. Raines, *Protein Sci.* **2003**, *12*, 1188-1194.

[14]   H. Borrmann, I. Persson, M. Sandstrom, C. M. V. Stalhandske, *J. Chem. Soc., Perkin Trans. 2* **2000**, 393-402.

[15]   a) M. L. DeRider, S. J. Wilkens, M. J. Waddell, L. E. Bretscher, F. Weinhold, R. T. Raines, J. L. Markley, *J. Am. Chem. Soc.* **2002**, *124*, 2497-2505; b) L. E. Bretscher, C. L. Jenkins, K. M. Taylor, M. L. DeRider, R. T. Raines, *J. Am. Chem. Soc.* **2001**, *123*, 777-778.

[16]   G. J. Bartlett, A. Choudhary, R. T. Raines, D. N. Woolfson, *Nat. Chem. Biol.* **2010**, *6*, 615-620.

[17]   a) H. B. Bürgi, J. D. Dunitz, J. M. Lehn, G. Wipff, *Tetrahedron* **1974**, *30*, 1563-1572; b) H. B. Bürgi, J. D. Dunitz, E. J. Shefter, *J. Am. Chem. Soc.* **1973**, *95*, 5065-5067; c) H. B. Bürgi, J. D. Dunitz, E. Shefter, *Acta Crystallogr., Sect. B: Struct. Sci.* **1973**, *30*, 1517-1527; d) I. Fleming, in *Molecular Orbitals and Organic Chemical Reactions: Reference Edition*, John Wiley and Sons, **2010**, pp. 214–215.

[18]   J. A. Hodges, R. T. Raines, *Org. Lett.* **2006**, *8*, 4695-4697.

[19]   C. Renner, S. Alefelder, J. H. Bae, N. Budisa, R. Huber, L. Moroder, *Angew. Chem., Int. Ed. Engl.* **2001**, *40*, 923-925.

[20]   V. W. Magaard, R. M. Sanchez, J. W. Bean, M. L. Moore, *Tetrahedron Lett.* **1993**, *34*, 381-384.

[21]   N. G. Delaney, V. Madison, *J. Am. Chem. Soc.* **1982**, *104*, 6635-6641.

[22]   L. S. Sonntag, S. Schweizer, C. Ochsenfeld, H. Wennemers, *J. Am. Chem. Soc.* **2006**, *128*, 14697-14703.

[23]   a) M. Karplus, *J. Phys. Chem.* **1959**, *30*, 11-15; b) R. S. Hotchkiss, K. W. McConnell, K. Bullok, C. G. Davis, K. C. Chang, S. J. Schwulst, J. C. Dunne, G. P. Dietz, M. Bahr, J. E. McDunn, I. E. Karl, T. H. Wagner, J. P. Cobb, C. M. Coopersmith, D. Piwnica-Worms, *J. Immunol.* **2006**, *176*, 5471-5477; c) R. P. Bennett, B. Dalby, P. M. Guy, *Nat. Biotechnol.* **2002**, *20*, 20.

[24]   J. R. Durig, J. Liu, T. S. Little, V. F. Kalaskinsky, *J. Phys. Chem.* **1992**, *96*, 8224-8233.

[25]   L. E. Zimmer, C. Sparr, R. Gilmour, *Angew. Chem., Int. Ed. Engl.* **2011**, *50*, 11860-11871.

[26]   a) M. Kumin, L. S. Sonntag, H. Wennemers, *J. Am. Chem. Soc.* **2007**, *129*, 466-467; b) M. Kuemin, Y. A. Nagel, S. Schweizer, F. W. Monnard, C. Ochsenfeld, H. Wennemers, *Angew. Chem., Int. Ed. Engl.* **2010**, *49*, 6324-6327; c) K. M. Thomas, D. Naduthambi, G. Tririya, N. J. Zondlo, *Org. Lett.* **2005**, *7*, 2397-2400.

[27]   T. Steiner, P. Hess, J. H. Bae, B. Wiltschi, L. Moroder, N. Budisa, *PLoS One* **2008**, *3*, e1680.

[28]   S. S. A. An, C. C. Lester, J.-L. Peng, Y.-J. Li, D. M. Rothwarf, E. Welker, T. W. Thannhauser, L. S. Zhang, J. P. Tam, H. A. Scheraga, *J. Am. Chem. Soc.* **1999**, *121*, 11558-11566.

[29]   a) N. Panasik, Jr., E. S. Eberhardt, A. S. Edison, D. R. Powell, R. T. Raines, *Int. J. Pept. Protein Res.* **1994**, *44*, 262-269; b) F. W. Kotch, I. A. Guzei, R. T. Raines, *J. Am. Chem. Soc.* **2008**, *130*, 2952-2953.

[30]   a) R. S. Erdmann, H. Wennemers, *J. Am. Chem. Soc.* **2010**, *132*, 13957-13959; b) R. S. Erdmann, H. Wennemers, *Org. Biomol. Chem.* **2012**, *10*, 1982-1986.

[31]   R. S. Erdmann, H. Wennemers, *Angew. Chem., Int. Ed. Engl.* **2011**, *50*, 6835-6838.

[32]   a) P. Dumy, M. Keller, D. E. Ryan, B. Rohwedder, T. Woehr, M. Mutter, *J. Am. Chem. Soc.* **1997**, *119*, 918-925; b) M. Mutter, A. Nefzi, T. Sato, X. Sun, F. Wahl, T. Wohr, *Pept. Res.* **1995**, *8*, 145-153; c) T. Woehr, F. Wahl, A. Nefzi, B. Rohwedder, T. Sato, X. Sun, M. Mutter, *J. Am. Chem. Soc.* **1996**, *118*, 9218-9227.

[33]   a) F. Rabanal, M. D. Ludevid, M. Pons, E. Giralt, *Biopolymers* **1993**, *33*, 1019-1028; b) S. Kakinoki, Y. Hirano, M. Oka, *Polym. Bull.* **2005**, *53*, 109-115.

[34]   J. C. Horng, R. T. Raines, *Protein Sci.* **2006**, *15*, 74-83.

[35]   a) Y. A. Nagel, M. Kuemin, H. Wennemers, *Chimia* **2011**, *65*, 264-267; b) R. S. Erdmann, H. Wennemers, *Chimia* **2009**, *63*, 197-200.

[36]   B. W. Chellgren, T. P. Creamer, *Biochemistry* **2004**, *43*, 5864-5869.

[37] a) H. Yu, J. K. Chen, S. Feng, D. C. Dalgarno, A. W. Brauer, S. L. Schreiber, *Cell* **1994**, *76*, 933-945; b) A. B. Sparks, J. E. Rider, N. G. Hoffman, D. M. Fowlkes, L. A. Quillam, B. K. Kay, *Proc. Natl. Acad. Sci. U. S. A.* **1996**, *93*, 1540-1544.

[38] a) H. I. Chen, M. Sudol, *Proc. Natl. Acad. Sci. U. S. A.* **1995**, *92*, 7819-7823; b) M. J. Macias, M. Hyvonen, E. Baraldi, J. Schultz, M. Sudol, M. Saraste, H. Oschkinat, *Nature* **1996**, *382*, 646-649.

[39] a) M. Reinhard, K. Jouvenal, D. Tripier, U. Walter, *Proc. Natl. Acad. Sci. U. S. A.* **1995**, *92*, 7956-7960; b) M. Reinhard, K. Giehl, K. Abel, C. Haffner, T. Jarchau, V. Hoppe, B. M. Jockusch, U. Walter, *EMBO J.* **1995**, *14*, 1583-1589; c) M. Reinhard, M. Rudiger, B. M. Jockusch, U. Walter, *FEBS Lett.* **1996**, *399*, 103-107.

[40] a) K. Nishizawa, C. Freund, J. Li, G. Wagner, E. L. Reinherz, *Proc. Natl. Acad. Sci. U. S. A.* **1998**, *95*, 14897-14902; b) C. Freund, V. Dotsch, K. Nishizawa, E. L. Reinherz, G. Wagner, *Nat. Struct. Biol.* **1999**, *6*, 656-660.

[41] a) O. Pornillos, S. L. Alam, D. R. Davis, W. I. Sundquist, *Nat. Struct. Biol.* **2002**, *9*, 812-817; b) O. Pornillos, S. L. Alam, R. L. Rich, D. G. Myszka, D. R. Davis, W. I. Sundquist, *EMBO J.* **2002**, *21*, 2397-2406.

[42] a) N. M. Mahoney, P. A. Janmey, S. C. Almo, *Nat. Struct. Biol.* **1997**, *4*, 953-960; b) C. E. Schutt, J. C. Myslik, M. D. Rozycki, N. C. Goonesekere, U. Lindberg, *Nature* **1993**, *365*, 810-816.

[43] a) L. J. Ball, R. Kuhne, J. Schneider-Mergener, H. Oschkinat, *Angew. Chem., Int. Ed. Engl.* **2005**, *44*, 2852-2869; b) B. K. Kay, M. P. Williamson, M. Sudol, *FASEB J..* **2000**, *14*, 231-241.

[44] a) B. Brodsky, N. K. Shah, *FASEB J..* **1995**, *9*, 1537-1546; b) W. Traub, K. A. Piez, *Adv. Protein Chem.* **1971**, *25*, 243-352; c) H. P. Baechinger, J. Engel, in *Protein Folding Handbook,* Wiley-VCH, Weinheim, **2005**, pp. 1059-1110; d) J. Engel, H. P. Baechinger, *Top. Curr. Chem.* **2005**, *247*, 7-33.

[45] a) B. Bochicchio, A. M. Tamburro, *Chirality* **2002**, *14*, 782-792; b) A. Pepe, M. R. Armenante, B. Bochicchio, A. M. Tamburro, *Soft Matter* **2008**, *5*, 104-113.

[46] P. J. Ferris, J. P. Woessner, S. Waffenschmidt, S. Kilz, J. Drees, U. W. Goodenough, *Biochemistry* **2001**, *40*, 2978-2987.

[47] M. R. Holt, A. Koffer, *Trends Cell. Biol.* **2001**, *11*, 38-46.

[48] V. V. Rostovtsev, L. G. Green, V. V. Fokin, K. B. Sharpless, *Angew. Chem., Int. Ed. Engl.* **2002**, *41*, 2596-2599.

[49] C. W. Tornoe, C. Christensen, M. Meldal, *J. Org. Chem.* **2002**, *67*, 3057-3064.

[50] K. M. Bonger, V. V. Kapoerchan, G. M. Grotenbreg, C. J. van Koppen, C. M. Timmers, G. A. van der Marel, H. S. Overkleeft, *Org. Biomol. Chem.* **2010**, *8*, 1881-1884.

[51] a) L. Stryer, R. P. Haugland, *Proc. Natl. Acad. Sci. U. S. A.* **1967**, *58*, 719-726; b) B. Schuler, E. A. Lipman, P. J. Steinbach, M. Kumke, W. A. Eaton, *Proc. Natl. Acad. Sci. U. S. A.* **2005**, *102*, 2754-2759; c) R. B. Best, K. A. Merchant, I. V. Gopich, B. Schuler, A. Bax, W. A. Eaton, *Proc. Natl. Acad. Sci. U. S. A.* **2007**, *104*, 18964-18969.

[52] a) K. E. Sapsford, L. Berti, I. L. Medintz, *Angew. Chem., Int. Ed. Engl.* **2006**, *45*, 4562-4589; b) Z. K. Majumdar, R. Hickerson, H. F. Noller, R. M. Clegg, *J. Mol. Biol.* **2005**, *351*, 1123-1145; c) A. Roda, M. Guardigli, E. Michelini, M. Mirasoli, *Anal. Bioanal. Chem.* **2009**, *393*, 109-123.

[53]   a) W. L. Mattice, L. Mandelkern, *J. Am. Chem. Soc.* **1971**, *93*, 1769-1777; b) L. Tooke, L. Duitch, T. J. Measey, R. Schweitzer-Stenner, *Biopolymers* **2010**, *93*, 451-457; c) W. L. Mattice, L. Mandelkern, *Biopolymers* **1971**, *4*, 271-274.

[54]   a) B. Giese, M. Wang, J. Gao, M. Stoltz, P. Muller, M. Graber, *J. Org. Chem.* **2009**, *74*, 3621-3625; b) B. Giese, M. Graber, M. Cordes, *Curr. Opin. Chem. Biol.* **2008**, *12*, 755-759; c) M. Cordes, A. Kottgen, C. Jasper, O. Jacques, H. Boudebous, B. Giese, *Angew. Chem., Int. Ed. Engl.* **2008**, *47*, 3461-3463; d) S. A. Serron, W. S. Aldridge Iii, C. N. Fleming, R. M. Danell, M. H. Baik, M. Sykora, D. M. Dattelbaum, T. J. Meyer, *J. Am. Chem. Soc.* **2004**, *126*, 14506-14514; e) D. R. Striplin, S. Y. Reece, D. G. McCafferty, C. G. Wall, D. A. Friesen, B. W. Erickson, T. J. Meyer, *J. Am. Chem. Soc.* **2004**, *126*, 5282-5291.

[55]   a) M. A. Schmitt, B. Weisblum, S. H. Gellman, *J. Am. Chem. Soc.* **2004**, *126*, 6848-6849; b) D. Liu, W. F. DeGrado, *J. Am. Chem. Soc.* **2001**, *123*, 7553-7559.

[56]   a) J. W. Chin, A. Schepartz, *J. Am. Chem. Soc.* **2001**, *123*, 2929-2930; b) J. W. Chin, R. M. Grotzfeld, M. A. Fabian, A. Schepartz, *Bioorg. Med. Chem. Lett.* **2001**, *11*, 1501-1505; c) N. J. Zondlo, A. Schepartz, *J. Am. Chem. Soc.* **1999**, *121*, 6938-6939.

[57]   a) J. W. Chin, A. Schepartz, *Angew. Chem., Int. Ed. Engl.* **2001**, *40*, 3806-3809; b) S. E. Rutledge, J. W. Chin, A. Schepartz, *Curr. Opin. Chem. Biol.* **2002**, *6*, 479-485; c) J. A. Kritzer, R. Zutshi, M. Cheah, F. A. Ran, R. Webman, T. M. Wongjirad, A. Schepartz, *ChemBioChem* **2006**, *7*, 29-31.

[58]   a) E. S. Cobos, M. T. Pisabarro, M. C. Vega, E. Lacroix, L. Serrano, J. Ruiz-Sanz, J. C. Martinez, *J. Mol. Biol.* **2004**, *342*, 355-365; b) D. Golemi-Kotra, R. Mahaffy, M. J. Footer, J. H. Holtzman, T. D. Pollard, J. A. Theriot, A. Schepartz, *J. Am. Chem. Soc.* **2004**, *126*, 4-5.

[59]   E. Giralt, M. W. Peczuh, X. Salvatella, in *Protein surface recognition – Approaches for drug discovery*, John Wiley & Sons, Ltd, **2011**.

[60]   C. Kroll, R. Mansi, F. Braun, S. Dobitz, H.R. Maecke, H. Wennemers, *J. Am. Chem. Soc.* **2013,** *135(45),* 16793-16796.

[61]   G. Upert, F. Bouillere, H. Wennemers, *Angew. Chem., Int. Ed. Engl.* **2012**, *51*, 4231-4234.

[62]   a) L. E. O'Leary, J. A. Fallas, E. L. Bakota, M. K. Kang, J. D. Hartgerink, *Nat. Chem.* **2011**, *3*, 821-828; b) C. C. Chen, W. Hsu, T. C. Kao, J. C. Horng, *Biochemistry* **2011**, *50*, 2381-2383; c) U. Kusebauch, S. A. Cadamuro, H. J. Musiol, M. O. Lenz, J. Wachtveitl, L. Moroder, C. Renner, *Angew. Chem., Int. Ed. Engl.* **2006**, *45*, 7015-7018; d) M. M. Pires, D. E. Przybyla, C. M. Rubert Perez, J. Chmielewski, *J. Am. Chem. Soc.* **2011**, *133*, 14469-14471; e) K. Kar, S. Ibrar, V. Nanda, T. M. Getz, S. P. Kunapuli, B. Brodsky, *Biochemistry* **2009**, *48*, 7959-7968; f) F. W. Kotch, R. T. Raines, *Proc. Natl. Acad. Sci. U. S. A.* **2006**, *103*, 3028-3033.

[63]   K. Kamimura, T. Suda, G. Zhang, D. Liu, *Pharmaceut. Med.* **2011**, *25*, 293-306.

[64]   C. E. Thomas, A. Ehrhardt, M. A. Kay, *Nat. Rev. Genet.* **2003**, *4*, 346-358.

[65]   E. Check, *Nature* **2002**, *419*, 545-546.

[66]   T. Hollon, *Am. J. Ophthalmol.* **2000**, *129*, 701.

[67]   E. Check, *Nature* **2003**, *423*, 573-574.

[68]   A. D. Bangham, M. M. Standish, J. C. Watkins, *J. Mol. Biol.* **1965**, *13*, 238-252.

[69]   A. El-Aneed, *J. Controlled Release* **2004**, *94*, 1-14.

[70]   P. P. Karmali, A. Chaudhuri, *Med. Res. Rev.* **2007**, *27*, 696-722.

[71]   Invitrogen, *Lipofectamine*, http://www.invitrogen.com/site/us/en/home/

brands/Product-/lipofectamine.html

[72]   a) A. T. Stopeck, E. M. Hersh, E. T. Akporiaye, D. T. Harris, T. Grogan, E. Unger, J. Warneke, S. F. Schluter, S. Stahl, *J. Clin. Oncol.* **1997**, *15*, 341-349; b) A. T. Stopeck, A. Jones, E. M. Hersh, J. A. Thompson, D. M. Finucane, J. C. Gutheil, R. Gonzalez, *Clin. Cancer Res.* **2001**, *7*, 2285-2291.

[73]   a) P. R. Dash, M. L. Read, L. B. Barrett, M. A. Wolfert, L. W. Seymour, *Gene Ther.* **1999**, *6*, 643-650; b) C. M. Ward, M. L. Read, L. W. Seymour, *Blood* **2001**, *97*, 2221-2229.

[74]   a) Polyplus, *jetPEI, In vitro DNA Transfection Protocol*, http://www.polyplus-transfection.com; b) A. R. Klemm, D. Young, J. B. Lloyd, *Biochem. Pharmacol.* **1998**, *56*, 41-46.

[75]   A. Kichler, C. Leborgne, E. Coeytaux, O. Danos, *J. Gene Med.* **2001**, *3*, 135-144.

[76]   a) C. W. Pouton, P. Lucas, B. J. Thomas, A. N. Uduehi, D. A. Milroy, S. H. Moss, *J. Controlled Release* **1998**, *53*, 289-299; b) L. Shewring, L. Collins, S. L. Lightman, S. Hart, K. Gustafsson, J. W. Fabre, *Transplantation* **1997**, *64*, 763-769.

[77]   a) A. A. Chen, A. M. Derfus, S. R. Khetani, S. N. Bhatia, *Nucleic Acids Res.* **2005**, *33*, e190; b) M. X. Zhao, J. M. Li, L. Du, C. P. Tan, Q. Xia, Z. W. Mao, L. N. Ji, *Chemistry* **2011**, *17*, 5171-5179; c) X. Gao, Y. Cui, R. M. Levenson, L. W. Chung, S. Nie, *Nat. Biotechnol.* **2004**, *22*, 969-976; d) M. V. Yezhelyev, L. Qi, R. M. O'Regan, S. Nie, X. Gao, *J. Am. Chem. Soc.* **2008**, *130*, 9006-9012.

[78]   a) A. K. Lytton-Jean, R. Langer, D. G. Anderson, *Small* **2011**, *7*, 1932-1937; b) J. S. Lee, J. J. Green, K. T. Love, J. Sunshine, R. Langer, D. G. Anderson, *Nano Lett.* **2009**, *9*, 2402-2406; c) J. Shi, Z. Xiao, N. Kamaly, O. C. Farokhzad, *Acc. Chem. Res.* **2011**, *44*, 1123-1134; d) M. R. Papasani, G. Wang, R. A. Hill, *Nanomedicine* **2012**, *8*, 804-814.

[79]   a) Z. Medarova, W. Pham, C. Farrar, V. Petkova, A. Moore, *Nat. Med.* **2007**, *13*, 372-377; b) A. Curcio, R. Marotta, A. Riedinger, D. Palumberi, A. Falqui, T. Pellegrino, *Chem. Commun. (Cambridge, U.K.)* **2012**, *48*, 2400-2402.

[80]   T. Xia, M. Kovochich, M. Liong, H. Meng, S. Kabehie, S. George, J. I. Zink, A. E. Nel, *ACS Nano* **2009**, *3*, 3273-3286.

[81]   T. Tanaka, L. S. Mangala, P. E. Vivas-Mejia, R. Nieves-Alicea, A. P. Mann, E. Mora, H. D. Han, M. M. Shahzad, X. Liu, R. Bhavane, J. Gu, J. R. Fakhoury, C. Chiappini, C. Lu, K. Matsuo, B. Godin, R. L. Stone, A. M. Nick, G. Lopez-Berestein, A. K. Sood, M. Ferrari, *Cancer Res.* **2010**, *70*, 3687-3696.

[82]   N. W. Kam, Z. Liu, H. Dai, *J. Am. Chem. Soc.* **2005**, *127*, 12492-12493.

[83]   a) Y. Higuchi, S. Kawakami, M. Hashida, *BioDrugs* **2010**, *24*, 195-205; b) E. Miele, G. P. Spinelli, E. Miele, E. Di Fabrizio, E. Ferretti, S. Tomao, A. Gulino, *Int J Nanomedicine* **2012**, *7*, 3637-3657.

[84]   a) H. J. Johnston, G. Hutchison, F. M. Christensen, S. Peters, S. Hankin, V. Stone, *Crit. Rev. Toxicol.* **2010**, *40*, 328-346; b) N. Khlebtsov, L. Dykman, *Chem. Soc. Rev.* **2011**, *40*, 1647-1671.

[85]   F. Heitz, M. C. Morris, G. Divita, *Br. J. Pharmacol.* **2009**, *157*, 195-206.

[86]   K. M. Stewart, K. L. Horton, S. O. Kelley, *Org. Biomol. Chem.* **2008**, *6*, 2242-2255.

[87]   Ü. Langel, *Handbook of Cell-Penetrating Peptides*, 2nd ed., Taylor & Francis Group, **2007**.

[88]   Ü. Langel, *Cell-Penetrating Peptides: Methods and Protocols*, Humana Press, **2011**.

[89]   a) I. M. Kaplan, J. S. Wadia, S. F. Dowdy, *J. Controlled Release* **2005**, *102*, 247-253; b) J. P. Richard, K. Melikov, H. Brooks, P. Prevot, B. Lebleu, L. V. Chernomordik, *J. Biol. Chem.* **2005**, *280*, 15300-15306; c) J. P. Richard, K. Melikov, E. Vives, C. Ramos, B. Verbeure, M. J. Gait, L. V. Chernomordik, B. Lebleu, *J. Biol. Chem.* **2003**, *278*, 585-590.

[90]   a) B. Christiaens, J. Grooten, M. Reusens, A. Joliot, M. Goethals, J. Vandekerckhove, A. Prochiantz, M. Rosseneu, *Eur. J. Biochem.* **2004**, *271*, 1187-1197; b) D. Derossi, S. Calvet, A. Trembleau, A. Brunissen, G. Chassaing, A. Prochiantz, *J. Biol. Chem.* **1996**, *271*, 18188-18193; c) D. Derossi, A. H. Joliot, G. Chassaing, A. Prochiantz, *J. Biol. Chem.* **1994**, *269*, 10444-10450; d) A. Joliot, C. Pernelle, H. Deagostini-Bazin, A. Prochiantz, *Proc. Natl. Acad. Sci. U. S. A.* **1991**, *88*, 1864-1868.

[91]   A. Elmquist, M. Lindgren, T. Bartfai, U. Langel, *Exp. Cell Res.* **2001**, *269*, 237-244.

[92]   G. Elliott, P. O'Hare, *Cell* **1997**, *88*, 223-233.

[93]   a) C. Rousselle, P. Clair, J. M. Lefauconnier, M. Kaczorek, J. M. Scherrmann, J. Temsamani, *Mol. Pharmacol.* **2000**, *57*, 679-686; b) M. Mazel, P. Clair, C. Rousselle, P. Vidal, J. M. Scherrmann, D. Mathieu, J. Temsamani, *Anticancer Drugs* **2001**, *12*, 107-116.

[94]   E. Gros, S. Deshayes, M. C. Morris, G. Aldrian-Herrada, J. Depollier, F. Heitz, G. Divita, *Biochim. Biophys. Acta* **2006**, *1758*, 384-393.

[95]   M. Pooga, M. Hallbrink, M. Zorko, Ü. Langel, *FASEB J.* **1998**, *12*, 67-77.

[96]   L. Crombez, G. Aldrian-Herrada, K. Konate, Q. N. Nguyen, G. K. McMaster, R. Brasseur, F. Heitz, G. Divita, *Mol. Ther.* **2009**, *17*, 95-103.

[97]   a) J. Oehlke, E. Krause, B. Wiesner, M. Beyermann, M. Bienert, *FEBS Lett.* **1997**, *415*, 196-199; b) J. Oehlke, A. Scheller, B. Wiesner, E. Krause, M. Beyermann, E. Klauschenz, M. Melzig, M. Bienert, *Biochim. Biophys. Acta* **1998**, *1414*, 127-139.

[98]   a) S. Futaki, T. Suzuki, W. Ohashi, T. Yagami, S. Tanaka, K. Ueda, Y. Sugiura, *J. Biol. Chem.* **2001**, *276*, 5836-5840; b) P. A. Wender, D. J. Mitchell, K. Pattabiraman, E. T. Pelkey, L. Steinman, J. B. Rothbard, *Proc. Natl. Acad. Sci. U. S. A.* **2000**, *97*, 13003-13008.

[99]   K. Sadler, K. D. Eom, J. L. Yang, Y. Dimitrova, J. P. Tam, *Biochemistry* **2002**, *41*, 14150-14157.

[100]   D. S. Daniels, A. Schepartz, *J. Am. Chem. Soc.* **2007**, *129*, 14578-14579.

[101]   a) M. J. Kogan, I. Dalcol, P. Gorostiza, C. Lopez-Iglesias, M. Pons, F. Sanz, D. Ludevid, E. Giralt, *J. Mol. Biol.* **2001**, *312*, 907-913; b) M. J. Kogan, I. Dalcol, P. Gorostiza, C. Lopez-Iglesias, R. Pons, M. Pons, F. Sanz, E. Giralt, *Biophys J.* **2002**, *83*, 1194-1204; c) I. Martin, M. Teixido, E. Giralt, *ChemBioChem* **2011**, *12*, 896-903.

[102]   J. Tobaly-Tapiero, A. Zamborlini, P. Bittoun, A. Saib, *PLoS One* **2012**, *7*, e31108.

[103]   M. Green, P. M. Loewenstein, *Cell* **1988**, *55*, 1179-1188.

[104]   A. D. Frankel, C. O. Pabo, *Cell* **1988**, *55*, 1189-1193.

[105]   M. F. Laspia, A. P. Rice, M. B. Mathews, *Cell* **1989**, *59*, 283-292.

[106]   E. Vives, P. Brodin, B. Lebleu, *J. Biol. Chem.* **1997**, *272*, 16010-16017.

[107]   M. L. Lin, P. J. Bertics, *J. Cell. Physiol.* **1995**, *164*, 593-604.

[108]   M. C. Morris, P. Vidal, L. Chaloin, F. Heitz, G. Divita, *Nucleic Acids Res.* **1997**, *25*, 2730-2736.

[109]   L. Chaloin, P. Vidal, A. Heitz, N. Van Mau, J. Mery, G. Divita, F. Heitz, *Biochemistry* **1997**, *36*, 11179-11187.

[110] M. Y. Zhang, S. C. Sun, L. Bell, B. A. Miller, *Blood* **1998**, *91*, 4136-4144.

[111] L. Chaloin, P. Vidal, P. Lory, J. Mery, N. Lautredou, G. Divita, F. Heitz, *Biochem. Biophys. Res. Commun.* **1998**, *243*, 601-608.

[112] M. Pooga, M. Lindgren, M. Hallbrink, E. Brakenhielm, Ü. Langel, *Ann. N. Y. Acad. Sci.* **1998**, *863*, 450-453.

[113] J. Temsamani, P. Vidal, *Drug Discovery Today* **2004**, *9*, 1012-1019.

[114] D. J. Mitchell, D. T. Kim, L. Steinman, C. G. Fathman, J. B. Rothbard, *J. Pept. Res.* **2000**, *56*, 318-325.

[115] T. Jiang, E. S. Olson, Q. T. Nguyen, M. Roy, P. A. Jennings, R. Y. Tsien, *Proc. Natl. Acad. Sci. U. S. A.* **2004**, *101*, 17867-17872.

[116] D. Mandal, A. Nasrolahi Shirazi, K. Parang, *Angew. Chem., Int. Ed. Engl.* **2011**, *50*, 9633-9637.

[117] W. P. Verdurmen, P. H. Bovee-Geurts, P. Wadhwani, A. S. Ulrich, M. Hallbrink, T. H. van Kuppevelt, R. Brock, *Chem. Biol.* **2011**, *18*, 1000-1010.

[118] a) M. Rueping, Y. Mahajan, M. Sauer, D. Seebach, *ChemBioChem* **2002**, *3*, 257-259; b) D. Seebach, J. Gardiner, *Acc. Chem. Res.* **2008**, *41*, 1366-1375; c) T. Hitz, R. Iten, J. Gardiner, K. Namoto, P. Walde, D. Seebach, *Biochemistry* **2006**, *45*, 5817-5829; d) F. Kamena, B. Monnanda, D. Makou, S. Capone, K. Patora-Komisarska, D. Seebach, *Chem. Biodivers.* **2011**, *8*, 1-12; e) J. Frackenpohl, P. I. Arvidsson, J. V. Schreiber, D. Seebach, *ChemBioChem* **2001**, *2*, 445-455.

[119] N. Umezawa, M. A. Gelman, M. C. Haigis, R. T. Raines, S. H. Gellman, *J. Am. Chem. Soc.* **2002**, *124*, 368-369.

[120] J. Brugidou, C. Legrand, J. Mery, A. Rabie, *Biochem. Biophys. Res. Commun.* **1995**, *214*, 685-693.

[121] a) T. Darbre, J. L. Reymond, *Acc. Chem. Res.* **2006**, *39*, 925-934; b) J. L. Reymond, T. Darbre, *Org. Biomol. Chem.* **2012**, *10*, 1483-1492; c) H. H. Chung, G. Harms, C. M. Seong, B. H. Choi, C. Min, J. P. Taulane, M. Goodman, *Biopolymers* **2004**, *76*, 83-96.

[122] P. A. Wender, W. C. Galliher, E. A. Goun, L. R. Jones, T. H. Pillow, *Adv. Drug. Deliv. Rev.* **2008**, *60*, 452-472.

[123] a) N. W. Luedtke, T. J. Baker, M. Goodman, Y. Tor, *J. Am. Chem. Soc.* **2000**, *122*, 12035-12036; b) N. W. Luedtke, P. Carmichael, Y. Tor, *J. Am. Chem. Soc.* **2003**, *125*, 12374-12375.

[124] a) K. K. Maiti, O. Y. Jeon, W. S. Lee, D. C. Kim, K. T. Kim, T. Takeuchi, S. Futaki, S. K. Chung, *Angew. Chem., Int. Ed. Engl.* **2006**, *45*, 2907-2912; b) K. K. Maiti, O. Y. Jeon, W. S. Lee, S. K. Chung, *Chemistry* **2007**, *13*, 762-775.

[125] J. Fernandez-Carneado, M. Van Gool, V. Martos, S. Castel, P. Prados, J. de Mendoza, E. Giralt, *J. Am. Chem. Soc.* **2005**, *127*, 869-874.

[126] a) A. Dragulescu-Andrasi, P. Zhou, G. He, D. H. Ly, *Chem. Commun. (Cambridge, U.K.)* **2005**, 244-246; b) P. Zhou, M. Wang, L. Du, G. W. Fisher, A. Waggoner, D. H. Ly, *J. Am. Chem. Soc.* **2003**, *125*, 6878-6879.

[127] T. Ohmichi, M. Kuwahara, N. Sasaki, M. Hasegawa, T. Nishikata, H. Sawai, N. Sugimoto, *Angew. Chem., Int. Ed. Engl.* **2005**, *44*, 6682-6685.

[128] G. Deglane, S. Abes, T. Michel, P. Prevot, E. Vives, F. Debart, I. Barvik, B. Lebleu, J. J. Vasseur, *ChemBioChem* **2006**, *7*, 684-692.

[129] a) M. Park, J. W. Toporowski, T. C. Bruice, *Bioorg. Med. Chem.* **2006**, *14*, 1743-1749; b) R. O. Dempcy, O. Almarsson, T. C. Bruice, *Proc. Natl. Acad. Sci. U. S. A.*

1994, *91*, 7864-7868; c) M. Park, T. C. Bruice, *Bioorg. Med. Chem. Lett.* **2005**, *15*, 3247-3251.

[130] P. A. Wender, J. B. Rothbard, T. C. Jessop, E. L. Kreider, B. L. Wylie, *J. Am. Chem. Soc.* **2002**, *124*, 13382-13383.

[131] S. Pujals, E. Giralt, *Adv. Drug. Deliv. Rev.* **2008**, *60*, 473-484.

[132] a) J. Farrera-Sinfreu, E. Giralt, S. Castel, F. Albericio, M. Royo, *J. Am. Chem. Soc.* **2005**, *127*, 9459-9468; b) J. Farrera-Sinfreu, E. Giralt, M. Royo, F. Albericio, *Methods Mol. Biol.* **2007**, *386*, 241-267; c) J. Farrera-Sinfreu, L. Zaccaro, D. Vidal, X. Salvatella, E. Giralt, M. Pons, F. Albericio, M. Royo, *J. Am. Chem. Soc.* **2004**, *126*, 6048-6057.

[133] a) I. Geisler, J. Chmielewski, *Chem. Biol. Drug Des.* **2009**, *73*, 39-45; b) I. M. Geisler, J. Chmielewski, *Pharm. Res.* **2011**, *28*, 2797-2807; c) D. Kalafut, T. N. Anderson, J. Chmielewski, *Bioorg. Med. Chem. Lett.* **2012**, *22*, 561-563.

[134] a) L. Crespo, G. Sanclimens, B. Montaner, R. Perez-Tomas, M. Royo, M. Pons, F. Albericio, E. Giralt, *J. Am. Chem. Soc.* **2002**, *124*, 8876-8883; b) L. Crespo, G. Sanclimens, M. Pons, E. Giralt, M. Royo, F. Albericio, *Chem. Rev.* **2005**, *105*, 1663-1681.

[135] B. A. Smith, D. S. Daniels, A. E. Coplin, G. E. Jordan, L. M. McGregor, A. Schepartz, *J. Am. Chem. Soc.* **2008**, *130*, 2948-2949.

[136] J. Fernandez-Carneado, M. J. Kogan, S. Castel, E. Giralt, *Angew. Chem., Int. Ed. Engl.* **2004**, *43*, 1811-1814.

[137] S. Pujals, J. Fernandez-Carneado, M. J. Kogan, J. Martinez, F. Cavelier, E. Giralt, *J. Am. Chem. Soc.* **2006**, *128*, 8479-8483.

[138] M. Nanda, K. N. Ganesh, *J. Org. Chem.* **2012**, *77*, 4131-4135.

[139] a) Y. A. Fillon, J. P. Anderson, J. Chmielewski, *J. Am. Chem. Soc.* **2005**, *127*, 11798-11803; b) I. Geisler, J. Chmielewski, *Bioorg. Med. Chem. Lett.* **2007**, *17*, 2765-2768; c) L. Li, I. Geisler, J. Chmielewski, J. X. Cheng, *J. Controlled Release* **2010**, *142*, 259-266.

[140] a) F. Duchardt, M. Fotin-Mleczek, H. Schwarz, R. Fischer, R. Brock, *Traffic* **2007**, *8*, 848-866; b) J. R. Maiolo, M. Ferrer, E. A. Ottinger, *Biochim. Biophys. Acta* **2005**, *1712*, 161-172; c) I. Nakase, M. Niwa, T. Takeuchi, K. Sonomura, N. Kawabata, Y. Koike, M. Takehashi, S. Tanaka, K. Ueda, J. C. Simpson, A. T. Jones, Y. Sugiura, S. Futaki, *Mol. Ther.* **2004**, *10*, 1011-1022.

[141] a) S. Sandgren, F. Cheng, M. Belting, *J. Biol. Chem.* **2002**, *277*, 38877-38883; b) M. Tyagi, M. Rusnati, M. Presta, M. Giacca, *J. Biol. Chem.* **2001**, *276*, 3254-3261; c) A. Ziegler, J. Seelig, *Biophys J.* **2004**, *86*, 254-263; dE. Goncalves, E. Kitas, J. Seelig, *Biochemistry* **2005**, *44*, 2692-2702.

[142] A. Prochiantz, *Curr. Opin. Cell. Biol.* **2000**, *12*, 400-406.

[143] a) A. Ziegler, P. Nervi, M. Durrenberger, J. Seelig, *Biochemistry* **2005**, *44*, 138-148; b) J. C. Mai, H. Shen, S. C. Watkins, T. Cheng, P. D. Robbins, *J. Biol. Chem.* **2002**, *277*, 30208-30218.

[144] a) S. Pujals, J. Fernandez-Carneado, C. Lopez-Iglesias, M. J. Kogan, E. Giralt, *Biochim. Biophys. Acta* **2006**, *1758*, 264-279; b) H. Brooks, B. Lebleu, E. Vives, *Adv. Drug. Deliv. Rev.* **2005**, *57*, 559-577.

[145] a) K. A. Mislick, J. D. Baldeschwieler, *Proc. Natl. Acad. Sci. U. S. A.* **1996**, *93*, 12349-12354; b) M. Belting, P. Petersson, *Biochem. J.* **1999**, *342 (Pt 2)*, 281-286; c) C. M.

Wiethoff, J. G. Smith, G. S. Koe, C. R. Middaugh, *J. Biol. Chem.* **2001**, *276*, 32806-32813.

[146]   I. Nakase, H. Akita, K. Kogure, A. Graslund, U. Langel, H. Harashima, S. Futaki, *Acc. Chem. Res.* **2012**, *45*, 1132-1139.

[147]   a) P. E. Thoren, D. Persson, M. Karlsson, B. Norden, *FEBS Lett.* **2000**, *482*, 265-268; b) S. T. Henriques, J. Costa, M. A. Castanho, *Biochemistry* **2005**, *44*, 10189-10198.

[148]   R. Fischer, M. Fotin-Mleczek, H. Hufnagel, R. Brock, *ChemBioChem* **2005**, *6*, 2126-2142.

[149]   a) M. Nishihara, F. Perret, T. Takeuchi, S. Futaki, A. N. Lazar, A. W. Coleman, N. Sakai, S. Matile, *Org. Biomol. Chem.* **2005**, *3*, 1659-1669; b) F. Perret, M. Nishihara, T. Takeuchi, S. Futaki, A. N. Lazar, A. W. Coleman, N. Sakai, S. Matile, *J. Am. Chem. Soc.* **2005**, *127*, 1114-1115; c) N. Sakai, S. Matile, *J. Am. Chem. Soc.* **2003**, *125*, 14348-14356; d) N. Sakai, T. Takeuchi, S. Futaki, S. Matile, *ChemBioChem* **2005**, *6*, 114-122; e) T. Takeuchi, M. Kosuge, A. Tadokoro, Y. Sugiura, M. Nishi, M. Kawata, N. Sakai, S. Matile, S. Futaki, *ACS Chem. Biol.* **2006**, *1*, 299-303.

[150]   J. P. Berlose, O. Convert, D. Derossi, A. Brunissen, G. Chassaing, *Eur. J. Biochem.* **1996**, *242*, 372-386.

[151]   T. Suzuki, S. Futaki, M. Niwa, S. Tanaka, K. Ueda, Y. Sugiura, *J. Biol. Chem.* **2002**, *277*, 2437-2443.

[152]   a) S. Console, C. Marty, C. Garcia-Echeverria, R. Schwendener, K. Ballmer-Hofer, *J. Biol. Chem.* **2003**, *278*, 35109-35114; b) G. Drin, S. Cottin, E. Blanc, A. R. Rees, J. Temsamani, *J. Biol. Chem.* **2003**, *278*, 31192-31201; c) A. Fittipaldi, A. Ferrari, M. Zoppe, C. Arcangeli, V. Pellegrini, F. Beltram, M. Giacca, *J. Biol. Chem.* **2003**, *278*, 34141-34149; d) S. M. Fuchs, R. T. Raines, *Biochemistry* **2004**, *43*, 2438-2444; e) R. Fischer, K. Kohler, M. Fotin-Mleczek, R. Brock, *J. Biol. Chem.* **2004**, *279*, 12625-12635.

[153]   a) S. D. Kramer, H. Wunderli-Allenspach, *Biochim. Biophys. Acta* **2003**, *1609*, 161-169; b) A. Ziegler, X. L. Blatter, A. Seelig, J. Seelig, *Biochemistry* **2003**, *42*, 9185-9194.

[154]   J. B. Rothbard, T. C. Jessop, P. A. Wender, *Adv. Drug. Deliv. Rev.* **2005**, *57*, 495-504.

[155]   S. Mukherjee, R. N. Ghosh, F. R. Maxfield, *Physiol. Rev.* **1997**, *77*, 759-803.

[156]   S. D. Conner, S. L. Schmid, *Nature* **2003**, *422*, 37-44.

[157]   a) I. Nakase, A. Tadokoro, N. Kawabata, T. Takeuchi, H. Katoh, K. Hiramoto, M. Negishi, M. Nomizu, Y. Sugiura, S. Futaki, *Biochemistry* **2007**, *46*, 492-501; b) E. Barany-Wallje, S. Keller, S. Serowy, S. Geibel, P. Pohl, M. Bienert, M. Dathe, *Biophys. J.* **2005**, *89*, 2513-2521.

[158]   S. T. Henriques, J. Costa, M. A. Castanho, *FEBS Lett.* **2005**, *579*, 4498-4502.

[159]   R. Brasseur, G. Divita, *Biochim. Biophys. Acta* **2010**, *1798*, 2177-2181.

[160]   S. B. Fonseca, M. P. Pereira, S. O. Kelley, *Adv. Drug. Deliv. Rev.* **2009**, *61*, 953-964.

[161]   E. Koren, V. P. Torchilin, *Trends Mol. Med.* **2012**, *18*, 385-393.

[162]   a) G. Tunnemann, R. M. Martin, S. Haupt, C. Patsch, F. Edenhofer, M. C. Cardoso, *FASEB J.* **2006**, *20*, 1775-1784; b) M. Mae, U. Langel, *Curr. Opin. Pharmacol.* **2006**, *6*, 509-514.

[163]   a) E. Eiriksdottir, I. Mager, T. Lehto, S. El Andaloussi, U. Langel, *Bioconjug. Chem.* **2010**, *21*, 1662-1672; b) L. R. Jones, E. A. Goun, R. Shinde, J. B. Rothbard, C. H. Contag, P. A. Wender, *J. Am. Chem. Soc.* **2006**, *128*, 6526-6527.

[164]   J. B. Rothbard, S. Garlington, Q. Lin, T. Kirschberg, E. Kreider, P. L. McGrane, P. A. Wender, P. A. Khavari, *Nat. Med.* **2000**, *6*, 1253-1257.

[165]   J. A. Baccile, M. A. Morrell, R. M. Falotico, B. T. Milliken, D. L. Drew, F. M. Rossi, *Tetrahedron Lett.* **2012**, *53*, 1933-1935.

[166]   a) S. M. Rozenzhak, M. P. Kadakia, T. M. Caserta, T. R. Westbrook, M. O. Stone, R. R. Naik, *Chem. Commun. (Cambridge, U.K.)* **2005**, 2217-2219; b) S. Santra, H. Yang, D. Dutta, J. T. Stanley, P. H. Holloway, W. Tan, B. M. Moudgil, R. A. Mericle, *Chem. Commun. (Cambridge, U.K.)* **2004**, 2810-2811; c) A. Webster, S. J. Compton, J. W. Aylott, *Analyst* **2005**, *130*, 163-170.

[167]   S. Santra, H. Yang, J. T. Stanley, P. H. Holloway, B. M. Moudgil, G. Walter, R. A. Mericle, *Chem. Commun. (Cambridge, U.K.)* **2005**, 3144-3146.

[168]   M. Hu, P. Chen, J. Wang, D. A. Scollard, K. A. Vallis, R. M. Reilly, *Eur. J. Nucl. Med. Mol. Imaging* **2007**, *34*, 368-377.

[169]   H. Y. Yeh, Y. C. Hwang, M. V. Yates, A. Mulchandani, W. Chen, *Appl. Environ. Microbiol.* **2008**, *74*, 2239-2243.

[170]   D. Maxwell, Q. Chang, X. Zhang, E. M. Barnett, D. Piwnica-Worms, *Bioconjug. Chem.* **2009**, *20*, 702-709.

[171]   E. A. Dubikovskaya, S. H. Thorne, T. H. Pillow, C. H. Contag, P. A. Wender, *Proc. Natl. Acad. Sci. U. S. A.* **2008**, *105*, 12128-12133.

[172]   a) E. A. Goun, T. H. Pillow, L. R. Jones, J. B. Rothbard, P. A. Wender, *ChemBioChem* **2006**, *7*, 1497-1515; b) T. A. Kirschberg, C. L. VanDeusen, J. B. Rothbard, M. Yang, P. A. Wender, *Org. Lett.* **2003**, *5*, 3459-3462.

[173]   a) M. Fritzer, T. Szekeres, V. Szuts, H. N. Jarayam, H. Goldenberg, *Biochem. Pharmacol.* **1996**, *51*, 489-493; b) J. F. Liang, V. C. Yang, *Bioorg. Med. Chem. Lett.* **2005**, *15*, 5071-5075.

[174]   M. Lindgren, K. Rosenthal-Aizman, K. Saar, E. Eiriksdottir, Y. Jiang, M. Sassian, P. Ostlund, M. Hallbrink, U. Langel, *Biochem. Pharmacol.* **2006**, *71*, 416-425.

[175]   C. T. McCusker, Y. Wang, J. Shan, M. W. Kinyanjui, A. Villeneuve, H. Michael, E. D. Fixman, *J. Immunol.* **2007**, *179*, 2556-2564.

[176]   a) M. Mutoh, F. D. Lung, Y. Q. Long, P. P. Roller, R. S. Sikorski, P. M. O'Connor, *Cancer Res.* **1999**, *59*, 3480-3488; b) M. Bonfanti, S. Taverna, M. Salmona, M. D'Incalci, M. Broggini, *Cancer Res.* **1997**, *57*, 1442-1446; c) R. Fahraeus, J. M. Paramio, K. L. Ball, S. Lain, D. P. Lane, *Curr. Biol.* **1996**, *6*, 84-91.

[177]   D. R. Gius, S. A. Ezhevsky, M. Becker-Hapak, H. Nagahara, M. C. Wei, S. F. Dowdy, *Cancer Res.* **1999**, *59*, 2577-2580.

[178]   a) J. L. Wang, Z. J. Zhang, S. Choksi, S. Shan, Z. Lu, C. M. Croce, E. S. Alnemri, R. Korngold, Z. Huang, *Cancer Res.* **2000**, *60*, 1498-1502; b) H. L. Vieira, P. Boya, I. Cohen, C. El Hamel, D. Haouzi, S. Druillenec, A. S. Belzacq, C. Brenner, B. Roques, G. Kroemer, *Oncogene* **2002**, *21*, 1963-1977; c) E. P. Holinger, T. Chittenden, R. J. Lutz, *J. Biol. Chem.* **1999**, *274*, 13298-13304; d) S. Fulda, W. Wick, M. Weller, K. M. Debatin, *Nat. Med.* **2002**, *8*, 808-815.

[179]   S. R. Schwarze, A. Ho, A. Vocero-Akbani, S. F. Dowdy, *Science* **1999**, *285*, 1569-1572.

[180]   G. Cao, W. Pei, H. Ge, Q. Liang, Y. Luo, F. R. Sharp, A. Lu, R. Ran, S. H. Graham, J. Chen, *J. Neurosci.* **2002**, *22*, 5423-5431.

[181]   a) E. Bleifuss, T. Kammertoens, A. Hutloff, D. Quarcoo, M. Dorner, P. Straub, W. Uckert, E. Hildt, *Cell. Mol. Life Sci.* **2006**, *63*, 627-635; b) N. A. Brooks, D. S. Pouniotis, C. K. Tang, V. Apostolopoulos, G. A. Pietersz, *Biochim. Biophys. Acta* **2010**, *1805*, 25-34.

[182]   a) S. D. Patil, D. G. Rhodes, D. J. Burgess, *AAPS J* **2005**, *7*, E61-77; b) S. Akhtar, R. L. Juliano, *Trends Cell Biol* **1992**, *2*, 139-144.

[183]   I. A. Ignatovich, E. B. Dizhe, A. V. Pavlotskaya, B. N. Akifiev, S. V. Burov, S. V. Orlov, A. P. Perevozchikov, *J. Biol. Chem.* **2003**, *278*, 42625-42636.

[184]   C. H. Tung, S. Mueller, R. Weissleder, *Bioorg. Med. Chem.* **2002**, *10*, 3609-3614.

[185]   S. A. Moschos, S. W. Jones, M. M. Perry, A. E. Williams, J. S. Erjefalt, J. J. Turner, P. J. Barnes, B. S. Sproat, M. J. Gait, M. A. Lindsay, *Bioconjug. Chem.* **2007**, *18*, 1450-1459.

[186]   a) A. Astriab-Fisher, D. Sergueev, M. Fisher, B. R. Shaw, R. L. Juliano, *Pharm. Res.* **2002**, *19*, 744-754; b) H. M. Moulton, M. C. Hase, K. M. Smith, P. L. Iversen, *Antisense Nucleic Acid Drug Dev.* **2003**, *13*, 31-43.

[187]   B. R. Meade, S. F. Dowdy, *Adv. Drug. Deliv. Rev.* **2007**, *59*, 134-140.

[188]   a) P. Lundberg, S. El-Andaloussi, T. Sutlu, H. Johansson, U. Langel, *FASEB J.* **2007**, *21*, 2664-2671; b) M. Mae, S. El Andaloussi, P. Lundin, N. Oskolkov, H. J. Johansson, P. Guterstam, Ü. Langel, *J. Controlled Release* **2009**, *134*, 221-227.

[189]   L. Crombez, G. Divita, *Methods Mol. Biol.* **2011**, *683*, 349-360.

[190]   E. Vives, J. Schmidt, A. Pelegrin, *Biochim. Biophys. Acta* **2008**, *1786*, 126-138.

[191]   a) H. Myrberg, L. Zhang, M. Mae, U. Langel, *Bioconjug. Chem.* **2008**, *19*, 70-75; b) M. Mäe, H. Myrberg, S. El-Andaloussi, Ü. Langel, *Int. J. Pept. Res. Therapeut.* **2009**, *15*, 11-15.

[192]   a) R. Pasqualini, E. Koivunen, E. Ruoslahti, *Nat. Biotechnol.* **1997**, *15*, 542-546; b) L. Sancey, E. Garanger, S. Foillard, G. Schoehn, A. Hurbin, C. Albiges-Rizo, D. Boturyn, C. Souchier, A. Grichine, P. Dumy, J. L. Coll, *Mol. Ther.* **2009**, *17*, 837-843.

[193]   a) E. Ruoslahti, T. Duza, L. Zhang, *Curr. Pharm. Des.* **2005**, *11*, 3655-3660; b) P. Laakkonen, M. E. Akerman, H. Biliran, M. Yang, F. Ferrer, T. Karpanen, R. M. Hoffman, E. Ruoslahti, *Proc. Natl. Acad. Sci. U. S. A.* **2004**, *101*, 9381-9386.

[194]   a) V. A. Sethuraman, K. Na, Y. H. Bae, *Biomacromolecules* **2006**, *7*, 64-70; b) M. Stubbs, P. M. McSheehy, J. R. Griffiths, C. L. Bashford, *Mol. Med. Today* **2000**, *6*, 15-19.

[195]   K. Ciftci, R. J. Levy, *Int. J. Pharm.* **2001**, *218*, 81-92.

[196]   T. Shiraishi, S. Pankratova, P. E. Nielsen, *Chem. Biol.* **2005**, *12*, 923-929.

[197]   S. Abes, H. M. Moulton, P. Clair, P. Prevot, D. S. Youngblood, R. P. Wu, P. L. Iversen, B. Lebleu, *J. Controlled Release* **2006**, *116*, 304-313.

[198]   S. L. Lo, S. Wang, *Biomaterials* **2008**, *29*, 2408-2414.

[199]   a) K. Berg, M. Folini, L. Prasmickaite, P. K. Selbo, A. Bonsted, B. O. Engesaeter, N. Zaffaroni, A. Weyergang, A. Dietze, G. M. Maelandsmo, E. Wagner, O. J. Norum, A. Hogset, *Curr. Pharm. Biotechnol.* **2007**, *8*, 362-372; b) K. Berg, L. Prasmickaite, P. K. Selbo, M. Hellum, A. Bonsted, A. Hogset, *Oftalmologia* **2003**, *56*, 67-71; c) J. R. Maiolo, 3rd, E. A. Ottinger, M. Ferrer, *J. Am. Chem. Soc.* **2004**, *126*, 15376-15377.

[200]   a) K. Saar, M. Lindgren, M. Hansen, E. Eiriksdottir, Y. Jiang, K. Rosenthal-Aizman, M. Sassian, U. Langel, *Anal. Biochem.* **2005**, *345*, 55-65; b) E. Barany-Wallje, J.

Gaur, P. Lundberg, U. Langel, A. Graslund, *FEBS Lett.* **2007**, *581*, 2389-2393; c) M. Magzoub, K. Oglecka, A. Pramanik, L. E. Goran Eriksson, A. Graslund, *Biochim. Biophys. Acta* **2005**, *1716*, 126-136.

[201]   a) S. Deshayes, T. Plenat, P. Charnet, G. Divita, G. Molle, F. Heitz, *Biochim. Biophys. Acta* **2006**, *1758*, 1846-1851; b) A. Ziegler, *Adv. Drug. Deliv. Rev.* **2008**, *60*, 580-597.

[202]   H. T. Chen, M. F. Neerman, A. R. Parrish, E. E. Simanek, *J. Am. Chem. Soc.* **2004**, *126*, 10044-10048.

[203]   G. P. Dietz, M. Bahr, *Mol. Cell. Neurosci.* **2004**, *27*, 85-131.

[204]   J. B. Rothbard, T. C. Jessop, R. S. Lewis, B. A. Murray, P. A. Wender, *J. Am. Chem. Soc.* **2004**, *126*, 9506-9507.

[205]   a) T. B. Potocky, A. K. Menon, S. H. Gellman, *J. Am. Chem. Soc.* **2005**, *127*, 3686-3687; b) J. Fernández-Carneado, M. J. Kogan, S. Pujals, E. Giralt, *Peptide Science* **2004**, *76*, 196-203.

[206]   P. Raschle, Master thesis, *University of Basel*, **2011**.

[207]   M. Kuemin, S. Schweizer, C. Ochsenfeld, H. Wennemers, *J. Am. Chem. Soc.* **2009**, *131*, 15474-15482.

[208]   F. W. Monnard, Master thesis, *University of Basel* **2007**.

[209]   M. Tamaki, G. Han, V. J. Hruby, *J. Org. Chem.* **2001**, *66*, 1038-1042.

[210]   K. Feichtinger, H. L. Sings, T. J. Baker, K. Matthews, M. Goodman, *J. Org. Chem.* **1998**, *63*, 8432-8439.

[211]   M. Fujino, M. Wakimasu, C. Kitada, *ChemComm* **1982**, 445-446.

[212]   a) J. Green, O. M. Ogunjobi, R. Ramage, A. S. J. Stewart, S. McCurdy, R. Noble, *Tetrahedron Lett.* **1988**, *29*, 4341-4344; b) R. Ramage, J. Green, *Tetrahedron Lett.* **1987**, *28*, 2287-2290.

[213]   a) L. A. Carpino, H. Shroff, S. A. Triolo, E.-S. M. E. Mansour, H. Wenschuh, F. Albericio, *Tetrahedron Lett.* **1993**, *34*, 7829-7832; b) A. Stierandova, N. F. Sepetov, G. V. Nikiforovich, M. Lebl, *Int. J. Pept. Protein Res.* **1994**, *43*, 31-38; c) C. G. Fields, G. B. Fields, *Tetrahedron Lett.* **1993**, *34*, 6661-6664.

[214]   M. Kümin, Dissertation, *University of Basel*, **2009**.

[215]   a) N. Greenfield, G. D. Fasman, *Biochemistry* **1969**, *8*, 4108-4116; b) R. K. Dukor, T. A. Keiderling, *Biopolymers* **1991**, *31*, 1747-1761.

[216]   A. T. C. C. (ATCC), http://www.atcc.org/

[217]   *Molecular Cell Biology*, 6th Ed. ed., W. H. Freeman and Company, New York, **2007**.

[218]   R. Fischer, H. Hufnagel, R. Brock, *Bioconjug. Chem.* **2010**, *21*, 64-73.

[219]   J. Mueller, I. Kretzschmar, R. Volkmer, P. Boisguerin, *Bioconjug. Chem.* **2008**, *19*, 2363-2374.

[220]   D. J. Yamashiro, F. R. Maxfield, *J. Cell. Biol.* **1987**, *105*, 2723-2733.

[221]   D. Seebach, J. Gardiner, *Acc. Chem. Res.* **2008**, *41*, 1366-1375.

[222]   N. Umezawa, M. A. Gelman, M. C. Haigis, R. T. Raines, S. H. Gellman, *J. Am. Chem. Soc.* **2001**, *124*, 368-369.

[223]   S. Ahmed, K. Kaur, *Chem. Biol. Drug Des* **2009**, *73*, 545-552.

[224]   a) C. Wrotnowski, *Gent. Eng. News* **1998**, *18*, 14; b) J. N. Adkins, S. M. Varnum, K. J. Auberry, R. J. Moore, N. H. Angell, R. D. Smith, D. L. Springer, J. G. Pounds, *Mol. Cell. Proteomics* **2002**, *1*, 947-955.

[225]   I. Rusu, A. Yaron, *Eur. J. Biochem.* **1992**, *210*, 93-100.

[226] S. Maruyama, T. Kobayashi, T. Ohmori, H. Tanaka, H. Maeda, *Biosci. Biotechnol. Biochem.* **1994**, *58*, 2107-2108.

[227] E. J. Holtzman, G. Pillay, T. Rosenthal, A. Yaron, *Anal. Biochem.* **1987**, *162*, 476-484.

[228] a) L. Polgar, *Cell. Mol. Life Sci.* **2002**, *59*, 349-362; b) V. Fulop, Z. Bocskei, L. Polgar, *Cell* **1998**, *94*, 161-170.

[229] a) T. Foulon, S. Cadel, P. Cohen, *Int. J. Biochem. Cell. Biol.* **1999**, *31*, 747-750; b) K. K. Makinen, K. K. Virtanen, *Clin. Chim. Acta* **1976**, *67*, 213-218.

[230] S. Asai, T. Sato, T. Tada, T. Miyamoto, N. Kimbara, N. Motoyama, H. Okada, N. Okada, *J. Immunol.* **2004**, *173*, 4669-4674.

[231] a) R. Trehin, H. M. Nielsen, H. G. Jahnke, U. Krauss, A. G. Beck-Sickinger, H. P. Merkle, *Biochem. J.* **2004**, *382*, 945-956; b) C. Palm, M. Jayamanne, M. Kjellander, M. Hällbrink, *Biochim. Biophysi. Acta - Biomembranes* **2007**, *1768*, 1769-1776.

[232] T. Mosmann, *J. Immunol. Methods* **1983**, *65*, 55-63.

[233] Sigma-Aldrich, *XTT sodium salt,* http://www.sigmaaldrich.com/catalog/product/sigma/x4626?lang=de&region =CH

[234] Sigma-Aldrich, *Thiazolyl Blue Tetrazolium Bromide,* http://www.sigmaaldrich.com/catalog/product/sigma/m5655?lang=de&region =CH

[235] H. Renz-Polster, S. Krautzig, J. Braun, *Basislehrbuch Innere Medizin*, Urban & Fischer Verlag, **2005**.

[236] http://medicalschool.tumblr.com/post/20782599252/a-carpet-of-red-blood-cells-clearly-showing-their

[237] J. Hall, *Chimia* **2005**, *59*, 803-807.

[238] a) J. Hall, *Nat. Rev. Genet.* **2004**, *5*, 552-557; b) T. N. Campbell, F. Y. Choy, *Curr. Issues. Mol. Biol.* **2005**, *7*, 1-6.

[239] H. Ledford, *Nature* **2010**, *468*, 487.

[240] A. Muratovska, M. R. Eccles, *FEBS Lett.* **2004**, *558*, 63-68.

[241] a) A. Eguchi, S. F. Dowdy, *Trends Pharmacol. Sci.* **2009**, *30*, 341-345; b) L. Crombez, M. C. Morris, S. Deshayes, F. Heitz, G. Divita, *Curr. Pharm. Des.* **2008**, *14*, 3656-3665.

[242] W. J. Kim, L. V. Christensen, S. Jo, J. W. Yockman, J. H. Jeong, Y. H. Kim, S. W. Kim, *Mol. Ther.* **2006**, *14*, 343-350.

[243] a) Promega, http://www.promega.com **2006**, *USA*; b) B. Guennewig, M. Stoltz, M. Menzi, A. M. Dogar, J. Hall, *Nucleic Acid Ther.* **2012**, *22*, 109-116.

[244] Invitrogen, *Transfecting siRNA into HeLa Cells Using Oligofectamine*, http://www.invitrogen.com/etc/medialib/en/filelibrary/pdf/protocols.Par.482 43.File.dat/sirna_oftsf_proc.pdf

[245] I. Ivanovska, A. S. Ball, R. L. Diaz, J. F. Magnus, M. Kibukawa, J. M. Schelter, S. V. Kobayashi, L. Lim, J. Burchard, A. L. Jackson, P. S. Linsley, M. A. Cleary, *Mol. Cell. Biol.* **2008**, *28*, 2167-2174.

[246] Promega, *RNA interference, protocols and applications guide* **2008**, http://www.promega.com

[247] a) K. V. Wood, J. R. de Wet, N. Dewji, M. DeLuca, *Biochem. Biophys. Res. Commun.* **1984**, *124*, 592-596; b) J. R. de Wet, K. V. Wood, D. R. Helinski, M. DeLuca, *Proc.*

Natl. Acad. Sci. U. S. A. **1985**, *82*, 7870-7873; c) J. C. Matthews, K. Hori, M. J. Cormier, *Biochemistry* **1977**, *16*, 85-91.

[248]   M. D. Shoulders, F. W. Kotch, A. Choudhary, I. A. Guzei, R. T. Raines, *J. Am. Chem. Soc.* **2010**, *132*, 10857-10865.

[249]   R. S. Erdmann, M. Kümin, H. Wennemers, *Chimia* **2009**, *63*, 197-200.

[250]   E. Kaiser, R. L. Colescott, C. D. Bossinger, P. I. Cook, *Anal. Biochem.* **1970**, *34*, 595-598.

[251]   T. Vojkovsky, *Pept. Res.* **1995**, *8*, 236-237.

[252]   W. S. Hancock, J. E. Battersby, *Anal. Biochem.* **1976**, *71*, 260-264.

6.2   General abbreviations

Å	Angström
abs.	absolut
Ac	Acetyl
Ac_2O	Acetic anhydride
AcOH	Acetic acid
Bn	Benzyl
Boc	*tert*-butyloxycarbonyle
Boc_2O	Di-*tert*-butyl dicarbonate
°C	Celsius degree
Cbz	Carbobenzyloxy
CD	Circular dichroism
CF	5,6-Carboxyfluoresceine
c	Concentration
$CDCl_3$	Deuterated chloroform
CH_2Cl_2	Dichloromethane
CH_3CN	Acetonitrile
CMP	Collagen Model Peptides
CPP	Cell-penetrating Peptide
d	Day(s)
d	Doublet
D_2O	Deuterium oxide
DAD	Diode Array Detector
DAPI	4',6-diamidino-2-phenylindole
DIPEA	*N,N'*-diisopropylethylamine
DMEM	Dulbecco's Modified Eagle Medium
DMF	*N,N*-dimethylformamide
DMSO	Dimethylsulfoxide
Eq	Equivalent
et al.	et alii
ESI-MS	Electrospray Ionization Mass Spectrometry
Et	Ethyl
EtOAc	Ethylacetate
EtOH	Ethanol
FACS	Fluorescence activated cell sorting

FCS	Fetal calf serum
Fmoc	9-Fluorenylmethoxycarbonyl
FRET	Fluorescence resonance energy transfer
g	Gram
h	Hour(s)
H_2O	Water
HCl	Hydrochloric acid
HCTU	2-(6-Chloro-1H-benzotriazole-1-yl)-1,1,3,3-tetramethyluronium hexafluorophosphate
HeLa	Human cervical adenocarcinoma cell line (Henrietta Lacks)
HIV-1	Human Immunodeficiency Virus Type 1
HOAc	Acetic acid
HPLC	High Performance Liquid Chromatography
HSPGs	Heparan sulphate proteoglycans
Hünig's base	*N,N*-Diisopropylamine
J	Coupling constant
m	Multipet
m_c	Centered multipet
M	Molar
MALDI	Matrix Assisted Laser Desorption or Ionization
Me	Methyl
MeOH	Methanol
MHz	Megahertz
min	Minute(s)
Ms	Methanesulfonyl (mesyl)
Mtr	4-Methoxy-2,3,6-trimethylbenzenesulphonyl
MTT	3-(4,5-Dimethylthiazol-2-yl)-2,5-diphenyltetrazolium bromide
NEt_3	Triethylamine
NMR	Nuclear Magnetic Resonance
θ_{MRW}	Mean Residue Weight Ellipticity
Pbf	2,2,4,6,7-pentamethyldihydrobenzofuran-5-sulfonyl
PBS	Phosphate buffered saline
Pbf	2,2,4,6,7-pentamethyldihydrobenzofuran-5-sulfonyl
Ph	Phenyl
PI	Propidium iodide
Pmc	2,2,5,7,8-pentamethyl-chroman-6-sulphonyl

PMe$_3$	Trimethylphosphine
PNA	Peptide Nucleic Acid
ppm	Parts per million
PPI	Polyproline I type helix
PPII	Polyproline II type helix
PRMs	Proline-rich motifs
PTD	Protein Transduction Domain
q	Quartet
quint	Quintet
R$_f$	Retention factor
R$_t$	Retention time
s	Singlet
SPPS	Solid Phase Peptide Synthesis
TFA	Trifluoroacetic acid
THF	Tetrahydrofurane
TLC	Thin Layer Chromatography
TMS	Trimethylslyl
UV	Ultraviolet

6.3   Abbreviations for amino acids

A	Ala	Alanine
U	(4*S*)Amp	(4*S*)-amino-L-proline
-	(4*R*)Amp	(4*R*)-amino-L-proline
-	(4*S*)Azp	(4*S*)-azido-L-proline
-	(4*R*)Azp	(4*R*)-azido-L-proline
X	(4*R*)Gup	(4*R*)-guanidinylated L-proline
x	D-(4*R*)Gup	(4*R*)-guanidinylated D-proline
Z	(4*S*)Gup	(4*S*)-guanidinylated L-proline
z	D-(4*S*)Gup	(4*S*)-guanidinylated D-proline
C	Cys	Cysteine
D	Asp	Aspartic acid
E	Glu	Glutamic acid
F	Phe	Phenylalanine
G	Gly	Glycine
H	Hys	Histidine
I	Ile	Isoleucine
K	Lys	Lysine
L	Leu	Leucine
M	Met	Methionine
N	Asn	Asparagine
P	L-Pro	L-proline
p	D-Pro	D-proline
Q	Gln	Glutamine
R	L-Arg	L-arginine
r	D-Arg	D-arginine
S	Ser	Serine
T	Thr	Threonine
V	Val	Valine
W	Trp	Tryptophan
Y	Tyr	Tyrosine

6.4   Analytical data of the peptides

Cell Penetrating Peptides (CPPs)

Alternating system

No.	Sequence	Purity 214 nm [%]	440 nm [%]	Yield [mg]	[%]	MS calc.	2+	3+	4+	5+
20	CF-G-UPU-UPU-CONH$_2$	100	98.0	19.2	29	1074.46	538.2	359.2	269.6	
21	CF-G-UPU-UPU-UPU-CONH$_2$	96.5	96.2	26.6	31	1395.64	698.8	466.2	349.9	280.1
22	CF-G-UPU-UPU-UPU-UPU-CONH$_2$	100	100	18.8	18	1716.82	859.4	573.3	430.2	344.4
23	CF-G-ZPZ-ZPZ-CONH$_2$	79.8	94.5	7.9	21	1242.54	622.3	415.2	311.6	
24	CF-G-ZPZ-ZPZ-ZPZ-CONH$_2$	98.5	97.8	4.0	8	1647.77	824.9	550.3	413.0	330.6
25	CF-G-ZPZ-ZPZ-ZPZ-ZPZ-CONH$_2$	94.7	96.1	7.0	11	2052.99	1027.5	685.3	514.3	411.6
26	CF-G-XPX-XPX-XPX-CONH$_2$	100	100	4.2	8	1647.77	824.9	550.3	413.0	330.6
27	CF-G-zpz-zpz-zpz-CONH$_2$[b]	99.5	100	8.4	17	1647.77	824.9	550.3	413.0	330.6
28	CF-G-xpx-xpx-xpx -CONH$_2$[b]	99.8	100	1.4	3	1647.77	824.9	550.3	413.0	330.6

***En bloc* system**

No.	Sequence	Purity 214 nm [%]	440 nm [%]	Yield [mg]	[%]	MS calc.	2+	3+	4+	5+
29	CF-G-PPP-ZZZ-ZZZ-CONH$_2$	95.0	96.0	2.5	5	1647.77	824.9	550.3	413.0	330.6
30	CF-G-ZZZ-ZZZ-PPP-CONH$_2$	100	100	9.6	19	1647.77	824.9	550.3	413.0	330.6
31	CF-G-ZZZ ZZZ-ZZP-PPP-CONH$_2$	94.3	98.7	10.1	15	2052.99	1027.5	685.3	514.3	411.6
32	CF-G-ppp-zzz-zzz-CONH$_2$[b]	95.2	98.7	4.3	9	1647.77	824.9	550.3	413.0	330.6
33	CF-G-zzz-zzz-ppp-CONH$_2$[b]	97.2	98.8	3.7	8	1647.77	824.9	550.3	413.0	330.6
34	CF-G PPP-XXX-XXX-CONH$_2$	100	100	2.6	5	1647.77	824.9	550.3	413.0	330.6
35	CF-G-XXX-XXX-PPP-CONH$_2$	97.1	93.2	3.5	7	1647.77	824.9	550.3	413.0	330.6
36	CF-G-ppp-xxx-xxx-CONH$_2$[b]	100	100	4.5	9	1647.77	824.9	550.3	413.0	330.6
37	CF-G-xxx-xxx-ppp-CONH$_2$[b]	100	100	4.3	9	1647.77	824.9	550.3	413.0	330.6
38	CF-G-ZZZ-ZZZ-CONH$_2$	97.0	97.5	3.5	9	1356.61	679.3	453.2	340.2	
39	CF-G-ZZZ-ZZZ-ZZ-CONH$_2$	98.3	98.7	6.4	13	1664.78	833.4	555.9	417.2	334.0
40	CF-G-ZZZ-ZZZ-ZZZ-Z-CONH$_2$	99.2	97.7	0.7	1	1972.95	987.5	658.6	494.2	395.6
41	CF-G-ZZZ-ZZZ-ZZZ-ZZZ-CONH$_2$	99.9	98.0	0.7	1	2281.12	1141.6	761.4	571.3	457.2

206

Observed Masses		Calculated for	HPLC cond.	R$_t$
LC-MS	**MALDI-TOF**			**[min]**
-	1078.3, 1100.4	C$_{53}$H$_{62}$N$_{12}$O$_{13}$	E	14.1
-	1400.1, 1422.4	C$_{68}$H$_{85}$N$_{17}$O$_{16}$	E	14.2
-	1741.6, 1762.7	C$_{83}$H$_{108}$N$_{22}$O$_{19}$	E	15.0
622.5, 415.4	-	C$_{57}$H$_{70}$N$_{20}$O$_{13}$	A	7.8
825.0, 550.6	-	C$_{74}$H$_{97}$N$_{29}$O$_{16}$	A	7.9
685.5, 557.5	-	C$_{91}$H$_{124}$N$_{38}$O$_{19}$	A	7.6
825.0, 550.6	-	C$_{74}$H$_{97}$N$_{29}$O$_{16}$	A	7.7
825.0, 550.6	-	C$_{74}$H$_{97}$N$_{29}$O$_{16}$	B	11.4, 11.5
825.4, 550.6	-	C$_{74}$H$_{97}$N$_{29}$O$_{16}$	B	11.5

Observed Masses		Calculated for	HPLC cond.	R$_t$
LC-MS	**MALDI-TOF**			**[min]**
825.0, 550.6	-	C$_{74}$H$_{97}$N$_{29}$O$_{16}$	A	8.3
825.1, 550.6, (602.0)*	-	C$_{74}$H$_{97}$N$_{29}$O$_{16}$	A	7.6, 7.7
685.7	-	C$_{91}$H$_{124}$N$_{38}$O$_{19}$	A	7.6, 7.8
825.4, 550.6	-	C$_{74}$H$_{97}$N$_{29}$O$_{16}$	B	11.8
550.6	-	C$_{74}$H$_{97}$N$_{29}$O$_{16}$	B	11.9
825.0, 550.6.	-	C$_{74}$H$_{97}$N$_{29}$O$_{16}$	A	8.3
825.1, 550.6	-	C$_{74}$H$_{97}$N$_{29}$O$_{16}$	A	7.5, 7.6
825.0, 550.6	-	C$_{74}$H$_{97}$N$_{29}$O$_{16}$	B	11.4
825.0, 550.6	-	C$_{74}$H$_{97}$N$_{29}$O$_{16}$	B	11.4
679.5, 453.5	-	C$_{59}$H$_{76}$N$_{26}$O$_{13}$	A	7.3, 7.5
833.5, 556.3, 417.4, (594.1)*	-	C$_{71}$H$_{96}$N$_{34}$O$_{15}$	A	7.3, 7.5
494.2 (522.7)*; 483.7[a] (512.7)[a]*	-	C$_{83}$H$_{116}$N$_{42}$O$_{17}$	D	10.0
457.4 (481.3)*; 449.2[a] (472.0)[a]*	-	C$_{95}$H$_{136}$N$_{50}$O$_{19}$	D	10.0

Reference peptides

No.	Sequence	Purity 214 nm [%]	440 nm [%]	Yield [mg]	[%]	MS calc.	2+	3+	4+	5+
42	CF-G-RKK-RRQ-RRR-PPQ-CONH$_2$	100	100	15.4	25	2075.12	1038.6	692.7	519.8	416.0
43	CF-G-RQI-KIW-FQN-RRM-KWK-K-CONH$_2$	95.0	95.0	6.5	8	2675.41	1338.7	892.8	669.9	536.1
44	CF-G-RRR-RRR-CONH$_2$	100	98.3	0.4	6	1368.70	685.4	457.2	343.2	
45	CF-G-RRR-RRR-RR-CONH$_2$	100	97.5	6.7	13	1680.90	841.5	561.3	421.2	337.2
46	CF-G-RRR-RRR-RRR-R-CONH$_2$	99.7	96.4	1.5	3	1993.1	997.6	665.4	499.3	399.6
47	CF-G-RRR-RRR-RRR-RRR-CONH$_2$	99.8	99.6	2.0	3	2305.3	1153.7	769.4	577.3	462.1
48	CF-G-rrr rrr-CONH$_2$[b]	97	100	7.9	19	1368.70	685.4	457.2	343.2	274.7
49	CF-G-PPP-PPP-CONH$_2$	99.4	100	12.0	40	1014.41	508.2	339.1	254.6	
50	CF-G-PPP-PPP-PPP-CONH$_2$	100	99.7	9.9	25	1305.57	653.8	436.2	327.4	262.1
51	CF-G-ppp-ppp-CONH$_2$	95	100	8.2	27	1014.41	508.2	339.1	254.6	
52	CF-G-ppp-ppp-ppp-CONH$_2$	96	100	9.0	23	1305.57	653.8	436.2	327.4	262.1

Peptides for Conformational Analyses

No.	Sequence	Purity 214 nm [%]	440 nm [%]	Yield [mg]	[%]	MS calc.	2+	3+	4+	5+
14S	Ac-[(4S)Amp-Pro-(4S)Amp]$_3$-COOH	100	-	14.1		1023.56	513.8	342.9	257.4	206.1
14R	Ac-[(4R)Amp-Pro-(4R)Amp]$_3$-COOH	99.8	-	11.5		1023.56	513.8	342.9	257.4	206.1

(a sideproducts containing one ammonium instead of a guanidinium function within the peptide)

(b peptides synthesized during the master thesis of P. Raschle)

(* TFA adducts)

HPLC conditions:

A   Reprosil gold 120 C128, 5 μm, 150 x 16 mm, 90% B to 55% B in 14 min, 50 °C, 1 mL/min

B   Reprosil gold 120 C128, 5 μm, 150 x 16 mm, 98% B to 70% B in 14 min, 50 °C, 1 mL/min

C   Reprosil gold 120 C128, 5 μm, 150 x 16 mm, 85% B to 65% B in 14 min, 50 °C, 1 mL/min

D   Reprosil gold 120 C128, 5 μm, 150 x 16 mm, 98% B to 70% B in 15 min, 50 °C, 0.5 mL/min

E   Lichrosphere 100 RP-18e, 5 μm, 250 x 4 mm, 90% B to 40% B in 24 min, 50 °C, 1.0 mL/min

F   Lichrosphere 100 RP-18e, 5 μm, 250 x 4 mm, 98% B to 75% B in 20 min, 50 °C, 1.0 mL/min

Observed Masses		Calculated for	HPLC cond.	R_t
LC-MS	MALDI-TOF			[min]
693.1, 520.1, (731.1)*	-	$C_{91}H_{142}N_{36}O_{21}$	B	11.8
888.2, 893.5	-	$C_{128}H_{186}N_{36}O_{26}S$	B	19.2
685.6, 457.5, (799.4, 685.6)*	-	$C_{59}H_{88}N_{26}O_{13}$	B	12.0
841.5, 561.7, 421.6, (599.5, 637.7)*	-	$C_{71}H_{112}N_{34}O_{15}$	B	12.0
499.3 (528.0, 556.3, 584,7)*, 399.8	-	$C_{83}H_{136}N_{42}O_{17}$	D	9.8
462.3 (485.2, 507.9, 530.6)*, 385.4 (6+)	-	$C_{95}H_{160}N_{50}O_{19}$	D	9.8
1369.8, 685.8	-	$C_{59}H_{88}N_{26}O_{13}$	B	7.7
1015.7, 508.5	-	$C_{53}H_{58}N_8O_{13}$	A	10.6, 10.7
654.1	-	$C_{68}H_{79}N_{11}O_{16}$	A	11.1, 11.2
1015.8, 1037.6	-	$C_{53}H_{58}N_8O_{13}$	C	11.0, 11.3
1307.2, 654.1	-	$C_{68}H_{79}N_{11}O_{16}$	C	12.2, 12.6

Observed Masses		Calculated for	HPLC cond.	R_t
LC-MS	MALDI-TOF			[min]
-	1024.2	$C_{47}H_{73}N_{15}O_{11}$	F	13.0
-	1023.8	$C_{47}H_{73}N_{15}O_{11}$	F	11.8

Abbreviations:

Modified building blocks:

U = (4*S*)Azp   z = D-(4*S*)Gup

Z = (4*S*)Gup   x = D-(4*R*)Gup

X = (4*R*)Gup

D-amino acid building blocks:

p = D-Pro

r = D-Arg

CF = 5(6)-carboxyfluorescein

Natural amino acid building blocks:

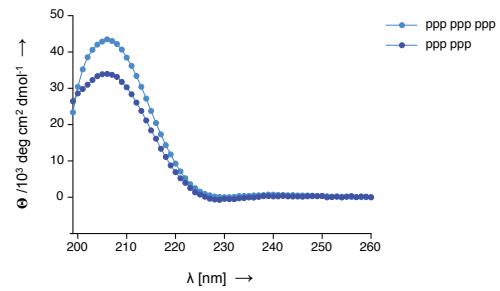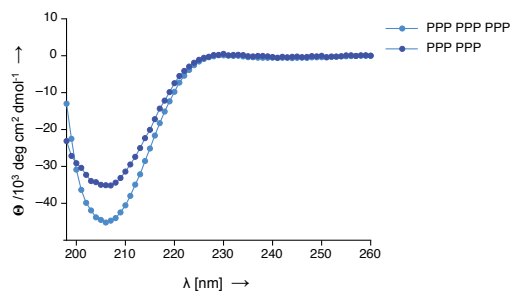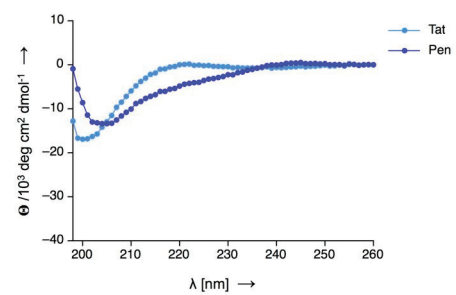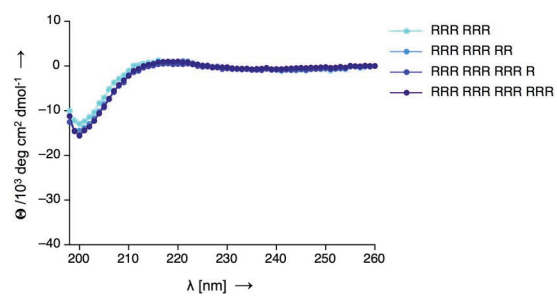|	
F = Phe	N = Asn
G = Gly	P = Pro
I = Ile	R = Arg
K = Lys	Q = Gln
M = Met	W = Trp

6.5 CD spectra

6.5.1 Functionalized oligoprolines
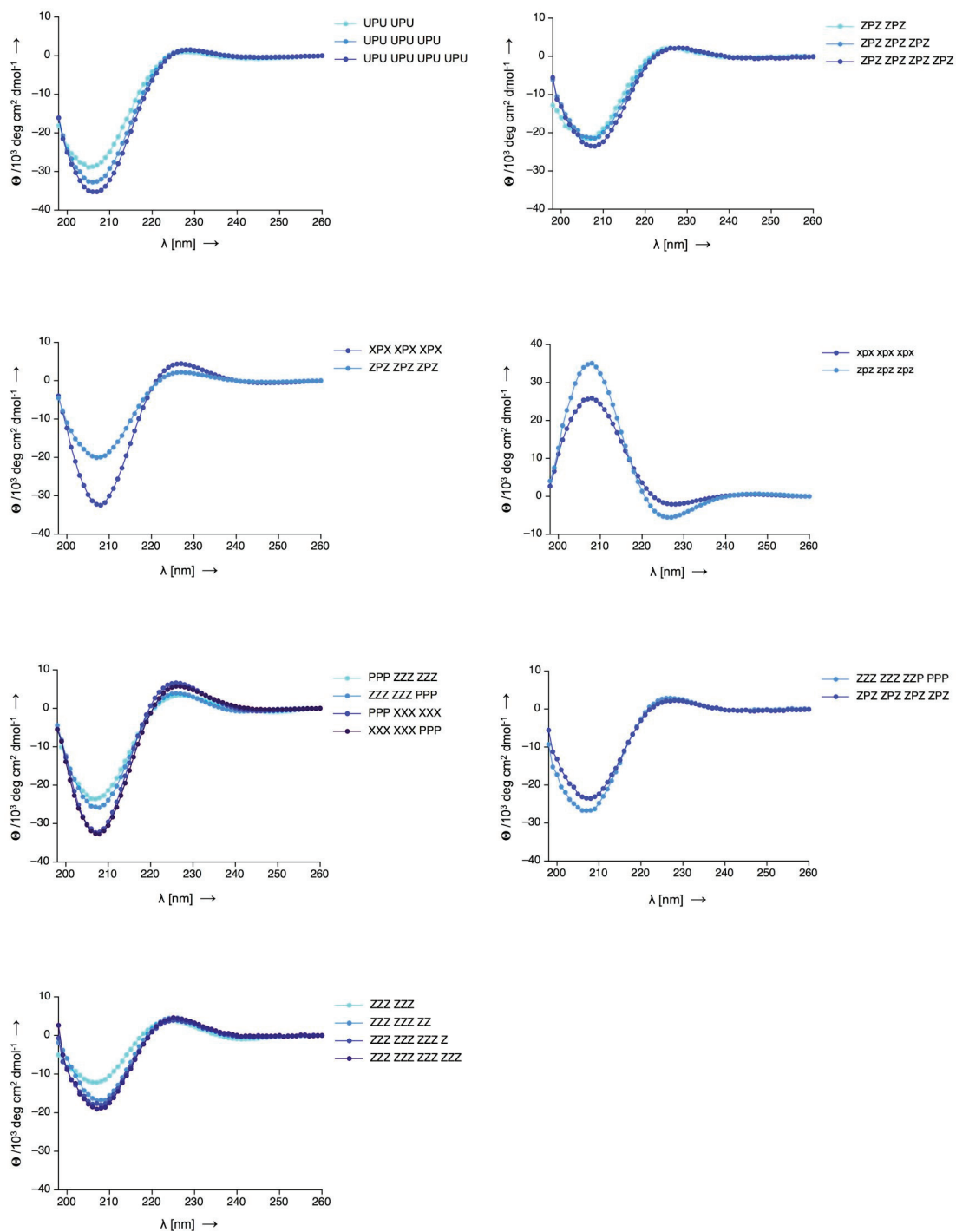
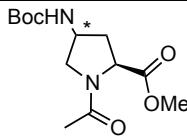### 6.5.1 Unfunctionalized oligoprolines

6.5.2 Reference peptides

211

6.6 ¹H NMR coupling constants

Values labeled with * might be inaccurate due to partially overlapping signals. "nd" indicates that the coupling constant could not be determined due to completely overlapping signals.

6.6.1 Ac-Amp(NHBoc)-OMe

Sample	Solvent	$K_{trans/cis}$ **8S**	$K_{trans/cis}$ **8R**
	D_2O	3.8	5.2

Ac-(4S)(NHBoc)Pro-OMe (8S)

$^3J_{(H,H)}$	D_2O	
	trans	*cis*
H^α-H^β	8.7	nd
H^α-$H^{\beta'}$	5.8	nd
H^β-H^γ	6.1	nd
$H^{\beta'}$-H^γ	nd	nd
H^γ-H^δ	6.5	nd
H^γ-$H^{\delta'}$	5.4	2.0
$H^{\beta'}$-$H^{\delta'}$	nd	nd

Ac-(4S)Amp(NHBoc)-OMe (8R)

$^3J_{(H,H)}$	D_2O	
	trans	*cis*
H^α-H^β	7.4	nd
H^α-$H^{\beta'}$	7.4	nd
H^β-$H^{\gamma'}$	nd	nd
$H^{\beta'}$-$H^{\gamma'}$	nd	nd
$H^{\gamma'}$-H^δ	4.8	nd
$H^{\gamma'}$-$H^{\delta'}$	6.1	6.1
H^β-H^δ	nd	nd

6.6.2 Ac-Amp-OMe*TFA

Sample	Solvent	$K_{trans/cis}$ 9S	$K_{trans/cis}$ 9R
$CF_3CO_2^{\ominus}$ $H_3N^{\oplus}$ (structure)	D_2O	5.7	3.5
	DMSO-d6	3.6	2.2
	CD_3OD	3.8	2.2
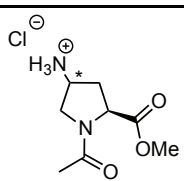
Ac-(4S)Amp-OMe*TFA (9S)

$^3J_{(H,H)}$	D_2O trans	D_2O cis	DMSO-d$_6$ trans	DMSO-d$_6$ cis	CD_3OD trans	CD_3OD cis
Hα-Hβ	9.1	9.4	8.2	9.0	9.2	9.3
Hα-Hβ'	5.8	4.3	8.2	6.6	5.4	4.6
Hβ-Hγ	7.0	7.4	8.4	8.3	7.0	7.8
Hβ'-Hγ	5.7	4.6	7.5	nd	5.2	5.0
Hγ-Hδ	nd	nd	7.7	8.1	7.3	7.0
Hγ-Hδ'	nd	nd	7.1	7.3	nd	5.7
Hβ'-Hδ'	nd	nd	nd	nd	≈1.2	nd

Ac-(4R)Amp-OMe*TFA (9R)

$^3J_{(H,H)}$	D_2O trans	D_2O cis	DMSO-d$_6$ trans	DMSO-d$_6$ cis	CD_3OD trans	CD_3OD cis
Hα-Hβ	8.0	8.9	7.9	8.0	8.5	8.8
Hα-Hβ'	7.0	4.2	7.0	5.5	6.1	4.4
Hβ-Hγ'	nd	6.8	4.6	5.8	nd	6.6
Hβ'-Hγ'	nd	6.9	6.6	nd	nd	6.7
Hγ'-Hδ	3.9	nd	5.9	nd	nd	nd
Hγ'-Hδ'	6.3	nd	nd	6.5	nd	nd
Hβ-Hδ	nd	nd	<1.0	nd	nd	nd

6.6.3 Ac-Amp-OMe*HCl

Sample	Solvent	$K_{trans/cis}$ **10S**	$K_{trans/cis}$ **10R**
	D_2O	5.7	3.5
	DMSO-d6	3.4*	2.6*
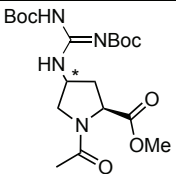
Ac-(4*S*)Amp-OMe*HCl (10S)

$^3J_{(H,H)}$	D_2O		DMSO-d$_6$	
	trans	*cis*	*trans*	*cis*
Hα-Hβ	9.2	9.3	8.3*	8.1*
Hα-Hβʻ	5.8	5.5	8.3*	8.1*
Hβ-Hγ	7.0	7.4	7.4*	8.3*
Hβʻ-Hγ	5.4	4.4	nd	nd
Hγ-Hδ	nd	nd	9.1	nd
Hγ-Hδʻ	nd	4.6	7.4*	7.3*
Hβʻ-Hδʻ	nd	nd	nd	nd

Ac-(4*R*)Amp-OMe*HCl (10R)

$^3J_{(H,H)}$	D_2O		DMSO-d$_6$	
	trans	*cis*	*trans*	*cis*
Hα-Hβ	7.9*	8.3*	8.3	8.7
Hα-Hβʻ	7.0*	6.8*	6.9	6.1
Hβ-Hγʻ	nd	nd	6.4*	nd
Hβʻ-Hγʻ	nd	nd	nd	nd
Hγʻ-Hδ	nd	nd	nd	nd
Hγʻ-Hδʻ	nd	nd	nd	nd
Hβ-Hδ	nd	nd	nd	nd

6.6.4 Ac-Gup(Boc)₂-OMe

Sample	Solvent	$K_{trans/cis}$ **11S**	$K_{trans/cis}$ **11R**
	DMSO-d6	2.5	3.6
	CDCl₃	3.6	4.4
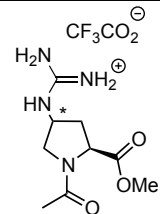
Ac-(4*S*)Gup(Boc)₂-OMe (11S)

³*J*(H,H)	CDCl₃		DMSO-d₆	
	trans	*cis*	*trans*	*cis*
Hα-Hβ	9.1	9.4	9.3	9.2
Hα-Hβ'	5.2	2.5	4.5	2.5
Hβ-Hγ	7.0	6.6	6.5	nd
Hβ'-Hγ	5.3	≈2.5	4.6	2.5
Hγ-Hδ	6.8	nd	6.6	6.6
Hγ-Hδ'	5.1	3.0	4.3	3.0
Hβ'-Hδ'	nd	nd	nd	nd

Ac-(4*R*)Gup(Boc)₂-OMe (11R)

³*J*(H,H)	CDCl₃		DMSO-d₆	
	trans	*cis*	*trans*	*cis*
Hα-Hβ	8.4	8.7	9.0	8.8
Hα-Hβ'	6.0	4.4	4.1	3.1
Hβ-Hγ'	6.3	nd	nd	nd
Hβ'-Hγ'	nd	6.3	6.5	nd
Hγ'-Hδ	4.5	5.0	6.5	6.6*
Hγ'-Hδ'	6.2	6.8	7.1	nd
Hβ-Hδ	nd	nd	nd	nd

6.6.5 Ac-Gup-OMe*TFA

Sample	Solvent	$K_{trans/cis}$ **12S**	$K_{trans/cis}$ **12R**
	D_2O	3.9	4.3
	DMSO-d6	3.3	2.9
	CD_3OD	3.0	2.9
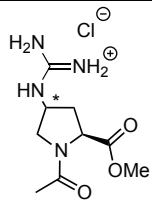
Ac-(4S)Gup-OMe*TFA (12S)

$^3J_{(H,H)}$	D_2O trans	cis	DMSO-d$_6$ trans	cis	CD_3OD trans	cis
Hα-Hβ	9.2	9.1	7.9	9.0	9.0	9.1
Hα-Hβ'	5.0	2.4	7.9*	3.9	5.9	3.2
Hβ-Hγ	5.8	5.2	7.8	nd	6.3	nd
Hβ'-Hγ	5.0	3.9	6.9	4.2	6.0	2.9
Hγ-Hδ	6.2	6.2	7.3	4.4	6.4	6.4
Hγ-Hδ'	4.4	≈1.6	6.8	6.6	5.6	3.4
Hβ'-Hδ'	≈0.7	nd	nd	nd	nd	nd

Ac-(4R)Gup-OMe*TFA (12R)

$^3J_{(H,H)}$	D_2O trans	cis	DMSO-d$_6$ trans	cis	CD_3OD trans	cis
Hα-Hβ	7.7*	8.6	8.2	8.8	8.3	8.7
Hα-Hβ'	7.7*	6.0	6.4	4.0	6.3	4.4
Hβ-Hγ'	4.9	6.7	6.0	7.3	nd	7.3*
Hβ'-Hγ'	5.9	5.1	nd	4.3	nd	6.2
Hγ'-Hδ	3.9	nd	4.6	5.5	4.6	5.4
Hγ'-Hδ'	5.7	5.2	6.0	6.5	6.0	5.8
Hβ-Hδ	1.0	<1	nd	nd	nd	nd

6.6.6 Ac-Gup-OMe*HCl

Sample	Solvent	$K_{trans/cis}$ **13S**	$K_{trans/cis}$ **13R**
	D$_2$O	3.4	4.1
	DMSO-d6	3.4	3.2

Ac-(4*S*)Gup-OMe*HCl (13S)

$^3J_{(H,H)}$	D$_2$O		DMSO-d$_6$	
	trans	*cis*	*trans*	*cis*
Hα-Hβ	9.2	9.1	8.1*	9.0
Hα-Hβ'	5.0	2.4	8.1*	4.0
Hβ-Hγ	6.0	nd	8.1	nd
Hβ'-Hγ	4.8	3.7	6.6	4.3
Hγ-Hδ	6.2	6.1	7.7	4.5
Hγ-Hδ'	4.4	≈1.5	6.8	6.7
Hβ'-Hδ'	nd	nd	nd	nd

Ac-(4*R*)Gup-OMe*HCl (13R)

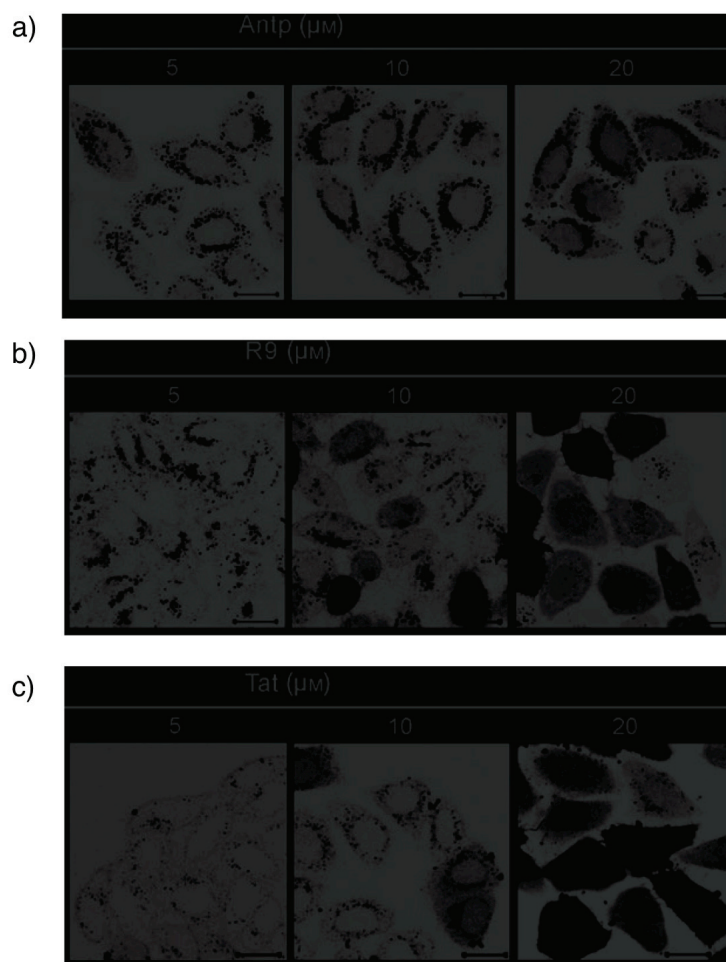| $^3J_{(H,H)}$	D$_2$O		DMSO-d$_6$	
	trans	*cis*	*trans*	*cis*
Hα-Hβ	7.7*	8.4	8.2	8.7
Hα-Hβ'	7.7*	5.0	6.3	4.4
Hβ-Hγ'	5.0*	nd	5.9	≈6.7
Hβ'-Hγ'	5.5*	nd	nd	nd
Hγ'-Hδ	3.8	4.8	4.5	5.0
Hγ'-Hδ'	5.7	nd	5.9	6.4
Hβ-Hδ	nd	nd	nd	nd

6.7 Microscopy images

Fig. 69: Distinct concentration-dependent phenotypes for the uptake of different CPPs. a–c) HeLa cells were incubated for 30 min with increasing concentrations of the indicated peptides (Antp, penetratin) by fluorescence microscopy. The scale bars represent 20 μm. From reference [140a].
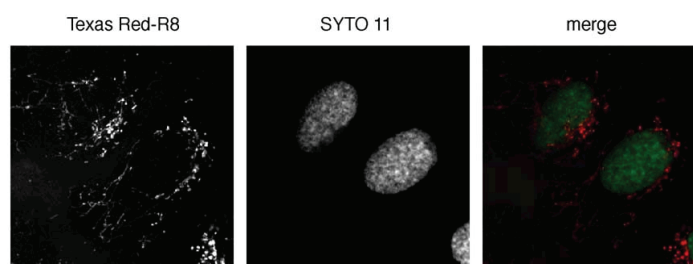

Fig. 70: Internalization of R_8 peptide into HeLa cells by confocal microscopy analysis of living HeLa cells incubated at 37°C for 1 h with the Texas red-labeled R_8 peptide (10 μM) (red). Nuclei were stained with SYTO (No. 11) (5 AM) (green). From reference [140c].
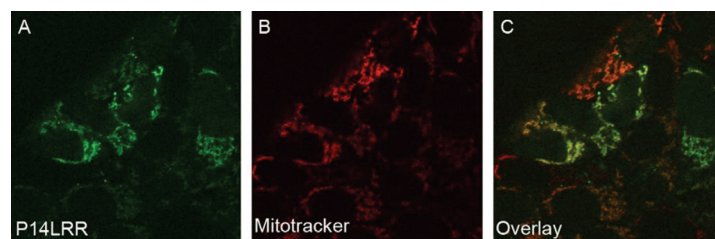
Fig. 71: Confocal images showing mitochondrial targeting of CF-G-P14LRR-CONH$_2$ (A), mitochondrial staining (B) and the overly (C) in HeLa cells at 5 µm, 30 min, 37°C. From reference [133c].
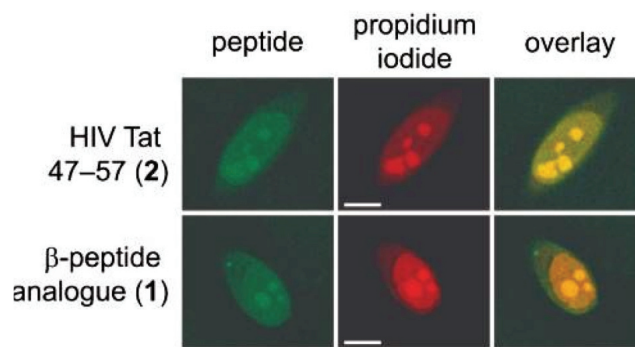

Fig. 72: Confocal microscopy images of HeLa cells incubated for 10 min at 37°C with a solution containing 0.10 µM fluorescein-labeled *β*-peptides, washed, permeabilized, and stained with propidium iodide. Scalebar: 10 µM. From reference [119].
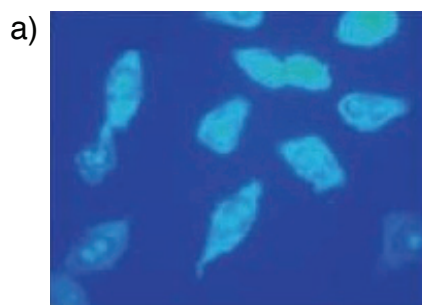

Fig. 73: Fluorescence microscopy of fluorescein-labeled *β*-hepta-arginine incubated at 1 µM peptide concentration for 40 min at 37°C to (a) HeLa cells. From reference [118a, 221]